JAERI-M
91-172

EVALUATION REPORT ON SCTF-III TEST S3-3, S3-4, AND S3-5
— COUNTER CURRENT FLOW LIMITATION PHENOMENA IN FULL RADIUS CORE —

October 1991

Tadashi IGUCHI, Isao SAKAKI*, Takamichi IWAMURA
Hajime AKIMOTO, Tsutomu OKUBO, Akira OHNUKI
Hiromichi ADACHI** and Yoshio MURAO

日本原子力研究所
Japan Atomic Energy Research Institute

JAERI-Mレポートは，日本原子力研究所が不定期に公刊している研究報告書です。
入手の問合わせは，日本原子力研究所技術情報部情報資料課（〒319-11茨城県那珂郡東海村）あて，お申しこしください。なお，このほかに財団法人原子力弘済会資料センター（〒319-11 茨城県那珂郡東海村日本原子力研究所内）で複写による実費頒布をおこなっております。

JAERI-M reports are issued irregularly.
Inquiries about availability of the reports should be addressed to Information Division Department of Technical Information, Japan Atomic Energy Research Institute, Tokai-mura, Naka-gun, Ibaraki-ken 319-11, Japan.

編集兼発行　日本原子力研究所
印　　刷　いばらき印刷㈱

Evaluation Report on SCTF-III Test S3-3, S3-4 and S3-5
- Counter Current Flow Limitation Phenomena in Full Radius Core -

Tadashi IGUCHI, Isao SAKAKI*, Takamichi IWAMURA
Hajime AKIMOTO, Tsutomu OKUBO, Akira OHNUKI
Hiromichi ADACHI** and Yoshio MURAO

Department of Reactor Engineering
Tokai Research Establishment
Japan Atomic Energy Research Institute
Tokai-mura, Naka-gun, Ibaraki-ken

(Received October 1, 1991)

In order to investigate the Counter Current Flow Limitation (CCFL) phenomena in full radius core, which is important for a LOCA of a German type PWR with a combined injection type ECCS, CCFL simulation tests (S3-3, S3-4 and S3-5) were performed using the Slab Core Test Facility (SCTF) Core-III.

In these tests, the pressure in the pressure vessel was maintained at 0.3 MPa. Steam upflow was established in the core by injecting steam into the cold leg and water was injected into the upper plenum. Intact loops and pressure-vessel-side broken loop were closed to establish the steam upflow in the core.

The break-through occurred in a localized region, while in the other region steam flowed up. Thus, the break-through occurrence was not uniform in full radius core. The radial break-through location was dependent mainly on the water subcooling distribution in the upper plenum. The break-through area decreased with decrease in steam injection rate. For typical PWR case, the ratio of the break-through area was approximately 20%.

The break-through rate increased with the increase in the injected

---

* Toshiba Coorporation

** Yamagata University

water subcooling and with the decrease in steam injection flow, similarly to small scale model tests. However, the quantitative relation between the break-through rate and the steam upflow rate was different from small scale model test. Two types of the relation were observed. When the steam upflow rate was high (corresponding to condition during early reflood phase), the break-through rate was nearly the same as one predicted with a typical one-dimensional CCFL correlation, indicating that the break-through behavior is almost one-dimensional even in a full radius core. However, when the steam upflow rate was decreased gradually (corresponding to condition during later reflood phase), the break-through rate increased suddenly at a certain steam upflow rate and could not be predicted with a typical one-dimensional CCFL correlation, indicating that the break-through behavior can switch to be nonuniform in full radius core.

Selected data from Tests S3-3, S3-4 and S3-5 are also presented in this report.

Keywords: Reactor Safety, ECCS, LOCA, PWR, Reflood, SCTF, CCFL, Break-through, Two-phase Flow, Fall-back

JAERI－M 91－172

SCTF第３次炉心試験S3－３，S3－４及びS3－５評価報告書
－実半径炉心に於ける対向流制限現象－

日本原子力研究所東海研究所原子炉工学部
井口　正・榊　勲*・岩村　公道・秋本　肇
大久保　努・大貫　晃・安達　公道**・村尾　良夫

（1991年10月１日受理）

複合注水型ECCSを備えた西ドイツ型PWR(GPWR）のLOCA時に重要な，大規模炉心における対向流抑制（CCFL）現象を解明するために，大型再冠水平板第３次試験装置（SCTF－Ⅲ）で３試験（S3－3，S3－４，S3－５試験）を実施した。

試験では，圧力容器内圧力を0.3MPaに設定し，上部プレナム内のエンドボックス上に水を注入した。また，健全コールドレグに蒸気を注入するとともに，健全ループおよび圧力容器側破断ループを閉鎖して，炉心内に上昇蒸気流を形成し炉心での蒸気発生を模擬した。

実半径炉心では，上部プレナムから炉心への落水は非一様であった。即ち，落水は局所的に生じ，他の領域を蒸気が集中して上昇した。落水位置は，主として上部プレナム内の水温分布に依存し，低水温の位置で落水が生じた。落水面積は蒸気流量の減少に伴い増加した。典型的なPWR の場合に対しては，落水面積比は約20％だった。

落水流量は，小規模試験結果と同様に，大サブクール程また小蒸気流量ほど，増加した。しかし，落水流量と蒸気上昇流量の定量的関係は小規模試験結果と異なり，２様の関係がみられた。蒸気上昇流量が大きい（再冠水初期に対応）と落水流量は一般的な１次元CCFL相関式で予測される流量とほぼ一致し，この条件では大規模炉心でも落水挙動が１次元的であることを示した。一方，蒸気上昇流量を次第に減少する（再冠水後期に対応）と，落水流量はある蒸気上昇流量で急激に増加し，以後は１次元CCFL相関式で予測できなくなった。これは，落水挙動が１次元的でなくなり，落水が局所的領域で集中する落水様式に遷移したことを示す。

なお，本報告書には試験S3－３，S3－４及びS3－５の試験結果の一部を付録として収録した。

東海研究所：〒319-11　茨城県那珂郡東海村白方字白根2-4
＊　東芝
＊＊　山形大学

Contents

目　　次

List of Tables

List of Figures

1. Introduction

SCTF program

The Slab Core Test Facility (SCTF) test program is a part of the large scale reflood test program[1] performed under contract with Atomic Energy Bureau of Science and Technology Agency of Japan together with the Cylindrical Core Test Facility (CCTF) test program.[2] The SCTF test program[3] is one of the research activities based on the trilateral agreement among Japan Atomic Energy Research Institute (JAERI), the United States Nuclear Regulatory Commission (USNRC) and the Federal Minister for Research and Technology (BMFT) of the Federal Republic of Germany (FRG).

The SCTF Core−I and Core−II test series have been performed mainly to investigate the two−dimensional thermal−hydraulic behavior in the core during the reflood phase of a loss−of−coolant accident (LOCA) of a Westinghouse−type (US/J−type) pressurized water reactor (PWR). On the other hand, one of the major objectives of the SCTF Core−III test series is to investigate the effectiveness of the combined−injection−type emergency−core−cooling−system (ECCS) for a German−type PWR (GPWR). In addition, simulation tests for a US/J−type PWR are also planned with the SCTF Core−III.

SCTF tests evaluated in this report

In the LOCA for a GPWR, it is expected that the the ECC water falls down through the upper plenum[4],[5] locally (Break−through) and floods up from the bottom of the core. And it is considered that one of major mechanism controlling the break−through is a Counter Current Flow Limitation (CCFL) at the tie plate of the end box, where the flow area is considered to be minimum between the core and the upper plenum, from the end−of−blowdown to the early reflood period. CCFL was investigated with experimental results using small scale model in the previous works. However, CCFL in full radius core has been little investigated.

Three tests were performed to investigate the CCFL phenomena in a full radius core for a GPWR using SCTF−III. This report describes the major results of these tests. The followings are brief description of these referred tests.

(1) Present test name

Tie plate CCFL tests for GPWR simulation

(2) Test number of the present tests

Test S3−3 (Run 707), Test S3−4 (Run 708) and Test S3−5 (Run 709)

Note; S3 : SCTF Core−III

3,4,5 : Sequential number of tests

(3) Object of the present tests

To investigate the tie plate CCFL phenomenon in full radius core during end-of-blowdown to reflood phase for a GPWR-LOCA

Presented in Appendix A is a brief description of the SCTF Core-III. Some selected data obtained in tests S3-3, S3-4 and S3-5 are presented in Appendix B, C and D, respectively.

2. Test description

2.1 Test facility[6]

SCTF was originally designed to study two-dimensional effect on thermal hydraulics during the reflood phase in the core of full radius.

The flow diagram of SCTF is shown in Fig. 2.1.1. The SCTF is simulating a 200 % cold-leg-break with a simplified primary system and can be operated at less than 0.6 MPa. It has a pressure vessel, an intact loop, a broken loop at a pressure vessel side, and a broken loop at a steam/water separator side.

Figure 2.1.2 shows a vertical cross section of the pressure vessel. The pressure vessel includes a simulated core, an upper plenum with internals, a lower plenum, a core baffle and a downcomer. The configurations of the upper plenum structure and the end box simulate those of a 1,300 MWe class GPWR as practically as possible.

The dimension of the core is a full-length, full-radius and one-bundle width core. The core flow area scaling ratio against a typical 1,300 MWe class PWR is 1/22. The 1,888 electrically heated rods simulating fuel rods are installed in the core. The dimension of a heated rod is 10.7 mm in diameter and 3,613 mm in heated length, which is nearly equal to that of PWRs. The maximum available power supplied to the core is 10 MW.

The heated rods are bundled to 16x16 with spacers, as similarly to those in PWRs. Eight bundles are installed in a row in the core, as shown in Fig. 2.1.2. In the SCTF, the leftmost bundle in the figure is called bundle 1 and orderly to the right the bundles are called bundle 2,3,...,8. Since the downcomer and the hot leg are connected to bundle 8 side, bundle 1 and 8 sides are corresponding to the central and the peripheral sides of PWR core, respectively.

The ECC water can be injected into the cold leg and the upper plenum in the SCTF. Since the SCTF has no injection port in the hot leg, the hot leg injection of ECC water in PWRs with combined-injection type ECCS was substituted by the upper plenum injection. The ECC water into the upper plenum can be injected from both top and side walls of the upper plenum.

The top core and the upper plenum are bounded with a top grid spacer, a tie plate of the end box and an upper core support plate (UCSP). They are perforated plate and have fluid flow pass from the core to the upper plenum. Although the top grid spacer was not shown in Fig.2.1.2, it was located just below the tie plate and used to support heated rods in the core. Geometry of tie plate and UCSP are exactly the same as those of German PWRs. Flow area of the tie plate is minimum, so that CCFL is expected to occur at the elevation of the tie plate. The pressure vessel are enveloped

by honeycomb thermal insulators with wall plates to minimize the wall thermal effects.

The description of SCTF Core−III is presented more in detail in Appendix A.

2.2 Objectives of present tests

Three tests discussed in this report are tests S3−3, S3−4 and S3−5, which are the tie plate CCFL tests for GPWRs using SCTF−III. Objective of these tests is to investigate CCFL phenomenon in a full radius core. In addition, each test has a special objective as described below.

(1) Test S3−3 : Uniform subcooled water test
Investigation of the effect of uniform subcooling in upper plenum on CCFL break−through phenomenon

(2) Test S3−4 : Local subcooled water test
Investigation of the effect of local subcooling in upper plenum on CCFL break−through location and CCFL break−through rate

(3) Test S3−5 : Distributed subcooled water test
Investigation of the effect of distributed subcooling in upper plenum on CCFL break−through location and CCFL break−through rate

2.3 Test condition and test procedure

The planned test condition for tests S3−3, S3−4 and S3−5 is summarized in Table 2.3.1. The measured test condition is described in a section 3.1.

Figure 2.3.1 shows the conceputual set−up of the facility for these CCFL tests. In these tests, the core was not heated, and the pressure vessel side blowdown valve was closed in order to prevent the steam to flow out directly from the downcomer to containment tank. In intact cold leg, a blind flange was installed at the pump simulator in order to block the intact loop.

Steam was injected into the pressure vessel through steam injection port at the intact cold leg. Water was injected into the upper plenum through ECC injection ports located just above the upper core support plate (called side injection ports as UCSP1, UCSP2, UCSP3 and UCSP4 in SCTF).

Liquid level in the upper plenum and the lower plenum were controlled using the upper plenum water extraction line and the lower plenum drain line, respectively. These are because of preventing the water entrainment into the steam flow at the upper plenum and at the lower plenum.

Figures 2.3.2, 2.3.3 and 2.3.4 show the test sequences for tests S3−3, S3−4 and S3−5, respectively. In these figures, the time when steam injection start is defined to

be 0 s.

Before the time '−3 s', the blowdown valves located at break point were closed and the pressure vessel was maintained at 0.3 MPa with saturated steam. The saturated water was stored in the lower plenum up to 0.15 m elevation. The pressure in containment tank was set at 0.17 MPa at −3 s. The blowdown valve 2 located between the steam/water separator and containment tank was quickly opened at −3 s.

For first 100 s, the pressure in the pressure vessel was nearly constant or decreased (test S3−3) due to discharge of steam through blowdown valve 2.

The pressure in containment tank was controlled to be constant at 0.17 MPa by adjusting of discharge rate of steam from containment tank to atomosphere after −3 s for tests S3−3 and S3−4. For test S3−5, it was increased from 0.17 MPa to 0.3 MPa with time to intend to keep the pressure in the pressure vessel constant during the test.

In these tests, steam was injected into pressure vessel through intact cold leg after 0 s. In test S3−3, steam flow rate was set at 5 kg/s until 180 s, and the flow rate after 180 s was decreased until 0 kg/s (at 300 s). On the other hand, in tests S3−4 and S3−5, steam flow rate were set at 7 kg/s until 40 s, and the flow rate after 40 s was decreased linearly to 0 kg/s (at 300 s).

Water was injected into upper plenum through side injection ports in these tests. In test S3−3 (Uniform subcooled water test), total water injection rate was 80 kg/s and water temperature was 133 °C at 0 s. The temperature was decreased gradually to 63 °C at 180 s. In test S3−4 (Distrubuted subcooled water test), total water injection rate was 60 kg/s, and water temperatures were set at 133 °C above bundle 1−6 and at 63 °C above bundle 7 and 8. In test S3−5 (Distrubuted subcooled water test), total water injection rate was 60 kg/s, and water temperatures were set at 50 °C above bundle 1 and 2, at 133 °C above bundle 3−6 and at 70 °C above bundle 7 and 8.

Liquid level in the upper plenum was controlled at about 0.5 m by using the upper plenum water extraction line, and liquid level in the lower plenum was controlled at about 0.2 m by using the lower plenum drain line.

3. Test results

3.1 Measured boundary conditions

Table 3.1.1 shows the chronology of major events that occurred during the present tests. Figures 3.1.1–3.1.18 show the measured conditions of test S3–3, S3–4 and S3–5.

(1) Pressure in pressure vessel and containment tanks

Pressure in the pressure vessel was intended to be constant during tests. However, it was not constant because of depressurization due to condensation and pressurization due to flow resistance across loops, as follows .

Figures 3.1.1–3.1.6 show the pressure in the pressure vessel and the containment tanks of test S3–3, S3–4 and S3–5.

In test S3–3 (Uniform subcooled water test), the pressures in the pressure vessel and the containment tanks were 0.29 MPa and 0.19 MPa at 0 s, respectively. After steam injection initiation, the pressure in the pressure vessel increased and the maximum pressure was 0.33 MPa at 46 s. In the period when injected water temperature decreased (80–198 s), the pressure in the pressure vessel decreased gradually by condensation. After 182 s, the pressure decreased further caused by decreasing of steam injection flow rate.

In test S3–4 (Local subcooled water test), the pressures in the pressure vessel and the containment tanks were 0.27 MPa and 0.18 MPa at 0 s ,respectively. After steam injection initiation, the pressure in the pressure vessel increased and reached 0.39 MPa at 53 s. After 53 s, the pressure in the pressure vessel decreased gradually by condensation and decrease in steam injection flow rate.

In test S3–5 (Distributed subcooled water test), the pressures in the pressure vessel and the containment tanks were 0.27 MPa and 0.18 MPa at 0 s, respectively. After steam injection initiation, the pressure in the pressure vessel increased and reached 0.38 MPa at 46 s. After 46 s, the pressure in the pressure vessel decreased gradually by condensation and decrease in steam injection flow rate.

(2) Water injection rate and temperature

Figures 3.1.7–3.1.12 show the water injection rate and the water temperature through the side injection ports in the upper plenum.

In all of present tests, the water injection started at 40 s. The total water injection rate was 80 kg/s for test S3–3 and 60 kg/s for tests S3–4 and S3–5, as intended.

In test S3–3 (Uniform subcooled water test), initial temperature of the water was

saturated temperature (133 °C) until 90 s, and the temperature was reduced gradually until 63 °C at 198 s. Temperature was uniform in the upper plenum.

In test S3-4 (Local subcooled water test), the subcooled water was injected into the upper plenum through only one injection port (UCSP1). The intended temperature was 63 °C, but the measured temperature was higher than 63 °C until 100 s. Injected water through other injection ports, i.e. UCSP2, UCSP3 and UCSP4, was the saturated water. Thus, one local subcooled water area was formed in the upper plenum.

In test S3-5 (Distributed subcooled water test), the subcooled water was injected through UCSP1 and UCSP4, and the temperatures were 70 °C and 50 °C after 100 s, respectively. Before that, it was higher than the intended. Injected water through UCSP2 and UCSP3 was the saturated water.

(3) Steam injection rate

Figure 3.1.13 shows the steam injection rate of the present tests. In all of present tests, the steam injection initiated at 0 s and the steam was injected through the intact cold leg.

In test S3-3 (Uniform subcooled water test), the steam injection flow rate was 4.7~4.9 kg/s until 182 s, and it was reduced gradually to 0 kg/s at 304 s. In test S3-4 (Local subcooled water test), the steam injection flow rate was 6.7 kg/s until 44 s, and it was reduced gradually to 0 kg/s at 293 s. In test S3-5 (Distributed subcooled water test), the steam injection flow rate was 6.6 kg/s until 46 s, and it was reduced gradually to 0 kg/s at 293 s. They were almost the same as the intended.

(4) Upper plenum liquid level

Upper plenum liquid level was controlled for preventing the water in the upper plenum from overflowing to the hot leg. To control the upper plenum liquid level, the upper plenum water extraction system was activated. In the facility, four extraction lines were provided, and they located above bundle 1 and 2, bundle 3 and 4, bundle 5 and 6 and bundle 7 and 8, respectively. Figures 3.1.14~3.1.16 show the measured upper plenum liquid level.

In the present tests, the upper plenum liquid level rose quickly after the water injection started. In test S3-3, the upper plenum water extraction started at 147 s because of the upper plenum liquid level exceeded the controlling range (0.5~0.53 m). However, the liquid level was not controlled well because of significantly much water injection into the upper plenum. In tests S3-4 and S3-5, the upper plenum water extraction started at 135 s and at 145 s, respectively, by using only one extraction line above bundles 7 and 8.

(5) Lower plenum liquid level

Lower plenum liquid level was controlled not to block the steam flow pass from the downcomer to the core. Figures 3.1.17 and 3.1.18 show the lower plenum liquid level and the lower plenum water drain rate.

In all of present tests, the liqui level in the lower plenum was 0.11 m before the water injection initiated at 40 s. After the water injection initiated, the lower plenum liquid level began to rise. And the lower plenum water drain initiated at 100 s, 141 s and 64 s for tests S3－3, S3－4 and S3－5, respectively. This is because the liquid level exceeded the controlling range (0.15–0.25 m). However, the liquid level was not controlled well because of large amount of water supply to the lower plenum due to massive CCFL break－through written later.

Around 200s the liquid level in the lower plenum exceeded 0.7 m, which elevation is the upper limit of the opening from the downcomer to the core. Therefore, after the time steam penetrates the liquid layer in the lower plenum to flow from the downcomer to the core.

3.2 CCFL break－through location and area

In CCFL tests, it is important to evaluate the CCFL break－through location, area and rate from the upper plenum to the core. In this section, the CCFL break－through location and area are described. The CCFL break－through rate is described in the next section.

The break－through locations and area were decided based on the data of the end box drag body (measuring drag force due to two－phase flow; Fig.3.2.1, Fig.3.2.4, and Fig.3.2.7), the differential pressure across the tie plate of the end box (Fig.3.2.2(1) and Fig.3.2.2(2), Fig.3.2.5(1) and Fig.3.2.5(2), and Fig.3.2.8(1) and Fig.3.2.8(2)) and the fluid temperature below the end box (Fig.3.2.3(1) and Fig.3.2.3(2), Fig.3.2.6(1) and Fig.3.2.6(2), and Fig.3.2.9(1) and Fig.3.2.9(2)). Combining the data of the end box drag body and the turbine meter, steam and water flow rates through the tie plate of the end box were calculated. Negative differential pressure across the tie plate indicates the fluid flow from the upper plenum to the core and then the occurrence of the break－through at the measuring location. However, positive differential pressure does not always mean the fluid flow from the core to the upper plenum because of the effect of the static head. Subcooled temperature, if measured below the tie plate, means the break－through of the subcooled water and indicates the location of the break－through.

In test S3-3 (Uniform subcooled water test), the break-through was observed above bundle 4 after 57 s, which was judged from Fig.3.2.2(1) showing negative differential pressure. In the period of the injected water temperature decreasing (80–182 s), only above bundle 4 was the break-through location in spite of uniform subcool condition. In the period of the steam injection rate decreasing (182 s–), the negative differential pressure is observed not only above bundle 4, as shown in Fig.3.2.2(1) and Fig.3.2.2(2), indicating the break-through area extended gradually with the decrease in the steam injection flow rate. Figures 3.2.10 shows more clearly the expansion of the break-through location.

In test S3-4 (Local subcooled water test), the subcooled water (63 °C) were injected only above bundles 7 and 8 and the steam flow rate was reduced gradually after 44 s. Based on the data shown in Fig.3.2.4–Fig.3.2.6, the location of the break-through was judged, as shown in Fig.3.2.11. The break-through with the short period is observed above bundle 1 at about 60 s. However, the break-through is observed mainly above bundle 6–8, where the subcooled water is injected and staying. And the no break-through was observed above bundle 3 and bundle 5.

In test S3-5 (Distributed subcooled water test), the subcooled water was injected above bundles 1 and 2 and above bundles 7 and 8. The water temperature were 50 °C and 70 °C, respectively. The steam flow rate was reduced gradually after 46 s. As shown in Fig.3.2.12, the break-through was observed after 62 s above bundles 1 and 2, where the high subcooled water were injected. The break-through area extended gradually with the steam flow decreasing. However, the break-through occurred mainly above bundles 1 and 2 and bundles 7 and 8, where the subcooled water were injected.

In summary, following characteristics were noticed.

(1) Concerning break-through location under high steam injection rate (more than 2.7kg/s in SCTF scale)
   (a) Break-through occurrence was not uniform even under uniform subcooling of water injected into the upper plenum. Break-through occurs locally in full radius core.
   (b) In the case of nonuniform subcooling in the upper plenum, the break-through location is affected by the distribution of the subcooling. In the case of one local subcool area in the upper plenum (as in test S3-4: Local subcooled water test), the break-through occurred locally below the subcool area and almost no break-through occurred below the saturated area. In addition, in the case of two subcool areas in the upper plenum (as in test S3-5: Distributed subcooled

water test), the break-through occurred locally only in higher subcool area and almost no break-through in lower subcool and saturated areas under more than steam flow rate typical in PWRs during reflood (around 5kg/s in SCTF scale(4),(5)). In less steam injection rate the break-through occurred locally below two subcool areas in the upper plenum.

(2) Concerning break-through location under low steam injection rate (less than 2.7kg/s in SCTF scale)
  (a) The break-through location was observed almost over the entire cross section. The distribution of the subcooling had little effect on the break-through location.

(3) Concerning break-through area
  (a) The break-through area extended gradually with the decrease in the steam injection flow rate, as shown in Fig. 3.2.13.
  (b) Following effect of water temperature distribution on the break-through area was observed from Fig. 3.2.13.
    i) Under high steam injection rate more than 2.7kg/s in SCTF scale, the ratio of the break-through area was less than 50% and the effect of water temperature distribution was little.
    ii) Under low steam injection rate less than 2.7kg/s in SCTF scale, the ratio was more than 50% and the steeper temperature distribution resulted in the smaller ratio of the break-through area. (Test S3-4 gave the smaller ratio than tests S3-3 and S3-5.)
  (c) The break-through occurrence was intermittent in the respective bundle. Break-through did not always continue at the same location. However when the break-through stopped at a location, the other break-through tended to start at the other location.
  (d) For typical PWR case (around 5kg/s in SCTF scale), the ratio of the break-through area was approximately 20%.

The reason why the break-through location is not always constant is considered as follows from the measurement of liquid level on the tie plate:

(1) When the massive break-through occurs, the water level on the tie plate of the end box decreases. In sometime, the water on the tie plate of the end box disappears.
(2) As the result, the break-through terminates in the break-through region.
(3) On the other hand, the water accumulates on the tie plate of the end box where the break-through has not occurred and hence the new break-through begins.

3.3 CCFL break−through rate

Figures 3.3.1−3.3.6 show the mass flow rate in the pressure vessel and the CCFL break−through rate. In these figures, the CCFL break−through rate were estimated by the following mass balance calculation.

$$m_{fb} = m_c + m_{LP} + m_{dm} + m_{DC}$$

where,

m_{fb} : break−through rate
m_c : water accumulation rate in core
m_{LP} : water accumulation rate in lower plenum
m_{dm} : water drain rate from lower plenum
m_{DC} : water accumulation rate in downcomer

In test S3−3 (Uniform subcooled water test), the CCFL break−through rate increased rapidly after 100 s, as shown in Fig. 3.3.2. Before 100 s, small CCFL break−through rate is detected. The timing of rapid increase of CCFL break−through (100 s) corresponds to the timing when the high subcooling begins to be detected below the tie plate, as shown in Fig. 3.2.3(1). After 100 s, the break−through rate increased with the increase in the injected water subcooling.

In test S3−4 (Local subcooled water test) and S3−5 (Distributed subcooled water test), the break−through rate increased rapidly after 134 s and 57 s, as shown in Figs. 3.3.4 and 3.3.6. In these tests, the break−through rate increased with the decrease in the injected steam flow rate.

4. Discussion

4.1 Effect of subcooling on CCFL break-through rate

Figure 4.1.1 shows the subcooling of ECC water injected into the upper plenum in a test S3-3 (Uniform subcooled water test). Figure 4.1.2 shows a relation of the water subcooling and CCFL break-through rate in the test. The test S3-3 was performed to investigate the effects of ECC water subcooling on CCFL break-through rate, under the constant ECC water and steam flow rate and the uniform subcooled water.

In a period of ECC water temperature decreasing (80-200 s), the break-through rate through the end box to the core increased with the increase in the injected water subcooling, as shown in Fig.4.1.2. This is caused by the increase in steam condensation rate in pressure vessel, resulted by decrease in the ECC water temperature.

Massive break-through were observed when the water subcooling exceeded at 20K.

4.2 Effect of steam flow rate on CCFL break-through rate

Figures 4.2.1 and 4.2.2 show a relation of break-through rate and steam injection rate into an intact cold leg in tests S3-4 (Local subcooled water test) and S3-5 (Distributed subcooled water test), respectively. Both tests were performed to investigate the effects of steam injection rate on CCFL break-through rate.

In both tests, the break-through rate increased with the decrease in the injected steam flow rate. The break-through were almost not observed under the condition of the high steam injection flow rate (more than 4.5 kg/s in test S3-4 and more than 6.2 kg/s in test S3-5) A difference in the threshold of the above steam injection flow rate were caused by the difference in the distribution of the subcooled water in the upper plenum.

4.3 Evaluation of break-through rate with a typical one-dimensional correlation

Figure 4.3.1 shows the relation between break-through rate and steam upflow rate through end box tie plate for a test S3-3 (Uniform subcooled water test). This steam upflow was estimated by (forced steam injection rate) − (steam condensation rate in

the core) due to subcooled break−through water. In the figure, prediction with a typical CCFL correlation[7](Wallis correlation) is shown.

Estimated break−through rate is much higher than predicted one. Possible reasons are considered to be two−dimensional effect and subcooling effect. As shown before, the break−through occurred locally in this test. Therefore, steam upflow and water downflow have little interference with each other. Thus, the nonuniform break−through occurrence and the significantly large break−through rate in comparison with the prediction by a typical one−dimensional correlation have occurred. Consequently, the nonuniform break−through is considered to be important for CCFL phenomena in a full radius core.

The previous report[8] described that the local break−through rate can be predicted with the local steam upflow rate in full radius core of PWRs under the water of the saturation temperature, by using one−dimensional typical CCFL correlation. Present result described above indicates that this approach to predict the break−through rate in the full radius core is not valid under the subcooled water condition.

4.4 Discussion on relation between break−through rate and steam flow rate

Data shown in Fig.4.2.1 and Fig.4.2.2 show jumps at respective steam injection flow rates for tests S3−4 and S3−5, i.e. about 4kg/s for S3−4 and about 6.2 kg/s for S3−5. This suggests that (1) if steam flow rate is large enough, little (almost no) break−through occurs and (2) if steam flow rate is small, massive break−through takes place. Once massive break−through takes place, the break−through rate is significantly large. This characteristics are well known in Fig.4.2.3 by the data in "A" and "B" regions indicated in the figure. "A" and "B" regions are common among the present tests and data in "A" regions are much larger than data in "B" region. Resultantly it is considered that there are two kinds of the stable relations between the break−through rate and steam injection flow rate. Data in "B" region is nearly equal to that predicted with a typical one−dimensional CCFL correlation, indicating that the break−through is uniform. On the other hand, data in "A" region indicate the effect of nonuniform break−through.

According to the present data, the switching from "B" region (Little break−through) to "A" region (Massive break−through) takes short time. Once mass break−through takes place, the massive break−through tends to continue.

In summary of this section, it is considered from the present data that

(1) Thc break-through rate through end box to core increased with increase in injected water subcooling and with decrease in steam injection flow rate, similarly to the characteristics observed in previous small scale model tests.

(2) However, the quantitative relation in full radius core is different from that in previous small scale model tests as follows:

i) There are two stable relations between break-through rate and steam injection flow rate, as shown ii) and iii) below.

ii) When the steam upflow rate was high (corresponding to condition during early reflood phase), the break-through rate was nearly the same as one predicted with a typical one-dimensional CCFL correlation (B region in Fig. 4.2.3), indicating that the break-through behavior is almost one-dimensional even in a full radius core. In this case temperature of falling water was nearly saturated, as noticed from Figs. 4.2.3, 3.1.13, 3.2.6(2) and 3.2.9(1).

iii) However, when the steam upflow rate was decreased gradually (corresponding to condition during later reflood phase), the break-through rate increased suddenly at a certain steam upflow rate and could not be predicted with a typical one-dimensional CCFL correlation (A region in Fig. 4.2.3), indicating that the break-through behavior can switch to be nonuniform in full radius core. In this core temperature of falling water was subcooled, as noticed from Figs. 4.2.3, 3.1.13, 3.2.6(2) and 3.2.9(1).

iv) Although the previous report described that the local break-through rate can be predicted with the local steam upflow rate in full radius core of PWRs under the water of the saturation temperature, by using one-dimensional typical CCFL correlation, the present result indicated that this approach to predict the break-through rate in the full radius core was not valid under the subcooled water condition.

v) Switching from ii) to iii) occurs in a short period. Once massive break-through takes place, the massive break-through tends to continue.

5. Conclusion

CCFL phenomena at the tie plate in full radius core of PWRs were investigated with the experimental result of SCTF tests S3−3 (Uniform subcooled water test), S3−4 (Local subcooled water test) and S3−5 (Distributed subcool water test). Following findings were obtained.

(1) Break−through location under high steam injection rate (more than 2.7kg/s in SCTF scale)

(a) Break−through occurrence was not uniform even under uniform subcooling of water injected into the upper plenum. Break−through occurs locally in full radius core.

(b) In the case of nonuniform subcooling in the upper plenum, the break−through location is affected by the distribution of the subcooling. In the case of one local subcool area in the upper plenum (as in test S3−4: Local subcooled water test), the break−through occurred locally below the subcool area and almost no break−through occurred below the saturated area. In addition, in the case of two subcool areas in the upper plenum (as in test S3−5: Distributed subcooled water test), the break−through occurred locally only in higher subcool area and almost no break−through in lower subcool and saturated areas under more than steam flow rate typical in PWRs during reflood (around 5 kg/s in SCTF scale). In less steam injection rate the break−through occurred locally below two subcool areas in the upper plenum.

(2) Break−through location under low steam injection rate (less than 2.7kg/s in SCTF scale)

The break−through location was observed almost over the entire cross section. The distribution of the subcooling had slight effect on the break−through location.

(3) Break−through area

(a) The break−through area extended gradually with the decrease in the steam injection flow rate.

(b) Under high steam injection rate more than 2.7kg/s in SCTF scale, the ratio of the break−through area was less than 50% and the effect of water temperature distribution was little.

Under low steam injection rate less than 2.7kg/s in SCTF scale the ratio was more than 50% and the steeper temperature distribution resulted in the smaller ratio of the break−through area.

(c) The break-through occurrence was intermittent in the respective bundle. Break-through did not always continue at the same location. However when the break-through stopped at a location, the other break-through tended to start at the other location.

(d) For typical PWR case, the ratio of the break-through area was approximately 20%.

(e) The reason why the break-through location is not always the same is considered as follows:

i) When the massive break-through occurs, the water level on the tie plate of the end box decreases. In some of this cases, the water on the tie plate of the end box disappears.

ii) As the result, the break-through terminates in the break-through region.

iii) On the other hand, the water accumulates on the tie plate of the end box where the break-through has not occurred and hence the new break-through begins.

(4) Break-through rate

(a) The break-through rate through end box to core increased with increase in injected water subcooling and with decrease in steam injection flow rate, similarly to the characteristics observed in previous small scale model tests.

(b) However, the quantitative relation in full radius core is different from that in previous small scale model tests as follows:

i) There are two stable relations between break-through rate and steam injection flow rate, as shown ii) and iii) below.

ii) When the steam upflow rate was high (corresponding to condition during early reflood phase), the break-through rate was nearly the same as one predicted with a typical one-dimensional CCFL correlation, indicating that the break-through behavior is almost one-dimensional even in a full radius core.

iii) However, when the steam upflow rate was decreased gradually (corresponding to condition during later reflood phase), the break-through rate increased suddenly at a certain steam upflow rate and could not be predicted with a typical one-dimensional CCFL correlation, indicating that the break-through behavior can switch to be nonuniform in full radius core.

iv) Although the previous report described that the local break-through rate can be predicted with the local steam upflow rate in full radius core of PWRs under the water of the saturation temperature, by using one-dimensional typical CCFL correlation, the present result indicated that this approach to

predict the break−through rate in the full radius core was not valid under the subcooled water condition.

v) Switching from ii) to iii) occurs in a short period. Once massive break−through takes place, the massive break−through tends to continue.

Acknowledgement

The authors would like to express their thanks to the 2D/3D project members of the U.S.A and the F.R.G.

References

(1) Hirano, K. and Murao, Y.: 'Large Scale Reflood Test', Nihon−Genshiryoku−Gakkai Shi (J. At. Energy Soc. Jpn.)[in Japanese], 2(10), 681 (1980)

(2) Iguchi, T. et al.: 'Analysis report on CCTF reflood tests' [in Japanese], to be published as a JAERI−M report

(3) Adachi, H. et al.: 'Design of Slab Core Test Facility (SCTF) in Large Scale Reflood Test Program, Part I: Core−I', JAERI−M 83−080 (1983)

(4) Iguchi, T. et al.: 'SCTF−III test plan and recent SCTF−III test result', Nucl. Eng. Des. v.108(1/2), 241−247 (1988)

(5) Iguchi, T. et al.: 'Recant results of analytical study on SCTF−III test for reflood phenomena of PWR with combined−injection−type ECCS under old−leg−large−break LOCA', NUREG/CP−0097 vol.4, 557−581 (1989)

(6) Adachi, H. et al.: 'Design of Slab Core Test Facility (SCTF) in Large Scale Reflood Test Program, Part III: Core−III', to be published as a JAERI−M report

(7) Wallis, G. B.:'One Dimensional Two Phase Flow', McGraw−Hill, NY (1969)

(8) Sobajima, M. et al.: 'Two−dimensional fall back flow and core cooling in the slab core test facility (SCTF)', Proc. second int. topical meeting on nucl. power plant thermal hydr. and operations, 2/129−2/135 (1986)

predict the break−through rate in the full radius core was not valid under the subcooled water condition.

v) Switching from ii) to iii) occurs in a short period. Once massive break−through takes place, the massive break−through tends to continue.

Acknowledgement

The authors would like to express their thanks to the 2D/3D project members of the U.S.A and the F.R.G.

References

(1) Hirano, K. and Murao, Y.: 'Large Scale Reflood Test', Nihon−Genshiryoku−Gakkai Shi (J. At. Energy Soc. Jpn.)[in Japanese], 2(10), 681 (1980)

(2) Iguchi, T. et al.: 'Analysis report on CCTF reflood tests' [in Japanese], to be published as a JAERI−M report

(3) Adachi, H. et al.: 'Design of Slab Core Test Facility (SCTF) in Large Scale Reflood Test Program, Part I: Core−I', JAERI−M 83−080 (1983)

(4) Iguchi, T. et al.: 'SCTF−III test plan and recent SCTF−III test result', Nucl. Eng. Des. v.108(1/2), 241−247 (1988)

(5) Iguchi, T. et al.: 'Recant results of analytical study on SCTF−III test for reflood phenomena of PWR with combined−injection−type ECCS under old−leg−large−break LOCA', NUREG/CP−0097 vol.4, 557−581 (1989)

(6) Adachi, H. et al.: 'Design of Slab Core Test Facility (SCTF) in Large Scale Reflood Test Program, Part III: Core−III', to be published as a JAERI−M report

(7) Wallis, G. B.:'One Dimensional Two Phase Flow', McGraw−Hill, NY (1969)

(8) Sobajima, M. et al.: 'Two−dimensional fall back flow and core cooling in the slab core test facility (SCTF)', Proc. second int. topical meeting on nucl. power plant thermal hydr. and operations, 2/129−2/135 (1986)

predict the break−through rate in the full radius core was not valid under the subcooled water condition.

v) Switching from ii) to iii) occurs in a short period. Once massive break−through takes place, the massive break−through tends to continue.

Acknowledgement

The authors would like to express their thanks to the 2D/3D project members of the U.S.A and the F.R.G.

References

(1) Hirano, K. and Murao, Y.: 'Large Scale Reflood Test', Nihon−Genshiryoku−Gakkai Shi (J. At. Energy Soc. Jpn.)[in Japanese], 2(10), 681 (1980)

(2) Iguchi, T. et al.: 'Analysis report on CCTF reflood tests' [in Japanese], to be published as a JAERI−M report

(3) Adachi, H. et al.: 'Design of Slab Core Test Facility (SCTF) in Large Scale Reflood Test Program, Part I: Core−I', JAERI−M 83−080 (1983)

(4) Iguchi, T. et al.: 'SCTF−III test plan and recent SCTF−III test result', Nucl. Eng. Des. v.108(1/2), 241−247 (1988)

(5) Iguchi, T. et al.: 'Recant results of analytical study on SCTF−III test for reflood phenomena of PWR with combined−injection−type ECCS under old−leg−large−break LOCA', NUREG/CP−0097 vol.4, 557−581 (1989)

(6) Adachi, H. et al.: 'Design of Slab Core Test Facility (SCTF) in Large Scale Reflood Test Program, Part III: Core−III', to be published as a JAERI−M report

(7) Wallis, G. B.:'One Dimensional Two Phase Flow', McGraw−Hill, NY (1969)

(8) Sobajima, M. et al.: 'Two−dimensional fall back flow and core cooling in the slab core test facility (SCTF)', Proc. second int. topical meeting on nucl. power plant thermal hydr. and operations, 2/129−2/135 (1986)

Table 2.3.1 Test conditions for Tests S3-3, S3-4 and S3-5

S3-3 : Uniform subcooled water test
S3-4 : Local subcooled water test
S3-5 : Distributed subcooled water test

(1) Common test condition

	Planned	Measured
Pressure in PV[*1]	0.3 MPa	(See Fig.3.1.1, 3.1.3 and 3.1.5)
Total power in Core	0.0 MW	0.0 MW
CL[*2] ECC[*7] injection mode		
Mass flow rate	0.0 kg/s	0.0 kg/s
Water extraction above UCSP[*3]	Yes	(See Fig.3.1.15, 3.1.17 and 3.1.19)
Initial liquid level in LP[*4]	0.02 m	(See Fig.3.1.20)
Water extraction from LP	Yes	(See Fig.3.1.21)

(2) Different test condition

	S3-3	S3-4	S3-5
Pressure in Containment Tank II	0.17 MPa	0.17 MPa	0.17 → 0.3 MPa
	(Measurement data are shown in Fig.3.1.2, 3.1.4 and 3.1.6.)		
UP[*5] ECC injection mode			
Mass flow rate	80.0 kg/s [*6]	60.0 kg/s [*6]	60.0 kg/s [*6]
	(Measurement data are shown in Fig.3.1.7, 3.1.9 and 3.1.11.)		
Temperature	133 → 63°C	133, 63°C	133, 70, 50°C
	(Measurement data are shown in Fig.3.1.8, 3.1.10 and 3.1.12.)		
Steam injection rate	5 → 0 kg/s	7 → 0 kg/s	7 → 0 kg/s
	(Measurement data are shown in Fig.3.1.13.)		

*1 Pressure Vessel
*2 Cold Leg
*3 Upper Core Suport Plate
*4 Lower Plenum
*5 Upper Plenum
*6 Side Injection
*7 Emergency Core Coolant

Table 3.1.1 Chronology of major events

(1) Test S3-3 (Run 707) (Uniform subcooled water test)

	Time after test starts
● Steam injection start (4.9 kg/s)	0 sec
● Water injection start (total 80.0 kg/s)	40
● Maximum pressure in pressure vessel (0.33 MPa)	46
● Initiation of water temperature decreasing (133°C →)	80
● Lower plenum water drain start	100
● Upper plenum water extraction start	147
● Initiation of steam flow rate decreasing (4.7 kg/s →)	182
● Maximum water level in upper plenum (above bundle 3 : 1.4 m)	192
● End of water temperature decreasing (→ 63 °C)	198
● End of steam flow rate decreasing (→ 0.0 kg/s)	304
● End of water injection	333

(2) Test S3-4 (Run 708) (Local subcooled water test)

	Time after test starts
● Steam injection start (6.7 kg/s)	0 sec
● Water injection start (total 60.0 kg/s)	40
● Initiation of steam flow rate decreasing (6.7 kg/s)	44
● Maximum pressure in pressure vessel (0.39 MPa)	53

Table 3.1.1 Chronology of mamor events (cont.)

● Upper plenum water extraction start (only above bundle 7,8)	135
● Maximum water level in upper plenum (above bundle 8 : 0.76 m)	138
● Lower plenum water drain start	141 sec
● End of steam flow rate decreasing (→ 0.0 kg/s)	293
● End of water injection	310

(3) Test S3-5 (Run 709) (Distributed subcooled water test)

	Time after test starts
● Steam injection start (6.6 kg/s)	0 sec
● Water injection start (total 60.0 kg/s)	40
● Maximum pressure in pressure vessel (0.38 MPa)	46
● Initiation of steam flow rate decreasing (6.6 kg/s)	46
● Lower plenum water drain start	64
● Maximum water level in upper plenum (above bundle 8 : 0.75 m)	125
● Upper plenum water extraction start (only above bundle 7,8)	145
● End of steam flow rate decreasing (→ 0.0 kg/s)	293
● End of water injection	330

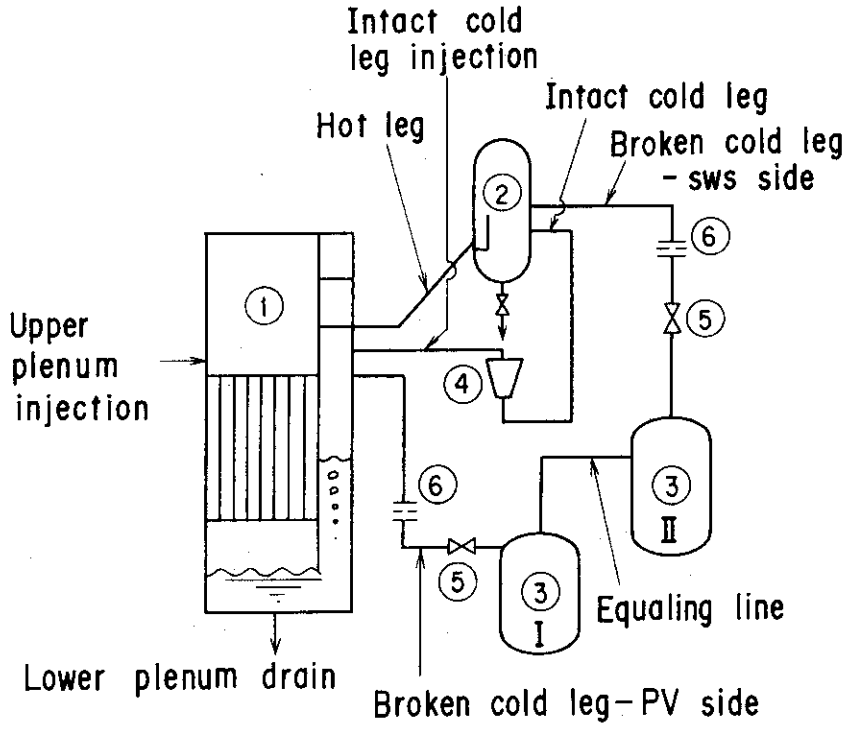

① Pressure vessel
② Steam/water separator
③ Containment tanks
④ Pump simulator
⑤ Blowdown valves
⑥ Flow resistance simulators

Upper plenum extraction system and steam injection system was deleted in the figure.

Fig. 2.1.1 Flow diagram of SCTF

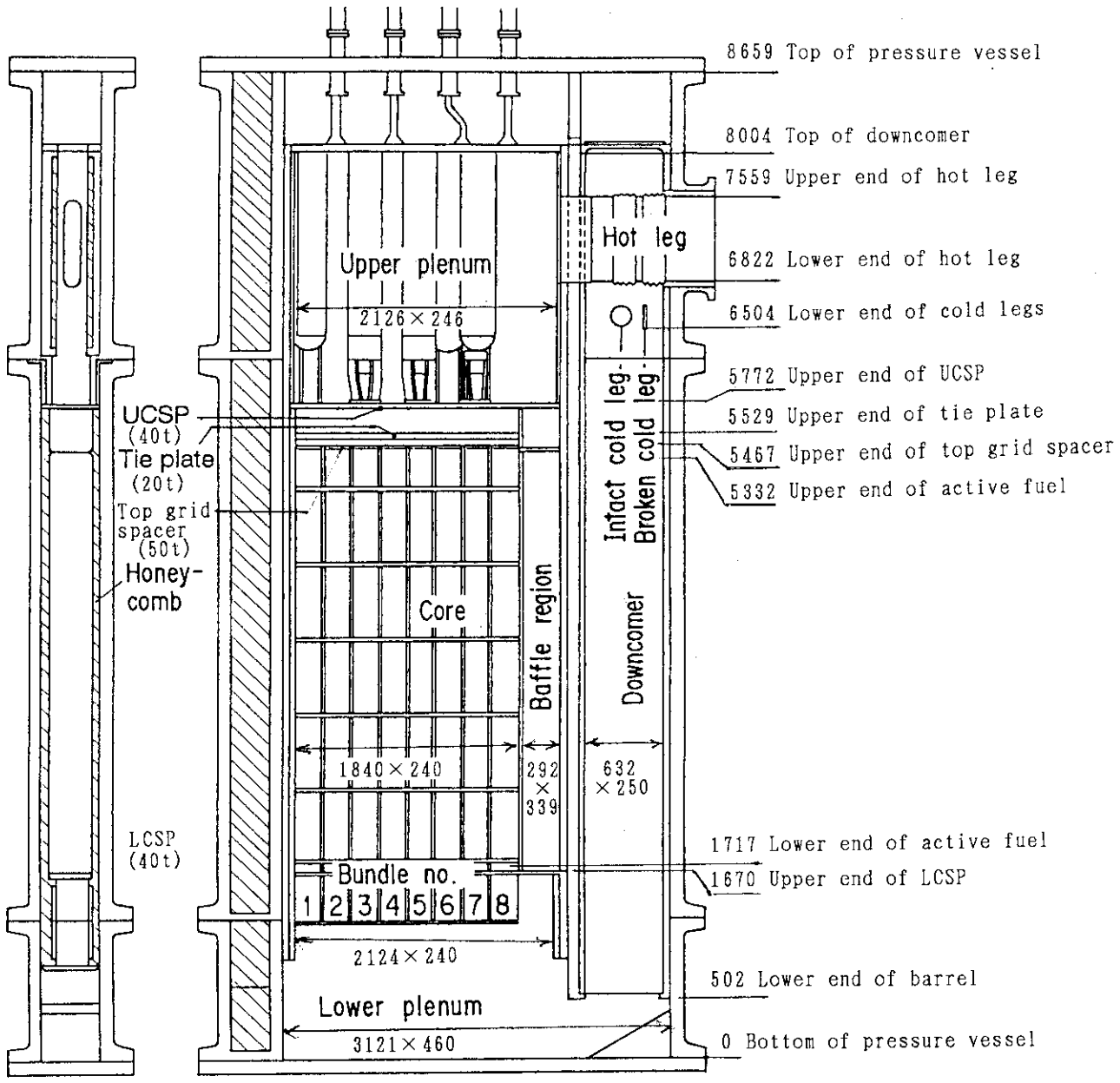

Fig. 2.1.2 Vertical cross section of pressure vessel

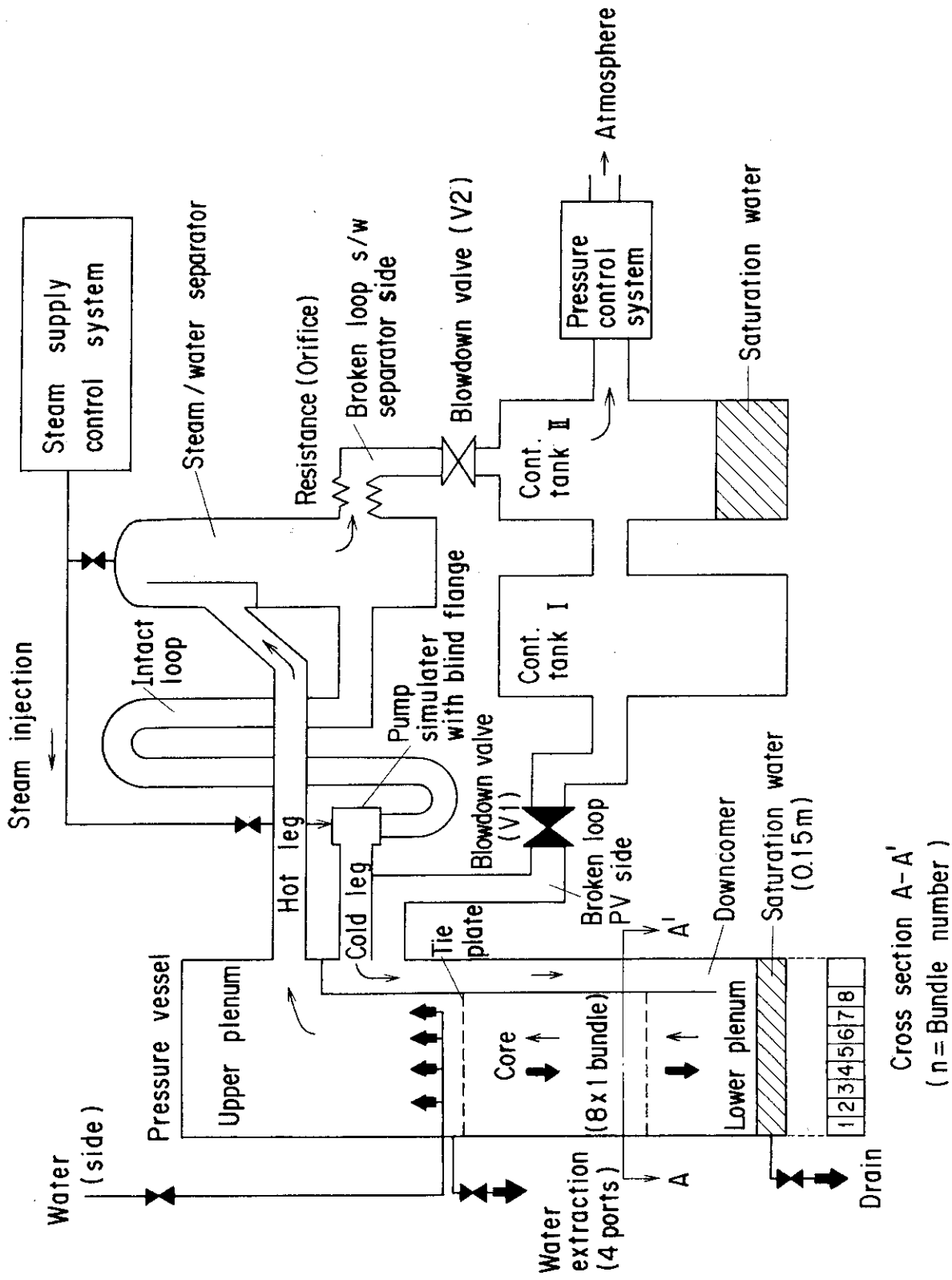

Fig. 2.3.1 Initial set-up for present CCFL tests

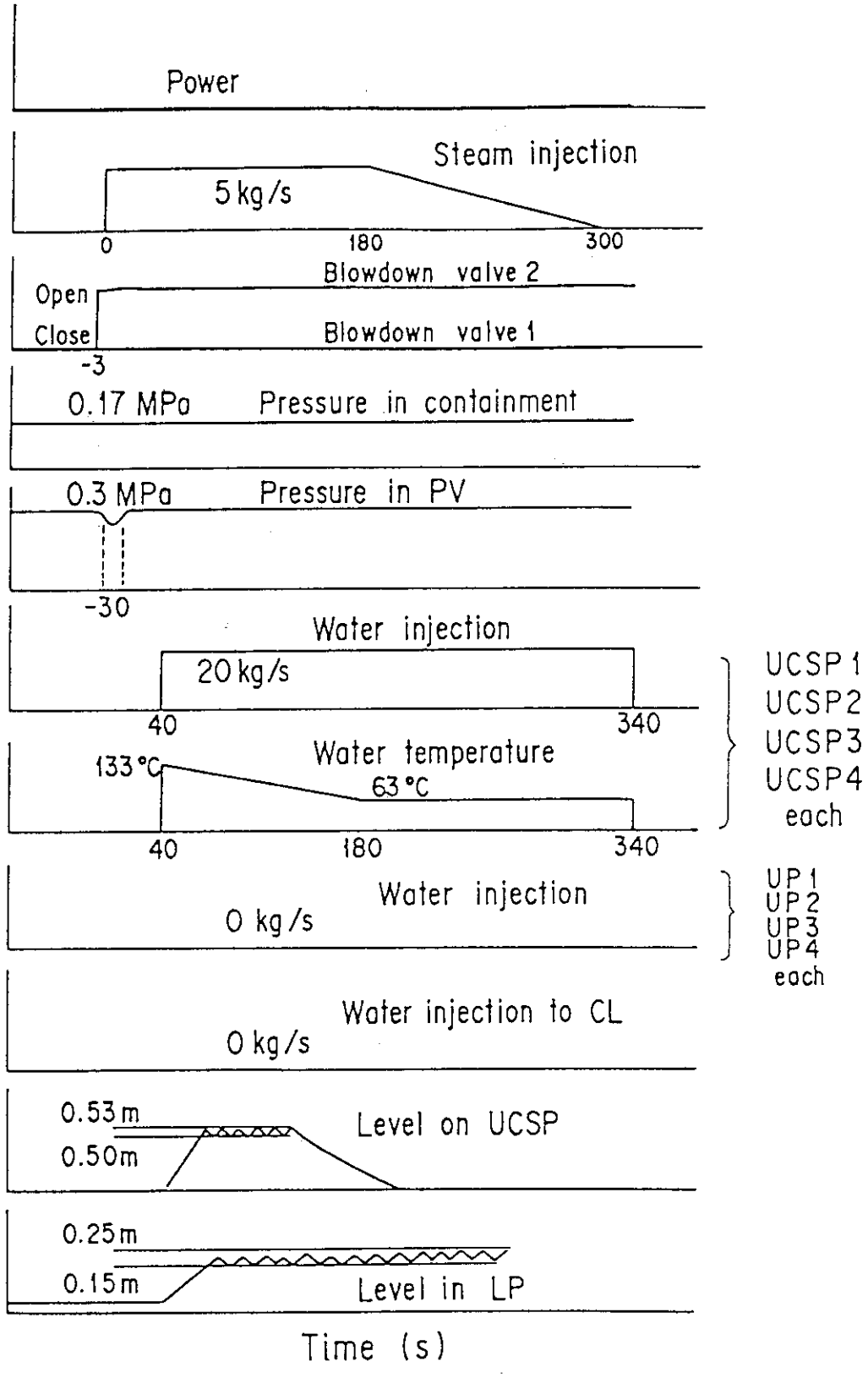

Fig. 2.3.2 Test sequence of Test S3-3 (Run 707)
(Uniform subcooled water test)

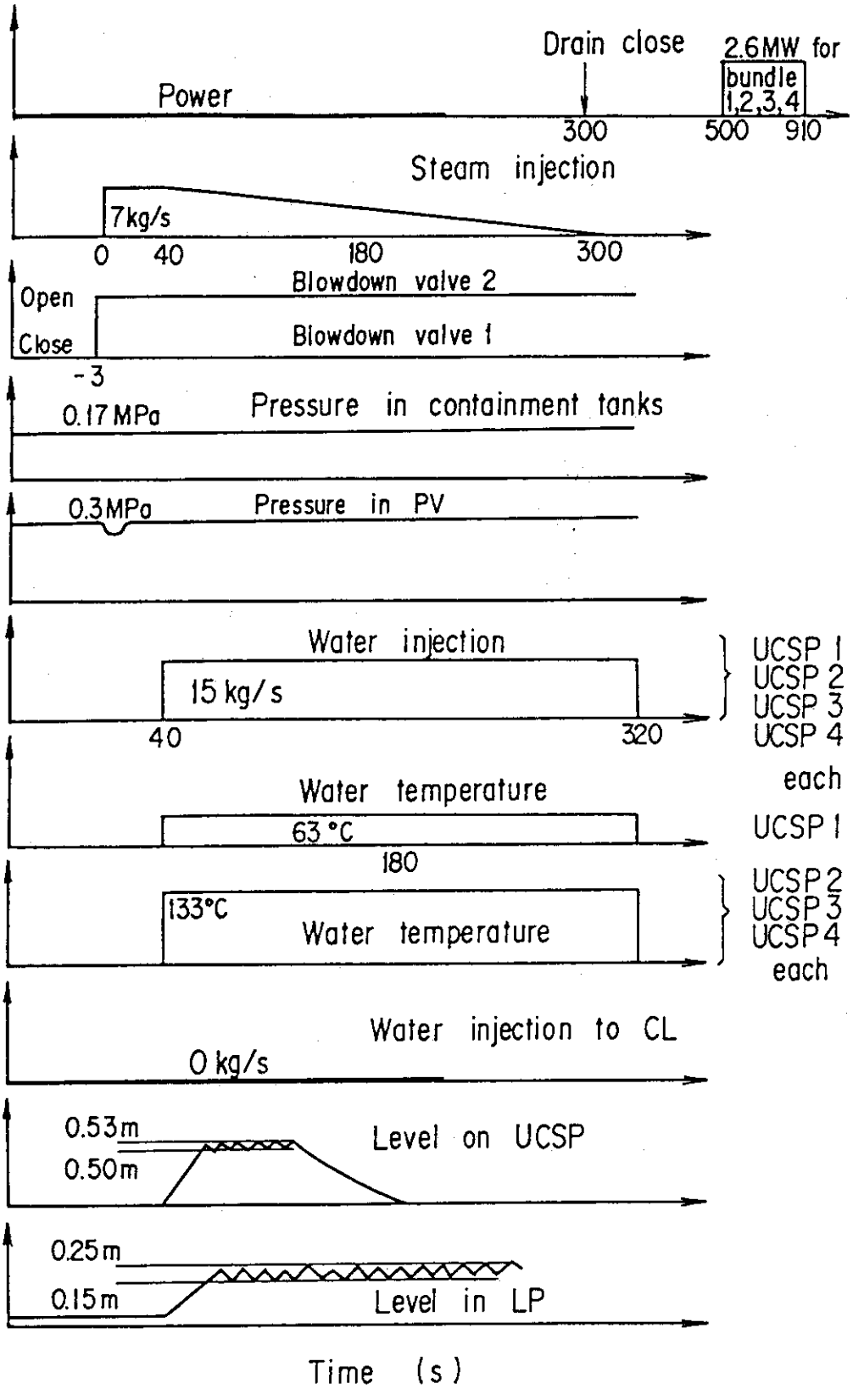

Fig. 2.3.3 Test sequence of Test S3-4 (Run 708)
(Local subcooled water test)

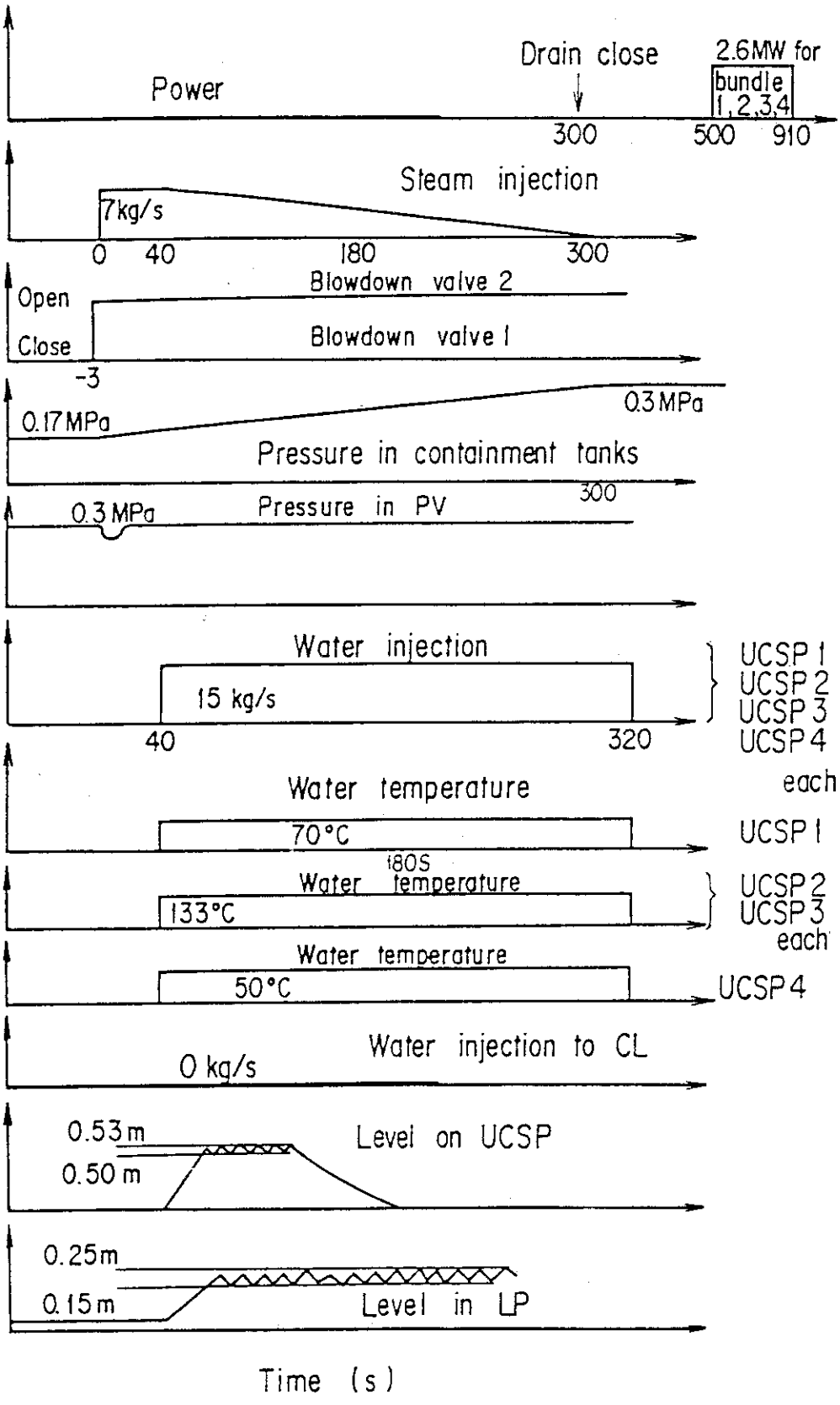

Fig. 2.3.4 Test sequence of Test S3-5 (Run 709)
(Distributed subcooled water test)

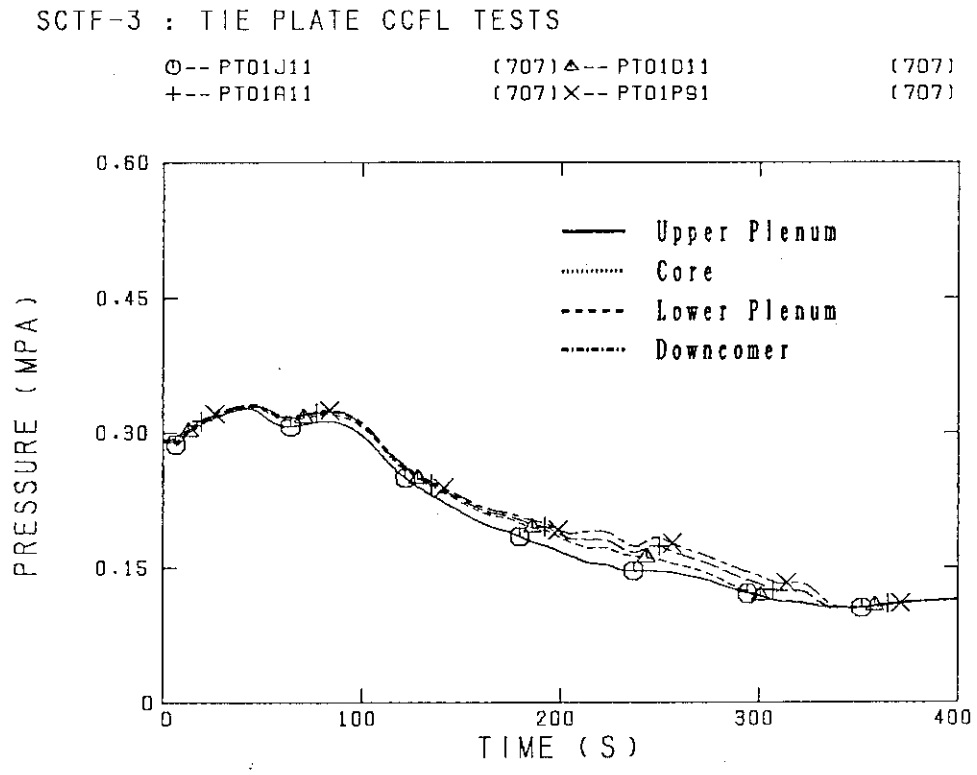

Fig. 3.1.1 Test S3-3: Pressure in pressure vessel

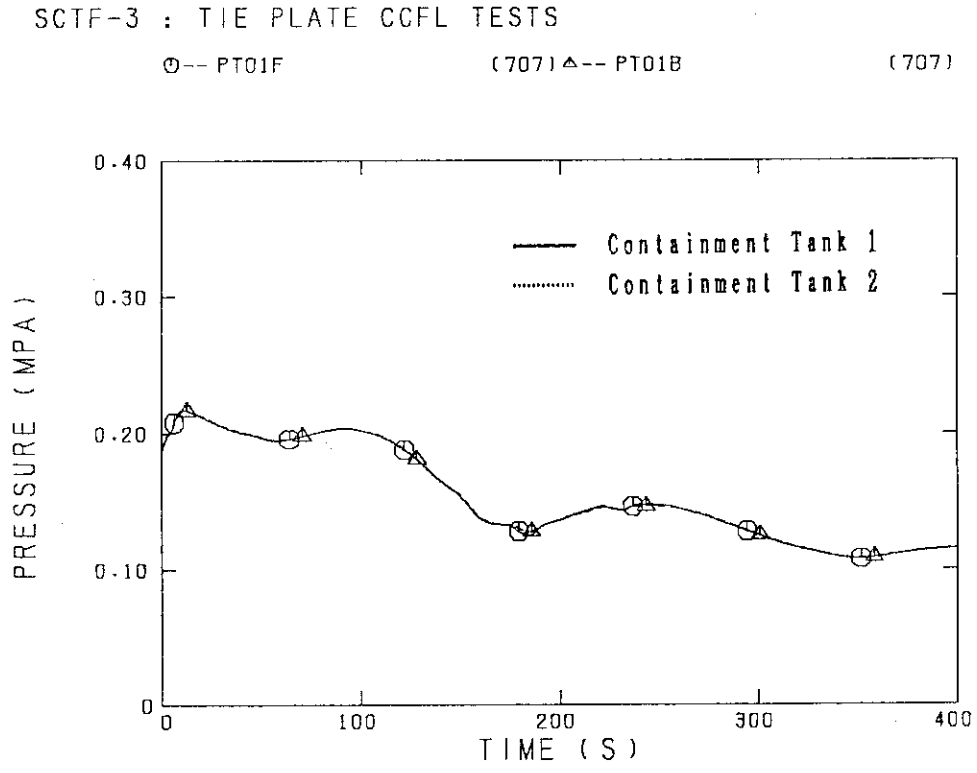

Fig. 3.1.2 Test S3-3: Pressure in containment tanks

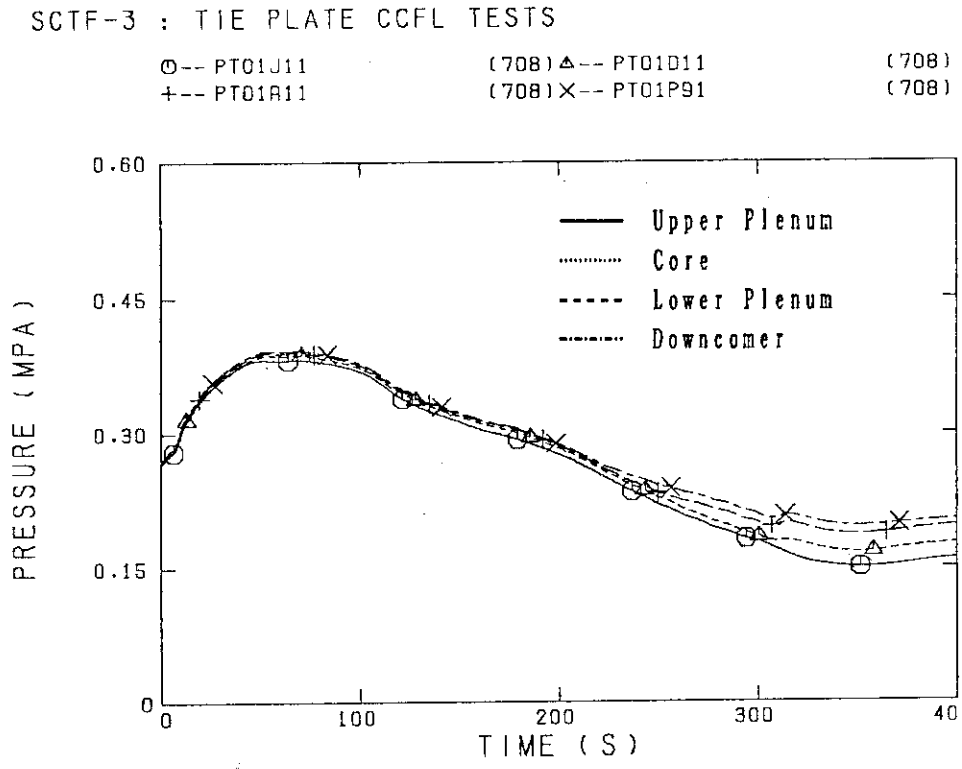

Fig. 3.1.3 Test S3-4: Pressure in pressure vessel

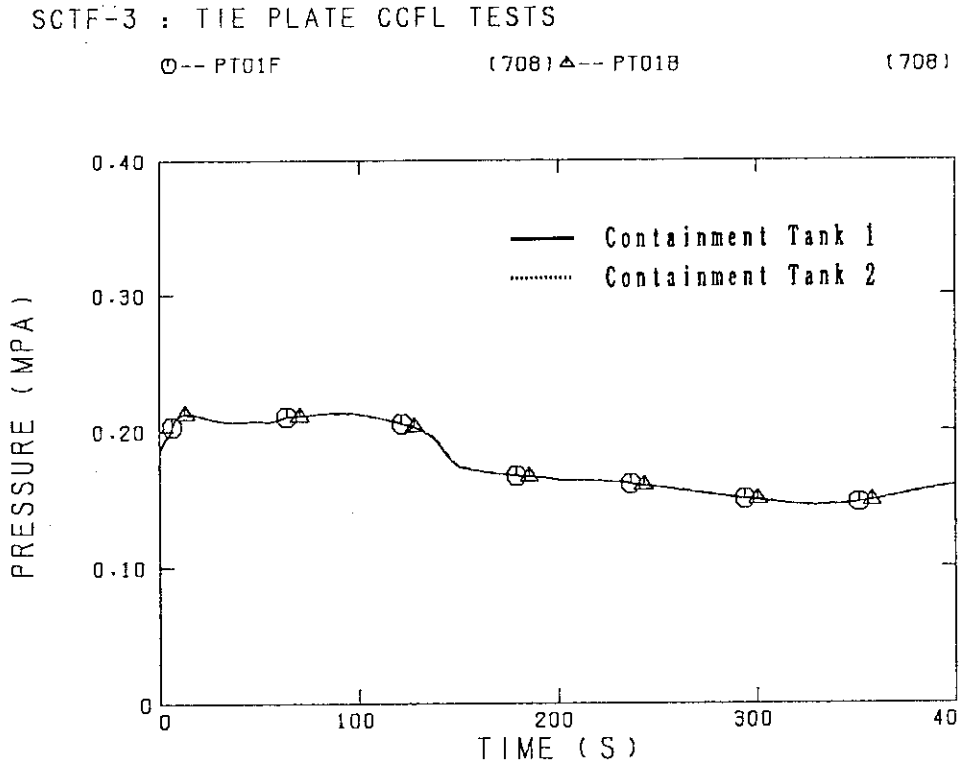

Fig. 3.1.4 Test S3-4: Pressure in containment tanks

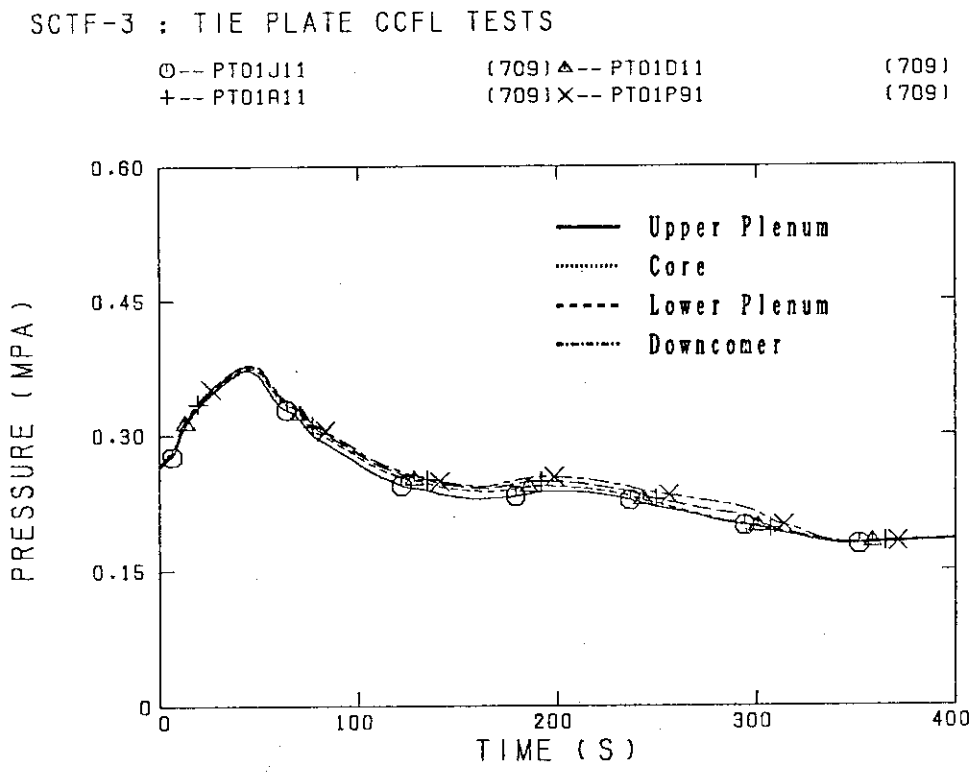

Fig. 3.1.5 Test S3-5: Pressure in pressure vessel

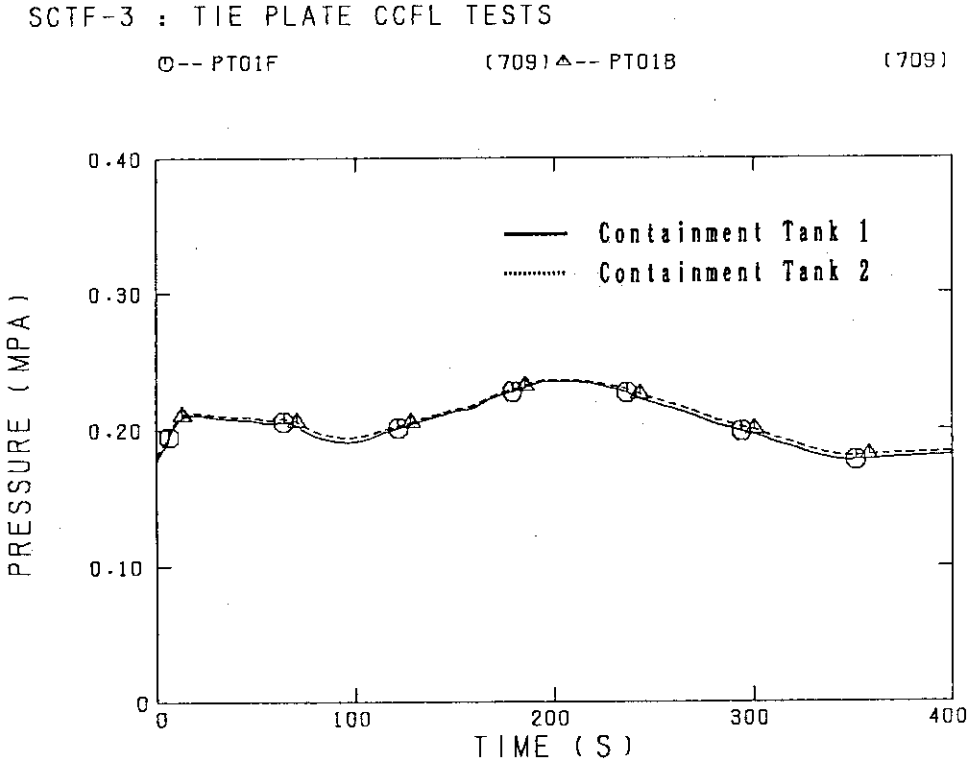

Fig. 3.1.6 Test S3-5: Pressure in containment tanks

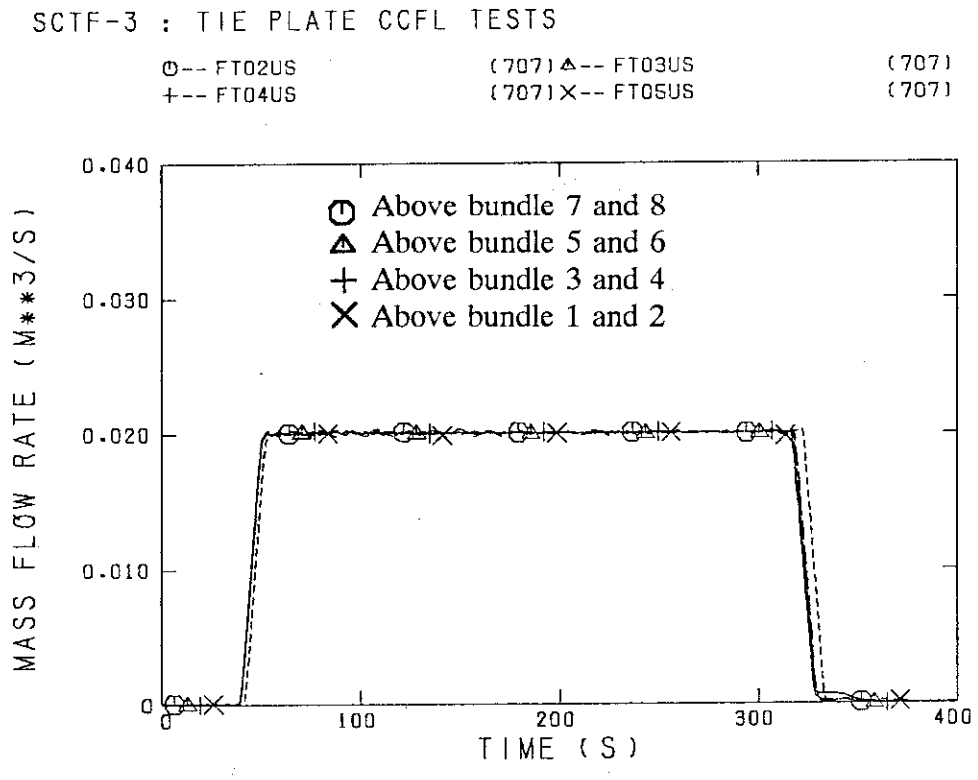

Fig. 3.1.7 Test S3-3: Water injection rate into upper plenum

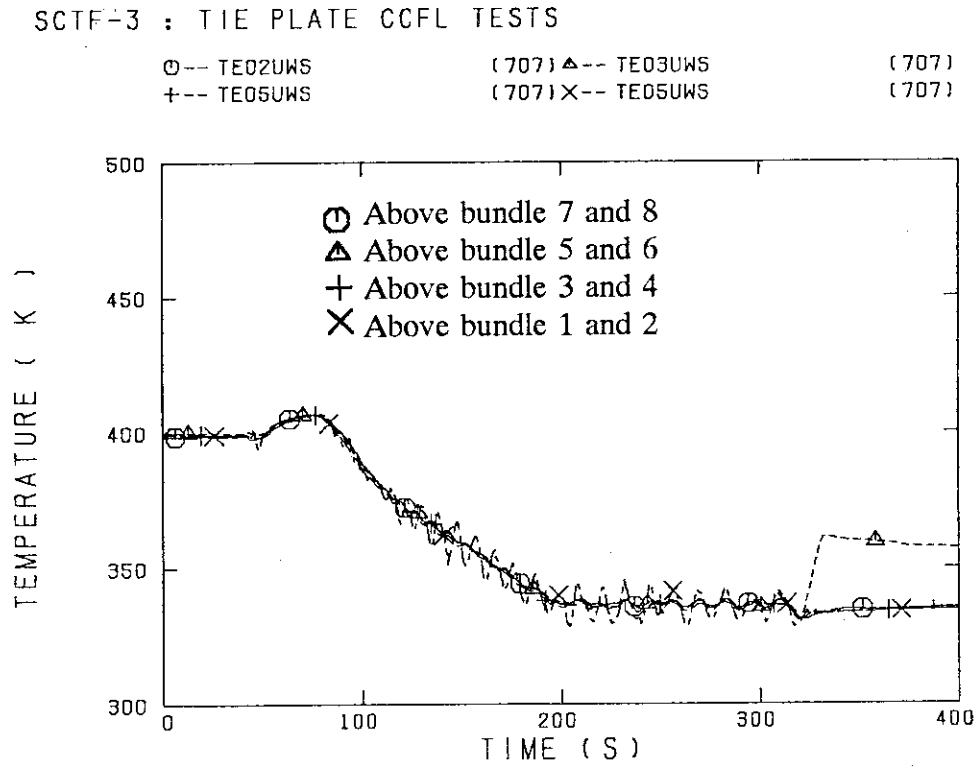

Fig. 3.1.8 Test S3-3: Temperature of water injected into upper plenum

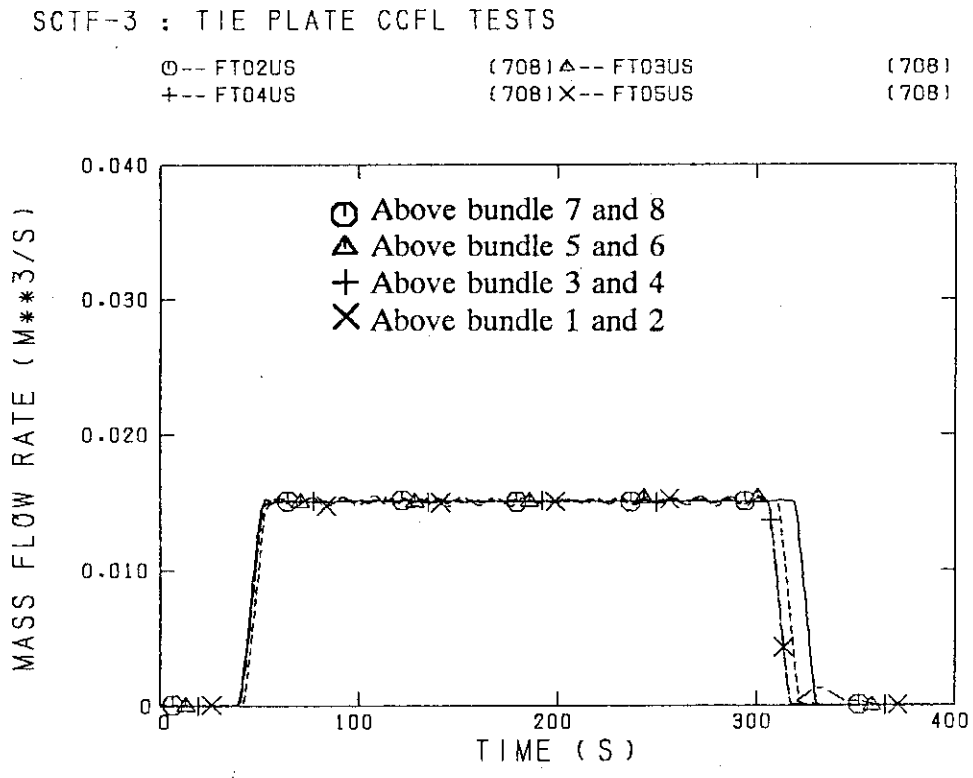

Fig. 3.1.9 Test S3-4: Water injection rate into upper plenum

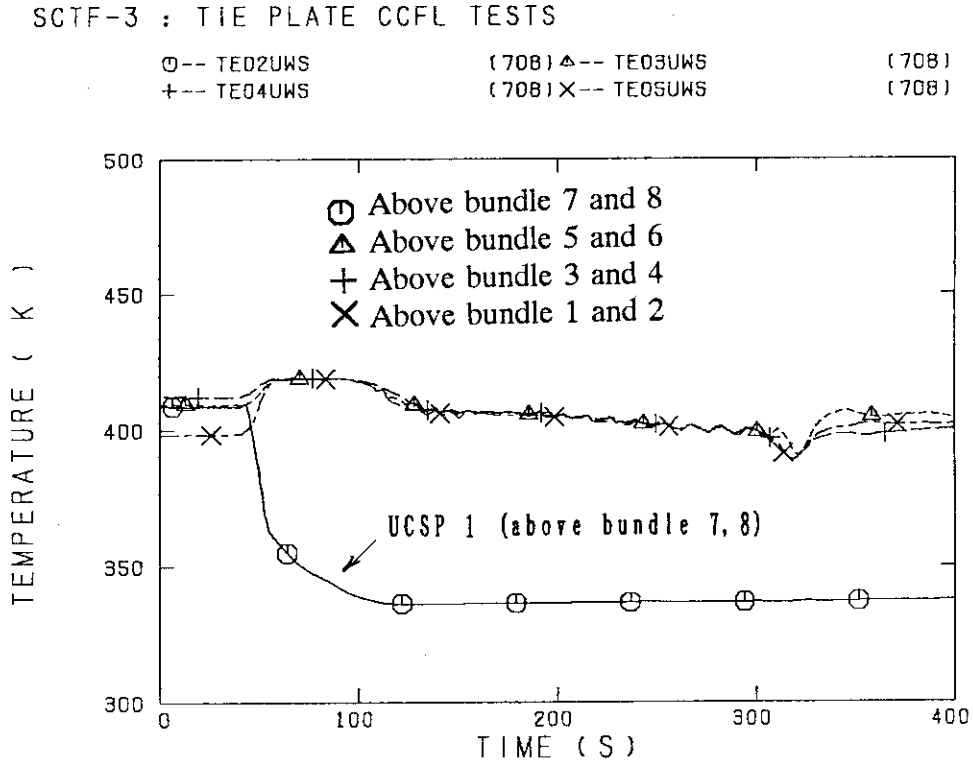

Fig. 3.1.10 Test S3-4: Temperature of water injected into upper plenum

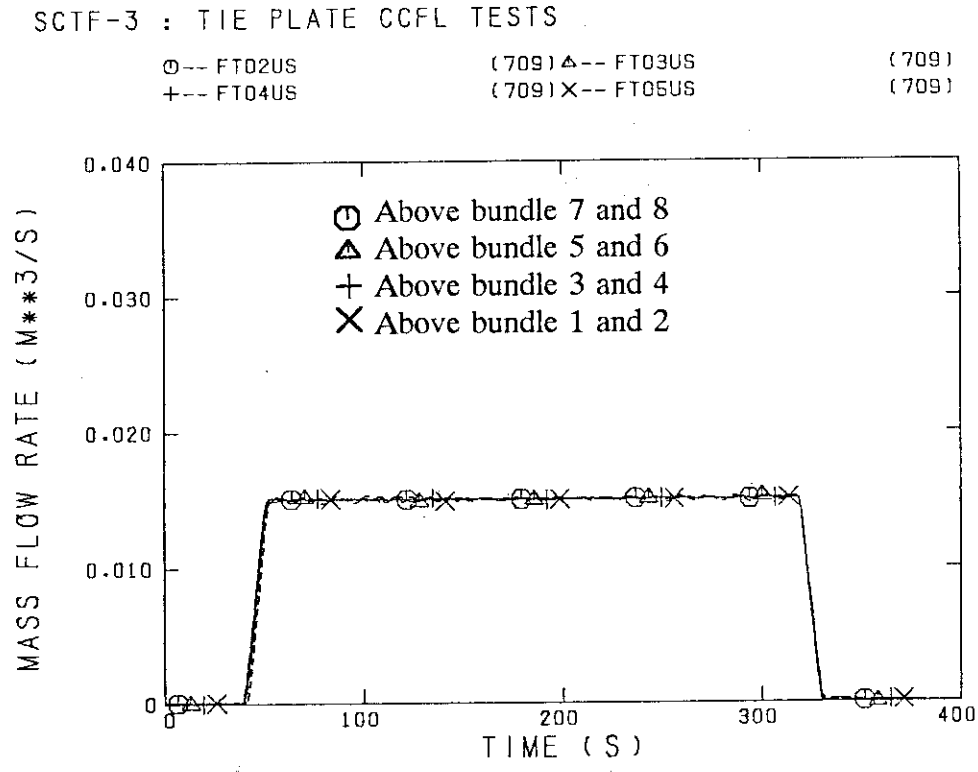

Fig. 3.1.11 Test S3-5: Water injection rate into upper plenum

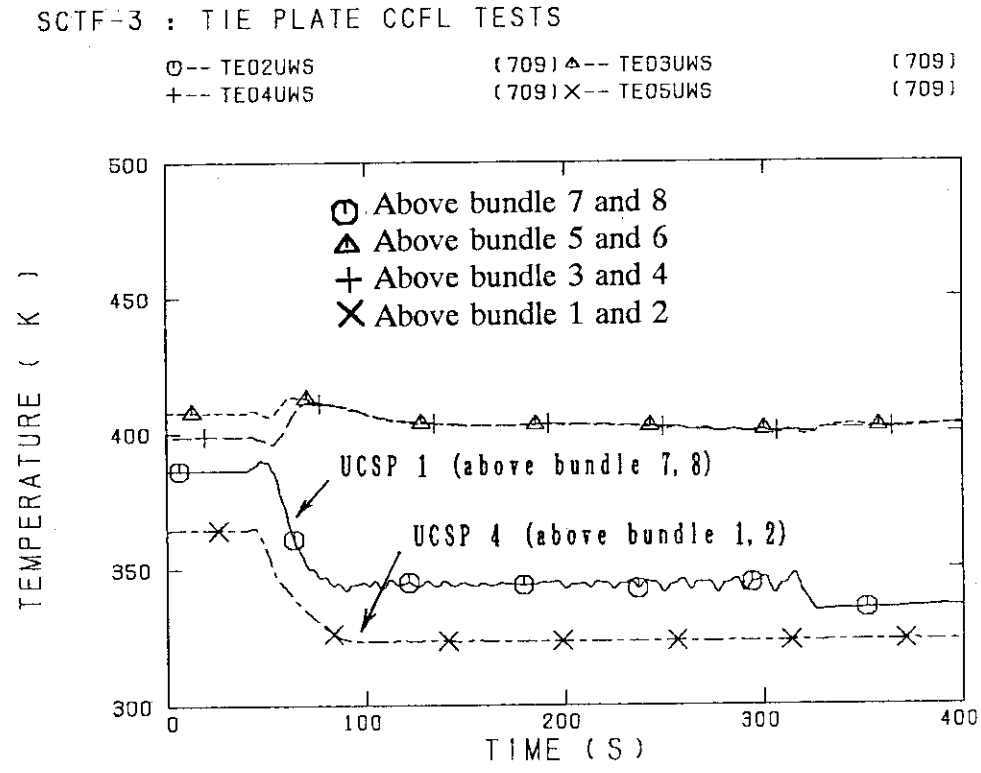

Fig. 3.1.12 Test S3-5: Temperature of water injected into upper plenum

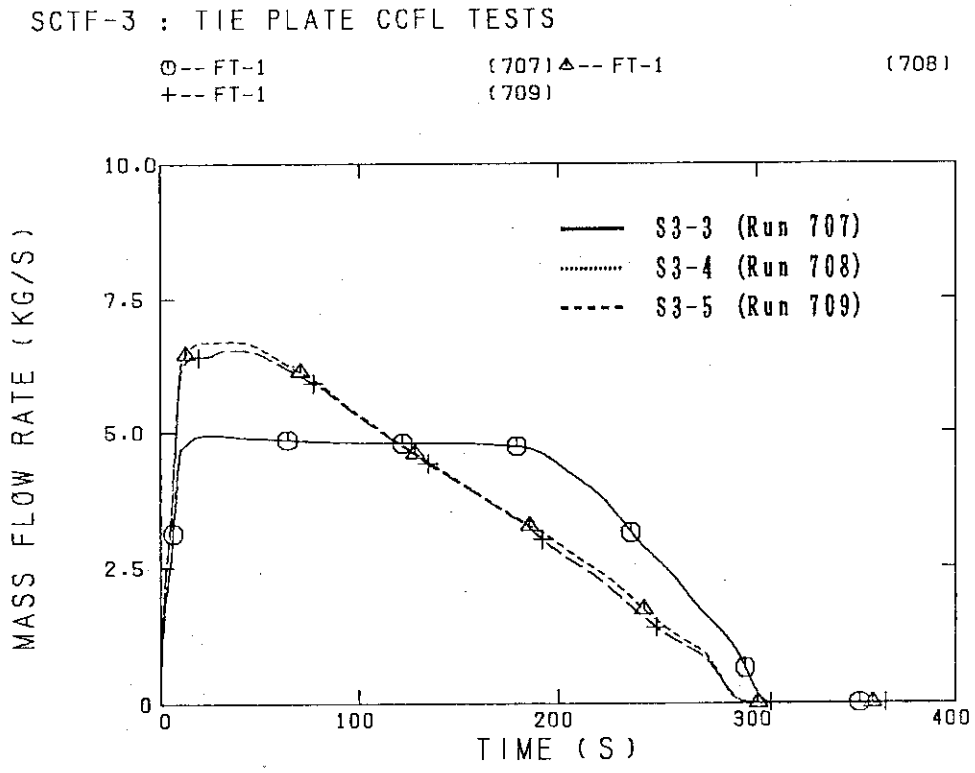

Fig. 3.1.13 Steam injection rate into intact cold leg

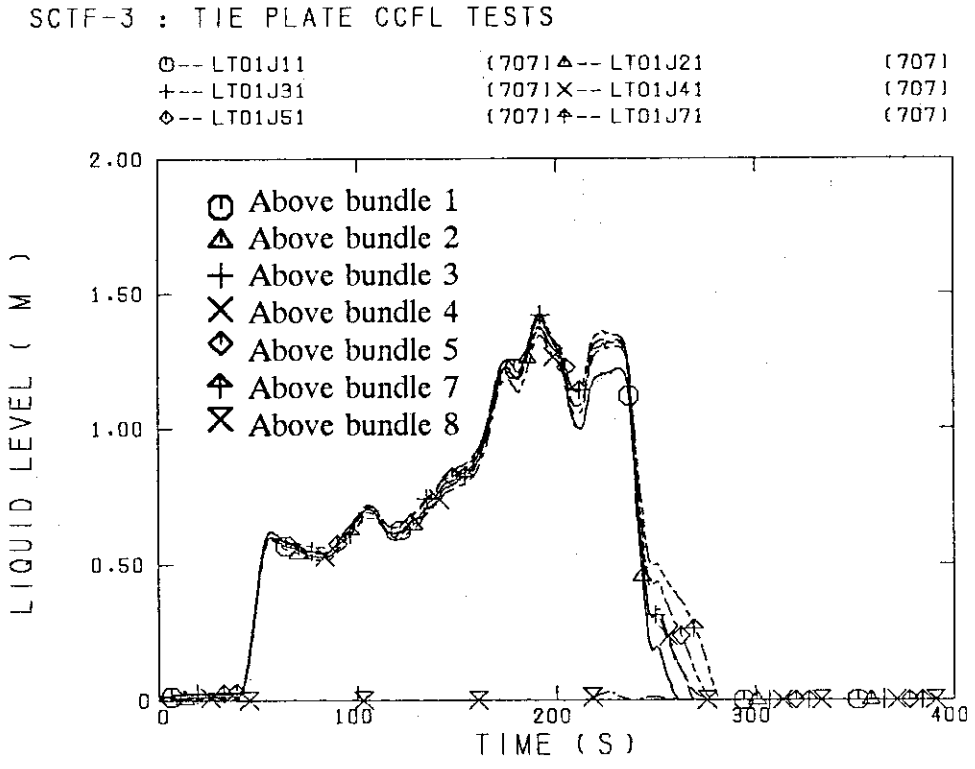

Fig. 3.1.14 Test S3-3: Upper plenum liquid level

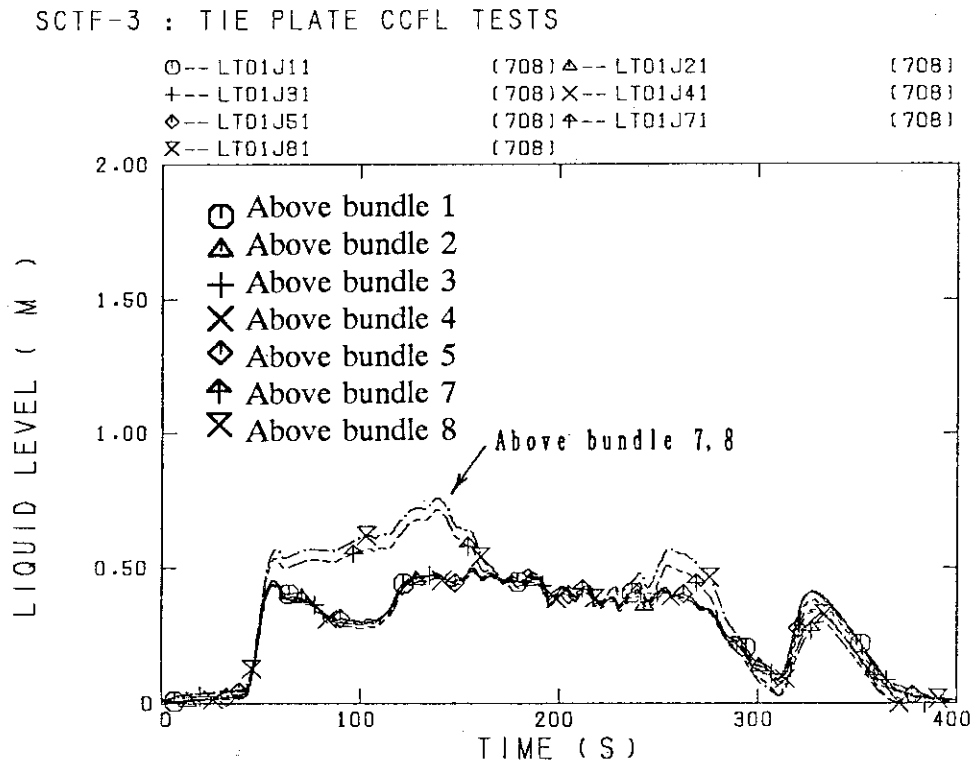

Fig. 3.1.15 Test S3-4: Upper plenum liquid level

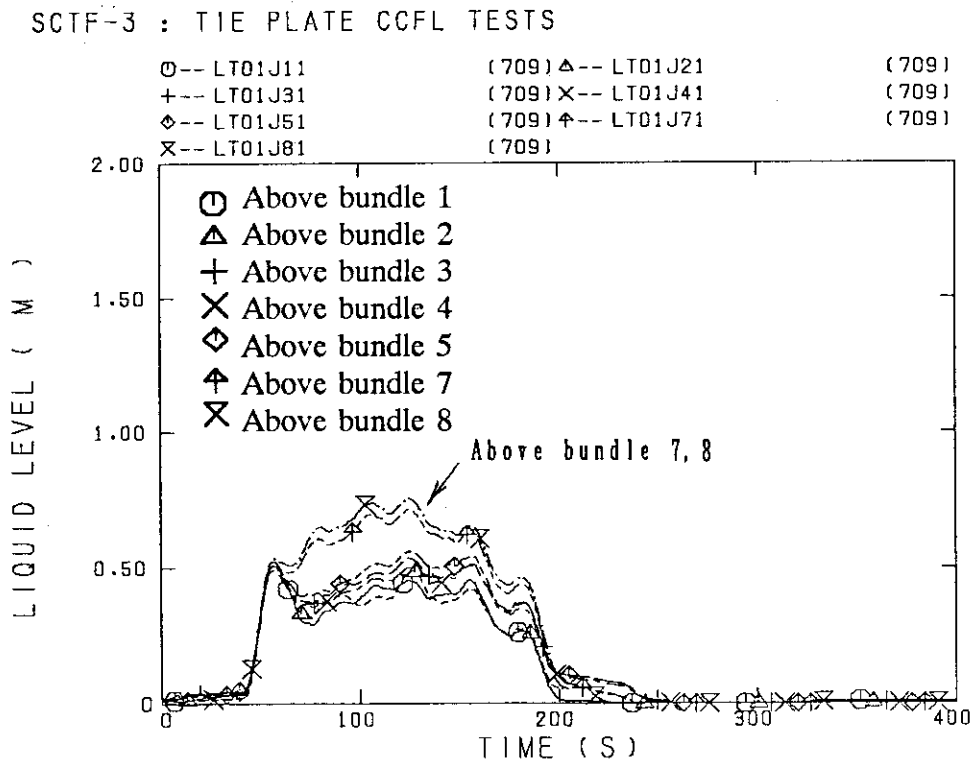

Fig. 3.1.16 Test S3-5: Upper plenum liquid level

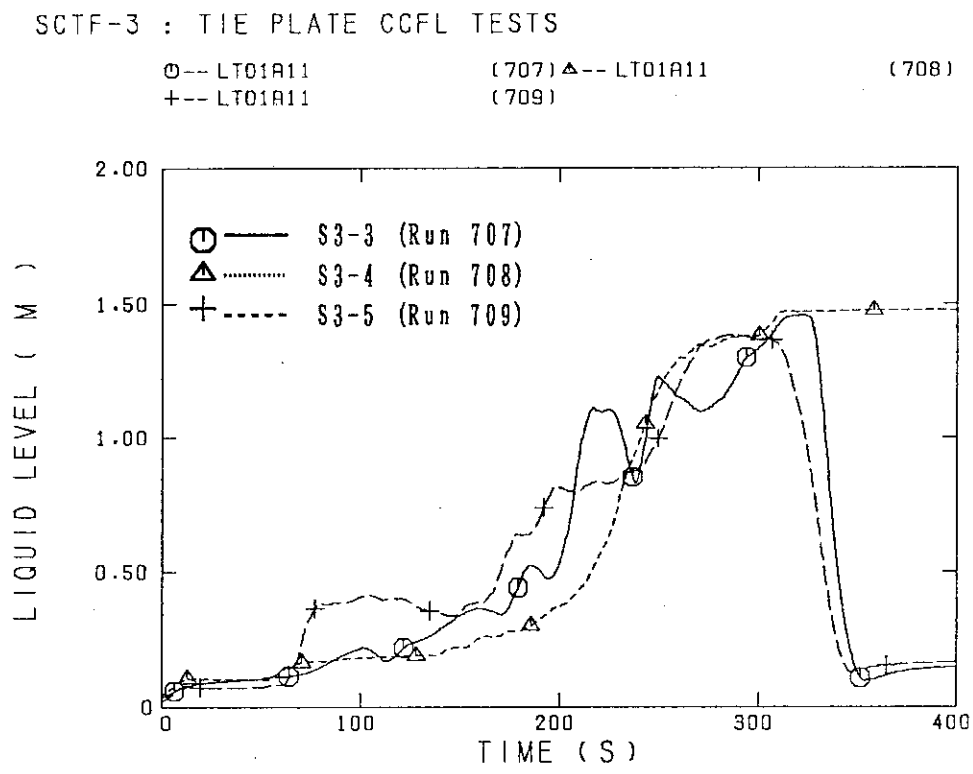

Fig. 3.1.17 Lower plenum liquid level

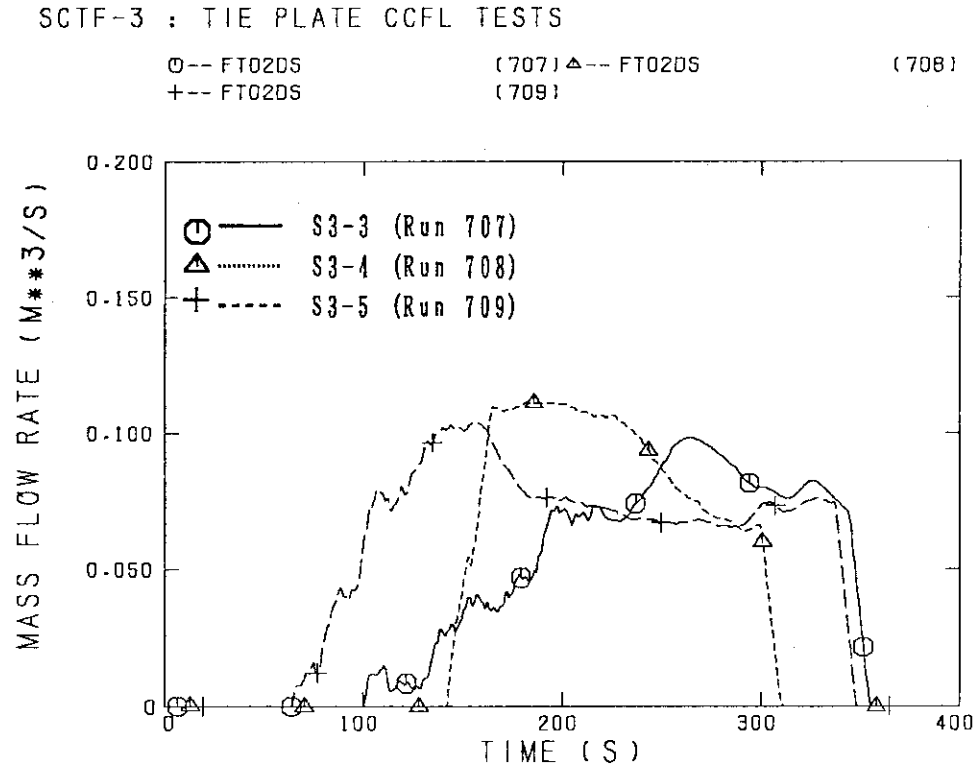

Fig. 3.1.18 Lower plenum water extraction rate

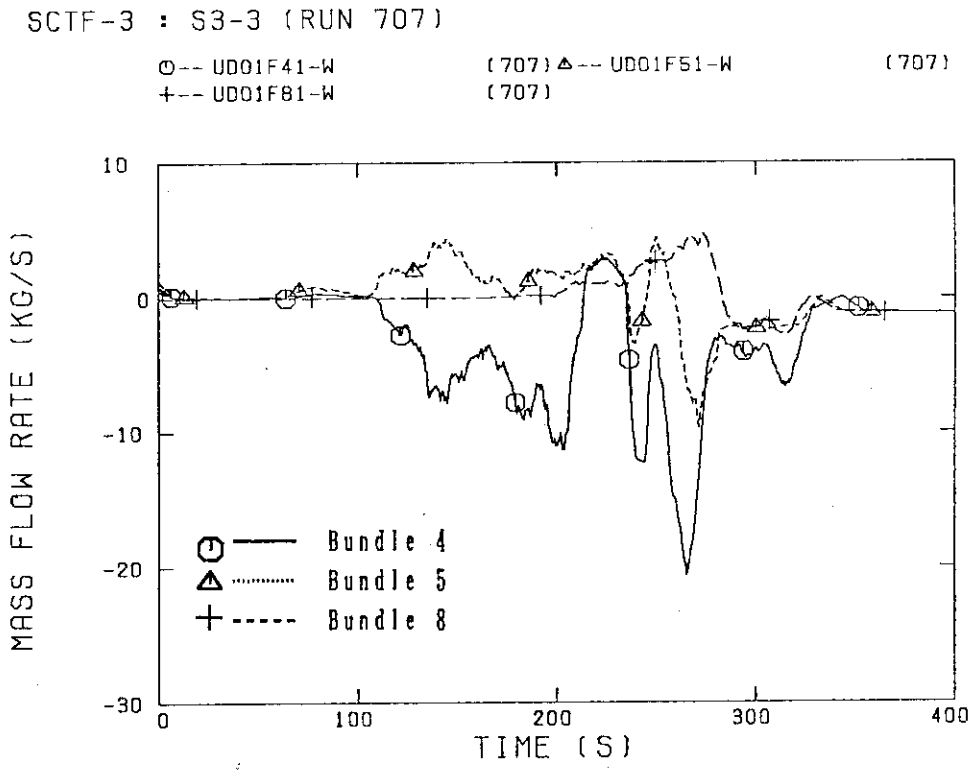

Fig. 3.2.1 Test S3-3: Water flow rate from core to upper plenum

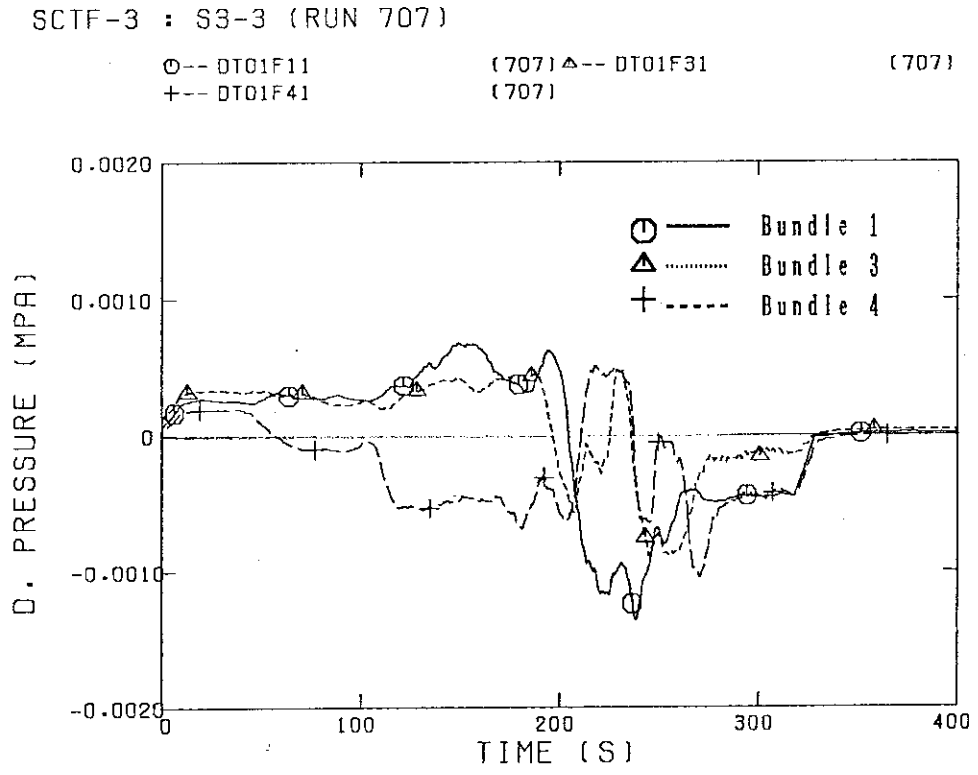

Fig. 3.2.2(1) Test S3-3: Differential pressure across end boxes

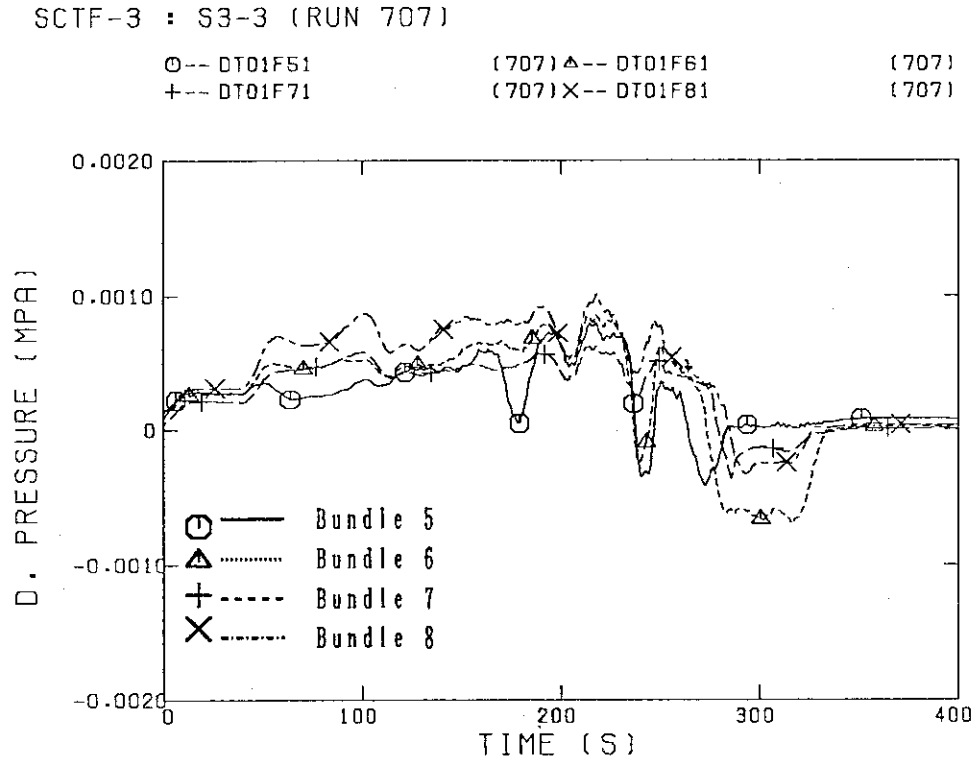

Fig. 3.2.2(2) Test S3-3: Differential pressure across end boxes

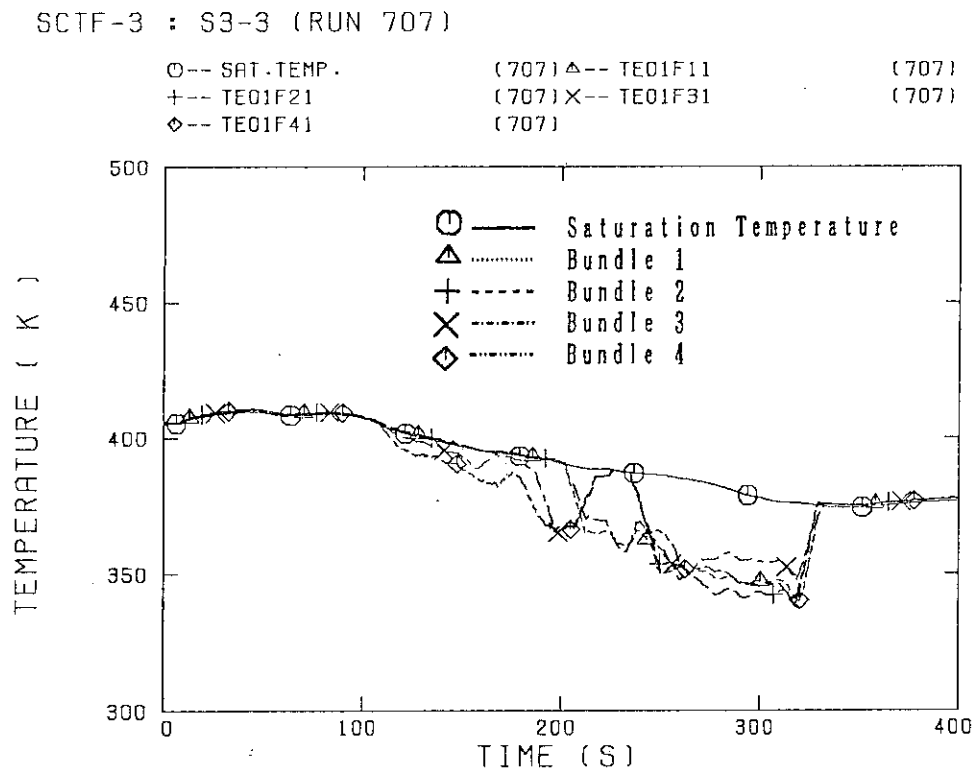

Fig. 3.2.3(1) Test S3-3: Fluid temperature below end box hole

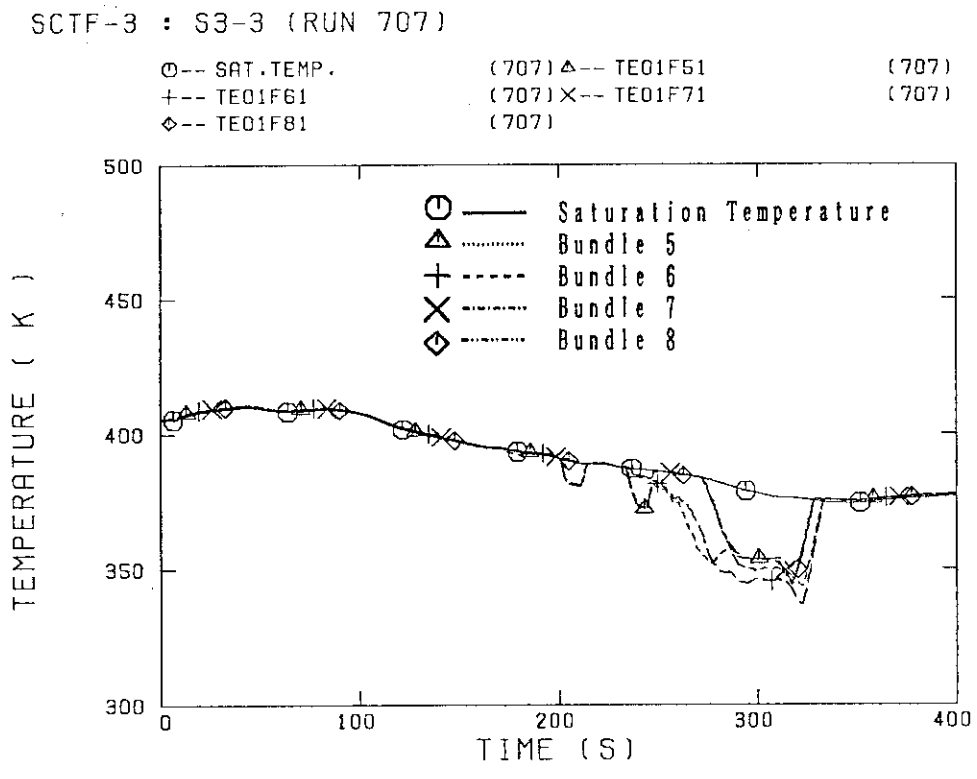

Fig. 3.2.3(2) Test S3-3: Fluid temperature below end box hole

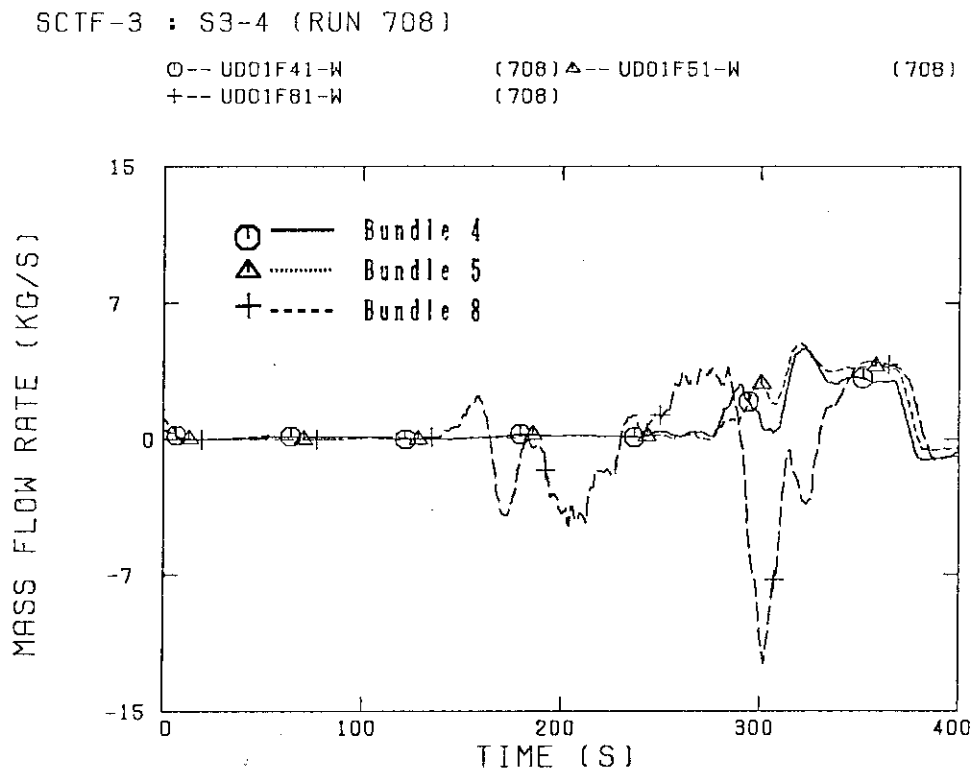

Fig. 3.2.4 Test S3-4: Water flow rate from core to upper plenum

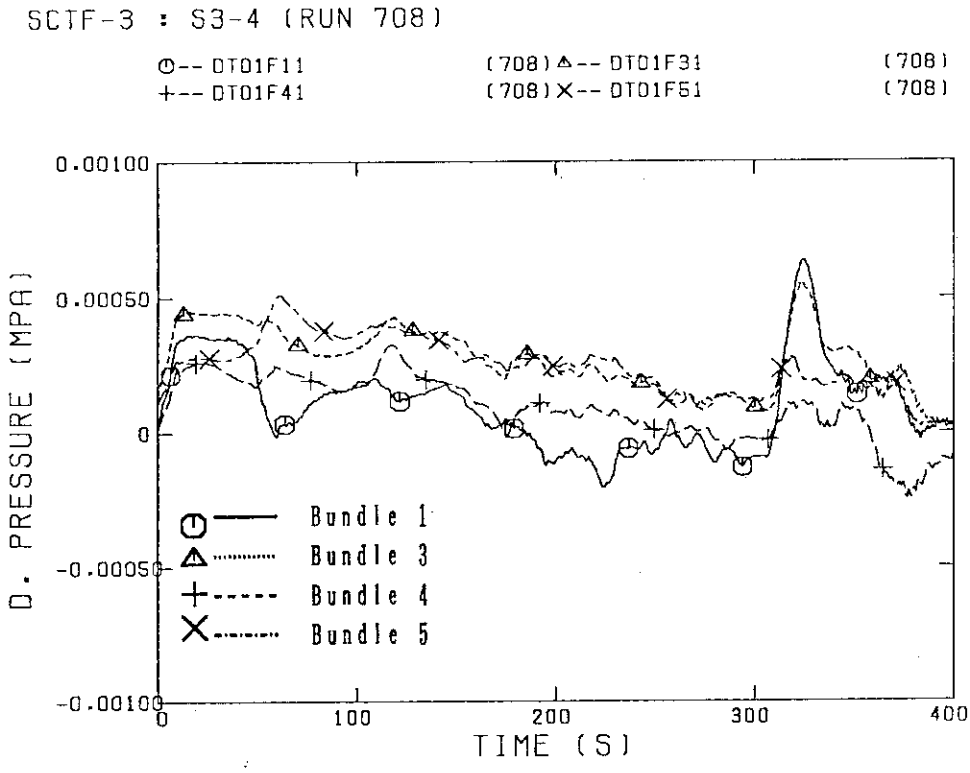

Fig. 3.2.5(1) Test S3-4: Differential pressure across end box

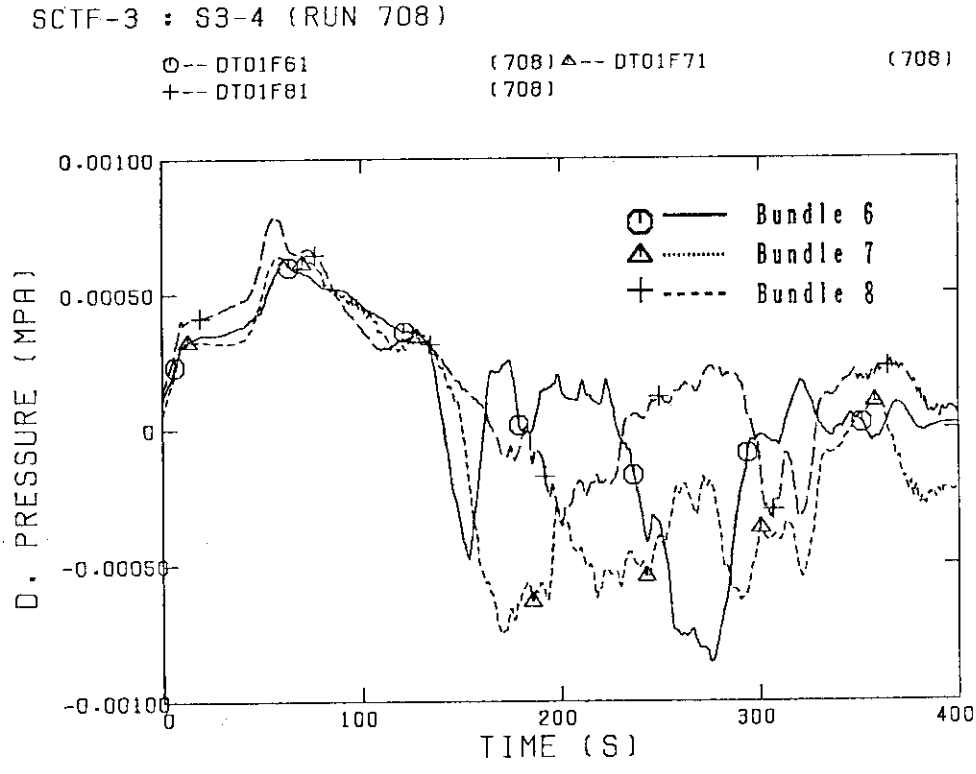

Fig. 3.2.5(2) Test S3-4: Differential pressure across end box

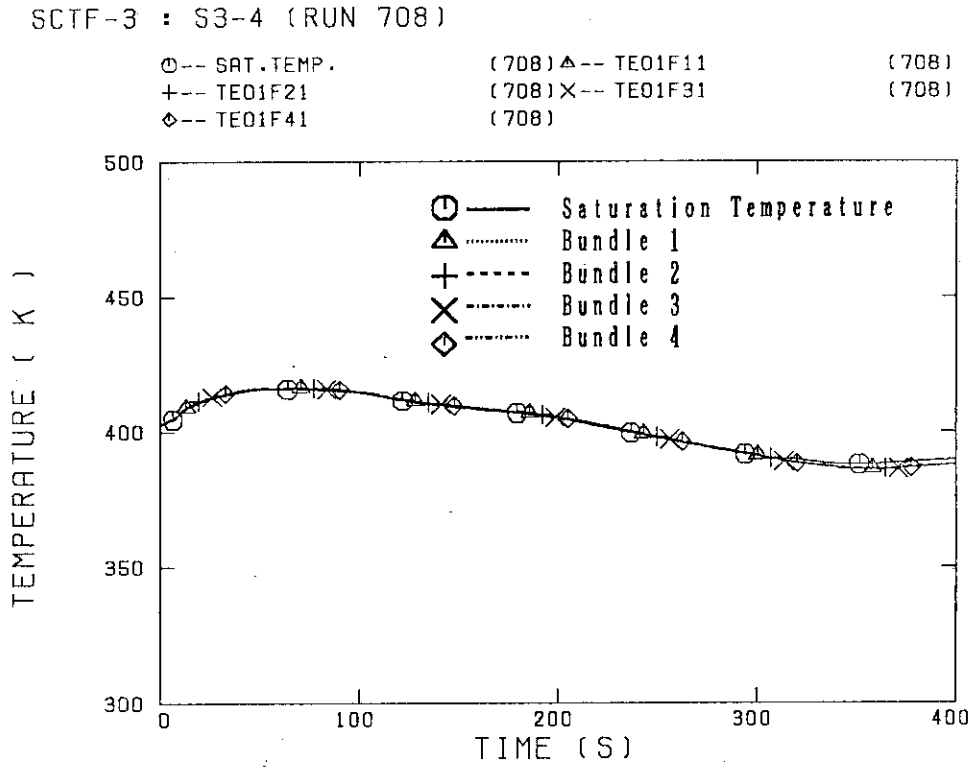

Fig. 3.2.6(1) Test S3-4: Fluid temperature below end box hole

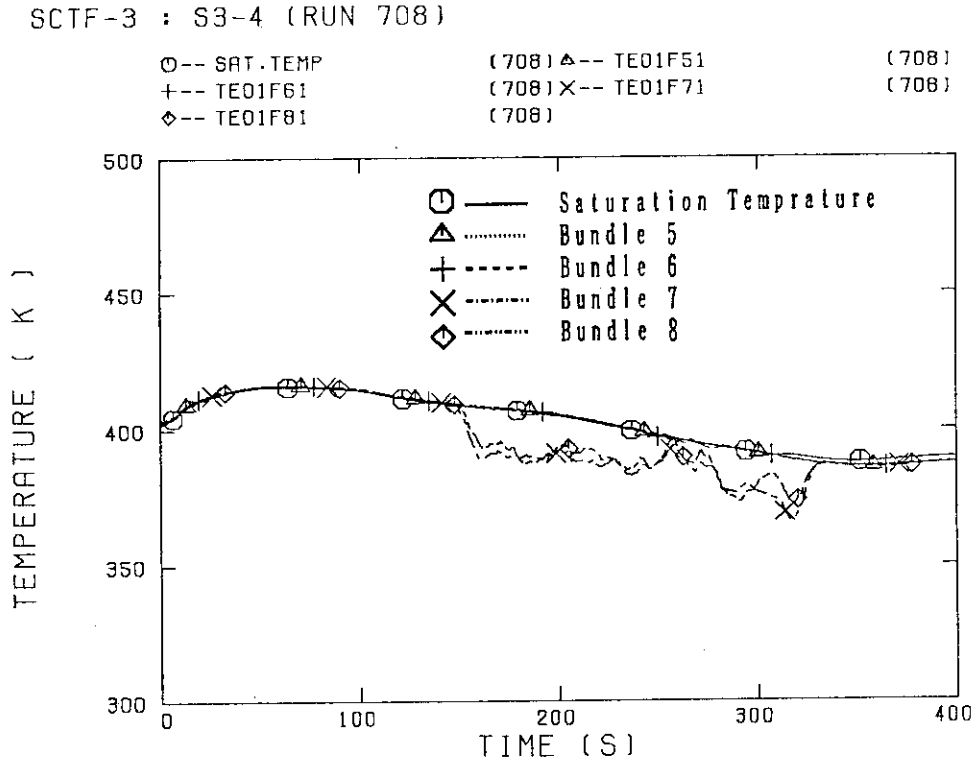

Fig. 3.2.6(2) Test S3-4: Fluid temperature below end box hole

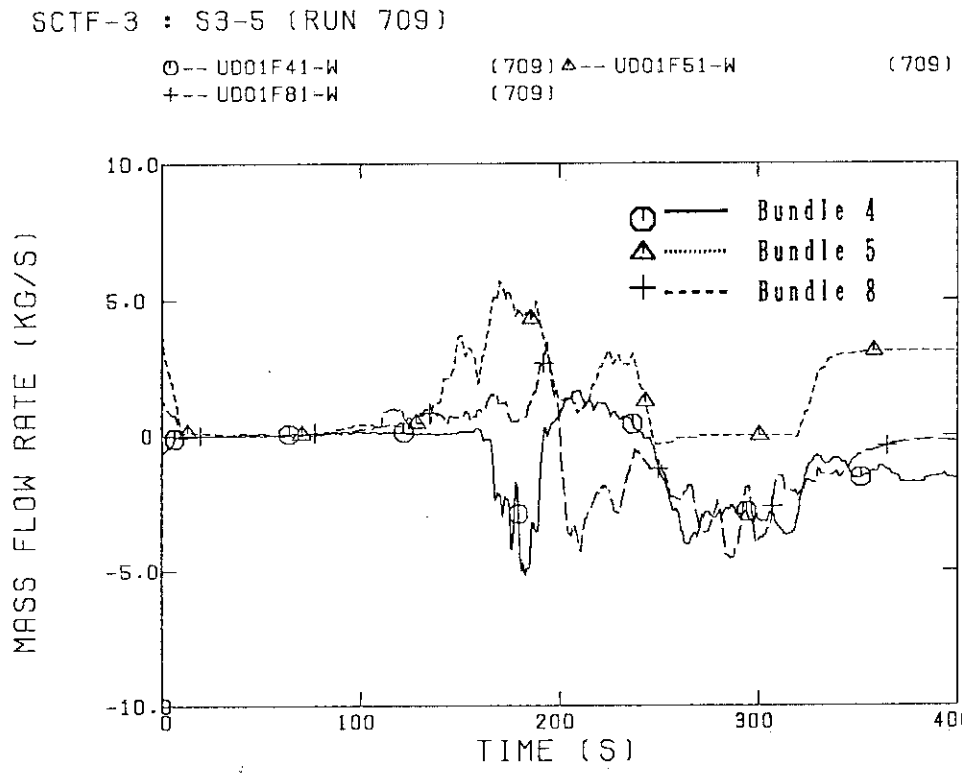

Fig. 3.2.7 Test S3-5: Water flow rate from core to upper plenum

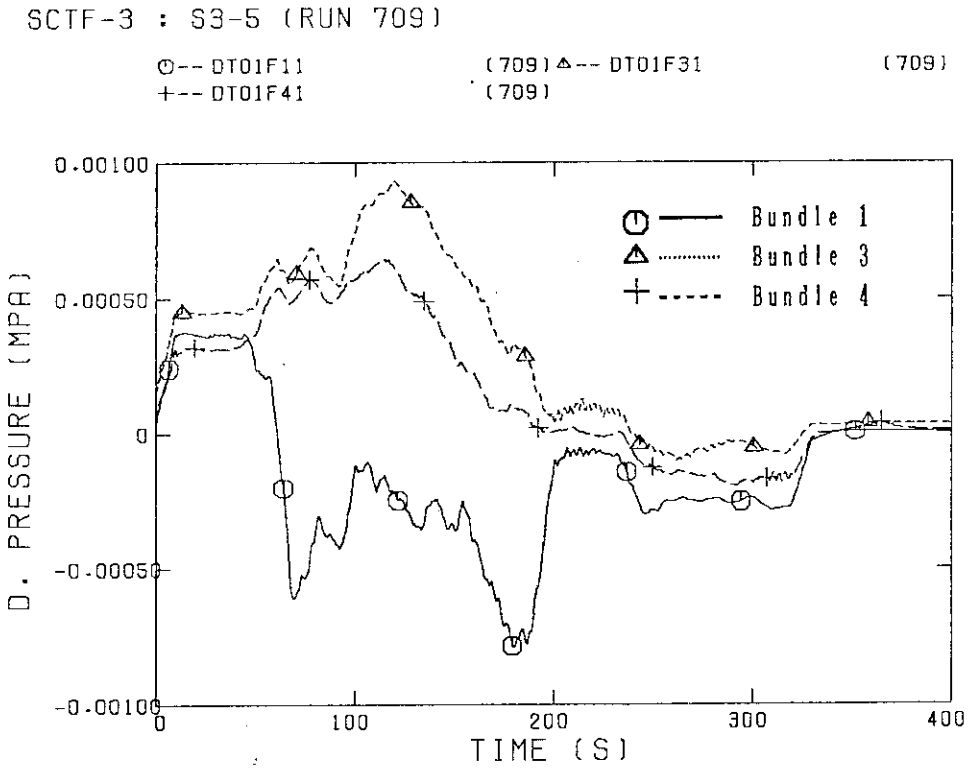

Fig. 3.2.8(1) Test S3-5: Differential pressure across end box

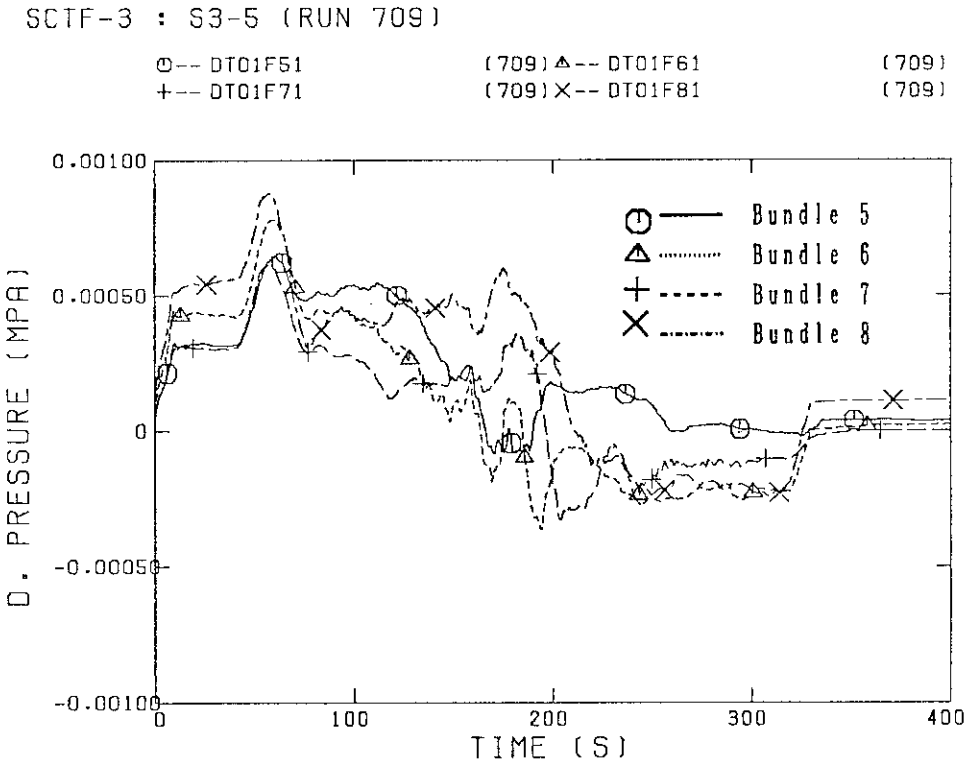

Fig. 3.2.8(2) Test S3-5: Differential pressure across end box

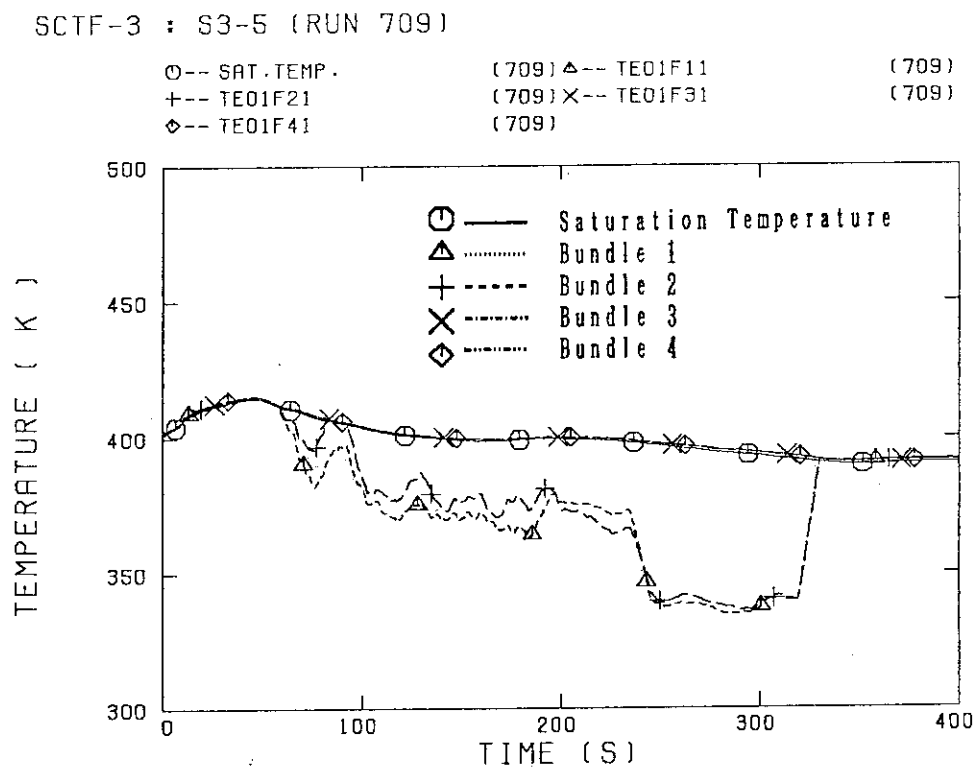

Fig. 3.2.9(1) Test S3-5: Fluid temperature below end box hole

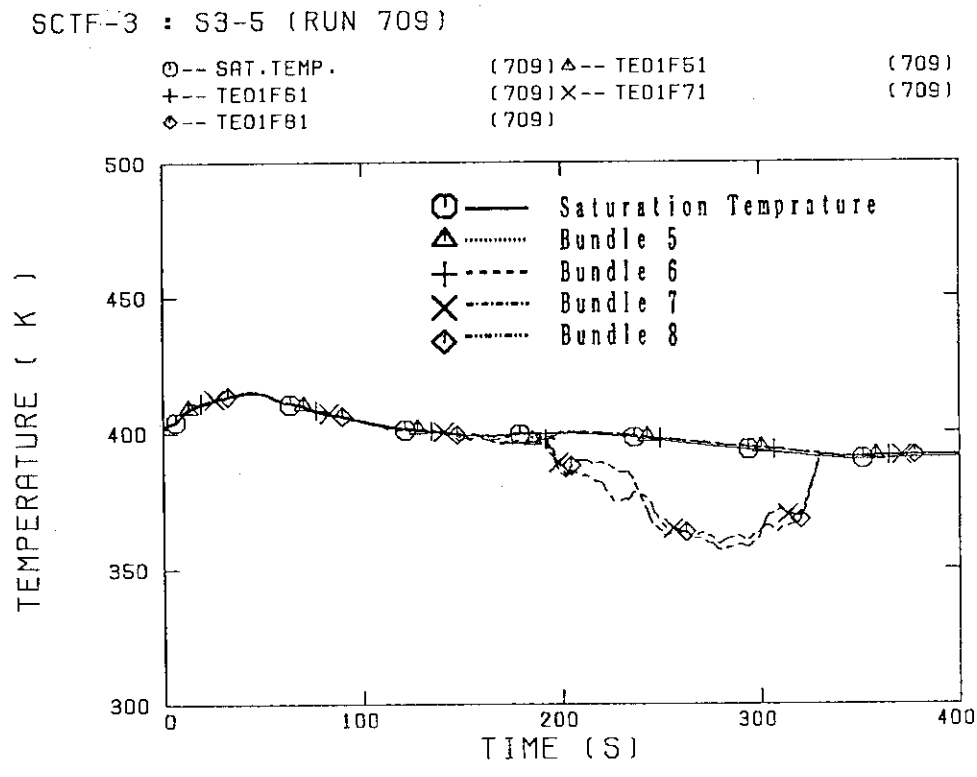

Fig. 3.2.9(2) Test S3-5: Fluid temperature below end box hole

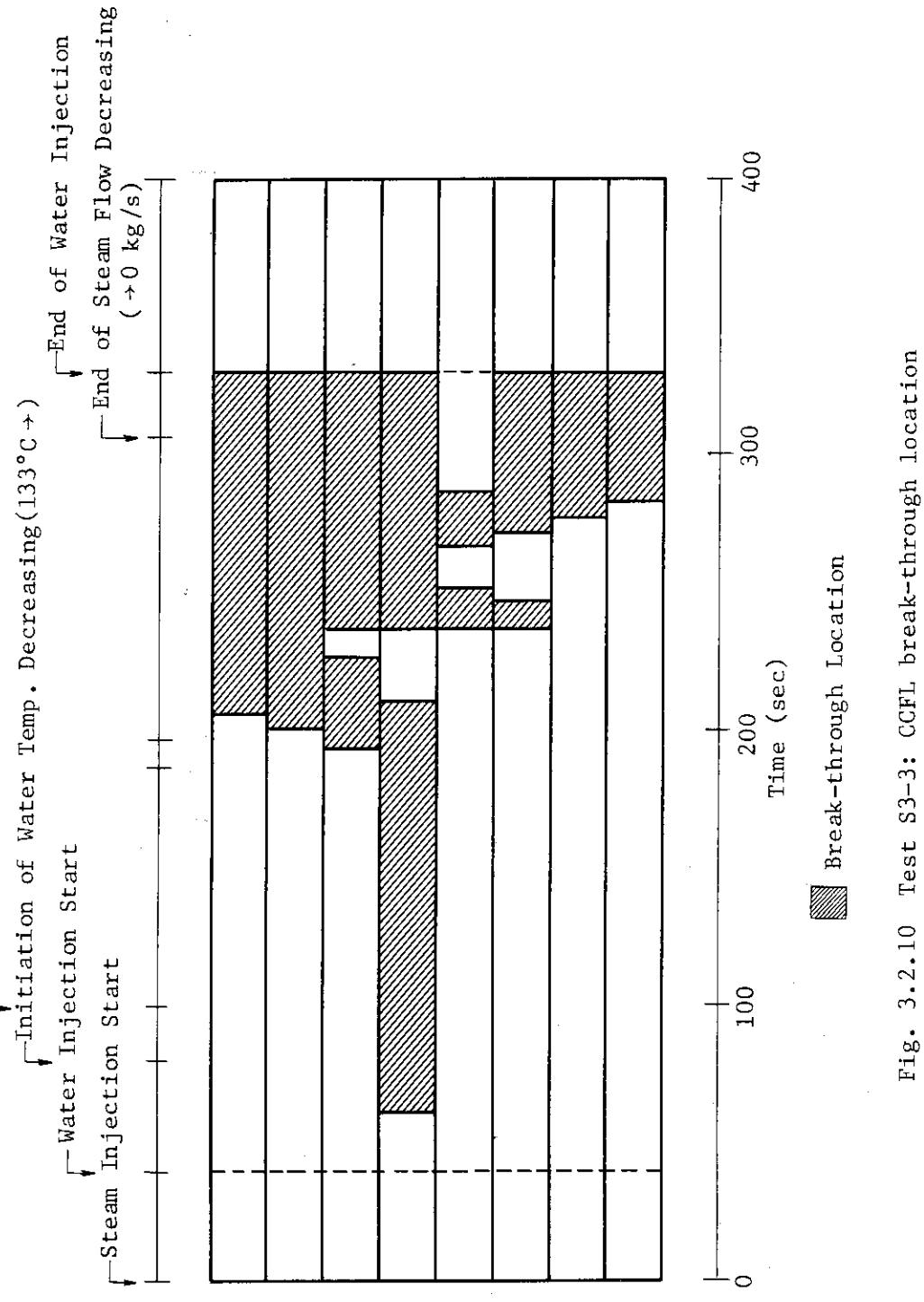

Fig. 3.2.10 Test S3-3: CCFL break-through location

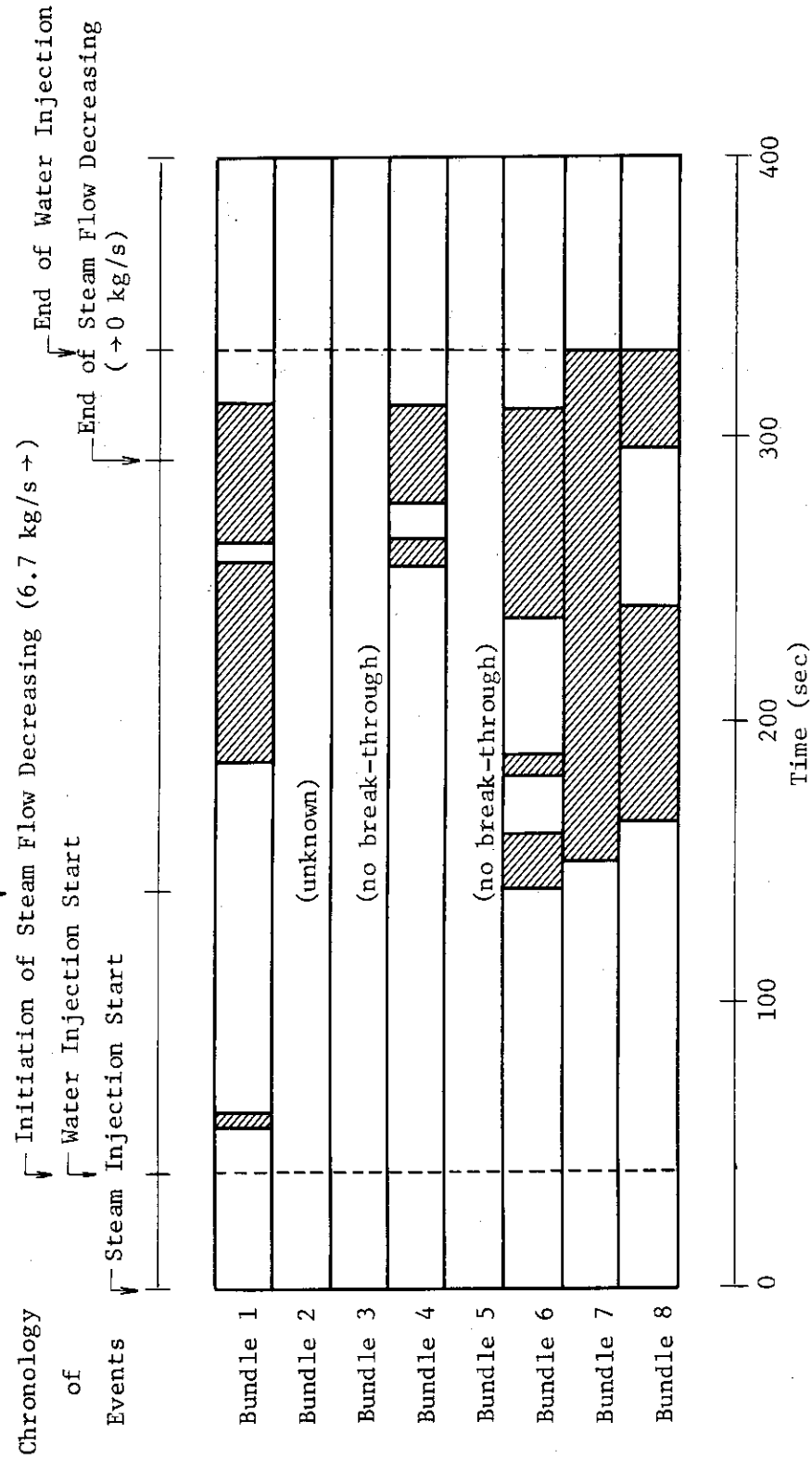

Fig. 3.2.11 Test S3-4: CCFL break-through location

Fig. 3.2.12 Test S3-5: CCFL break-through location

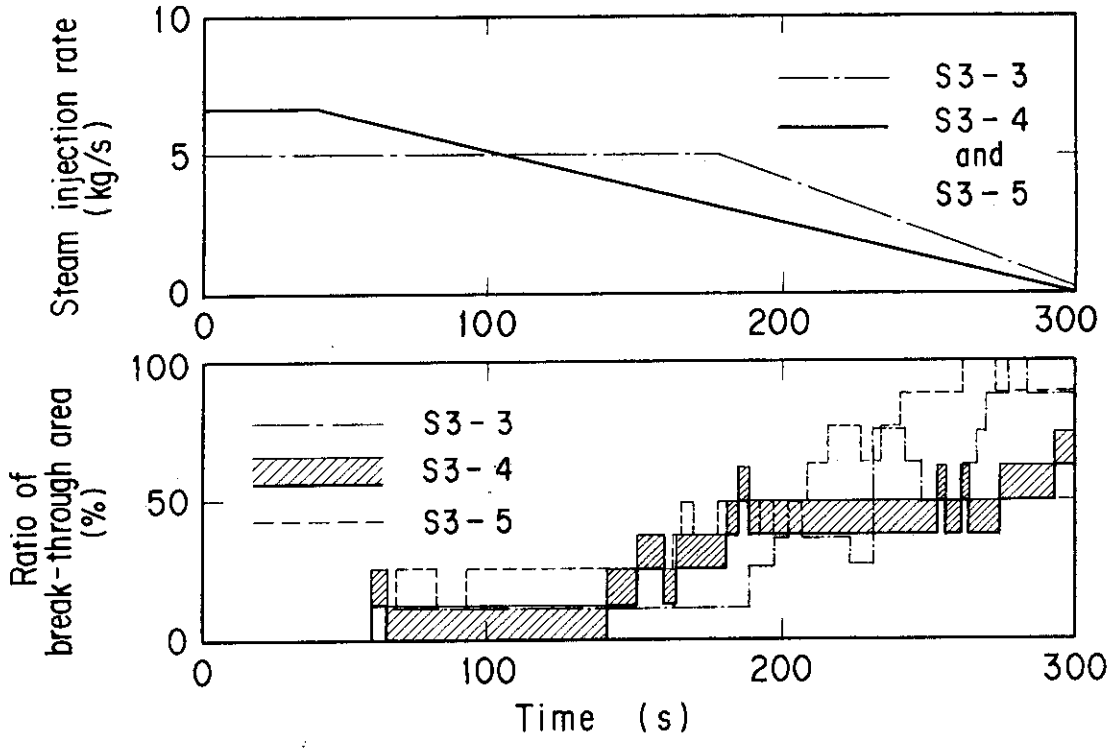

(a) Steam injection rate and ratio of break-through area vs time

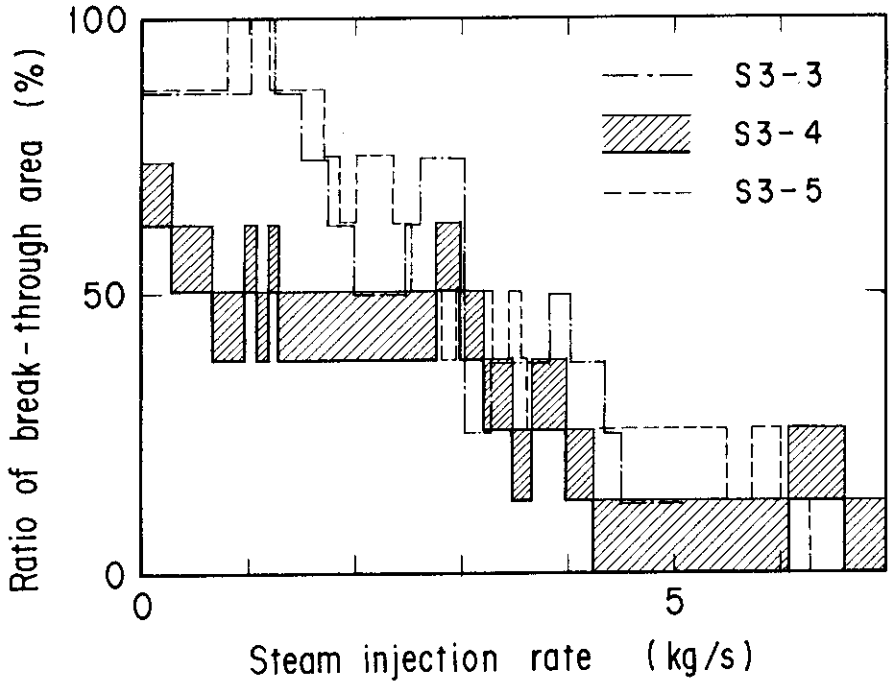

(b) Ratio of break-through area vs steam injection rate

Fig. 3.2.13 Relation between break-through area and steam injection flow rate

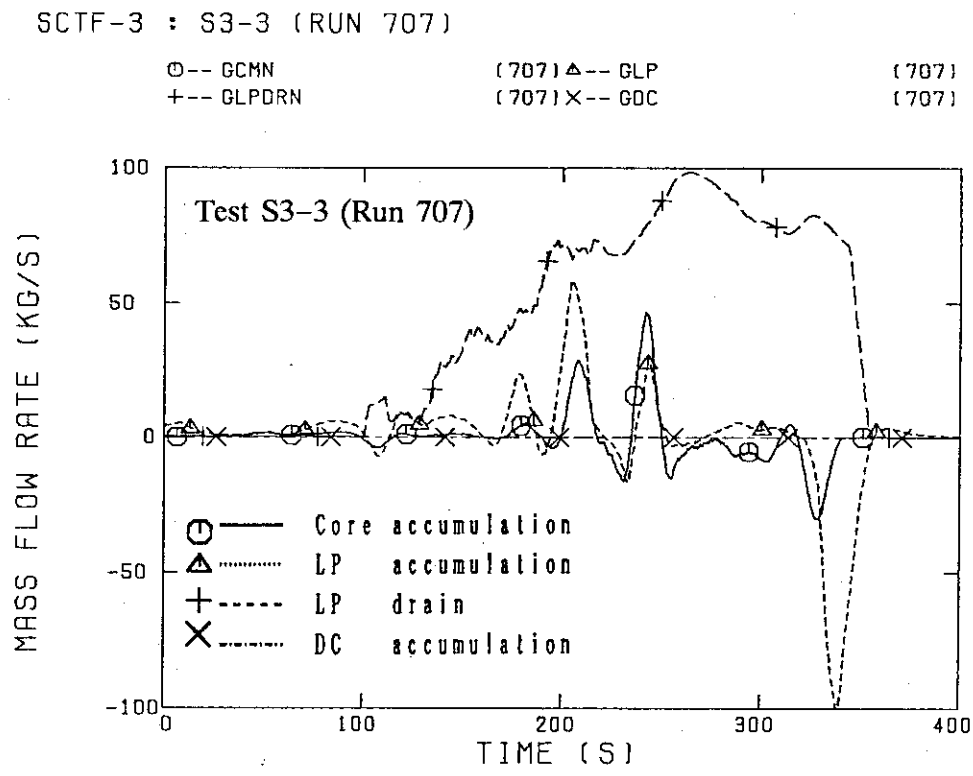

Fig. 3.3.1 Test S3-3: Mass flow rate in pressure vessel

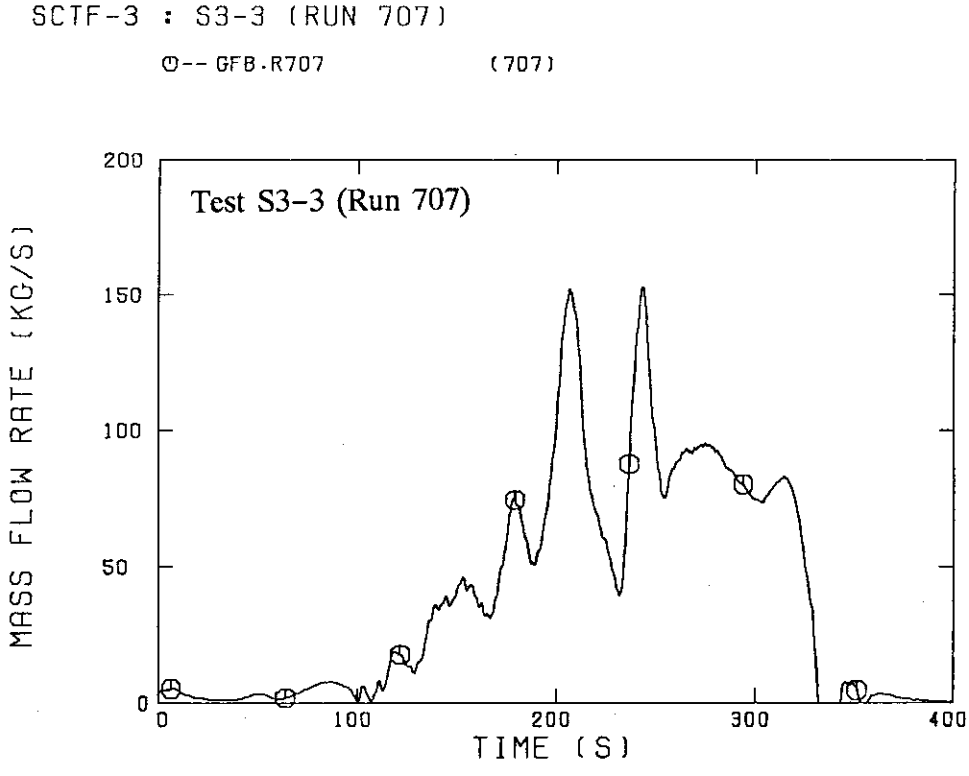

Fig. 3.3.2 Test S3-3: CCFL break-through rate

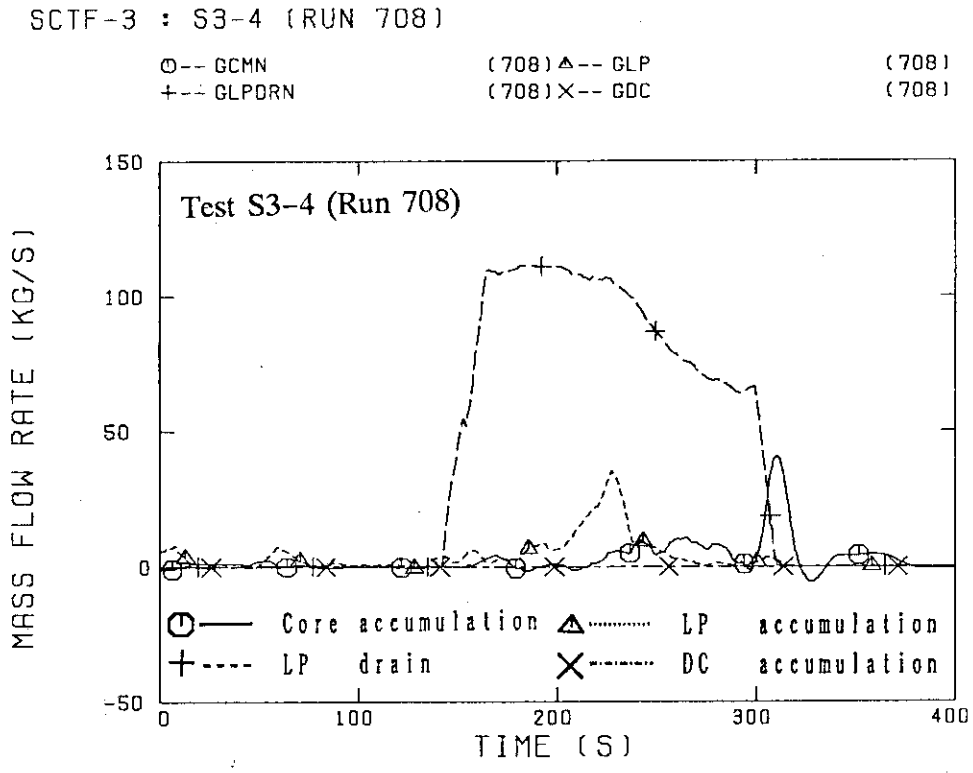

Fig. 3.3.3 Test S3-4: Mass flow rate in pressure vessel

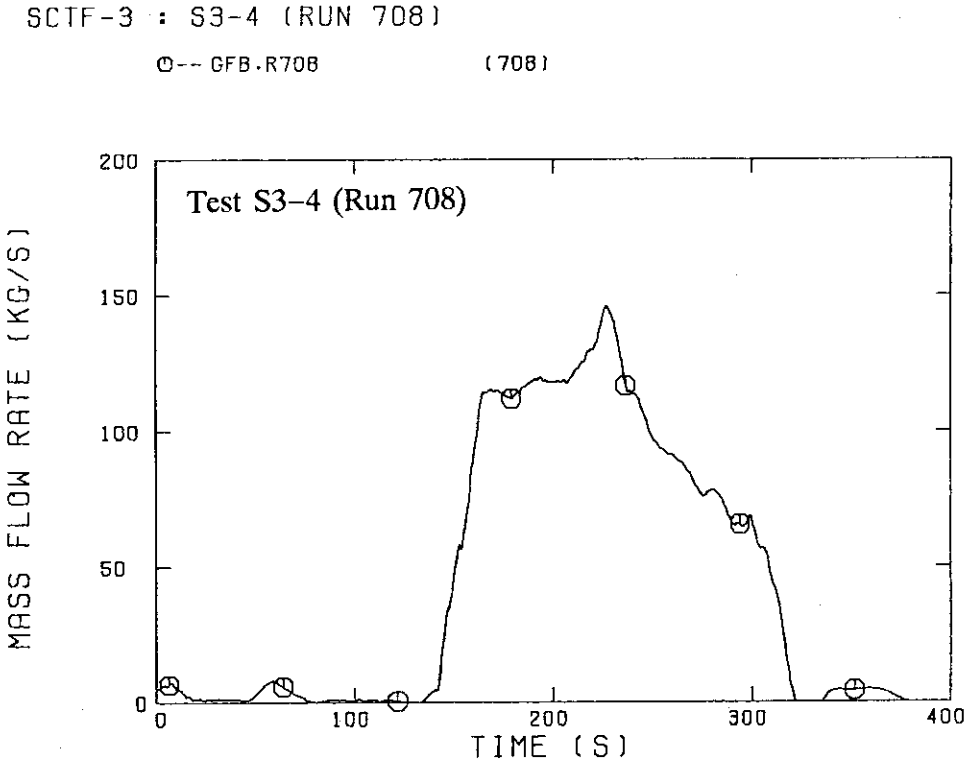

Fig. 3.3.4 Test S3-4: CCFL break-through rate

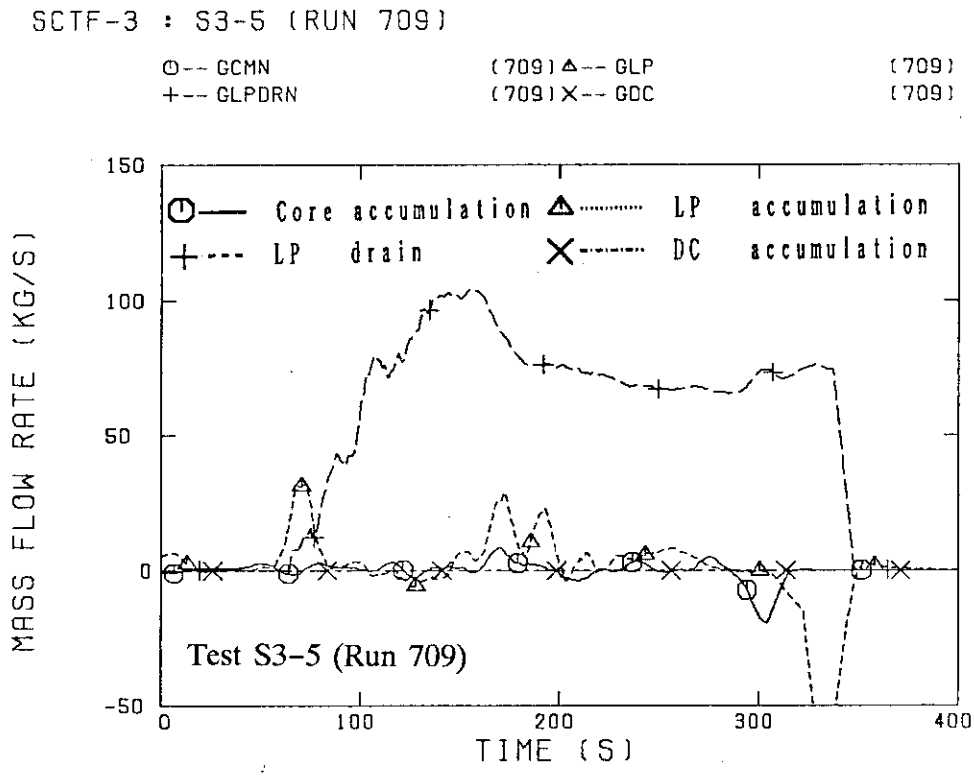

Fig. 3.3.5 Test S3-5: Mass flow rate in pressure vessel

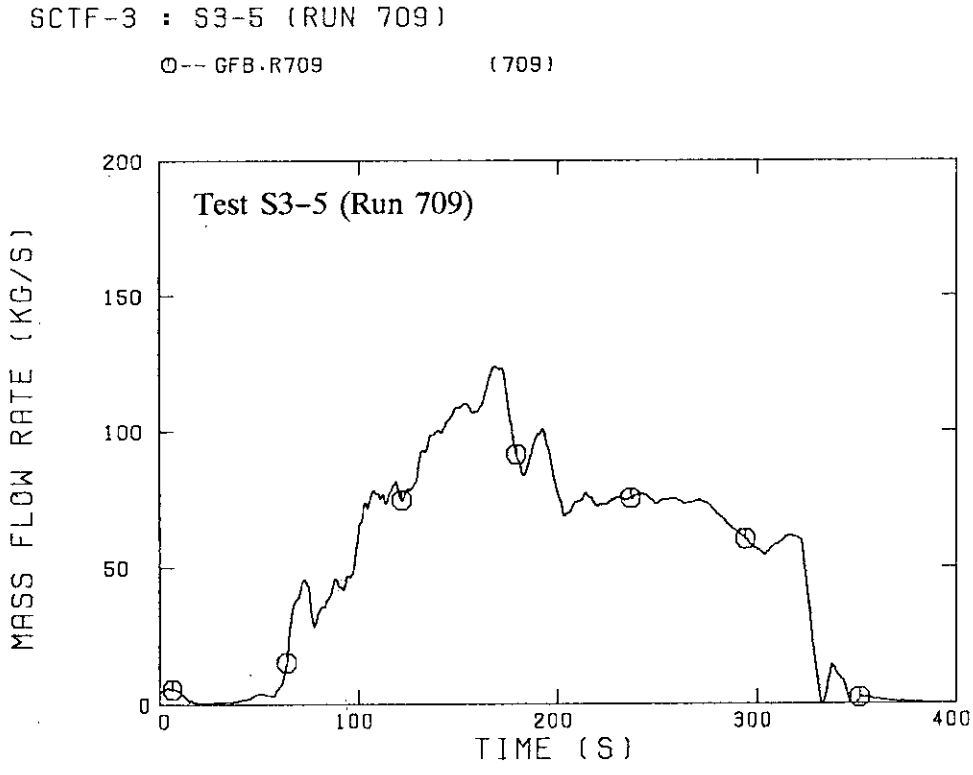

Fig. 3.3.6 Test S3-5: CCFL break-through rate

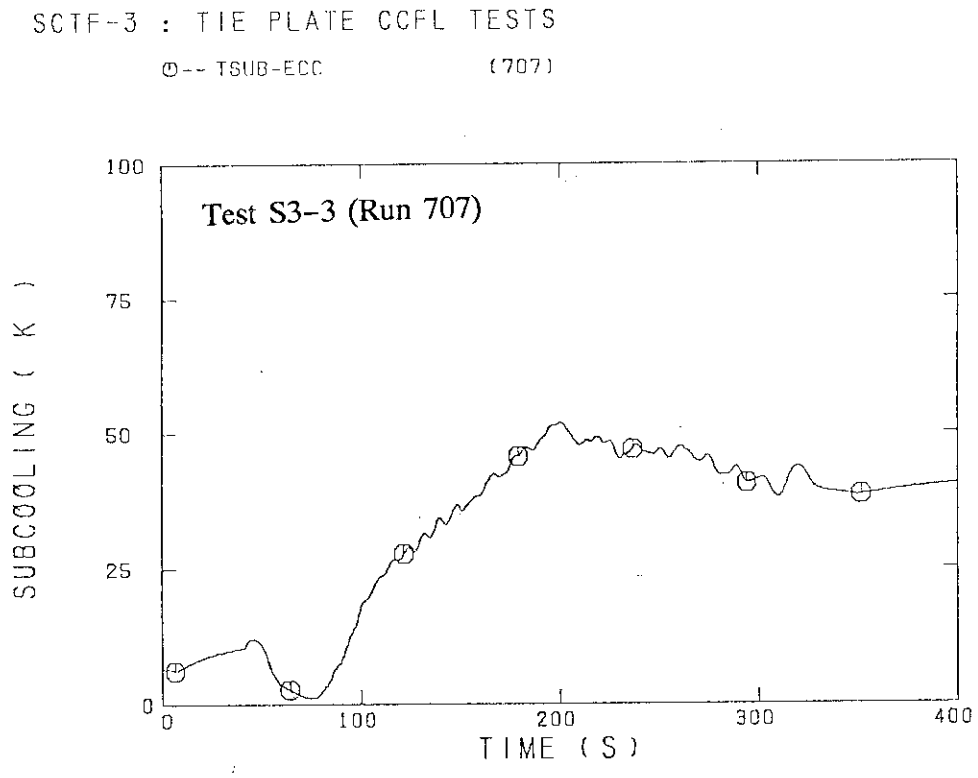

Fig. 4.1.1 Test S3-3: Subcooling of injected water

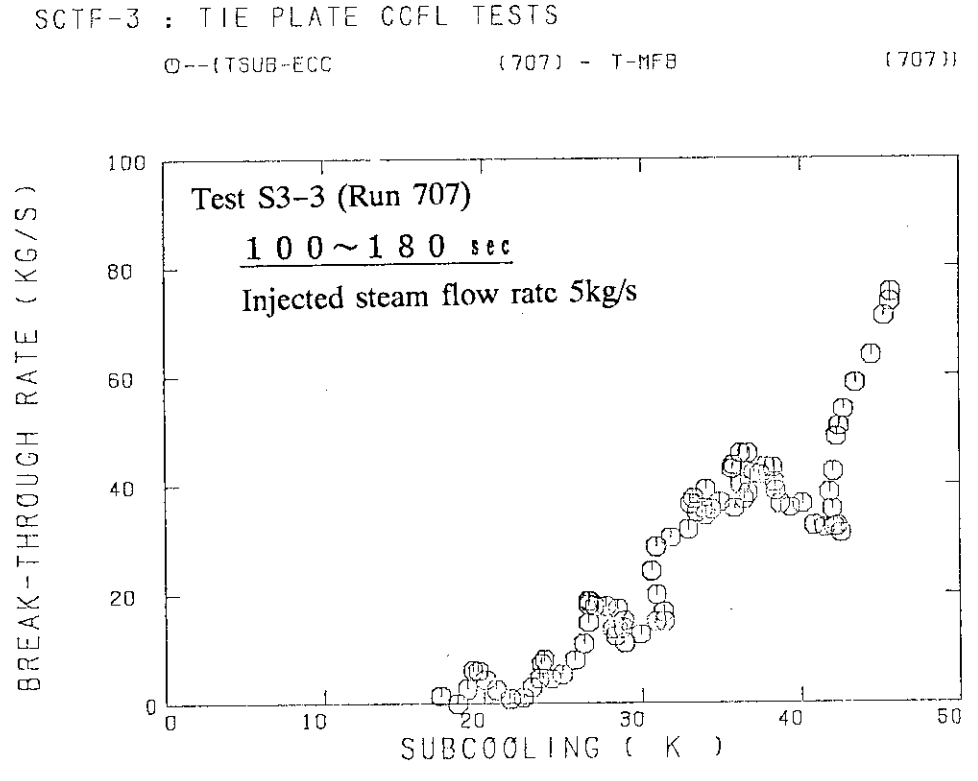

Fig. 4.1.2 Test S3-3: Effect of subcooling on break-through rate

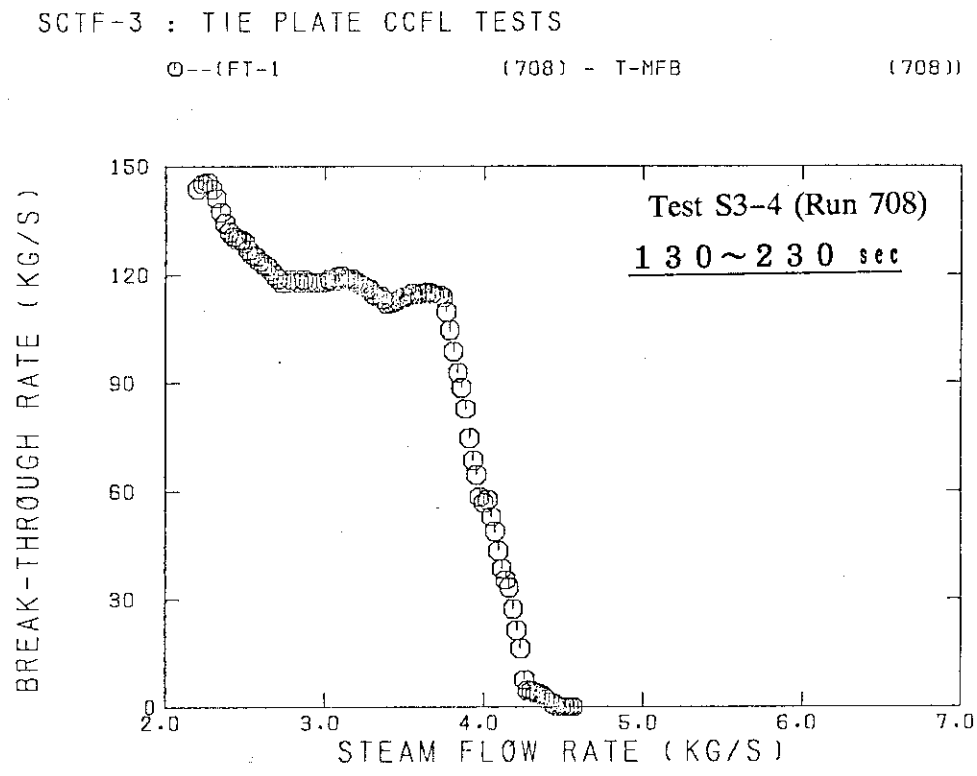

Fig. 4.2.1 Test S3-4: Effect of steam injection rate on break-through rate

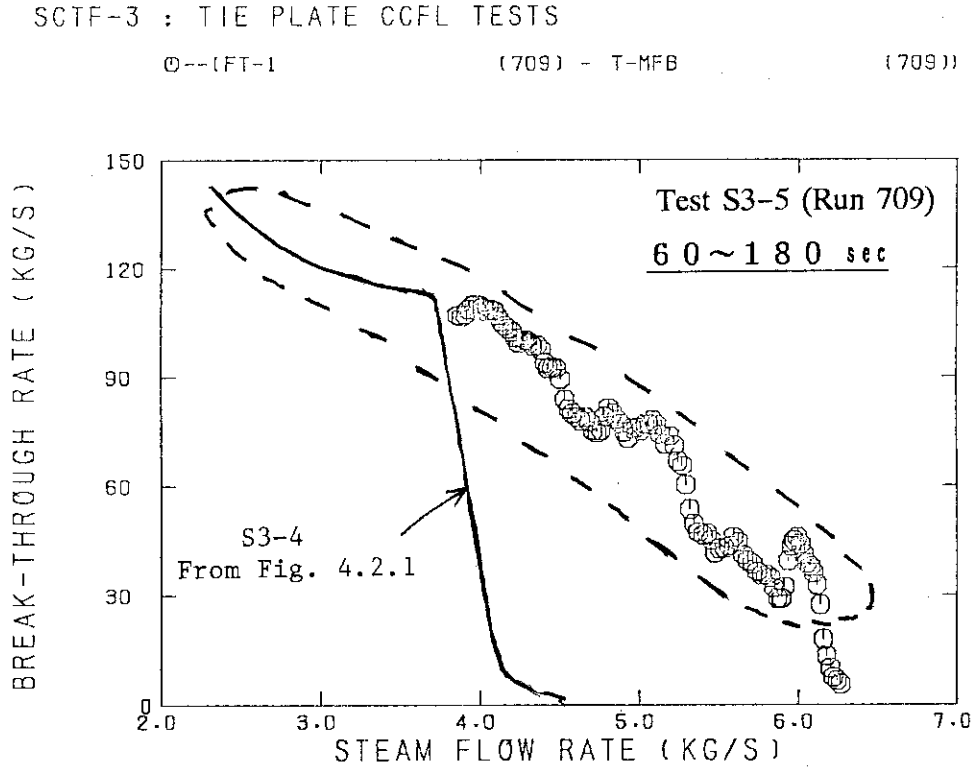

Fig. 4.2.2 Test S3-5: Effect of steam injection rate on break-through rate

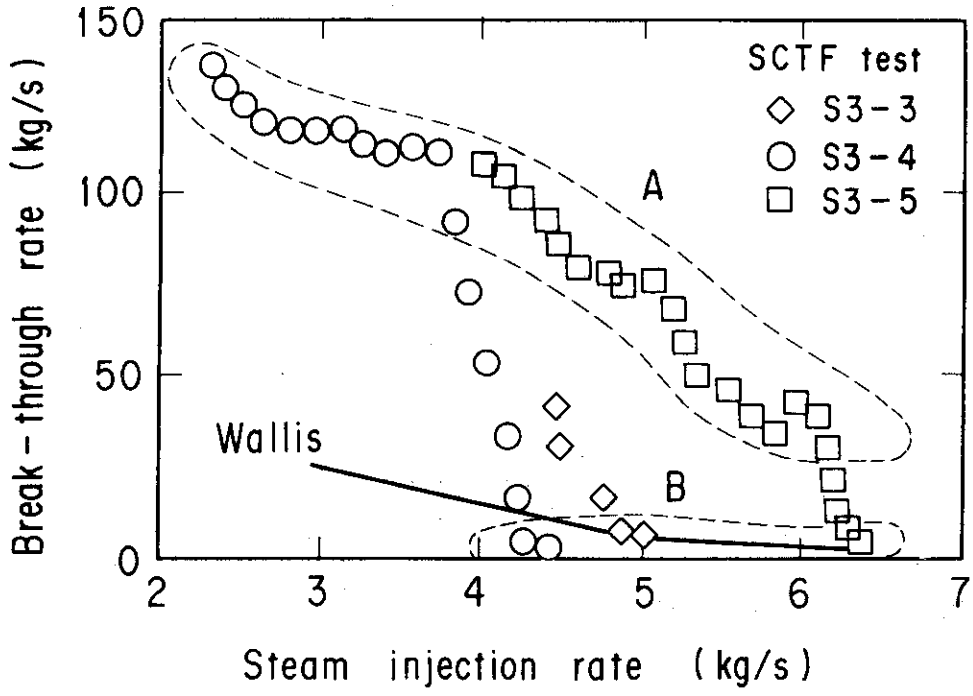

Fig. 4.2.3 Relation of break-through rate and steam flow rate

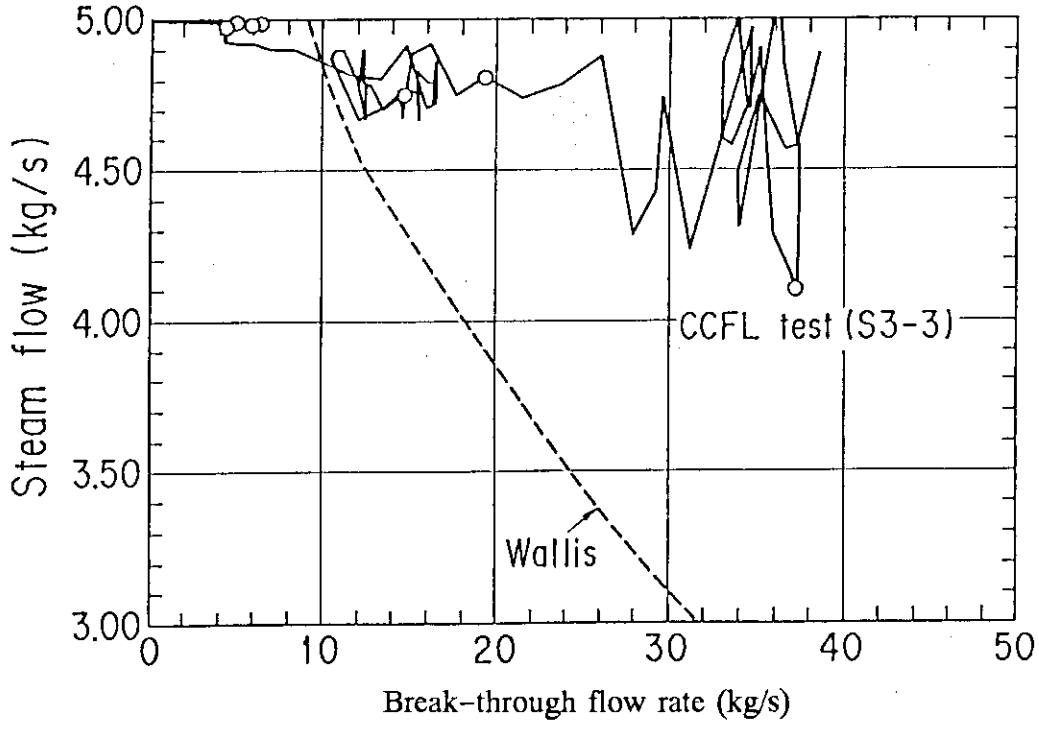

Fig. 4.3.1 Comparison between measured and predicted break-through rates

Appendix A Slab Core Test Facility Core-III

List of Table

List of Figures

Appendix A Slab Core Test Facility (SCTF) Core-III

A.1 Test Facility

The overall schematic diagram of SCTF is shown in Fig. A-1. The principal dimensions of the facility is shown in Table A-1, and the comparison of dimensions between SCTF and the reference PWR is shown in Fig. A-2.

A.1.1 Pressure Vessel

The pressure vessel is of slab geometry as shown in Fig. A-3. The height of the components in the pressure vessel is almost the same as the reference reactor's, and the flow area and the fluid volume of each component are scaled down based on the nominal core flow area scaling, 1/21.

The core consists of 8 bundles arranged in a row and each bundle includes heater rods and non-heated rods with 16×16 array. The core is enveloped by the honeycomb thermal insulator which is attached on the back surface of core wall plate.

The downcomer is located at one end of the pressure vessel which corresponds to the periphery of the actual reactor pressure vessel. The core baffle region located between the core and the downcomer is isolated for Core-III to minimize uncertainty in actual core flow. The cross sections of the pressure vessel at the upper head, upper plenum, core and lower plenum are shown in Fig. A-4.

A.1.2 Interface between Core and Upper Plenum

The interface between the core and the upper plenum consists of upper core support plate (UCSP), end box and various structures in the end box such as control rod spider which is paired with the control rod guid assembly (CRGA) and its support column bottom and special baffle plate spider which is paired with the hold-down bridge. These structures are exactly the same as those for a German PWR except some minor modifications.

Figure A-5 shows arrangement of the UCSP, the end box and the top grid spacer. The configuration of the end box is shown in Fig. A-6.

Detail of the end boxes with drag transducer device and other internals is shown in Fig. A-7. The UCSP shown in Fig. A-8 has two kinds of holes, i.e., the square holes correspond to the end boxes with control rod spider and the circular holes correspond to the end boxes with special baffle plate spider.

A.1.3 Upper Plenum and Upper Head

The vertical and horizontal cross sections of the upper plenum are shown in Figs. A-9 and A-4, respectively. In the SCTF Core-III, the slab cut of the upper plenum of a German (KWU) PWR is simulated. The splitted and staggered arrangement of the CRGA support columns was chosen to make good simulation of horizontal flow in the upper plenum.

As shown in Fig. A-10, there are three kinds of CRGA support column. Support column-1 is installed above Bundles 3 and 5 and connected to the CRGA support column bottom with the transition cone. Cross section of the CRGA support calumn changes from a circle to a half circle in this transition cone. Support column 2 is installed above Bundles 6 and 7 and the bottom is closed with the half conical bottom seal plate with many flow holes. Support column 3 is essentially the same as support column 2 but the edge of one side is cut off in order to install above Bundle 1. Each CRGA support column has ten or eleven baffle plates with flow holes. Top flow paths to the upper head bottom and to the upper plenum top are also provided.

Figure A-11 shows vertical cross section of the bottom part of the upper plenum and the interface between the core and the upper plenum. There are eight side flow injection nozzles and eight side flow extraction nozzles just at the opposite side of the upper plenum bottom, corresponding to each bundle.

The upper plenum is separated from the upper head by an upper support plate. Four top injection nozzles penetrate the upper head and open the top of upper plenum as shown in Fig. A-12. Outlet part of the top injection nozzle has a rectangular cross section and double mesh screen with 45 degree cross angle is attached at the mouth.

A.1.4 Simulated Core

The simulated core for the SCTF Core-III consists of 8 heater rod bundles arranged in a row. Each bundle has 236 electrically heated rods and 20 non-heated rods. The arrangement of rods in a bundle is shown in Fig. A-13. The dimensions of the heater rods are based on 15×15 fuel rods bundle for a PWR and the heated length and the outer diameter of each heater rod are 3.613 m and 10.7 mm, respectively. A heater rod consists of a nichrome heater element, boron nitride (BN) or magnesium oxide (MgO) depending on elevation in the heated zone and Nichrofer 7216 (equivalent to Inconel 600) sheath. The sheath thickness is about 1.0 mm and is thicker than the actual fuel cladding because of the requirements for thermocouple installation. The heater element is a helical coil and has a 17 step chopped cosine axial power profile as shown in Fig. A-14. The peaking factor is 1.4.

Non-heated rods are either pipes or solid rods of stainless steel with 13.8 mm O.D. The heater rods and non-heated rods are fixed at the top of the core allowing downward expansion. In Fig. A-15, relative elevation of rods and spacers is shown.

For better simulation of flow resistance in the lower plenum, the simulated fuel rods end in the lower plenum and do not penetrate through the bottom plate of the lower plenum as shown in Fig. A-15.

A.1.5 Primary Loops

Primary loops consist of a hot leg equivalent to four hot legs in area, a steam/water separator for simulating single steam phase flow downstream of the steam generator and for measuring flow rate of carry over water, an intact cold leg equivalent to three intact loops, a broken cold leg on the pressure vessel side and a broken cold leg on the steam/water separator side. These two broken cold legs are connected to two containment tanks through break valves, respectively. The arrangement of the primary loops is shown in Fig. A-16. The flow area of each loop is scaled down based on the core flow area scaling, 1/21. It should be emphasized that the cross section of the hot leg is an elongated circle with an actual height to realize proper flow pattern in the hot leg. The steam/water separator has a steam generator inlet plenum simulator to correctly simulate the flow

characteristics of carryover water into the U-tubes. The cross section of the hot leg and the configuration of the steam genrator inlet plenum simulator are shown in Fig. A-17.

A pump simulator and a loop seal part are provided for the intact cold leg. The arangement of the intact cold leg is shown in Fig. A-18. The pump simulator consists of the casing and duct simulators and an orifice plate as shown in Fig. A-19. The loop resistance is adjusted with the orifice plates attached to the intact cold leg, the steam/water separator side and pressure vessel side broken cold legs and the pump simulator.

A.1.6 ECC Water Injection System

Three kinds of ECCSs are provided, i.e., the accumulator injection system (Acc), low pressure coolant injection system (LPCI) and combined injection system. Available injection locations for the former two are the intact and broken cold legs, the hot leg, the lower plenum and the downcomer. On the other hand, those for the last one are the top and bottom-side of the upper plenum and the intact and broken cold legs.

A.1.7 Containment Tanks and Auxiliary System

Two containment tanks are provided to SCTF. The containment tank-I is connected with the downcomer through the pressure vessel side broken cold leg and the containment tank-II is connected with the steam/water separator through the steam/water separator side broken cold leg. Especially in the containment tank-I, carryover water from the downcomer is measured by the differentiation of the liquid level. These containment tanks and auxiliary system such as a pressurizer for injecting water from the Acc tanks, etc. are shared with CCTF.

A.2 Instrumentation

The instrumentation in SCTF has been provided both by JAERI and USNRC. The JAERI-provided instrumentation includes the measurement of temperatures, pressures, differential pressures, liquid levels, flow velocities, and heating powers. USNRC has provided film probes, impedance probes, string probes, liquid level detectors (LLDs), fluid distribution grids (FDGs), turbine meters, drag disks, densitometers, spool pieces, drag bodies, break through detectors and video optical probes. Locations of the JAERI-provided instruments are shown in Figs. A-20 through A-43.

Table A-1 Principal dimensions of the SCTF

1.	Core Dimension		
	(1) Quantity of Bundle	8 Bundles	
	(2) Bundle Array	1 × 8	
	(3) Bundle Pitch	230 mm	
	(4) Rod Array in a Bundle	16 × 16	
	(5) Rod Pitch in a Bundle	14.3 mm	
	(6) Quantity of Heater Rod in a Bundle	236 rods	
	(7) Quantity of Non-Heated Rod in a Bundle	20 rods	
	(8) Total Quantity of Heater Rods	236×8=1,888	rods
	(9) Total Quantity of Non-Heated Rods	20×8=160	rods
	(10) Effective Heated Length of Heater Rod	3613 mm	
	(11) Diameter of Heater Rod	10.7 mm	
	(12) Diameter of Non-Heated Rod	13.8 mm	
2.	Flow Area & Fluid Volume		
	(1) Core Flow Area	0.25	m^2
	(2) Core Fluid Volume	0.903	m^3
	(3) Baffle Region Flow Area (isolated)	(0.096)	m^2
	(4) Baffle Region Fluid Volume (nominal)	0.355	m^3
	(5) Cross-Sectional Area of Core Additional Fluid Volumes Including Gap between Core Barrel and Pressure Vessel Wall and Various Penetration Holes	0.07 0.10	m^2 m^2
	(6) Downcomer Flow Area	0.158	m^2
	(7) Upper Annulus Flow Area	0.158	m^2
	(8) Upper Plenum Horizontal Flow Area (max.)	0.541	m^2
	(9) Upper Plenum Vertical Flow Area	0.525	m^2
	(10) Upper Plenum Fluid Volume	1.156	m^3
	(11) Upper Head Fluid Volume	0.86	m^3
	(12) Lower Plenum Fluid Volume (excluding below downcomer)	1.305	m^3
	(13) Steam Generator Inlet Plenum Simulator Flow Area	0.626	m^2
	(14) Steam Generator Inlet Plenum Simulator Fluid Volume	0.931	m^3
	(15) Steam Water Separator Fluid Volume	5.3	m^3
	(16) Flow Area at the Top Plate of Steam Generator Inlet Plenum Simulator	0.195	m^2
	(17) Hot Leg Flow Area	0.0826	m^2

Table A-1 (cont.)

(18)	Intact Cold Leg Flow Area (Diameter = 297.9 mm) Inverted U-Tube with 0.0314 m^2 Cross-Sectional Area (Diameter = 200 mm) and 10 m Height from the Top of Steam Generator Inlet Plenum Simulator Can Be Added As an Option.	0.0697 m^2
(19)	Broken Cold Leg Flow Area (Diameter = 151.0 mm)	0.0197 m^2
(20)	Containment Tank-I Fluid Volume	30 m^3
(21)	Containment Tank-II Fluid Volume	50 m^3
(22)	Flow Area of Exhausted Steam Line from Containment Tank-II to the Atmosphere	see Fig. 3-63

3. Elevation & Height

(1)	Top Surface of Upper Core Support Plate (UCSP)	0 mm
(2)	Bottom Surface of UCSP	- 40 mm
(3)	Top of the Effective Heated Length of Heater Rod	- 444 mm
(4)	Bottom of the Effective Heated Length of Heater Rod	-4,057 mm
(5)	Bottom of the Skirt in the Lower Plenum	-5,270 mm
(6)	Bottom of Intact Cold Leg	+ 724 mm
(7)	Bottom of Hot Leg	+1,050 mm
(8)	Top of Upper Plenum	+2,200 mm
(9)	Bottom of Steam Generator Inlet Plenum Simulator	+1,933 mm
(10)	Centerline of Loop Seal Bottom	-2,281 mm
(11)	Bottom Surface of End Box	- 263 mm
(12)	Top of Upper Annulus of Downcomer	+2,234 mm
(13)	Height of Steam Generator Inlet Plenum Simulator	1,595 mm
(14)	Height of Loop Seal	3,140 mm
(15)	Inner Height of Hot Leg Pipe	737 mm
(16)	Bottom of Lower Plenum	-5,772 mm
(17)	Top of Upper Head	+2,887 mm

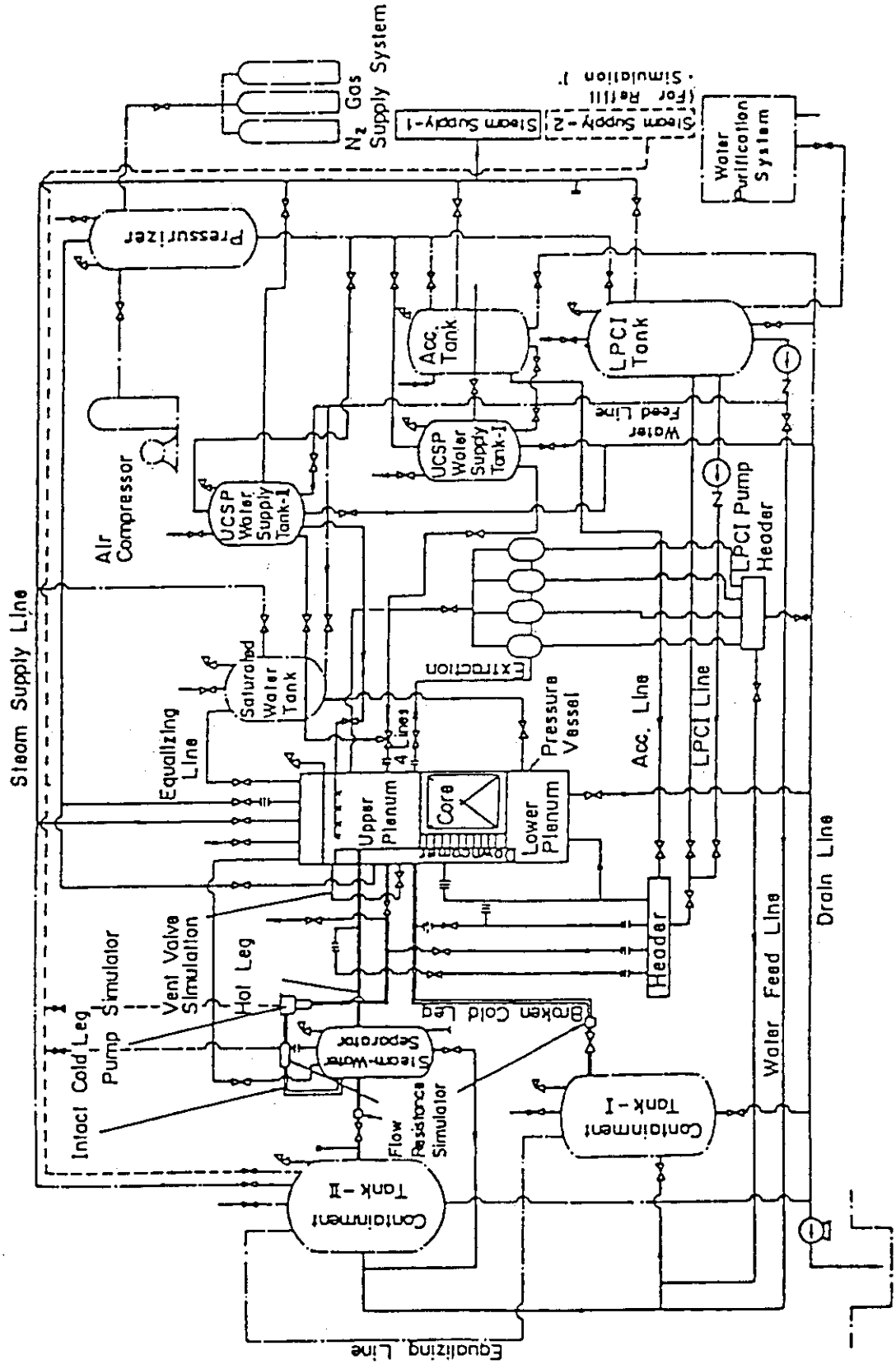

Fig. A-1 Schematic diagram of Slab Core Test Facility

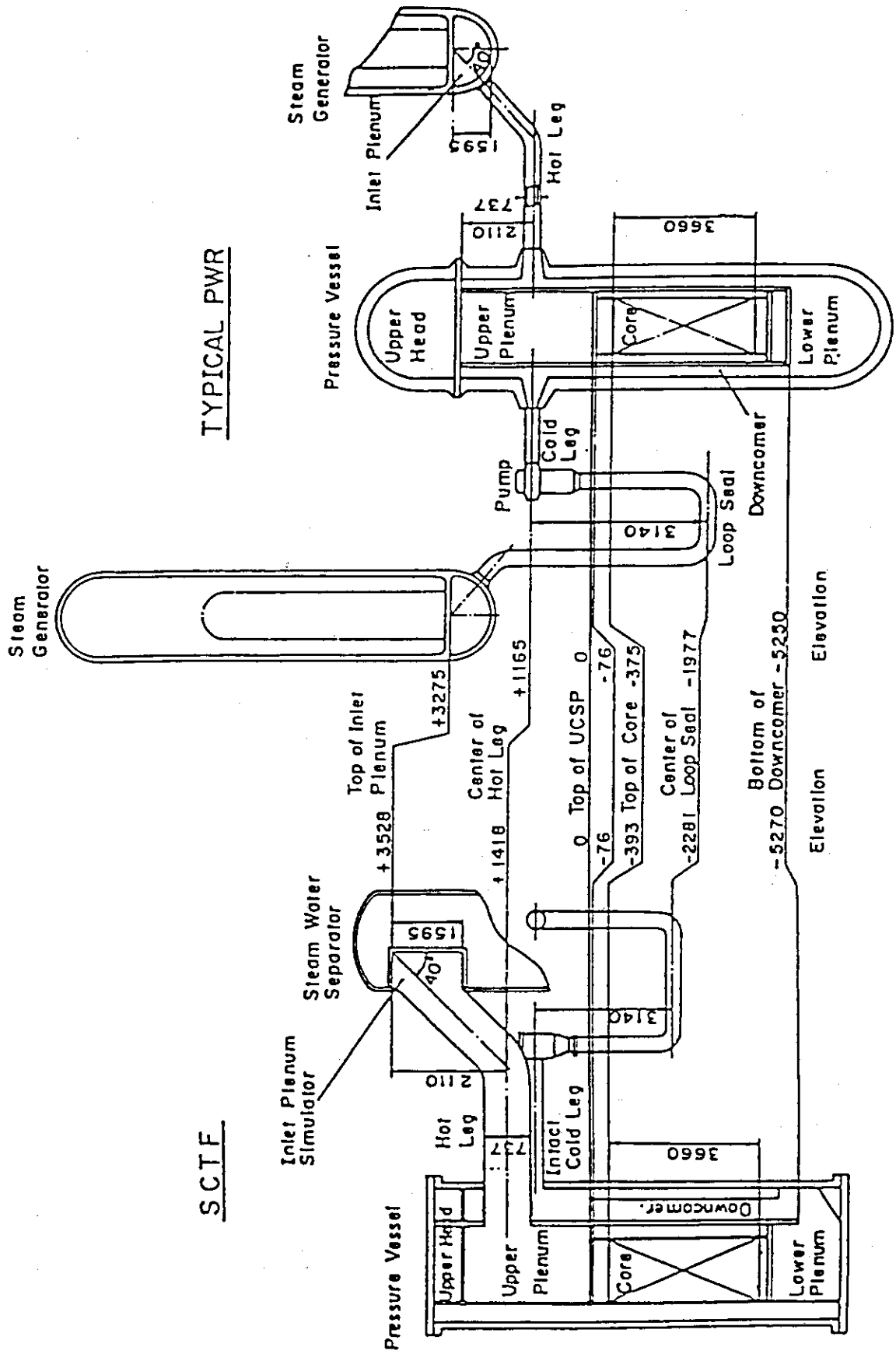

Fig. A-2 Comparison of dimensions between SCTF and a reference PWR

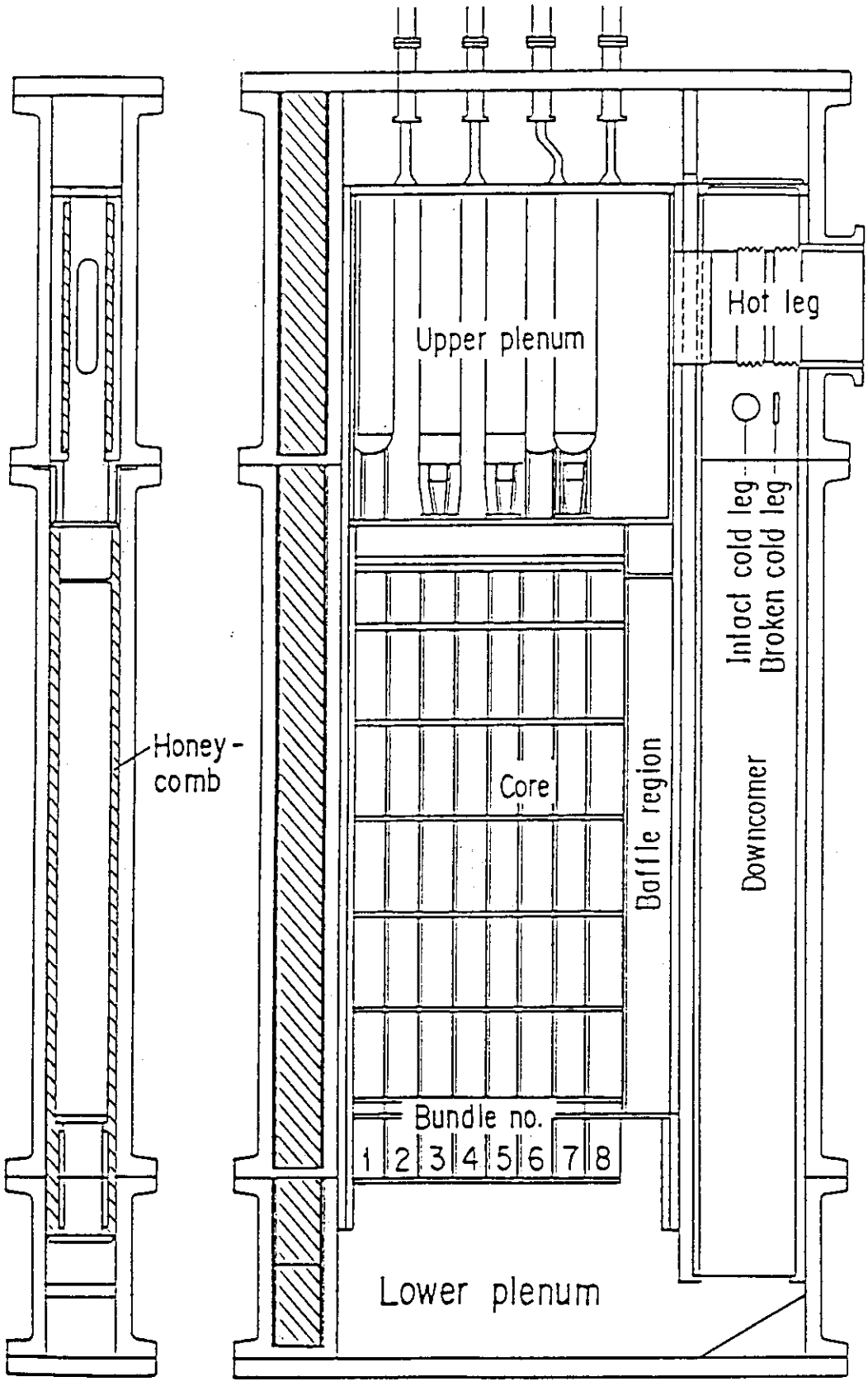

Fig. A-3 Vertical cross sections of pressure vessel

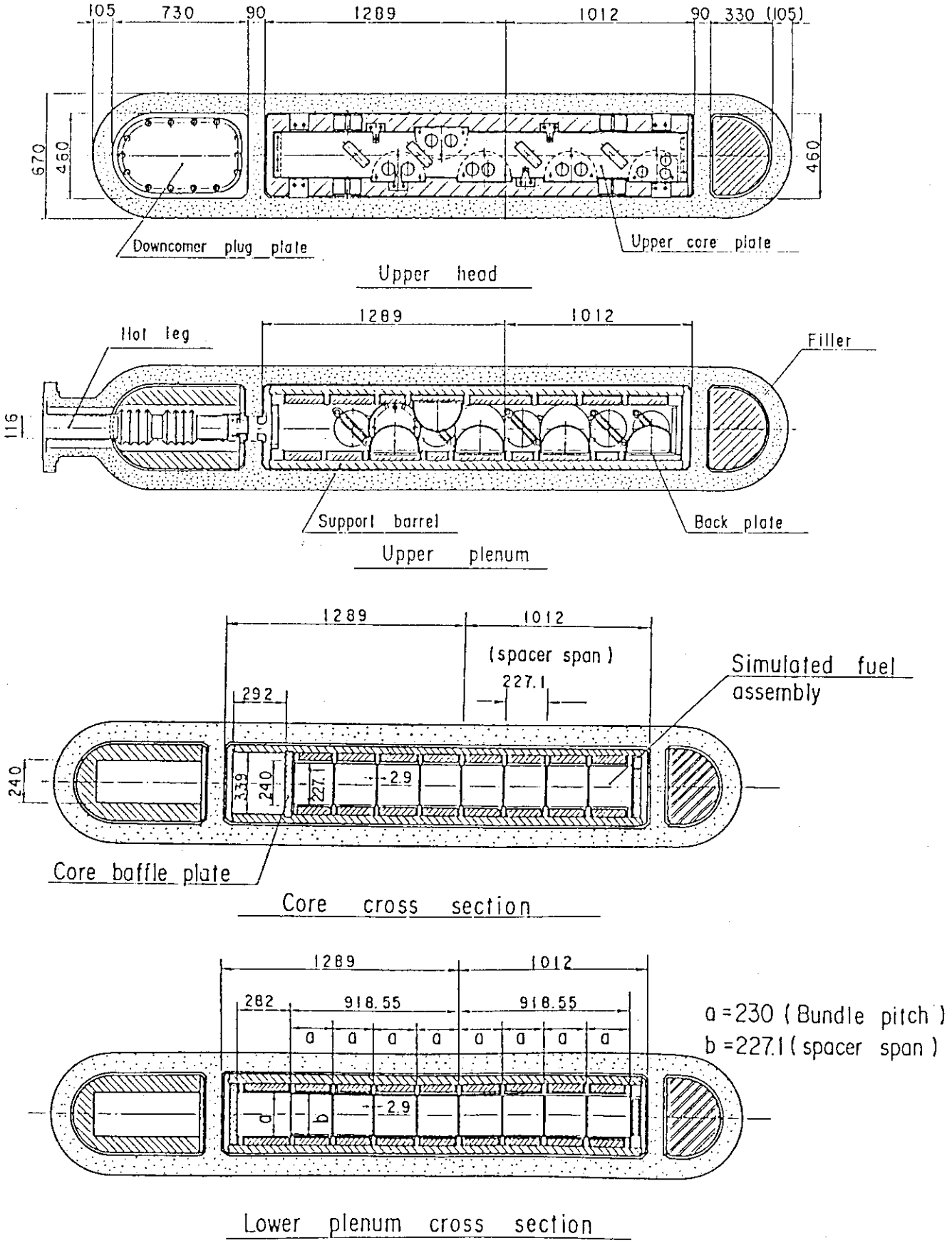

Fig. A-4 Horizontal cross sections of pressure vessel

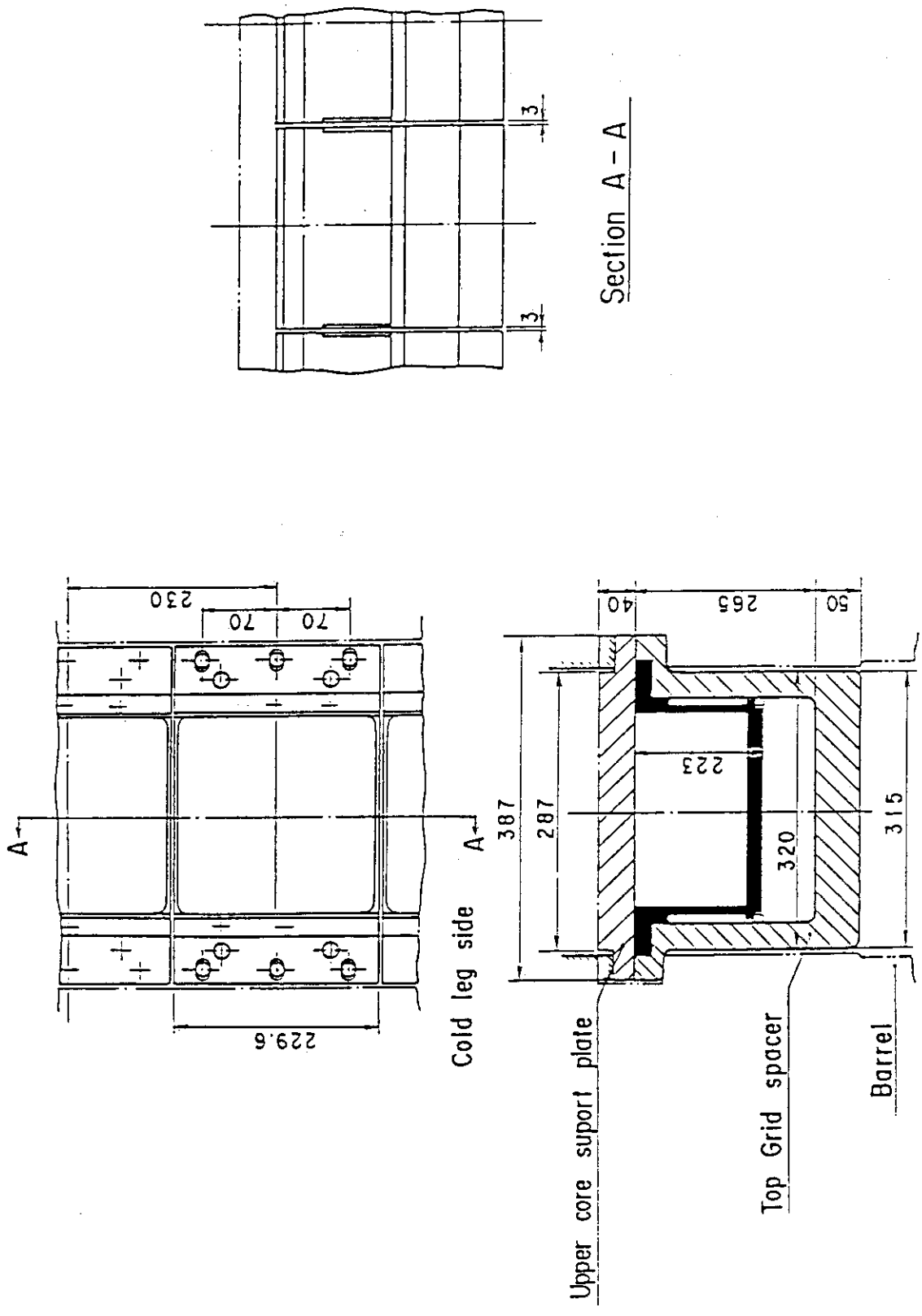

Fig. A-5 Arrangement and principal dimension of end boxes and top grid spacers

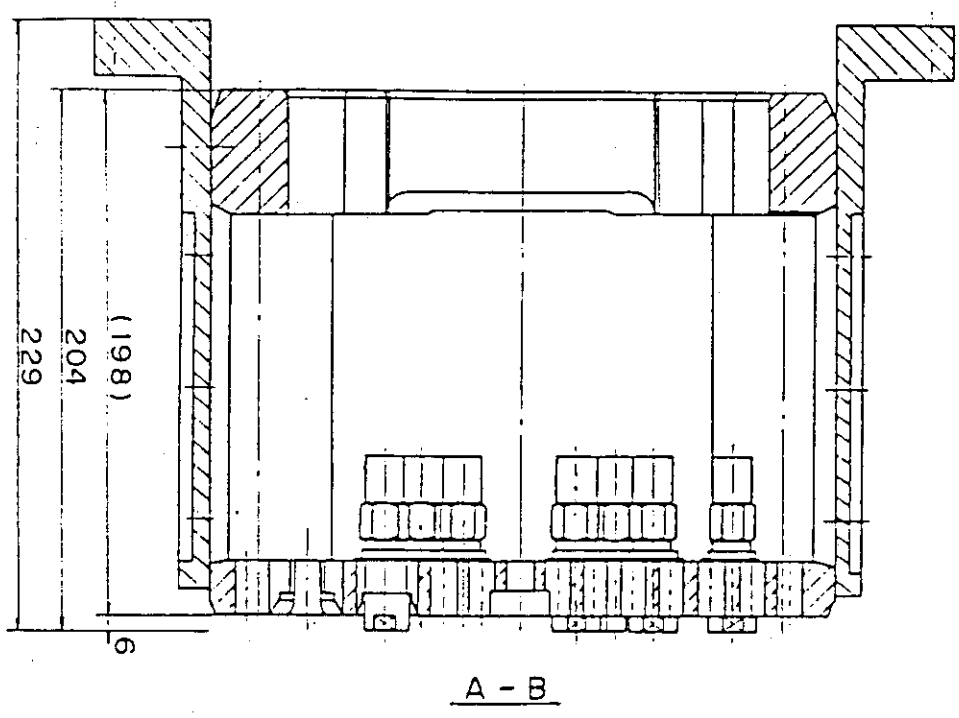

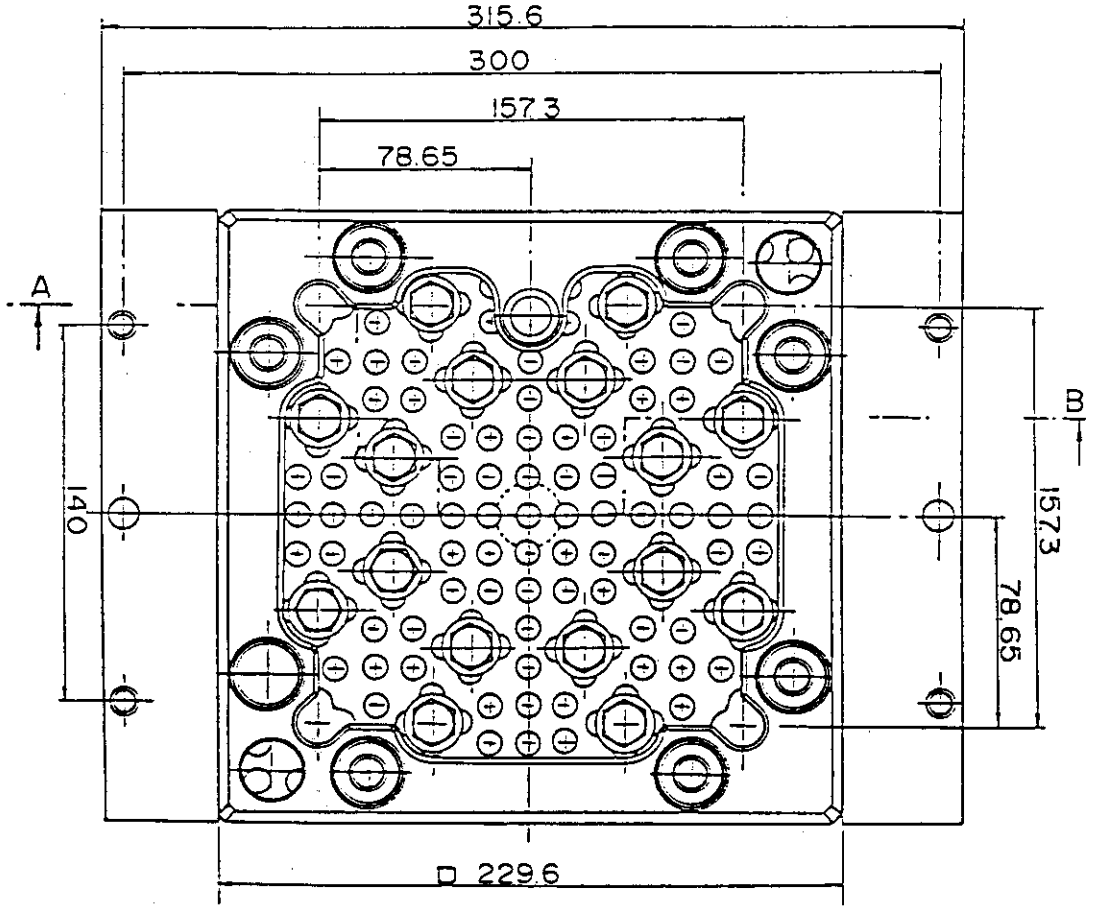

Fig. A-6 Configuration and dimension of end boxes

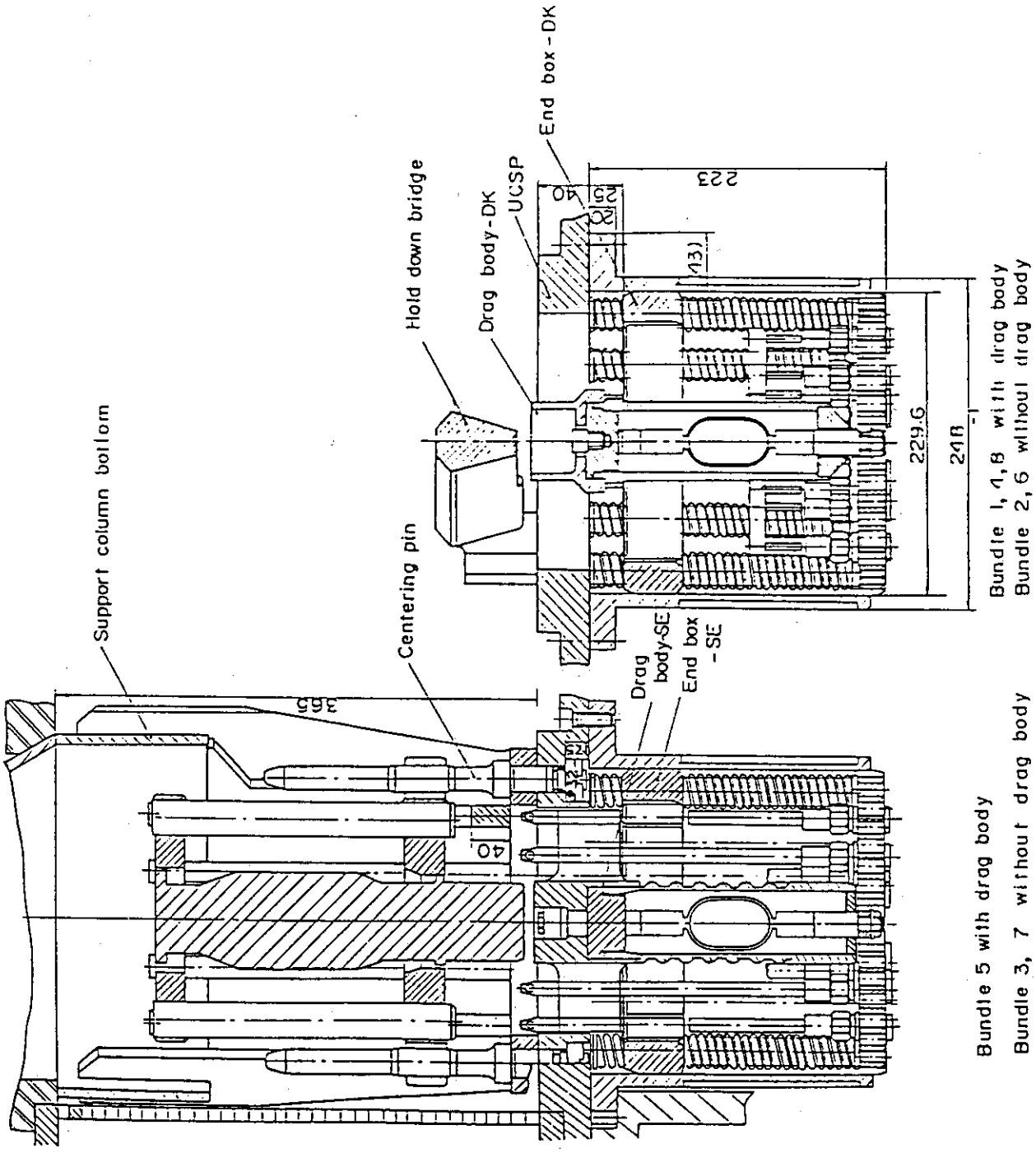

Fig. A-7 Detail of end boxes with drag bodies

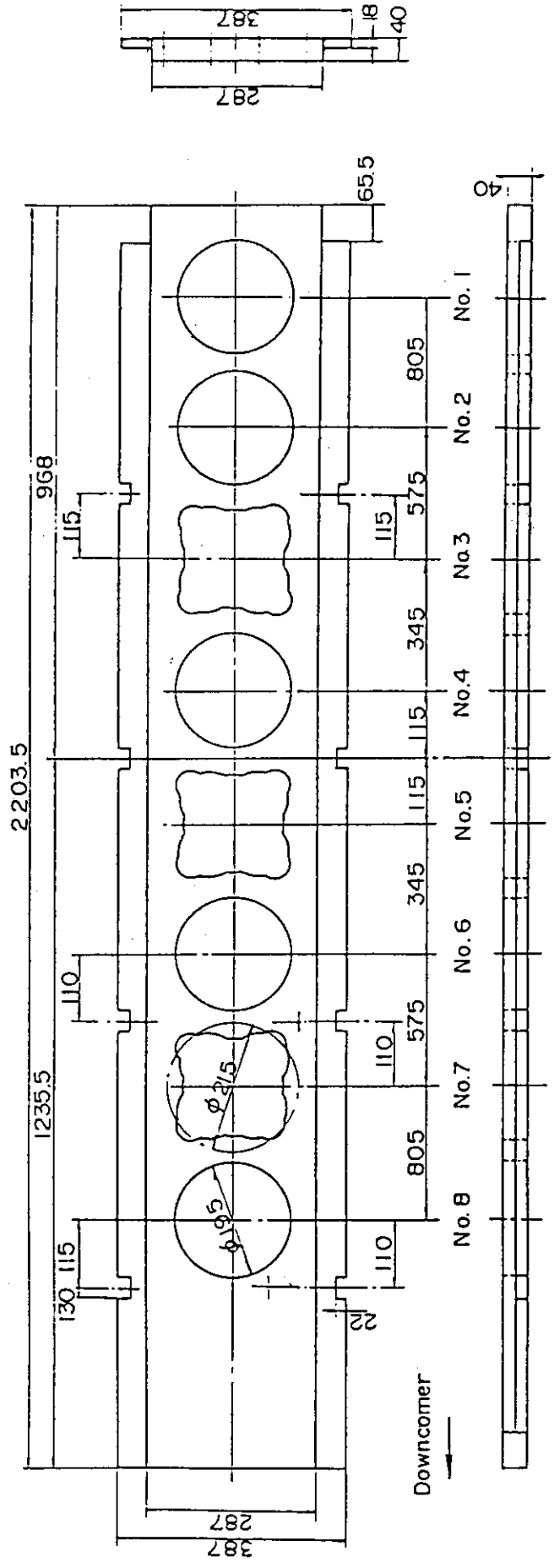

Fig. A-8 Dimension of upper core support plate

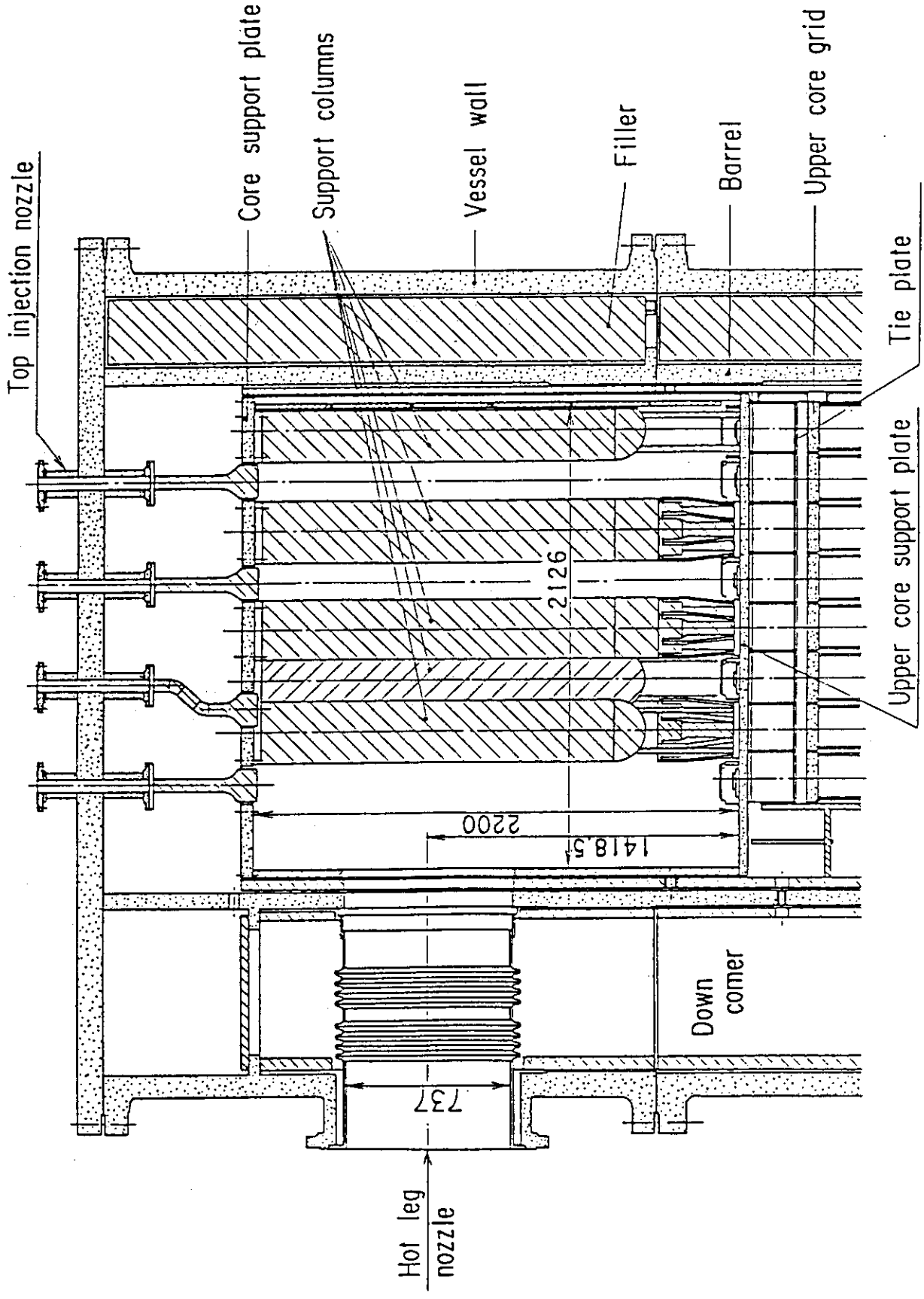

Fig. A-9 Vertical cross section of upper plenum internals

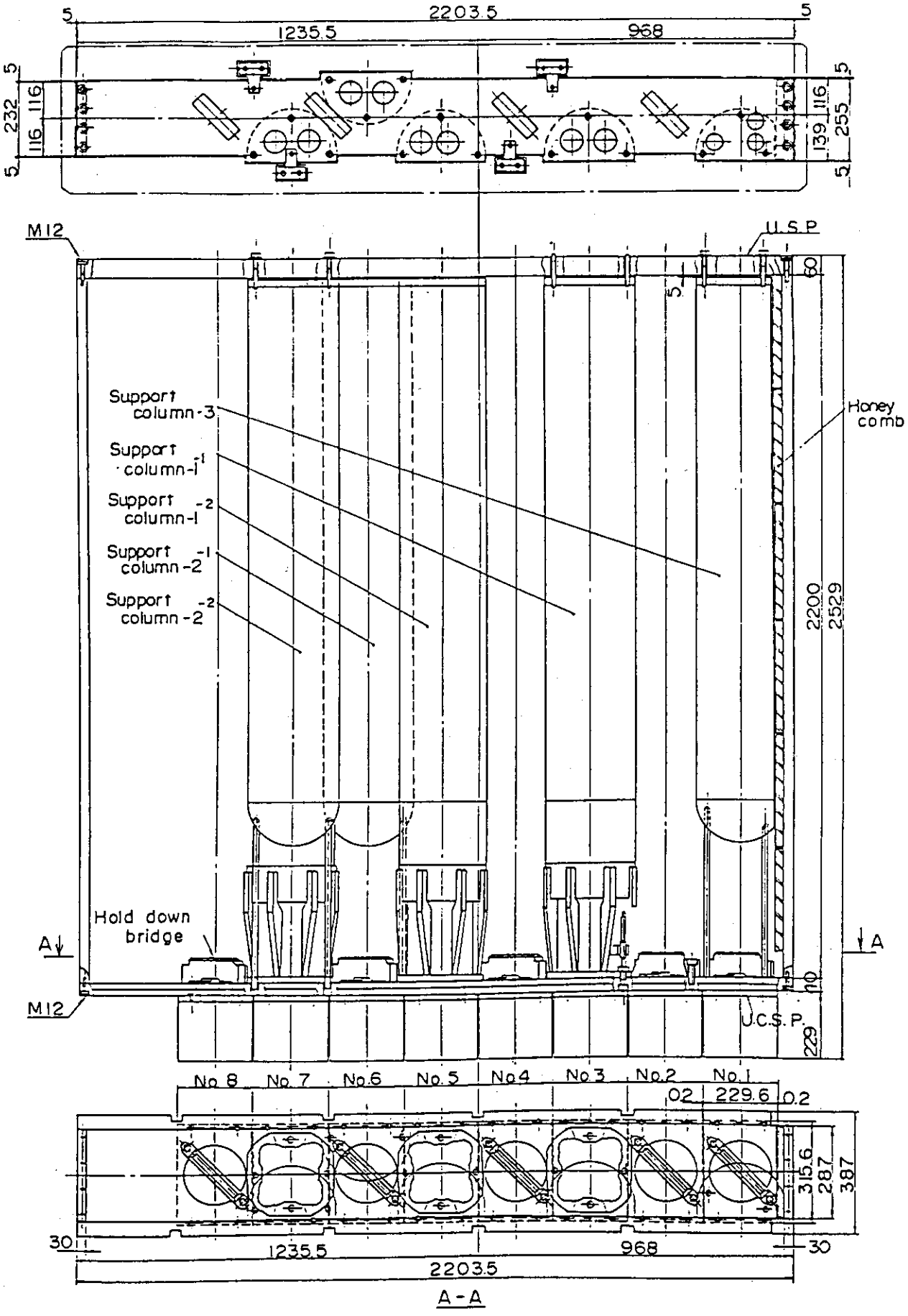

Fig. A-10 Three kinds of CRGA support column

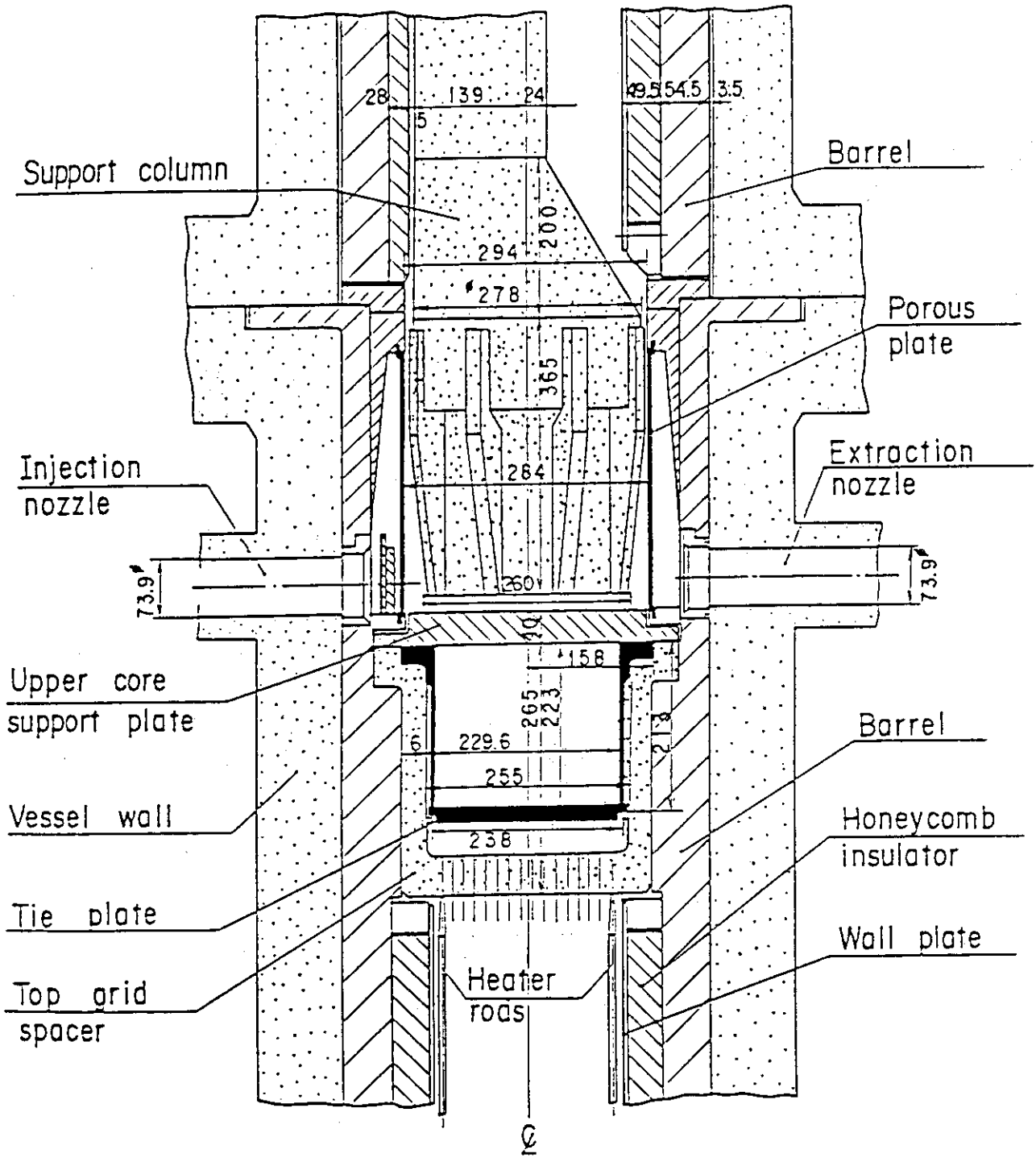

Fig. A-11 Vertical cross section of interface between core and upper plenum

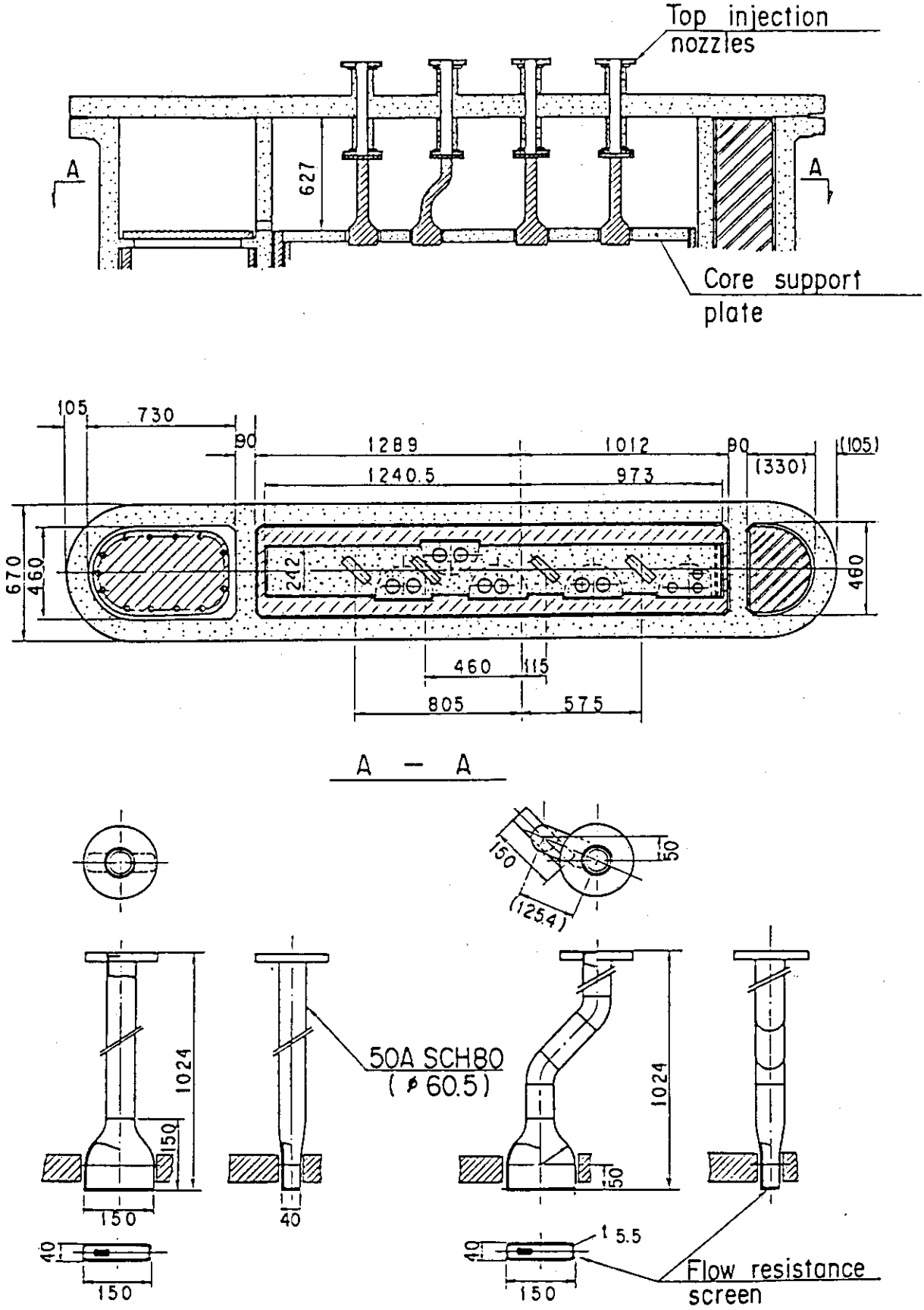

Fig. A-12 Schematic of upper head

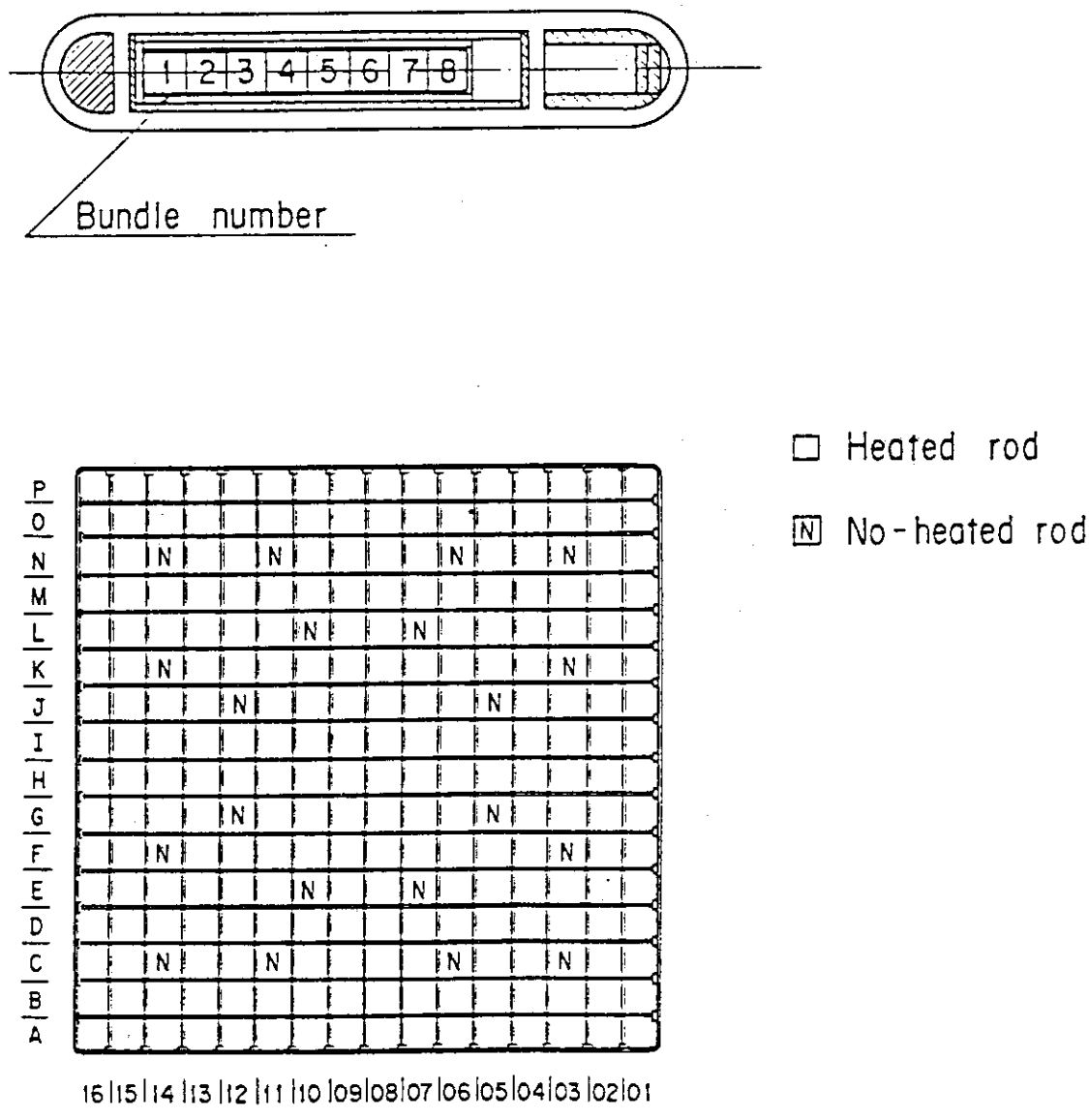

Fig. A-13 Arrangement of heater rod bundles

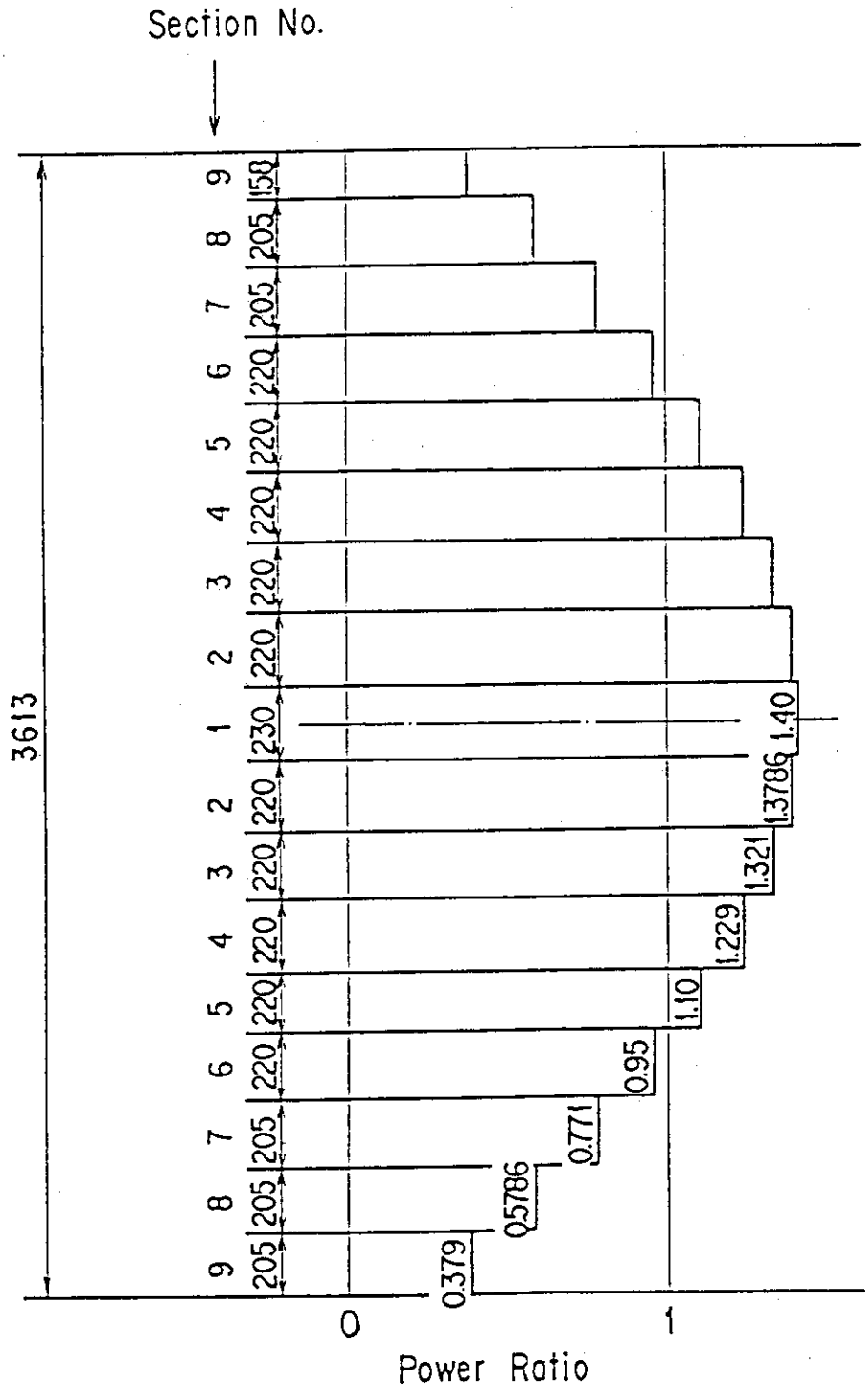

Fig. A-14 Axial power distribution of heater rods

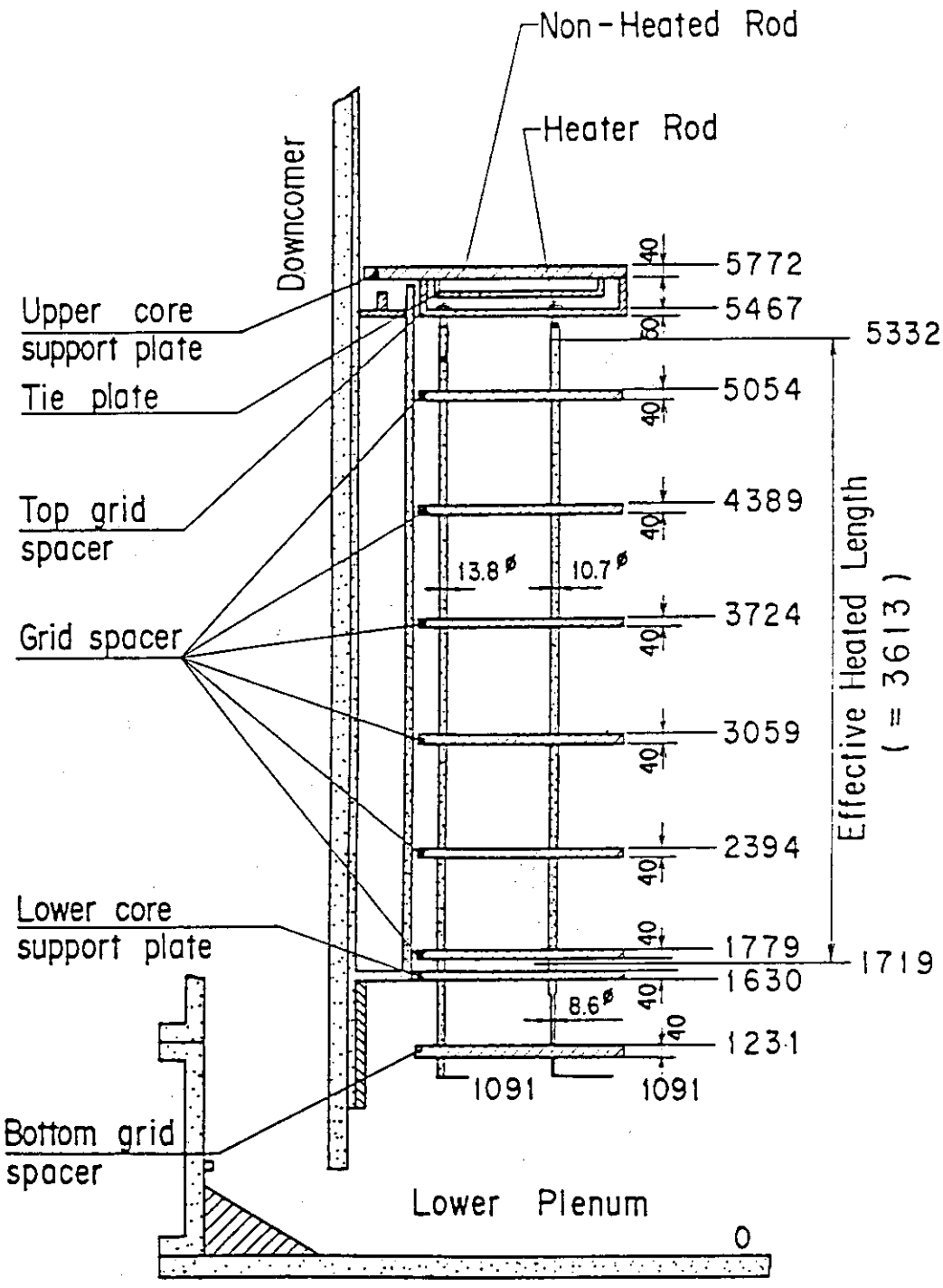

Fig. A-15 Relative elevation and dimension of core

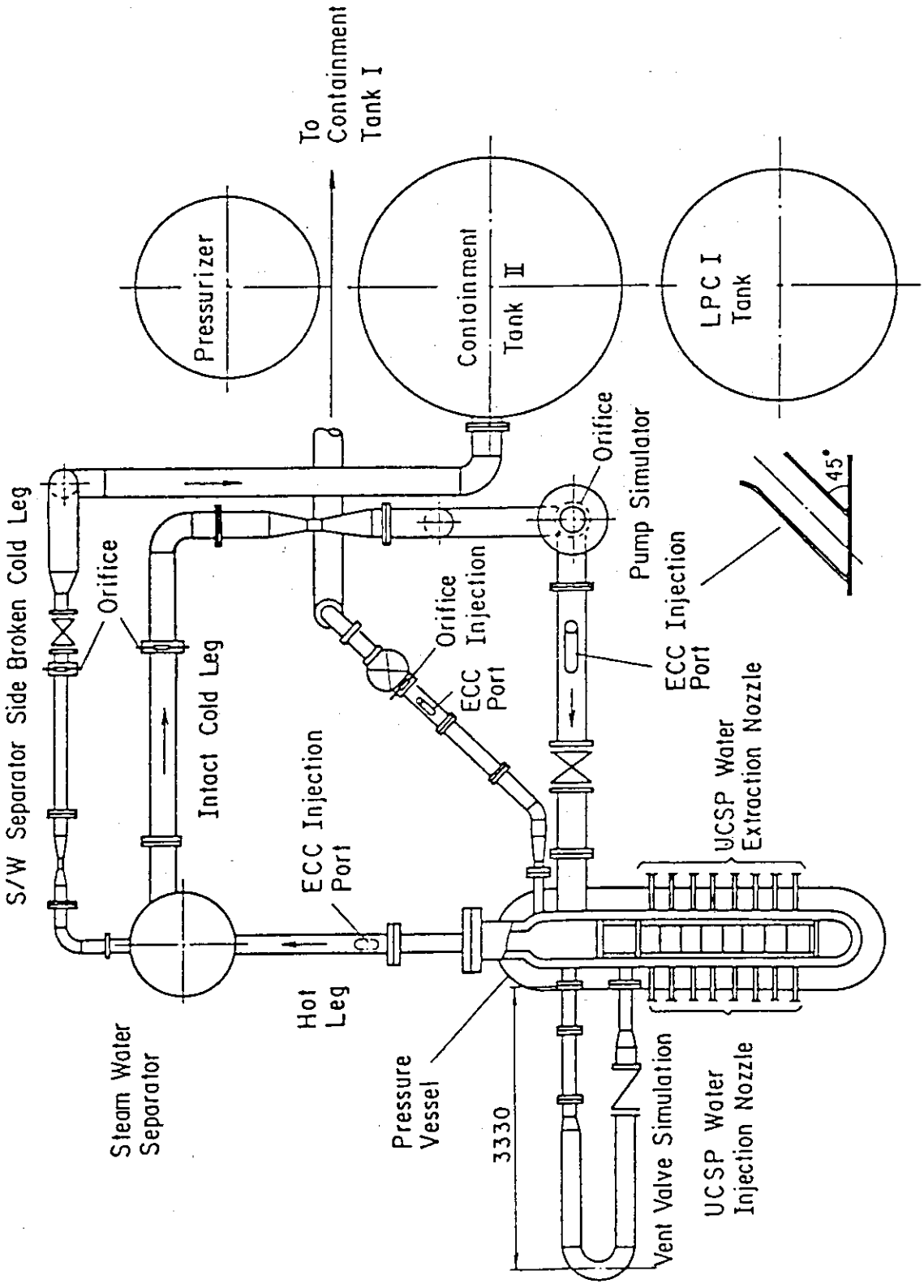

Fig. A-16 Overview of the arrangements of SCTF

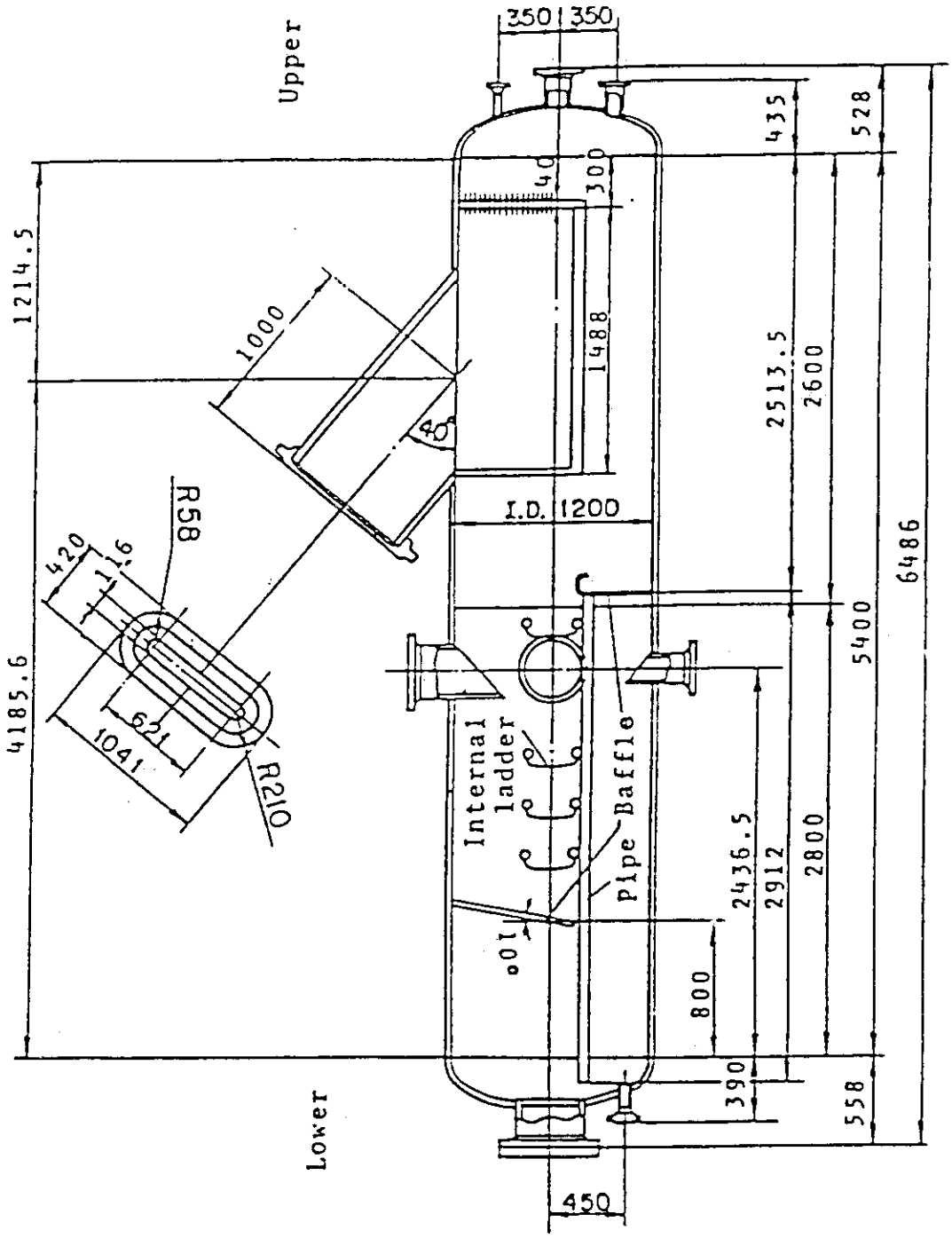

Fig. A-17 Steam/water separator

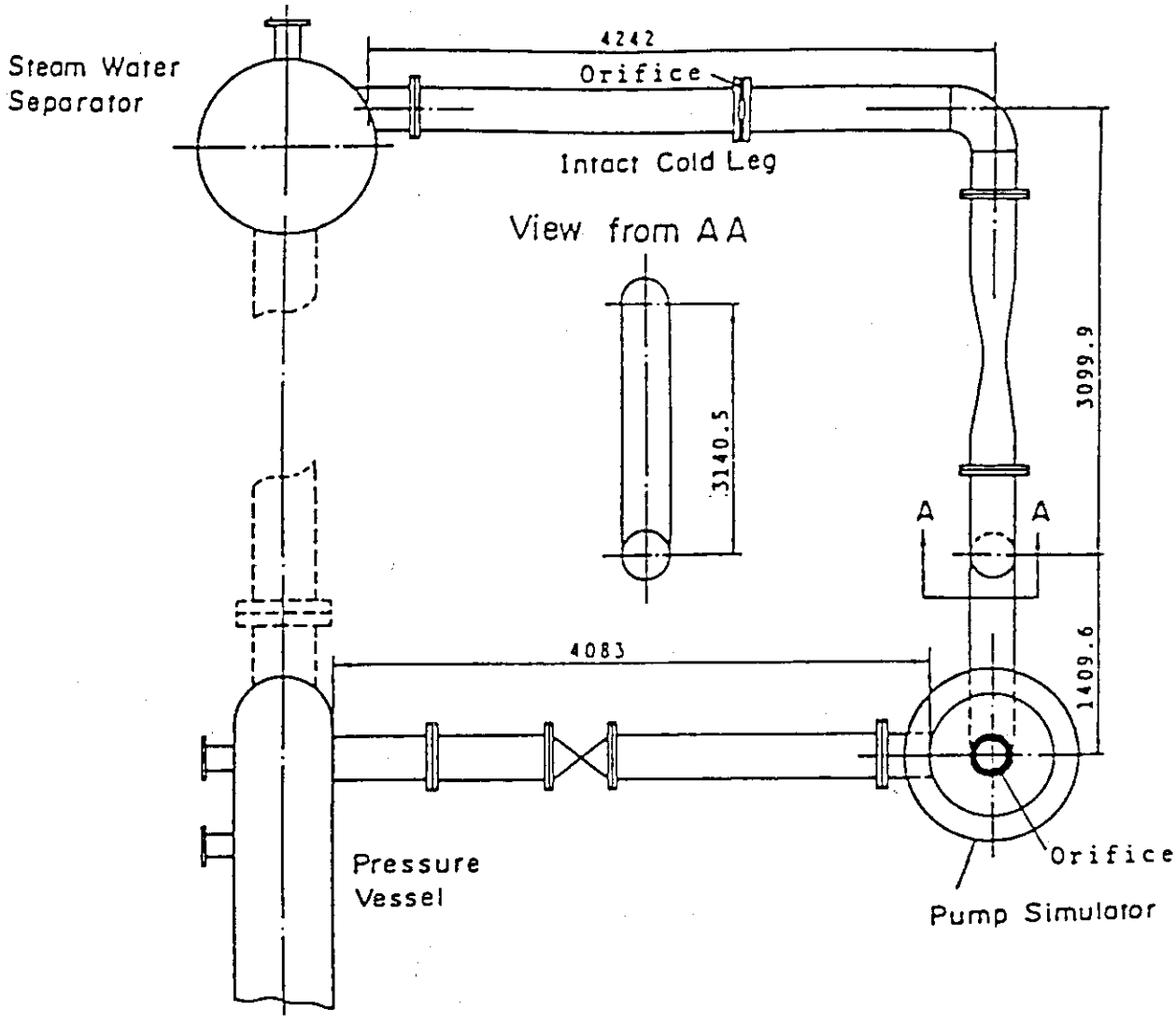

Fig. A-18 Arrangement of intact cold leg

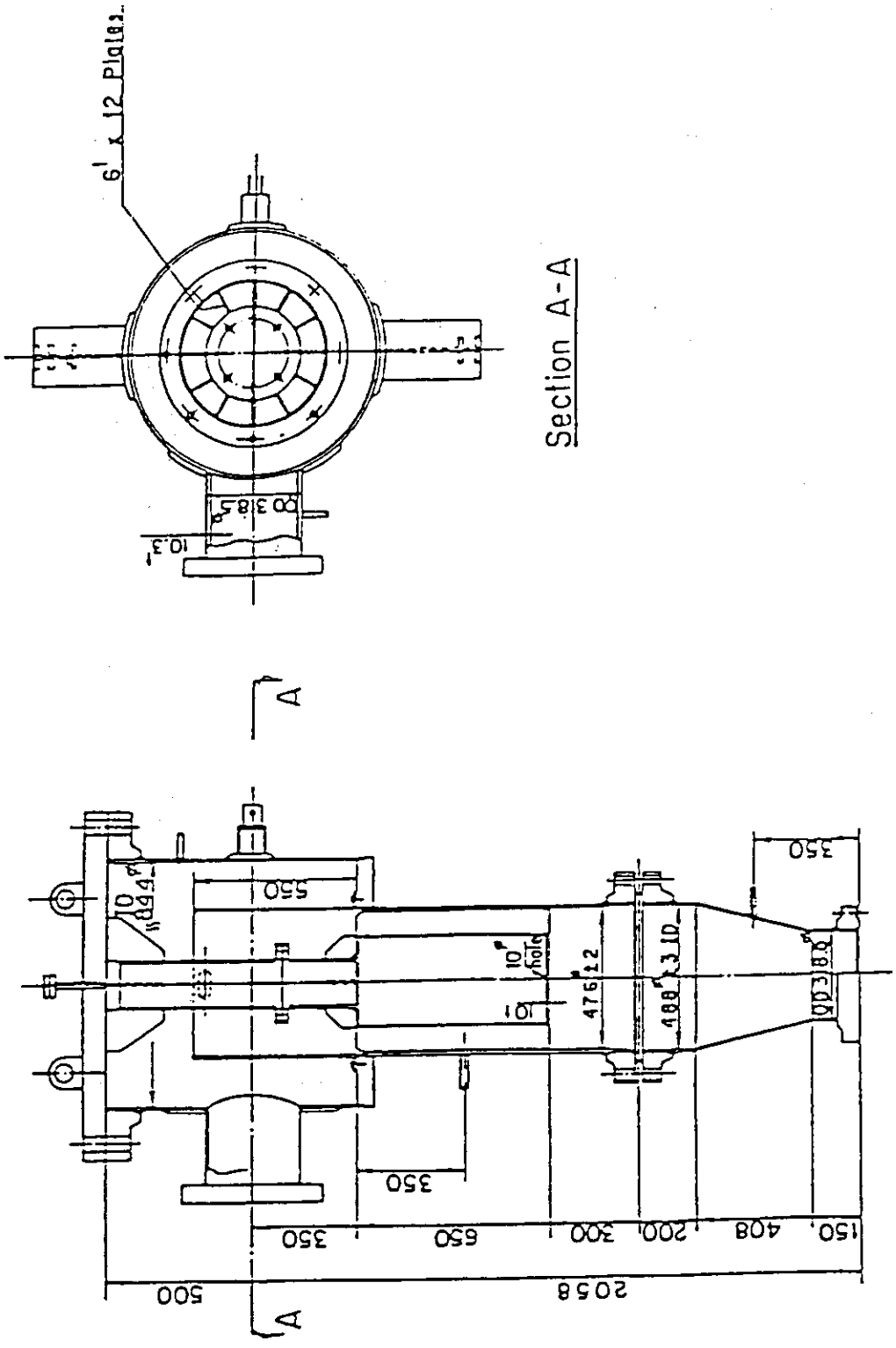

Fig. A-19 Configuration and dimension of pump simulator

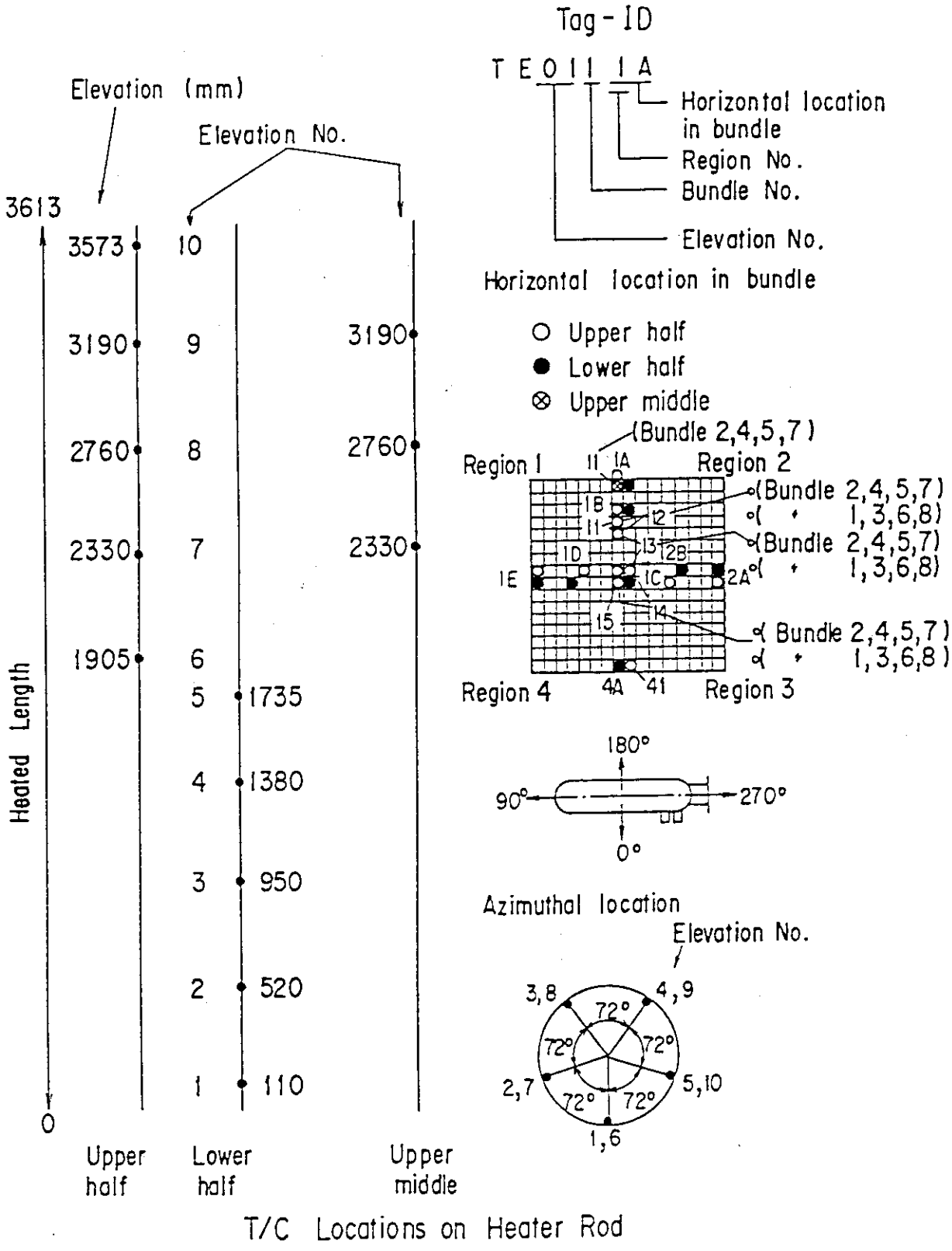

T/C Locations on Heater Rod

Fig. A-20 Thermocouple locations of heater rod surface temperature measurements

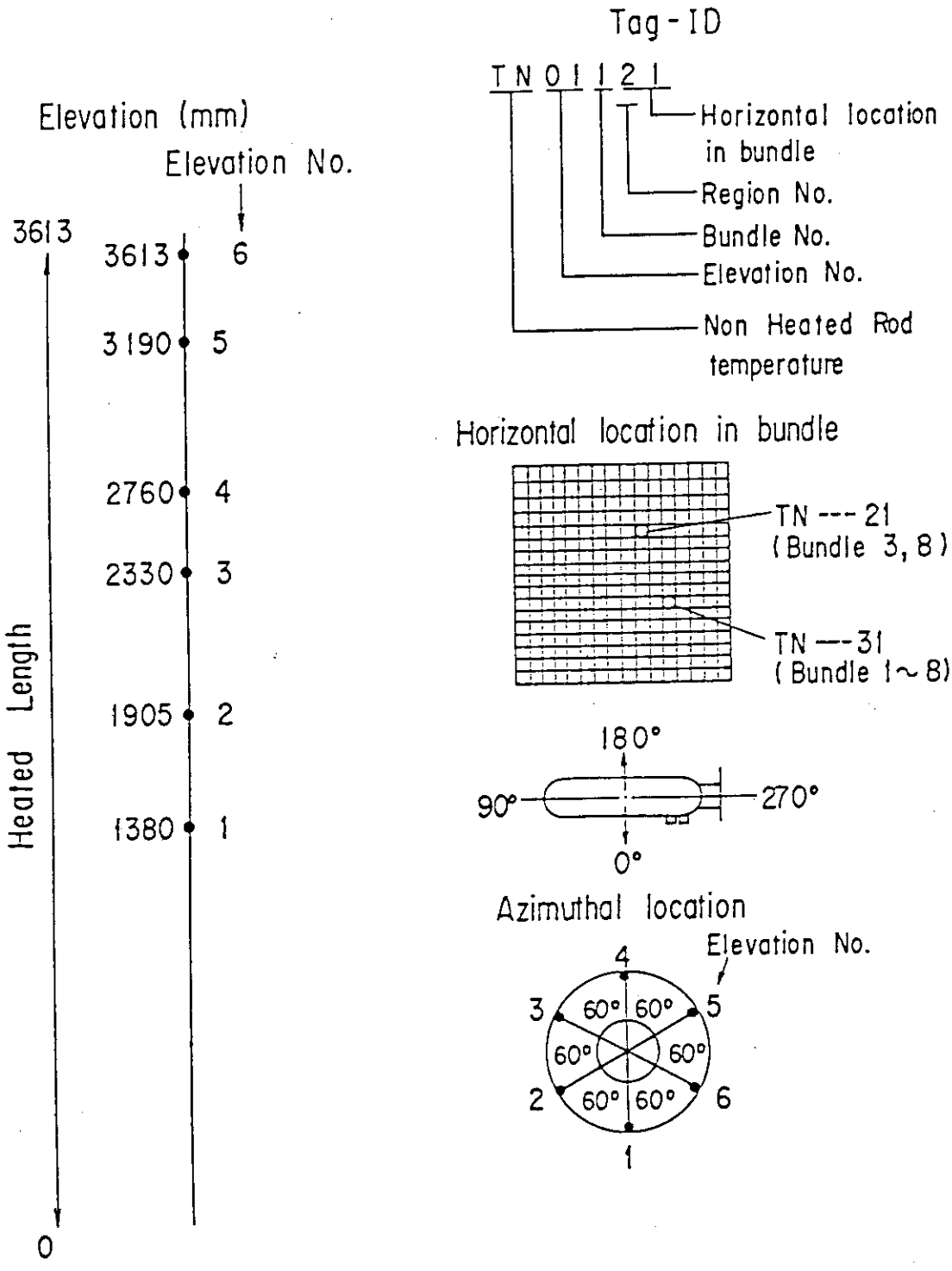

Fig. A-21 Thermocouple locations of non-heated rod surface temperature measurements

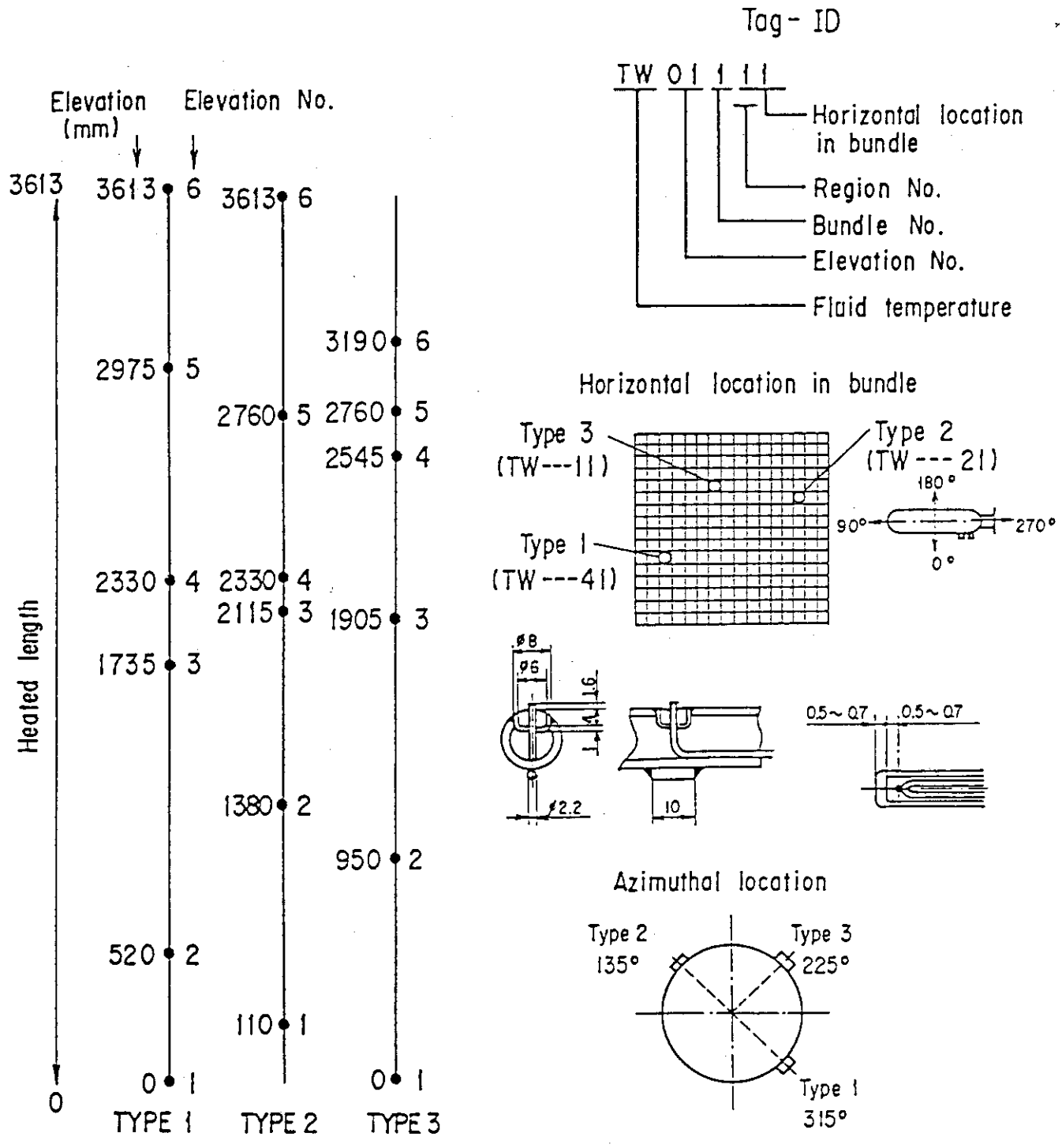

Fig. A-22 Thermocouple locations of fluid temperature measurements in core

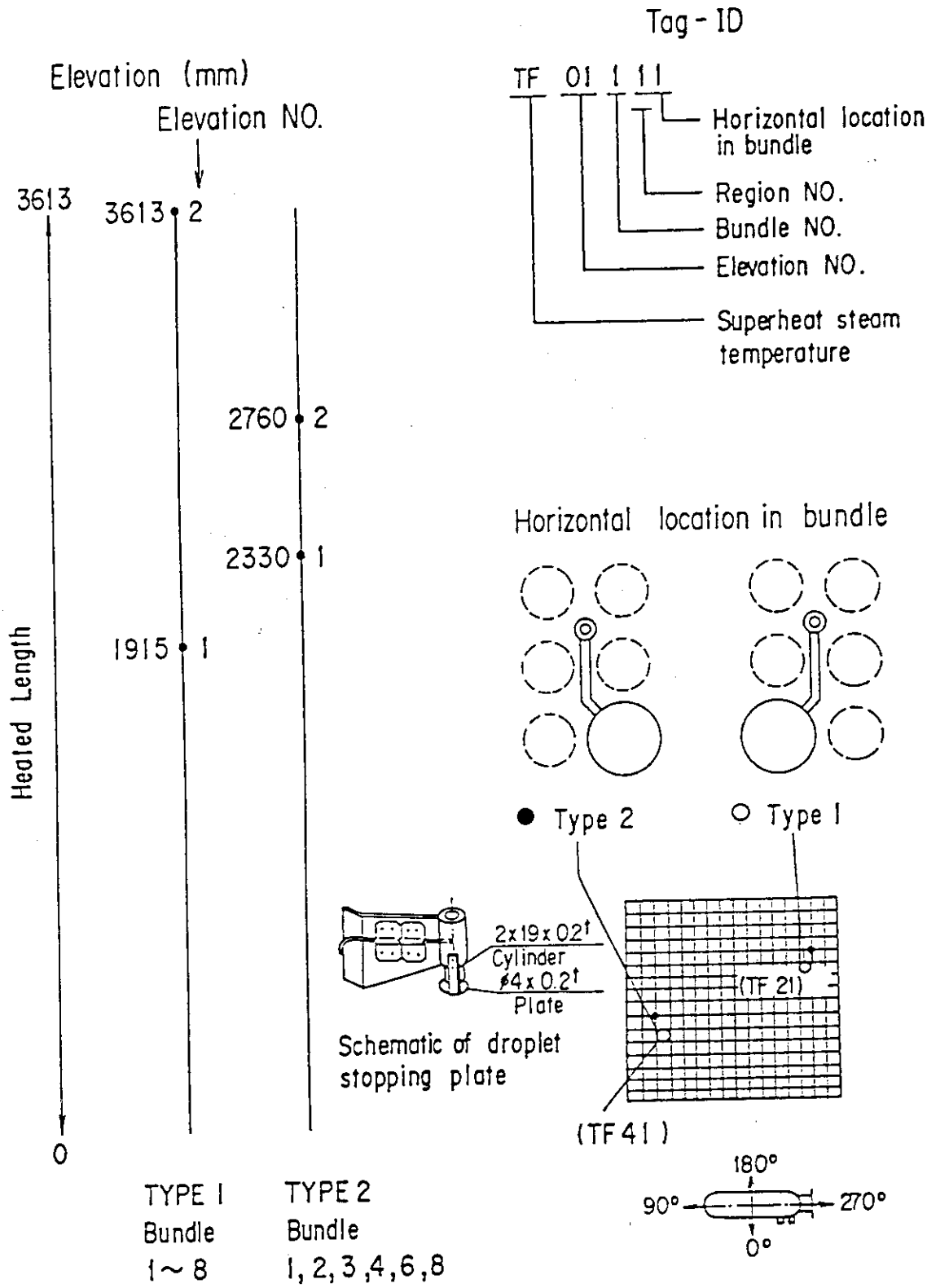

Fig. A-23 Thermocouple locations of steam temperature measurements in core

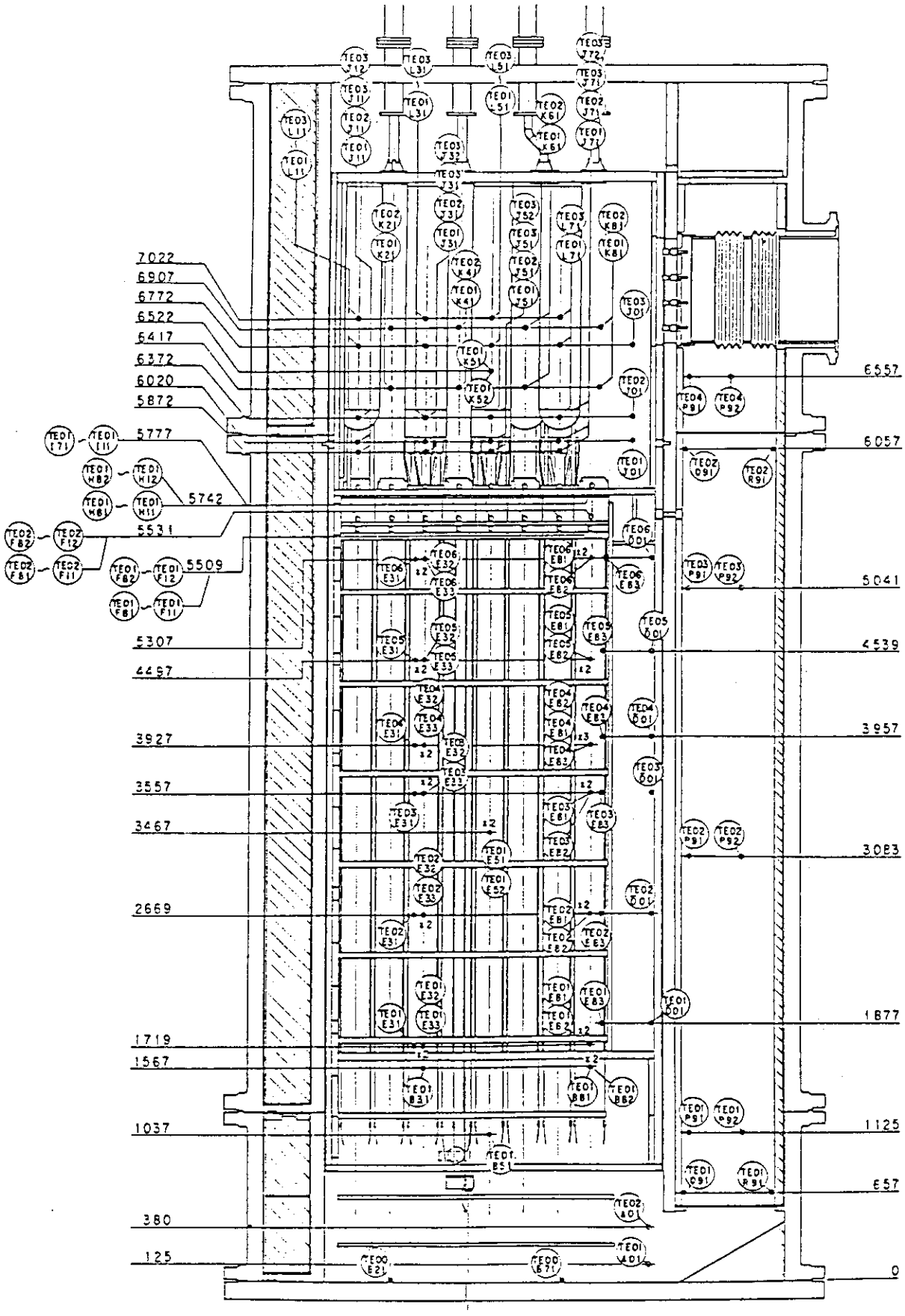

Fig. A-24 Thermocouple locations of temperature measurements in pressure vessel except core region (vertical view)

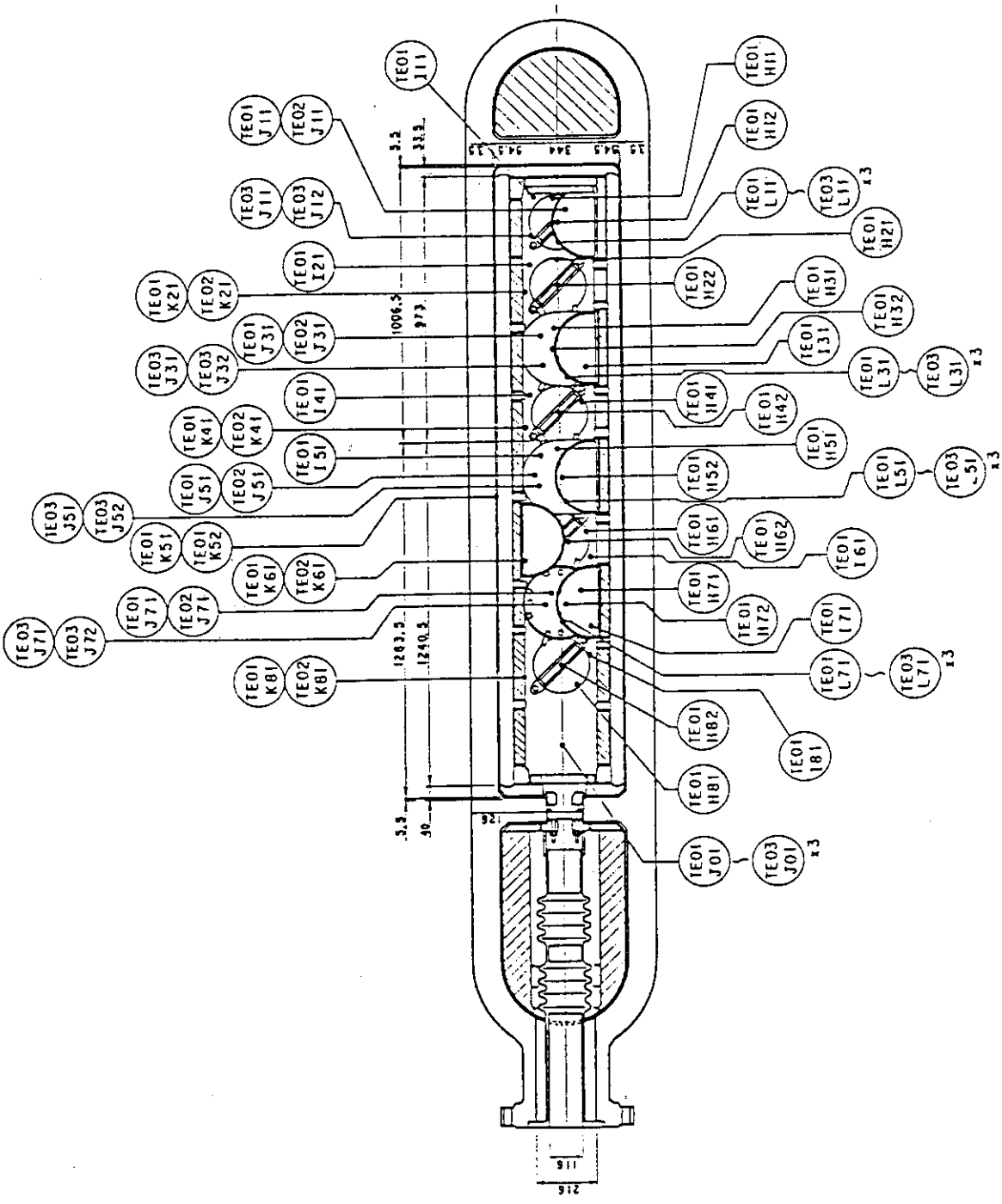

Fig. A-25 Thermocouple locations of temperature measurements in upper plenum (horizontal view)

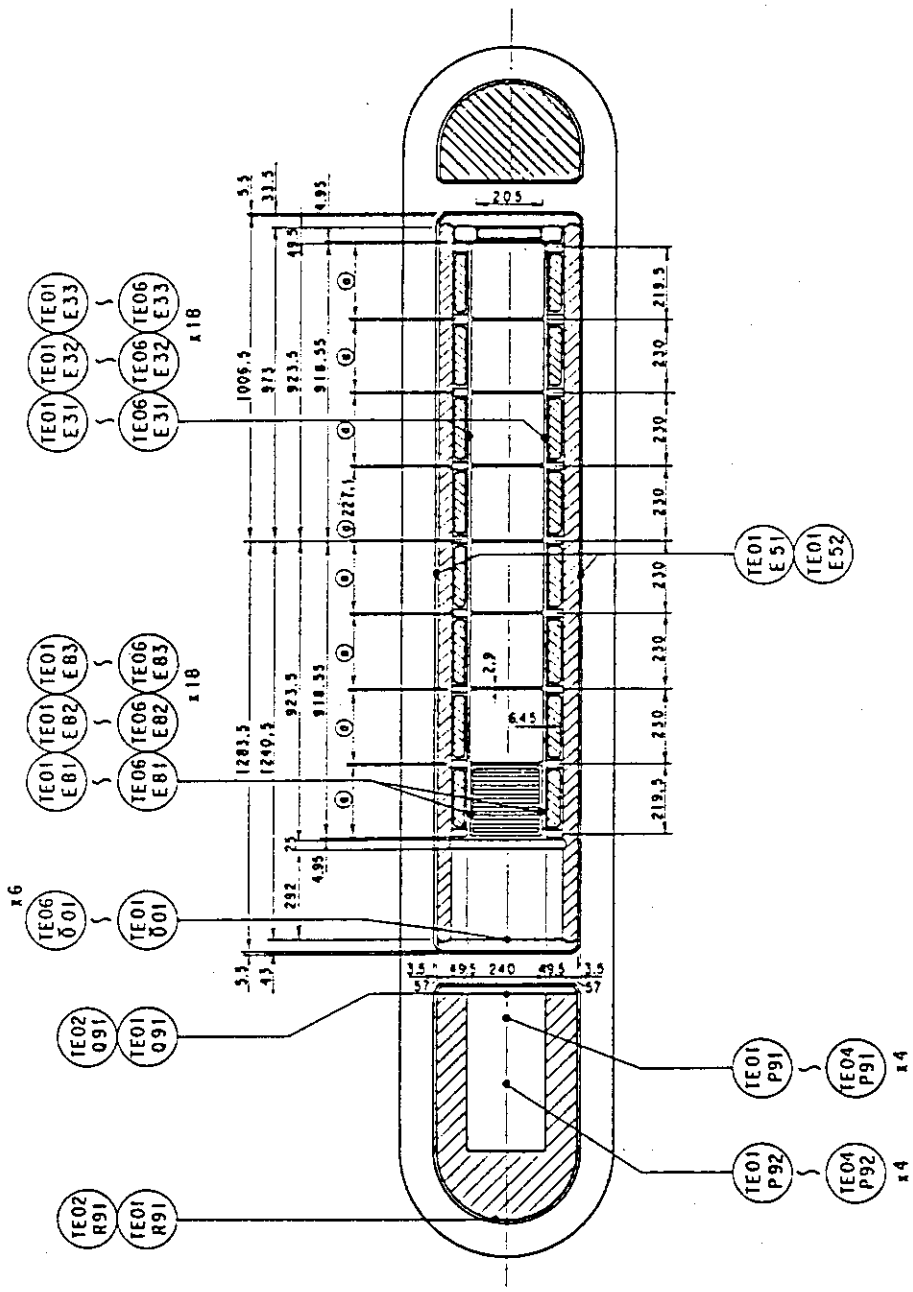

Fig. A-26 Thermocouple locations of temperature measurements in pressure vessel except upper plenum (horizontal view)

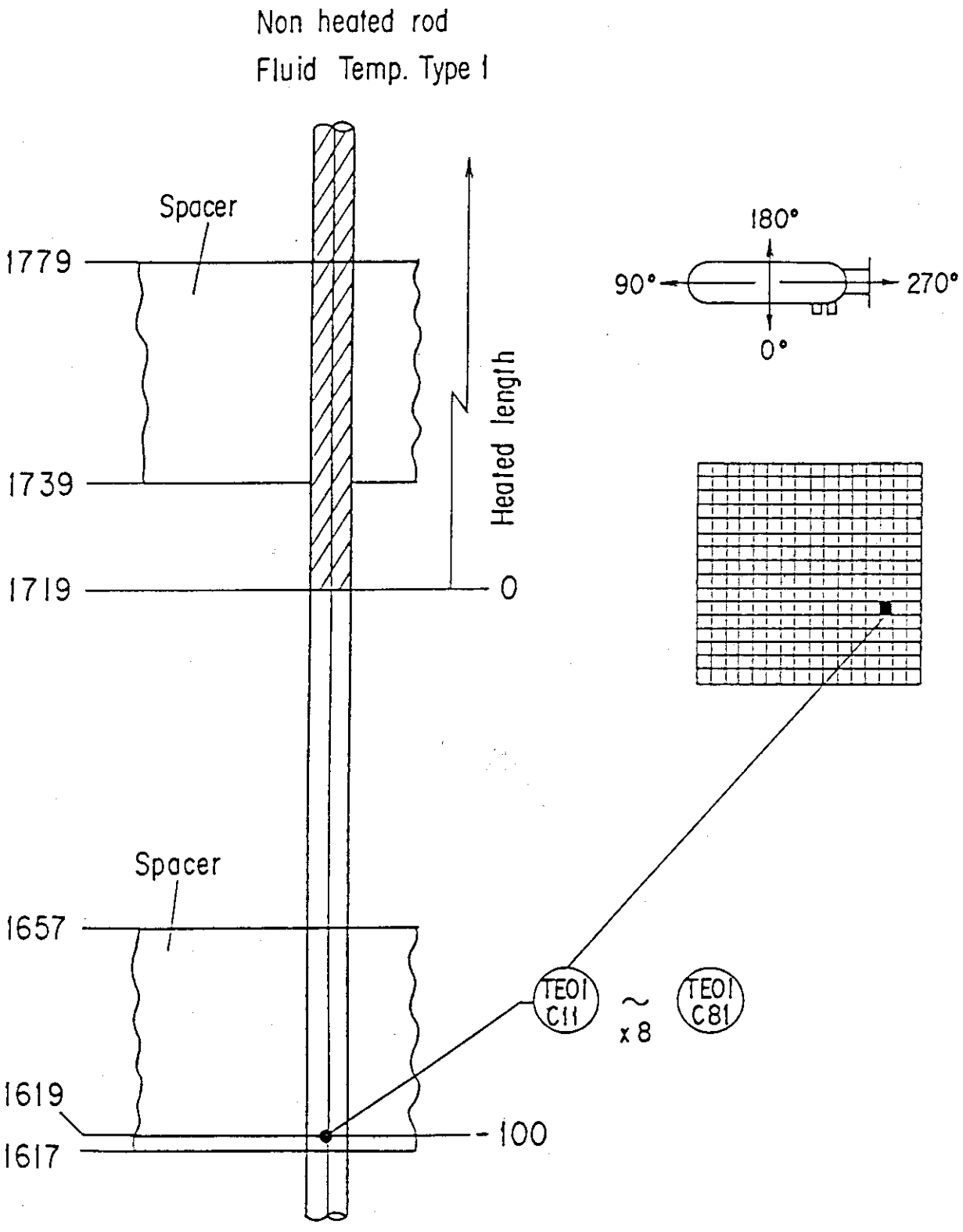

Fig. A-27 Thermocouple locations of fluid temperature measurements at core inlet

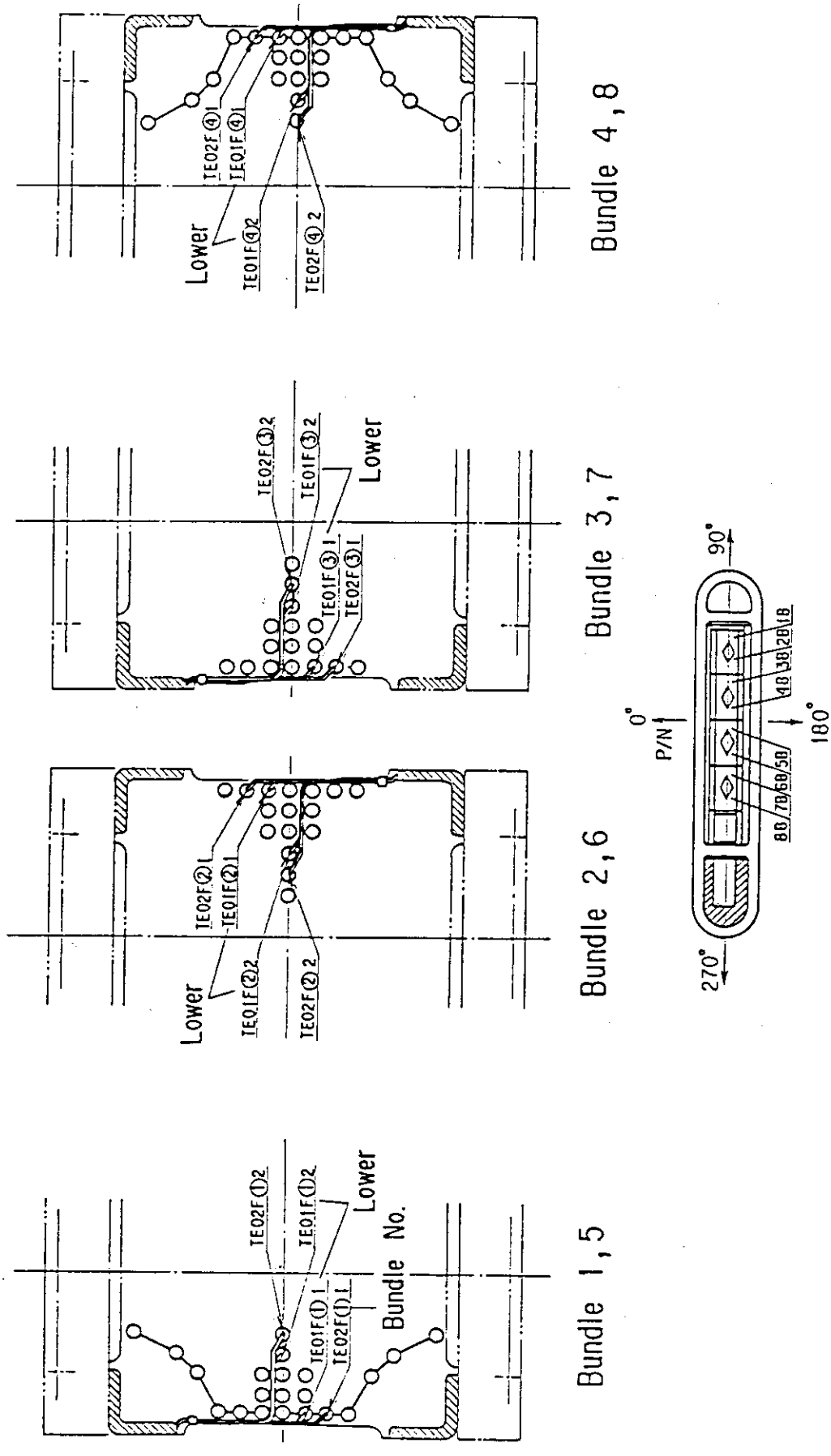

Fig. A-28 Thermocouple locations of fluid temperature measurements just above and below end box tie plates

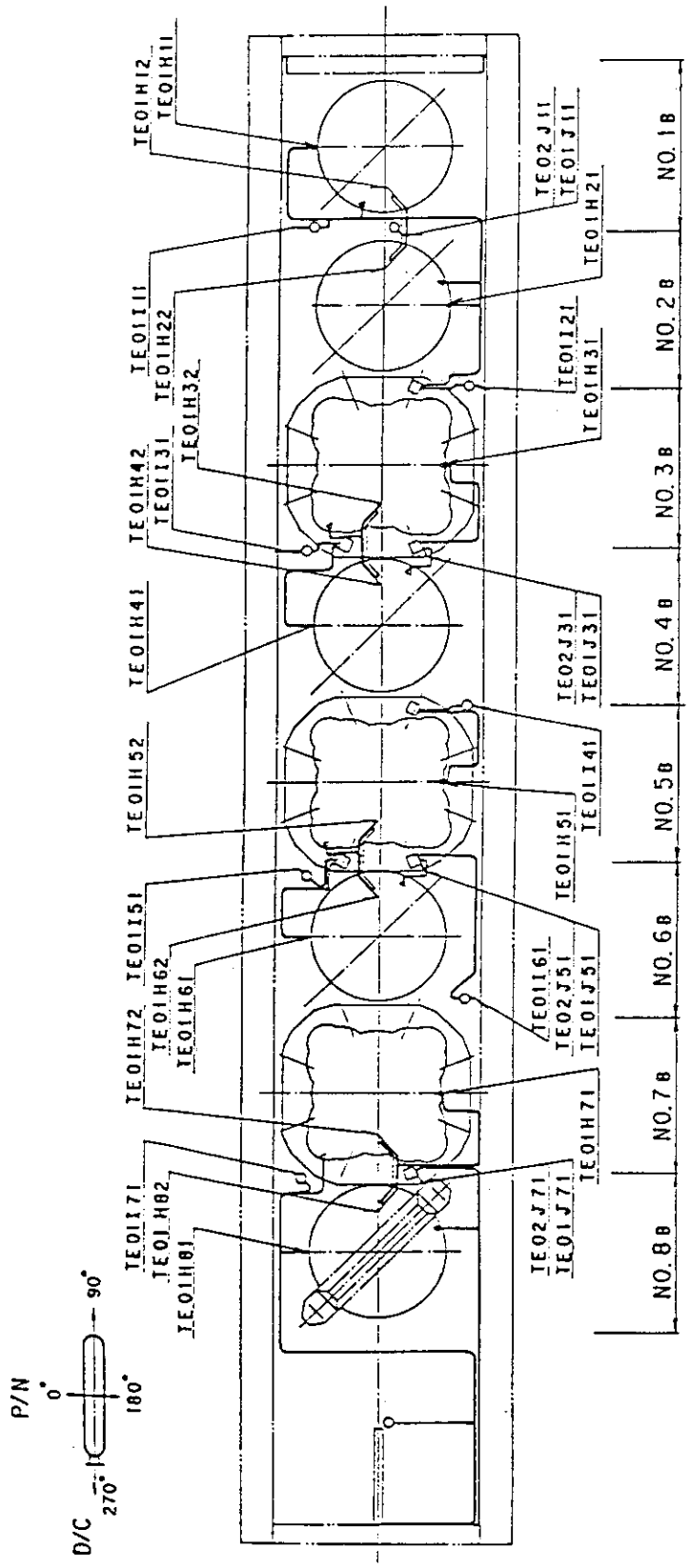

Fig. A-29 Thermocouple locations of fluid temperature measurements on UCSP and at inside and periphery of UCSP holes

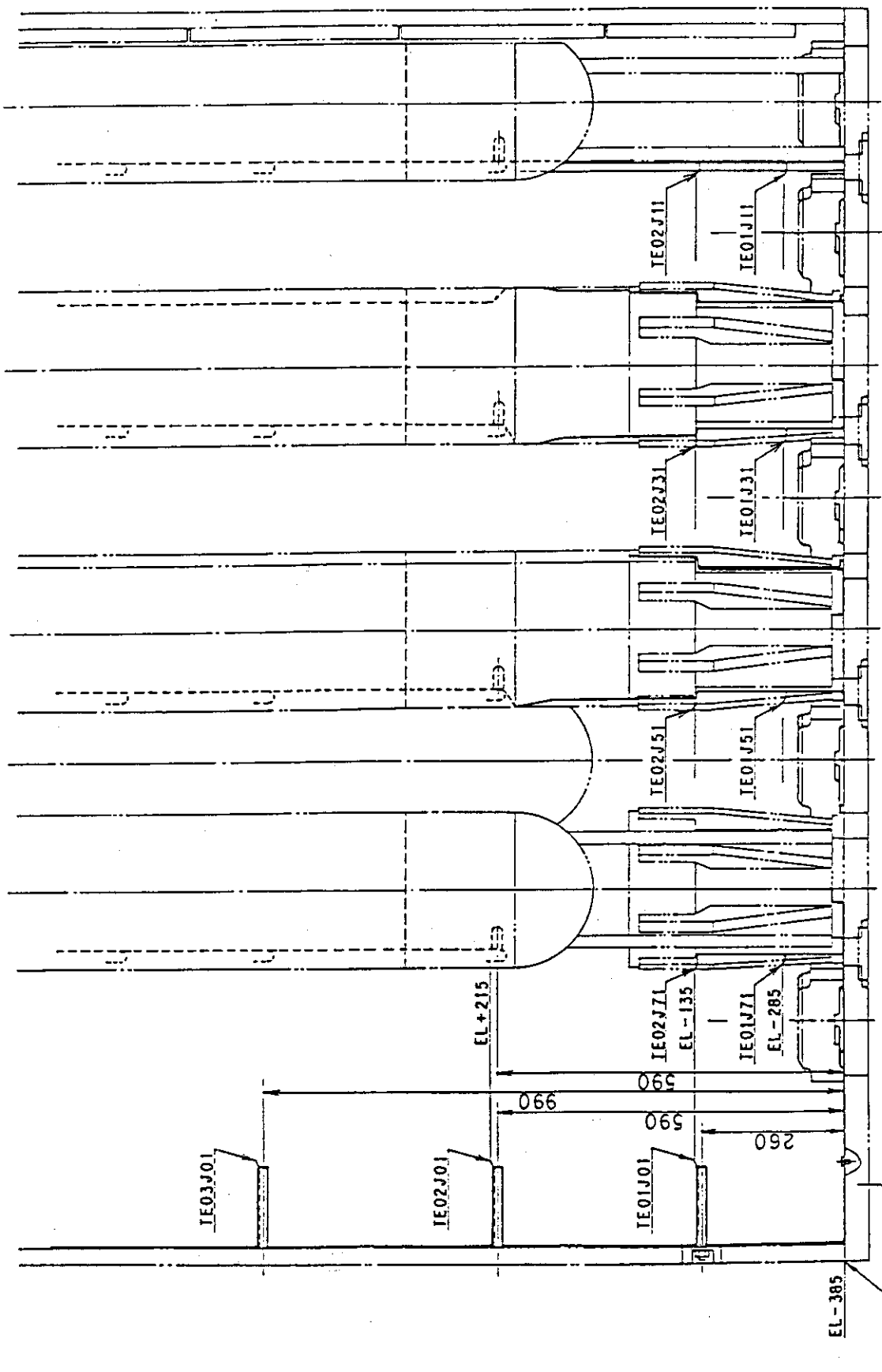

Fig. A-30 Thermocouple locations of fluid temperature measurements on and above UCSP

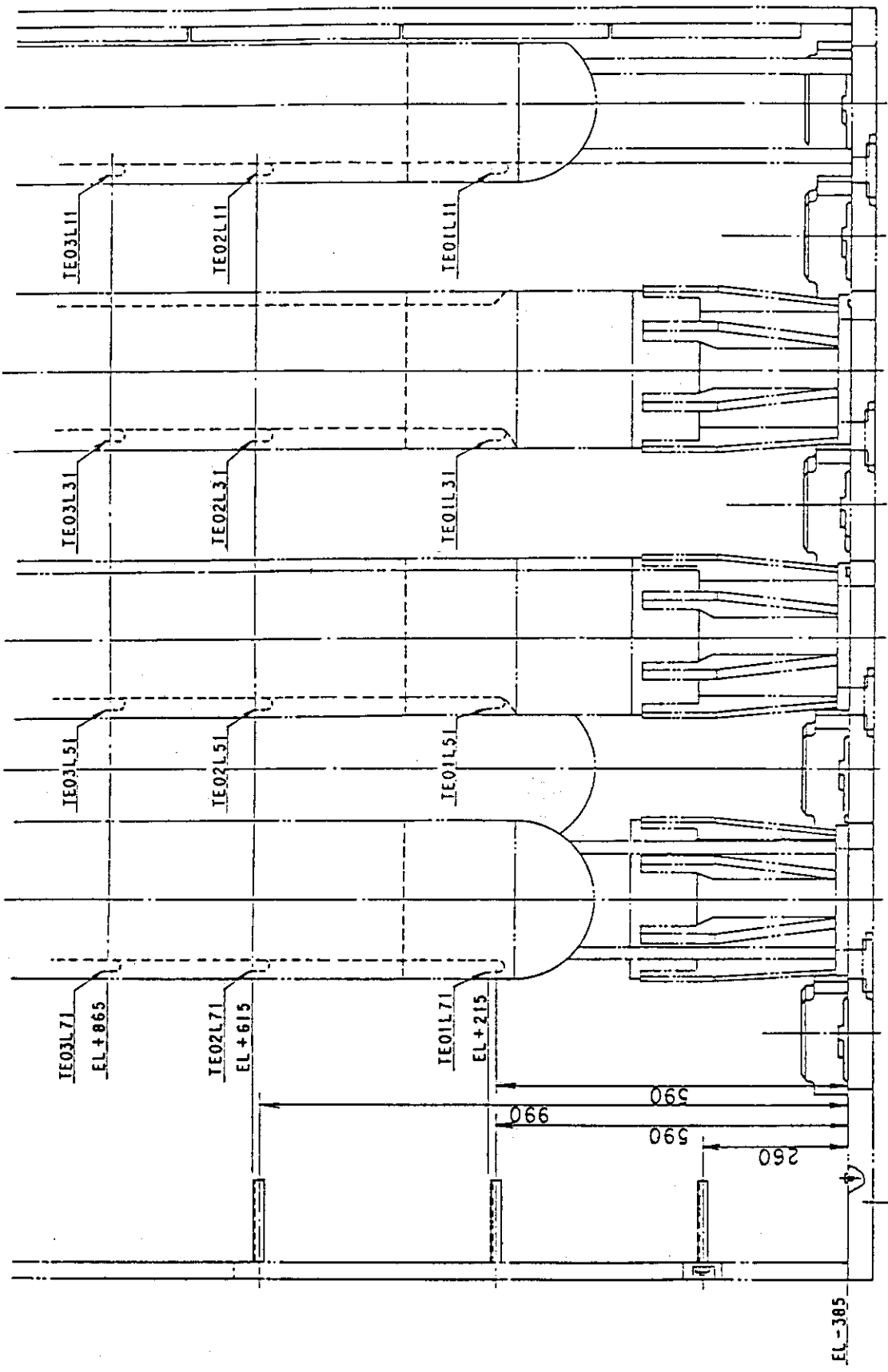

Fig. A-31 Thermocouple locations of surface temperature measurements of upper plenum structures

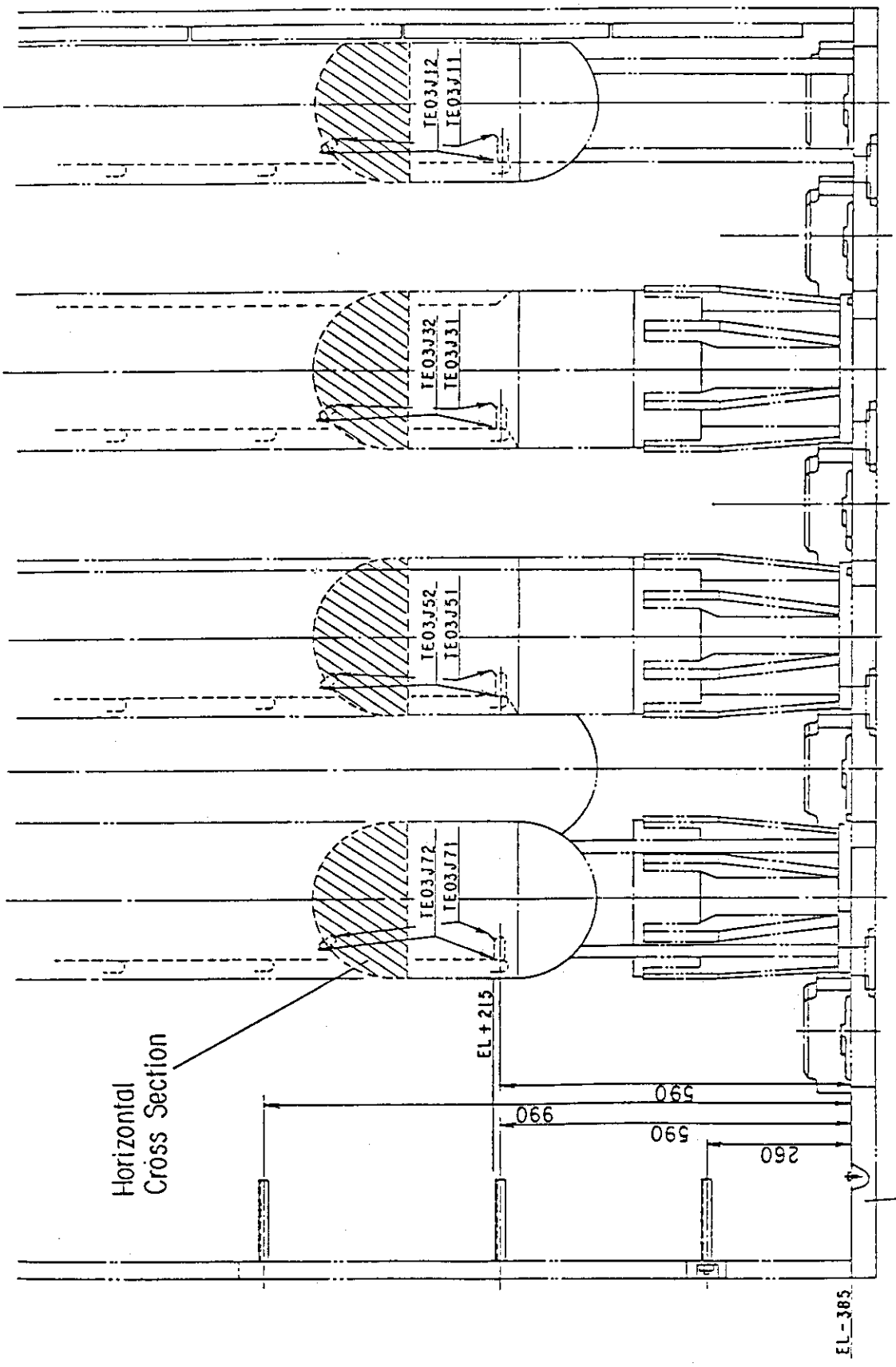

Fig. A-32 Thermocouple locations of steam temperature measurements above UCSP holes

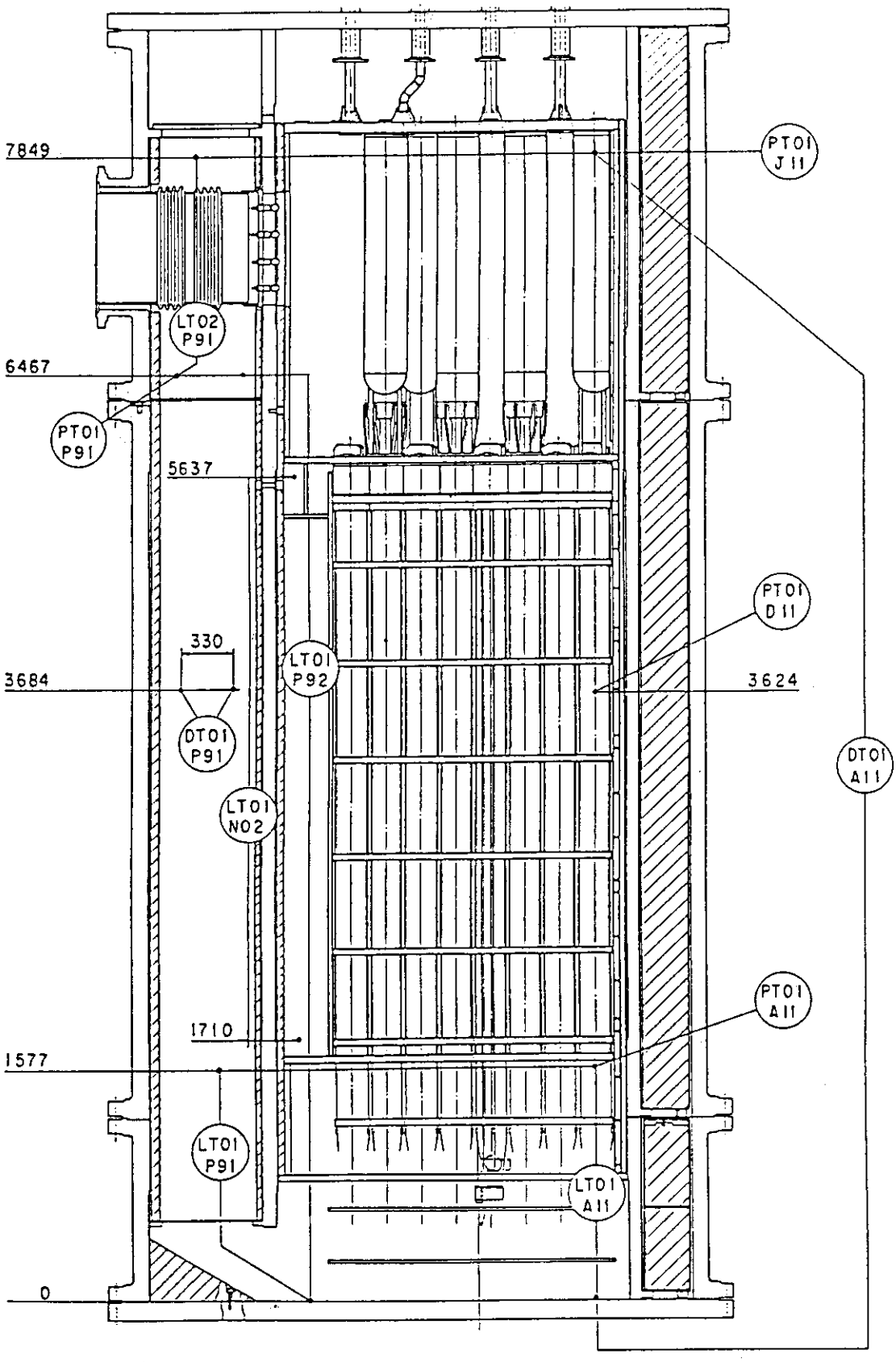

Fig. A-33 Locations of pressure measurements in pressure vessel, differential pressure measurements between upper and lower plenums and liquid level measurements in downcomer and lower plenums

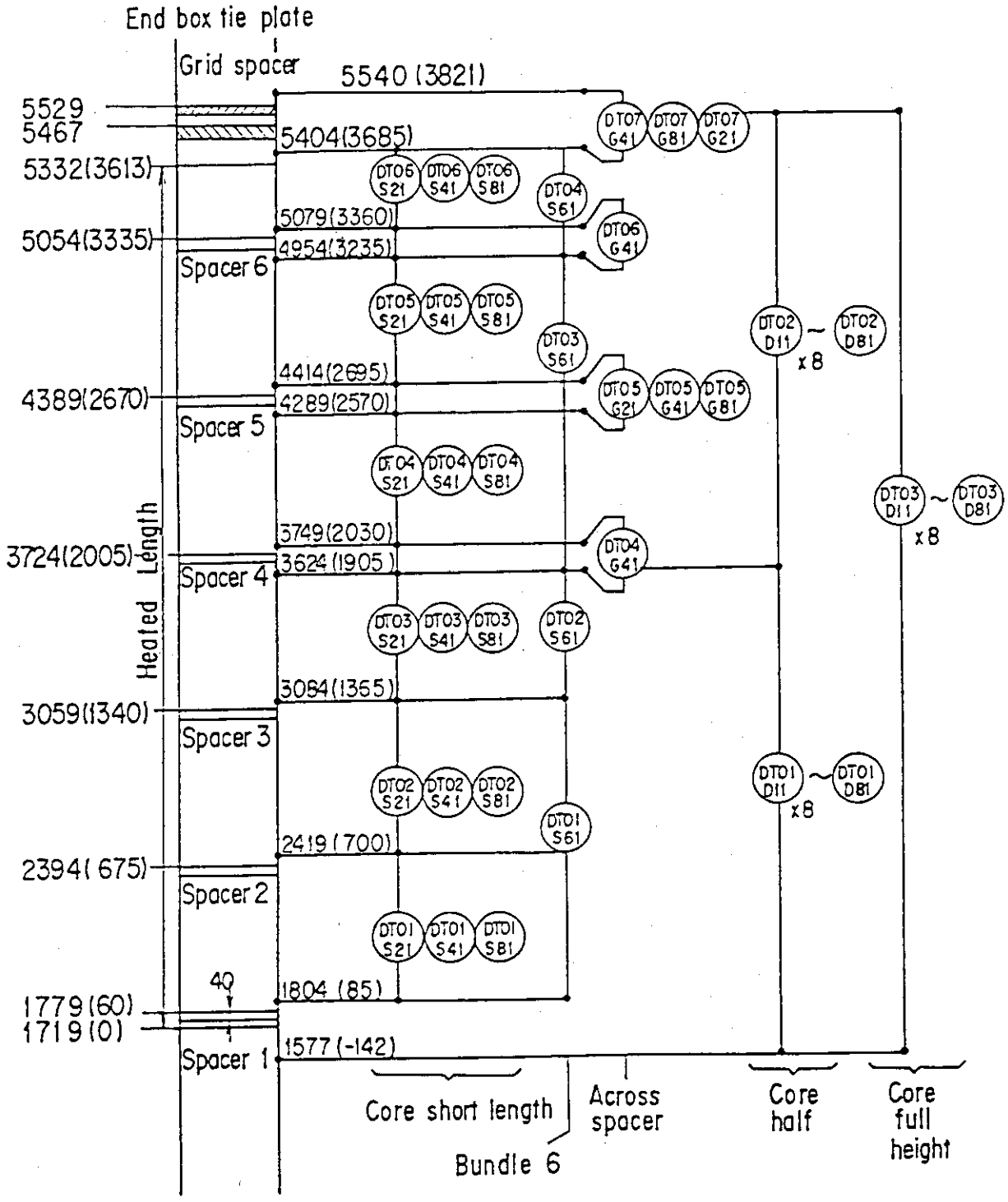

Fig. A-34 Locations of vertical differential pressure measurements in core

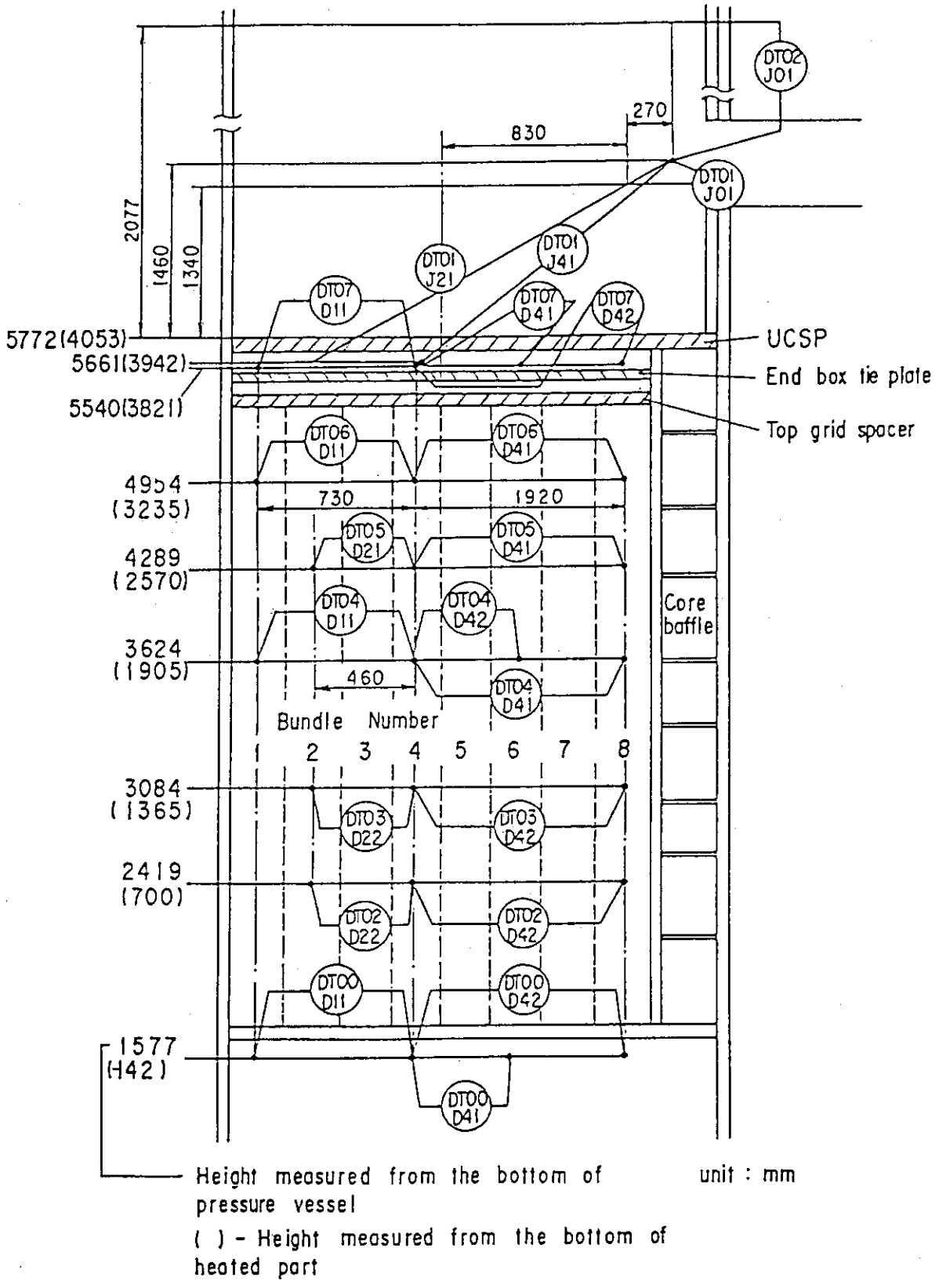

Fig. A-35 Locations of horizontal differential pressure measurements in core and differential pressure measurements between end boxes and inlet of hot leg

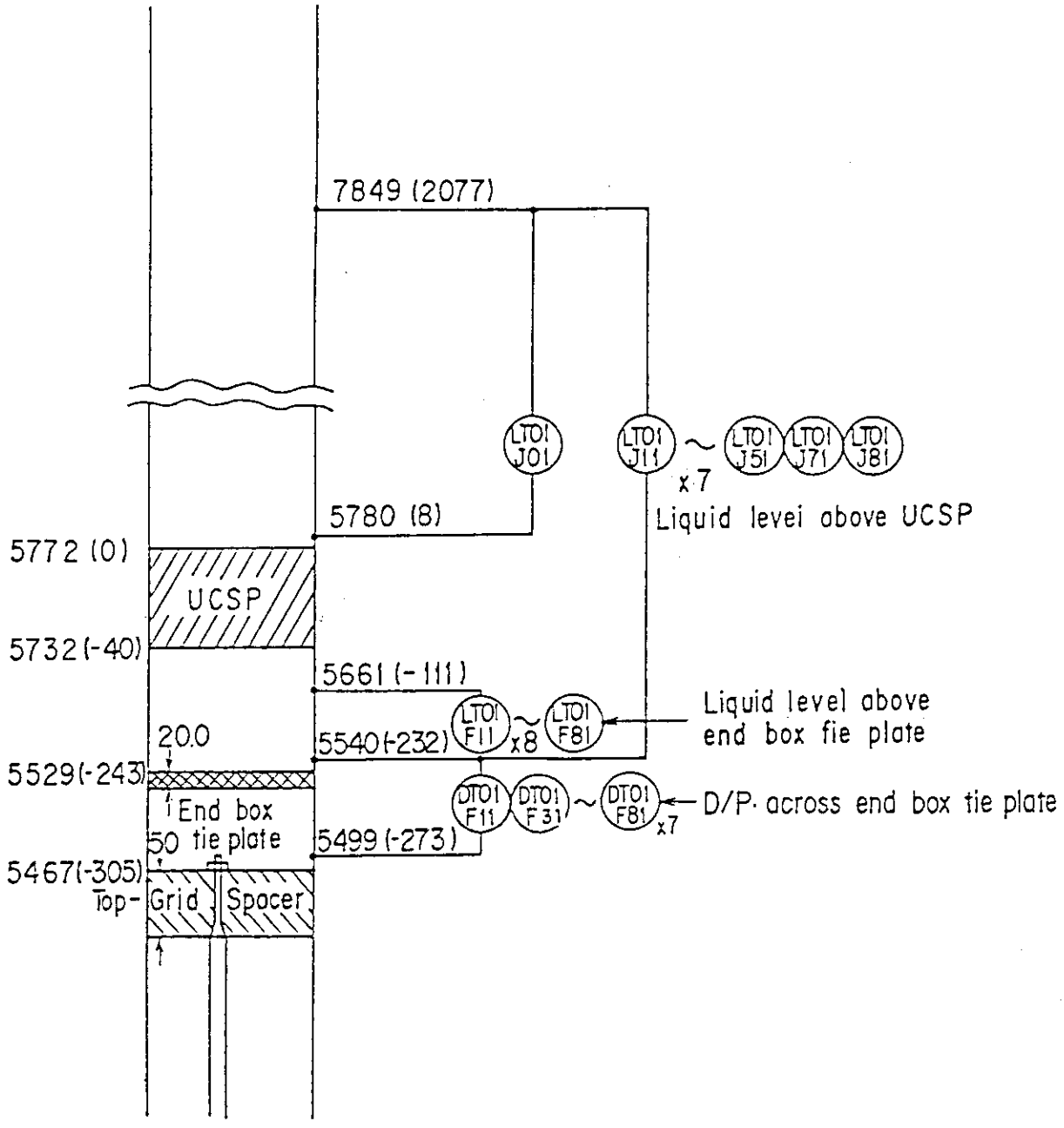

Fig. A-36 Locations of differential pressure measurements across end box tie plate

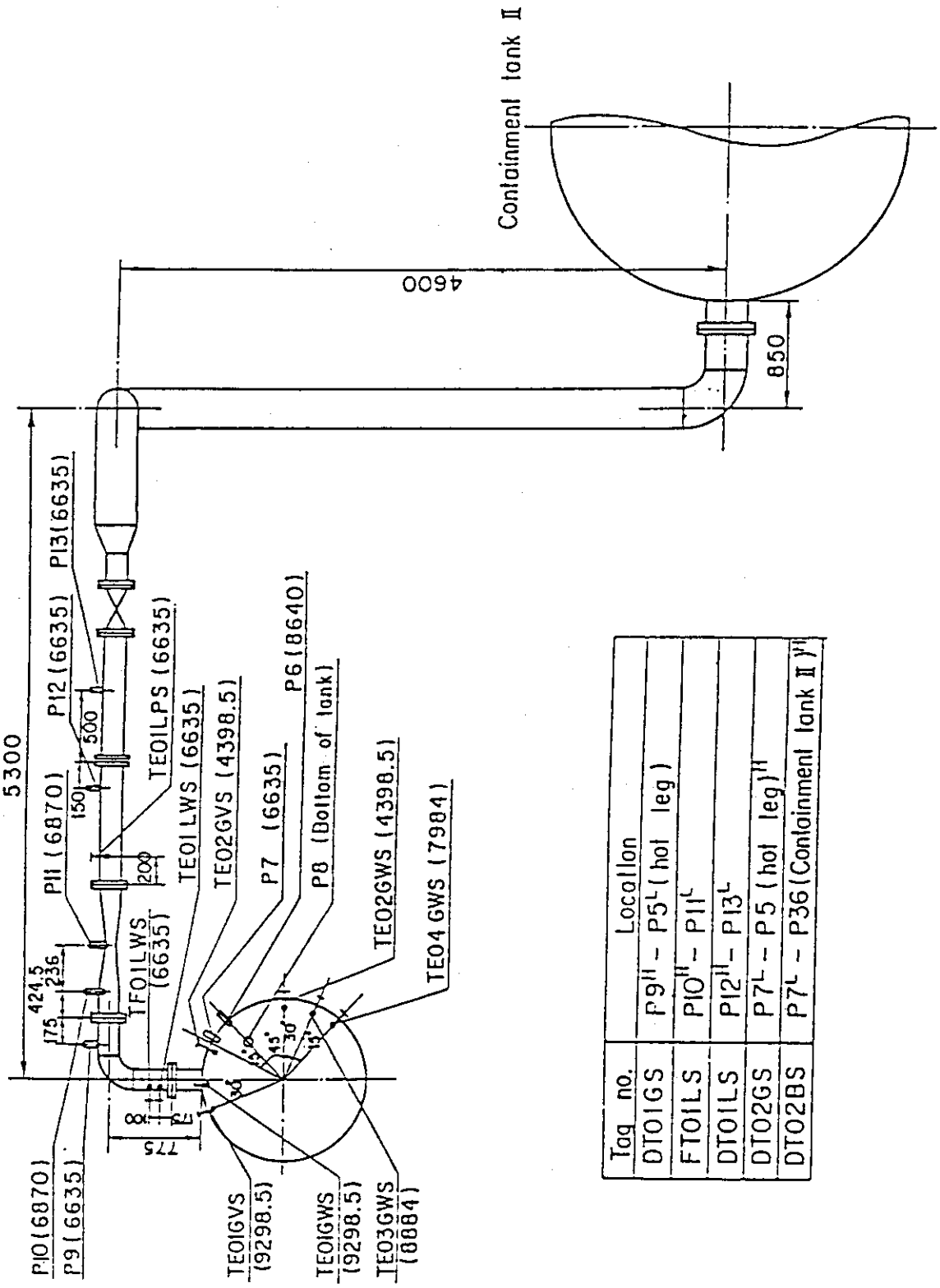

Tag no.	Location
DT01GS	$P9^{H}$ − $P5^{L}$ (hot leg)
FT01LS	$P10^{H}$ − $P11^{L}$
DT01LS	$P12^{H}$ − $P13^{L}$
DT02GS	$P7^{L}$ − P5 (hot leg)^{H}
DT02BS	$P7^{L}$ − P36(Containment tank II)^{H}

Fig. A-37 Locations of broken cold leg instruments (steam-water separator side)

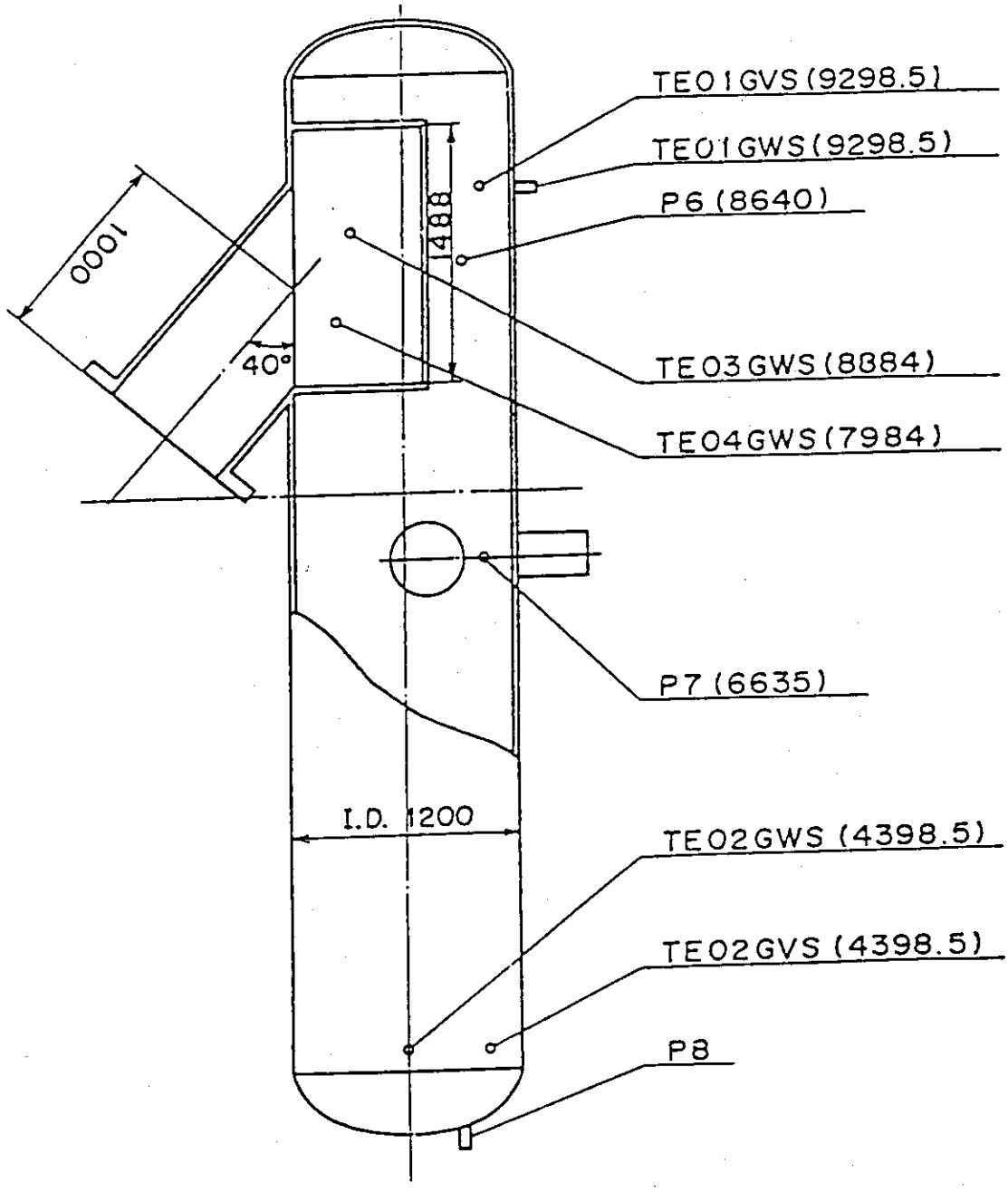

Fig. A-38 Locations of steam-water separator instruments

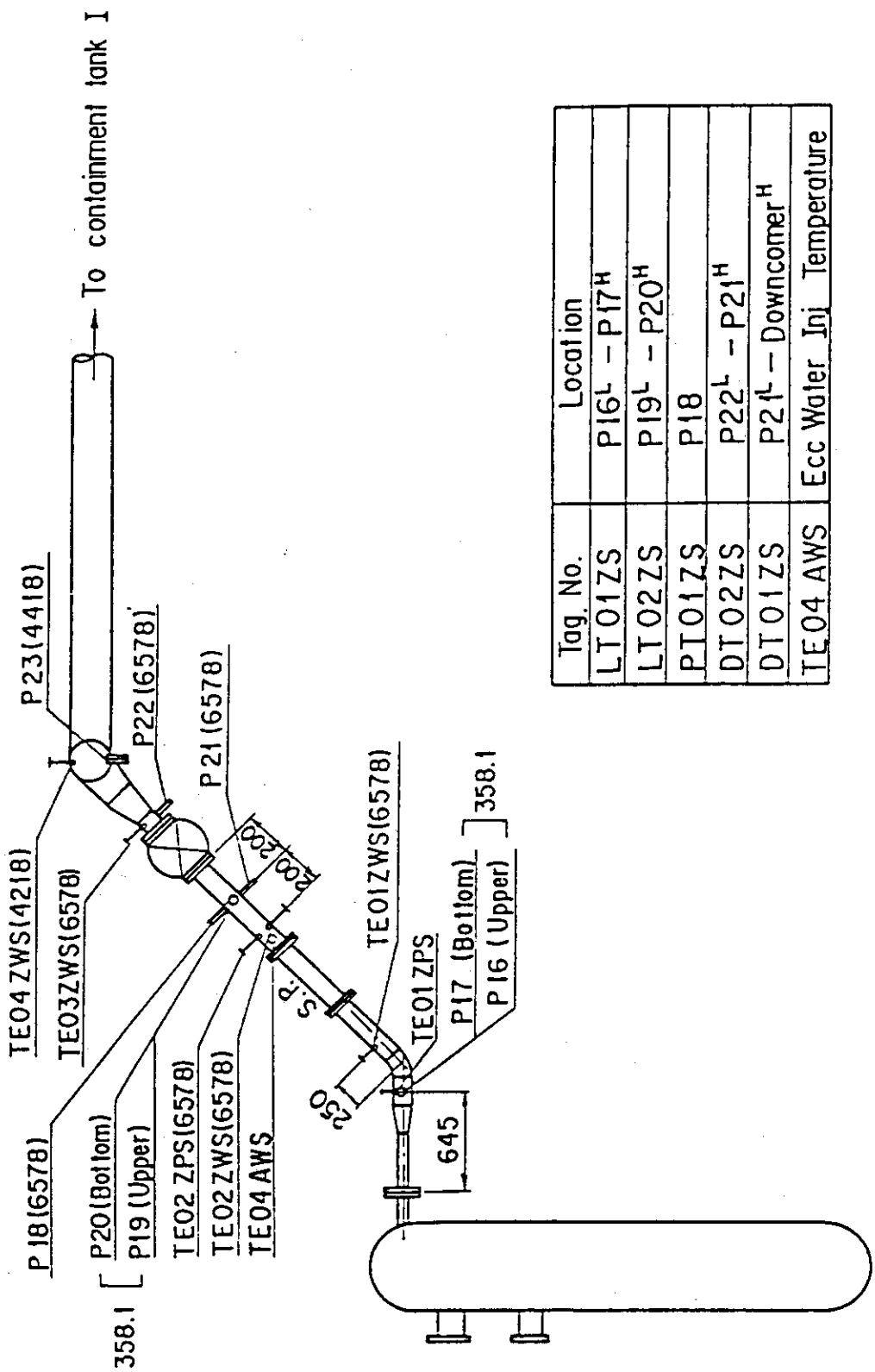

Tag. No.	Location
LT01ZS	$P16^{L} - P17^{H}$
LT02ZS	$P19^{L} - P20^{H}$
PT01ZS	P18
DT02ZS	$P22^{L} - P21^{H}$
DT01ZS	$P21^{L}$ — Downcomer^{H}
TE04 AWS	Ecc Water Inj Temperature

Fig. A-39 Locations of broken cold leg instruments (pressure vessel side)

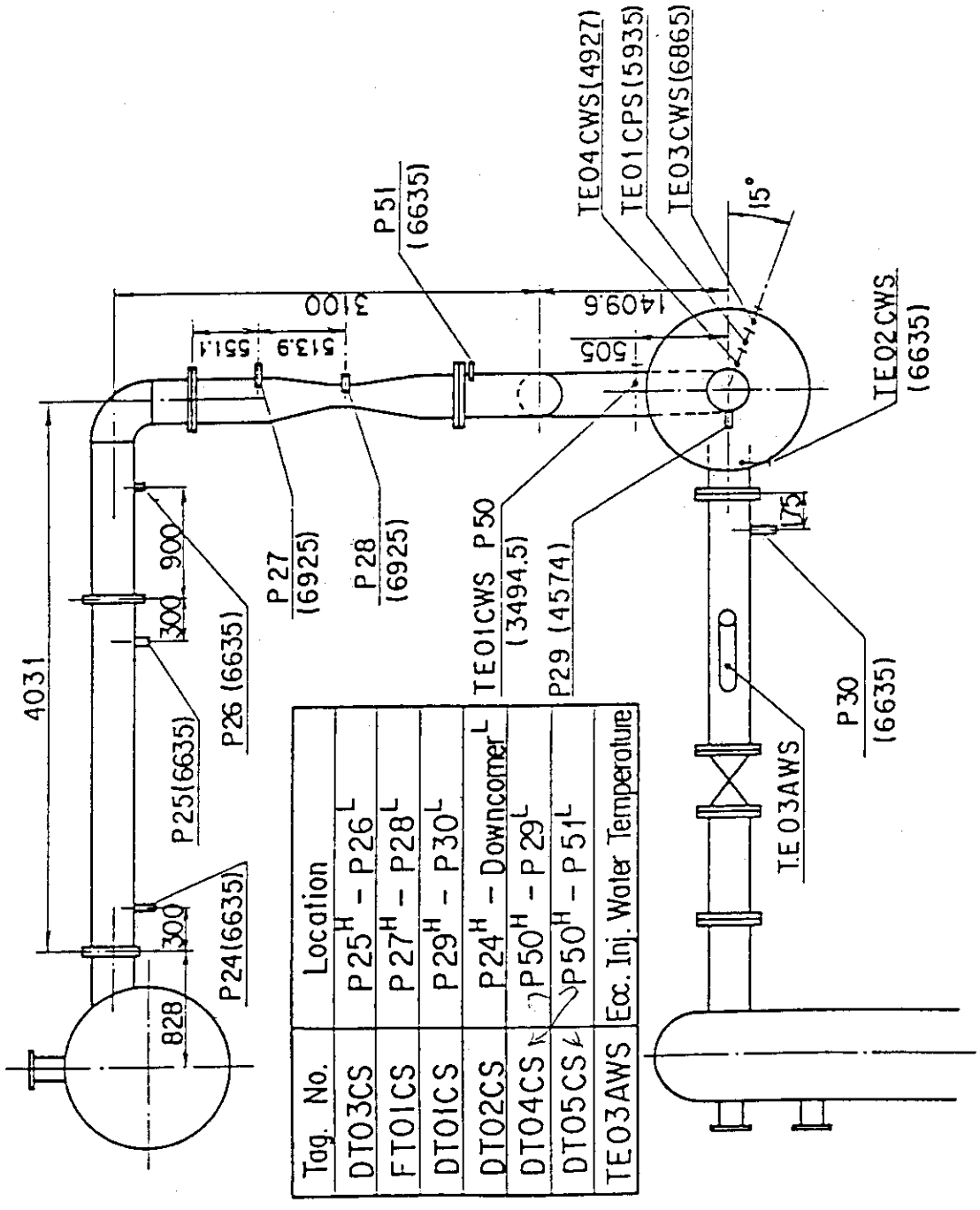

Fig. A-40 Locations of intact cold leg instruments

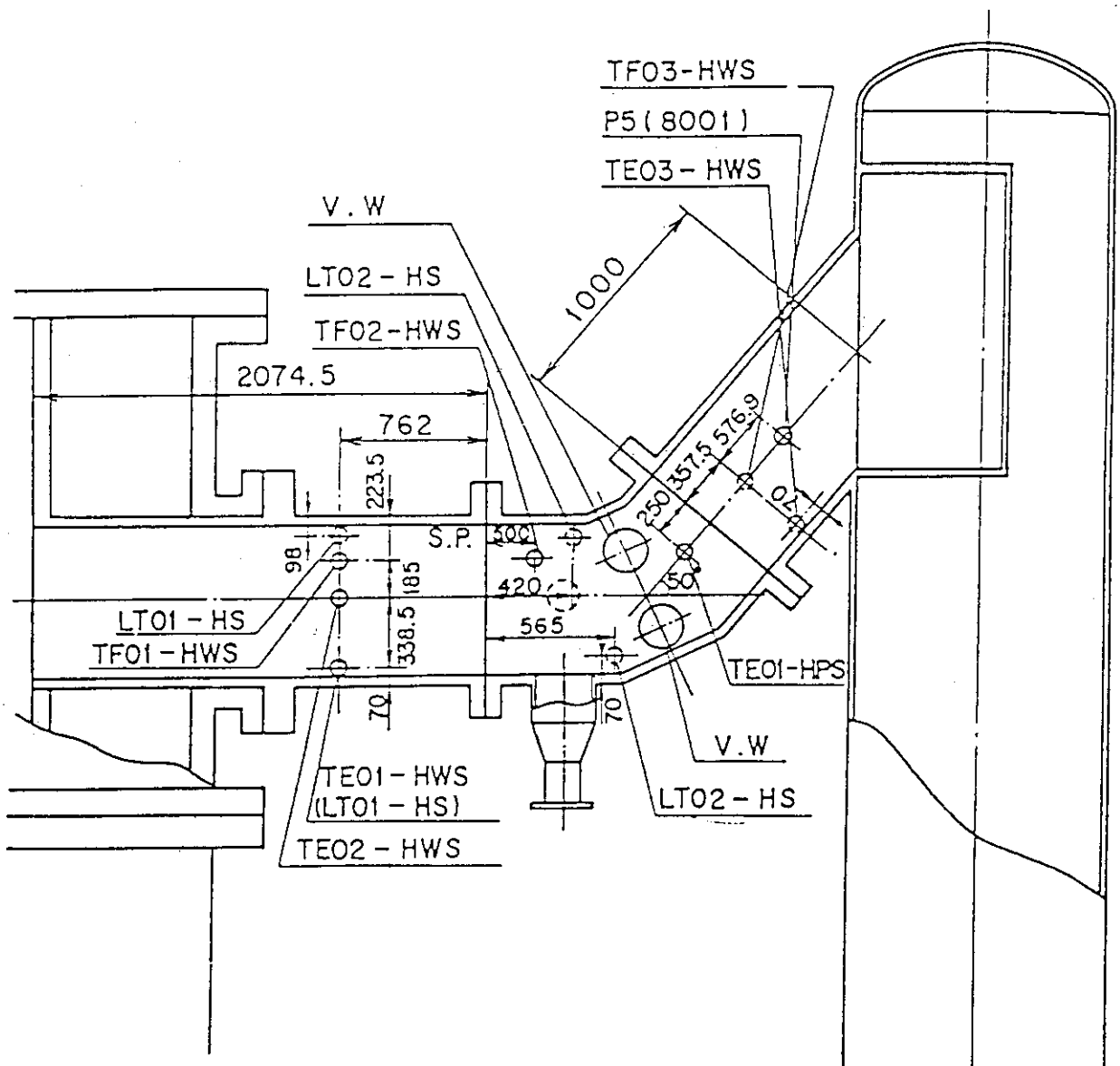

Tag no.	Location
DT01HS	P5^{L}－Inlet of hot leg^{H}
DT01GS	P5^{L}－Broken cold leg (S-W separator side)^{H}
DT02GS	P5^{H}－S-W separator tank^{L}

Fig. A-41 Locations of hot leg instruments

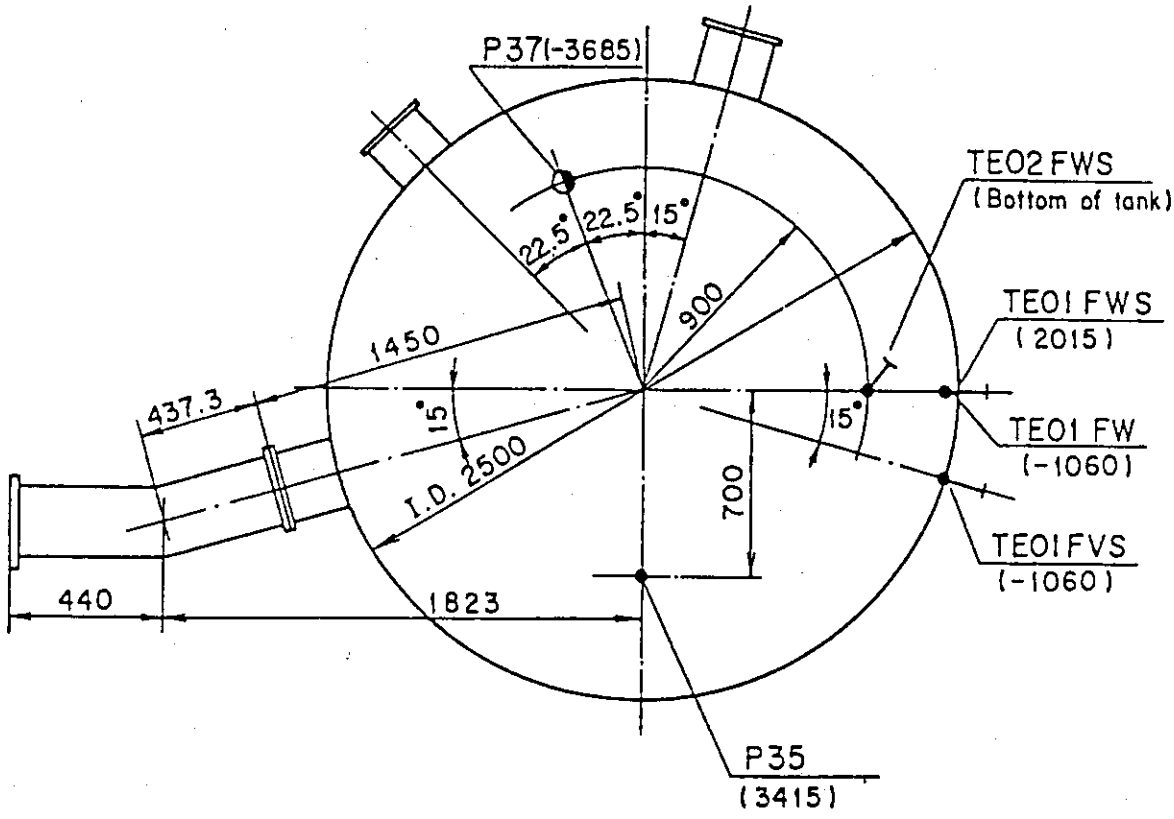

Tag. no.	Location
LT01FS	$P35^{L}$ – $P37^{H}$
DT01FS	$P35^{H}$ – $Downcomer^{L}$
DT01E	$P35^{L}$ – P36(C.T. II)^{H}
PT01F	P35

Fig. A-42 Locations of containment tank-I instruments

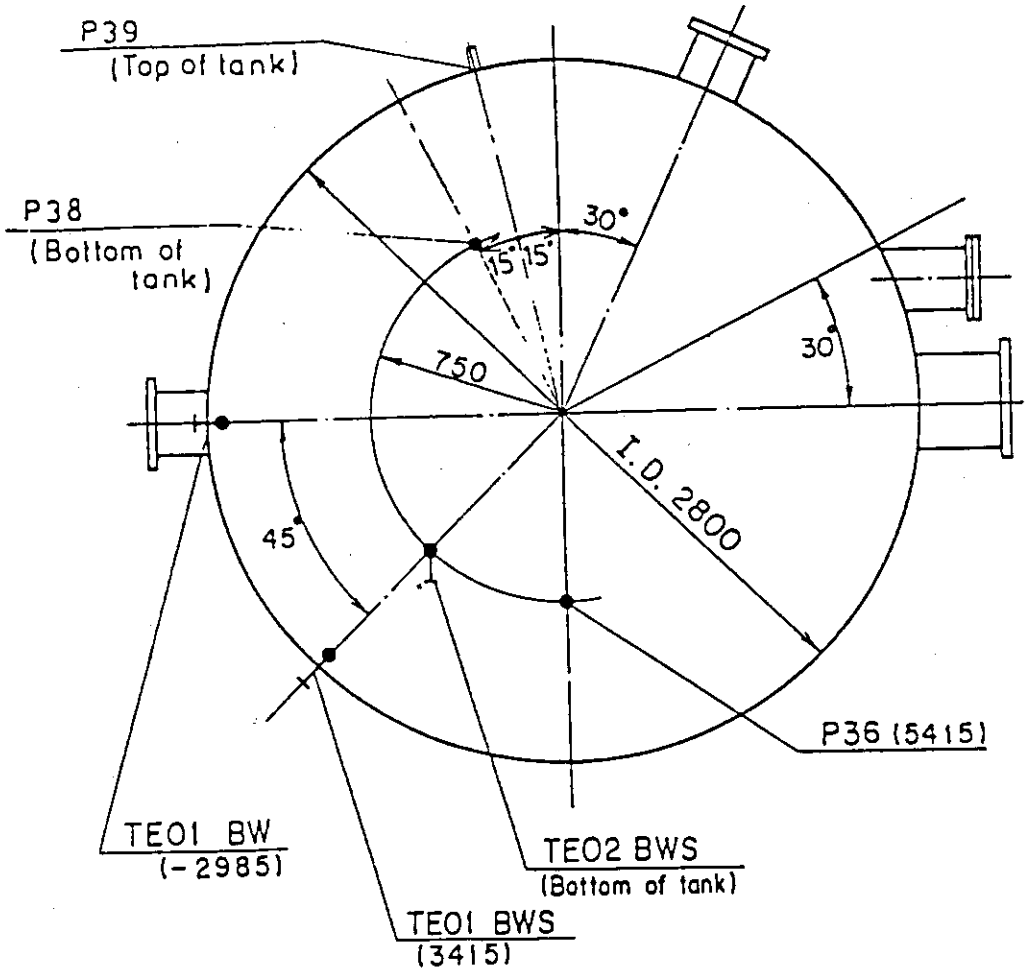

Tag no.	Location
DT01 BS	P36^{H}– Upper plenum^{L}
DT02 BS	P36^{H}– S-W Separator^{L}
DT01 E	P36^{H}– P35 (C.T.I)^{L}
PT01 B	P36
LT01 1B	P38^{H}– P39^{L}

Fig. A-43 Locations of containment tank-II instruments

Appendix B Selected data of Test S3-3

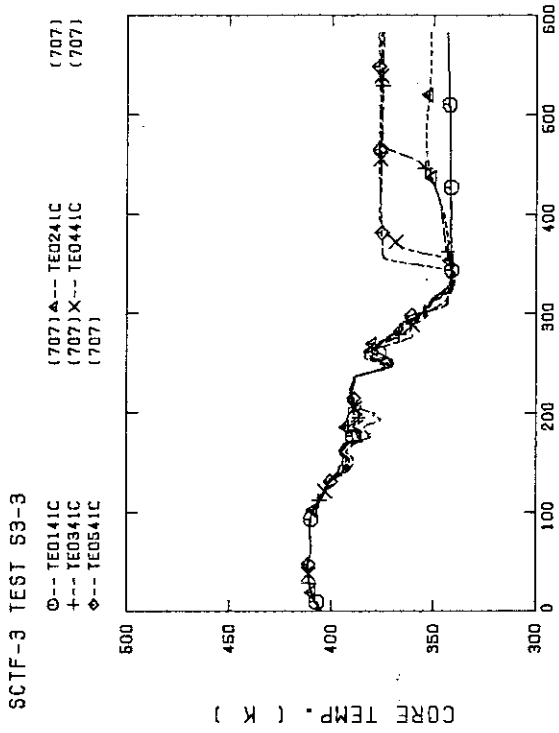

FIG. B-03 HEATER ROD TEMPERATURE
(BUNDLE 4-1C, LOWER HALF)

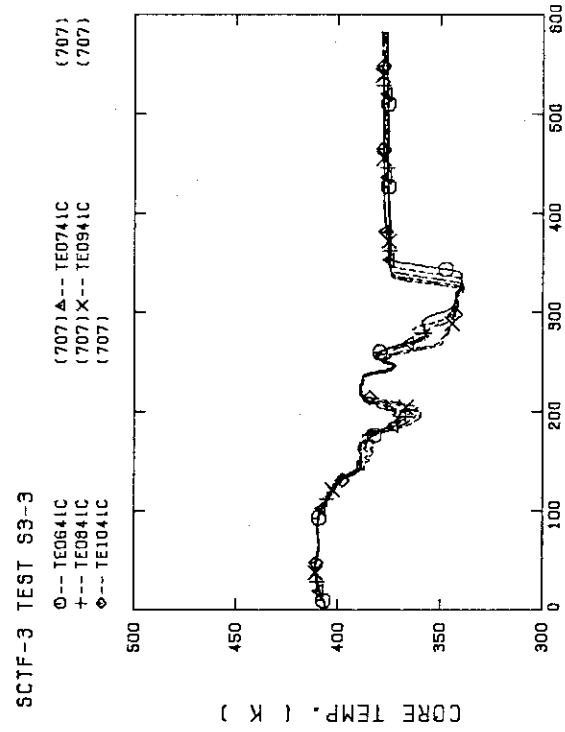

FIG. B-04 HEATER ROD TEMPERATURE
(BUNDLE 4-1C, UPPER HALF)

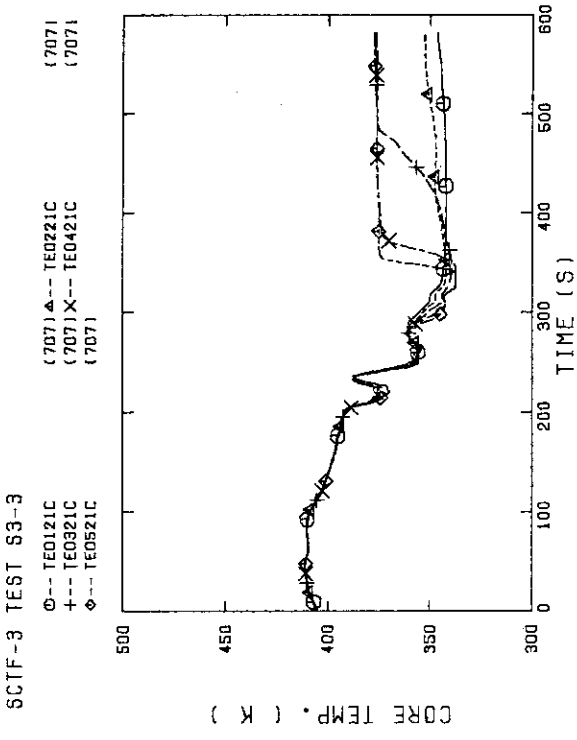

FIG. B-01 HEATER ROD TEMPERATURE
(BUNDLE 2-1C, LOWER HALF)

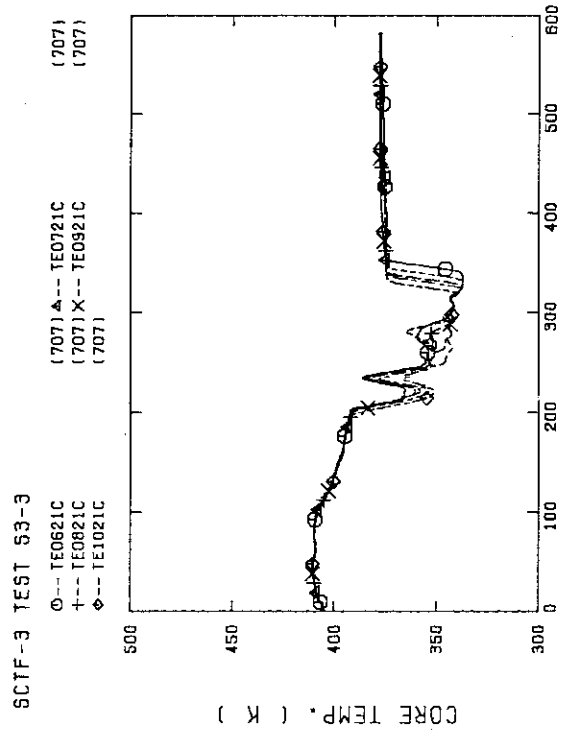

FIG. B-02 HEATER ROD TEMPERATURE
(BUNDLE 2-1C, UPPER HALF)

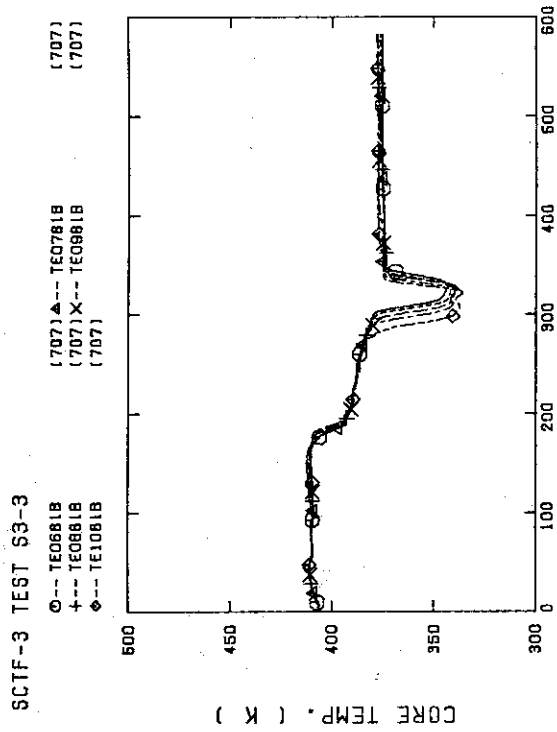

FIG. B-07 HEATER ROD TEMPERATURE (BUNDLE 8-1B, UPPER HALF)

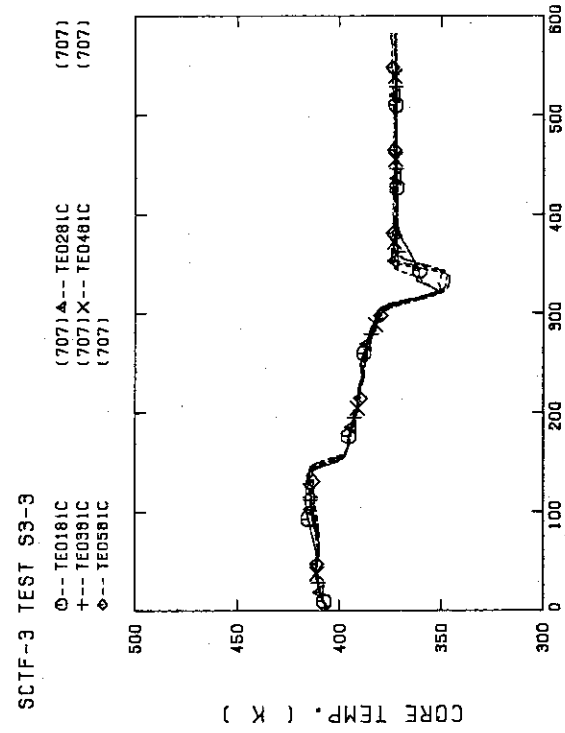

FIG. B-08 HEATER ROD TEMPERATURE (BUNDLE 8-1C, LOWER HALF)

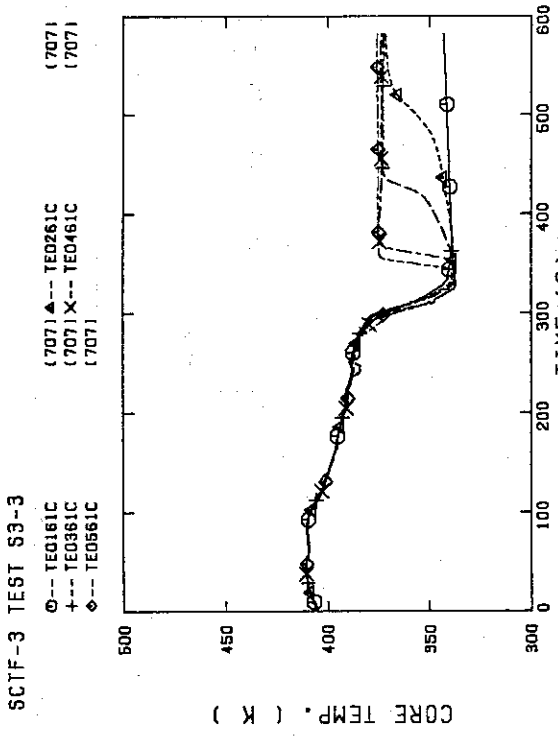

FIG. B-05 HEATER ROD TEMPERATURE (BUNDLE 6-1C, LOWER HALF)

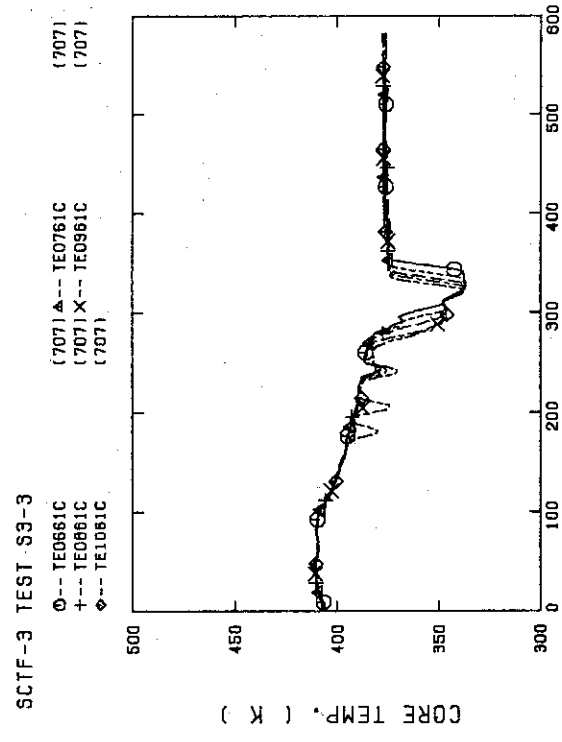

FIG. B-06 HEATER ROD TEMPERATURE (BUNDLE 6-1C, UPPER HALF)

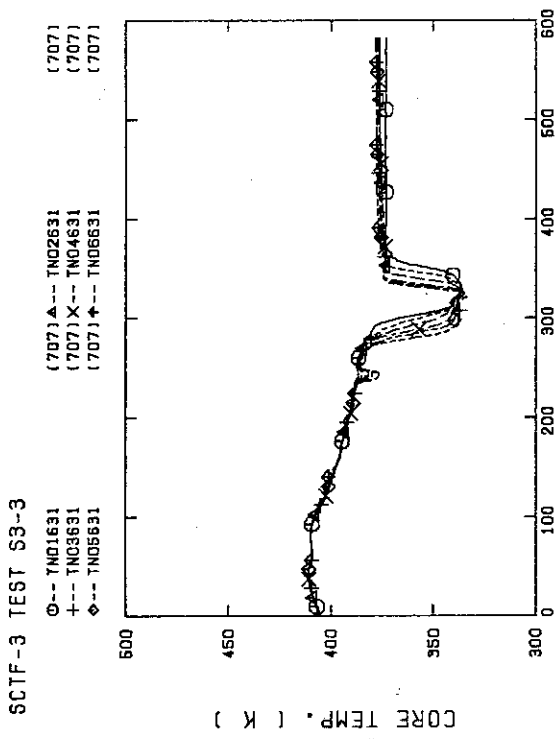

FIG. B-11 NON-HEATED ROD TEMPERATURE (BUNDLE 6-31)

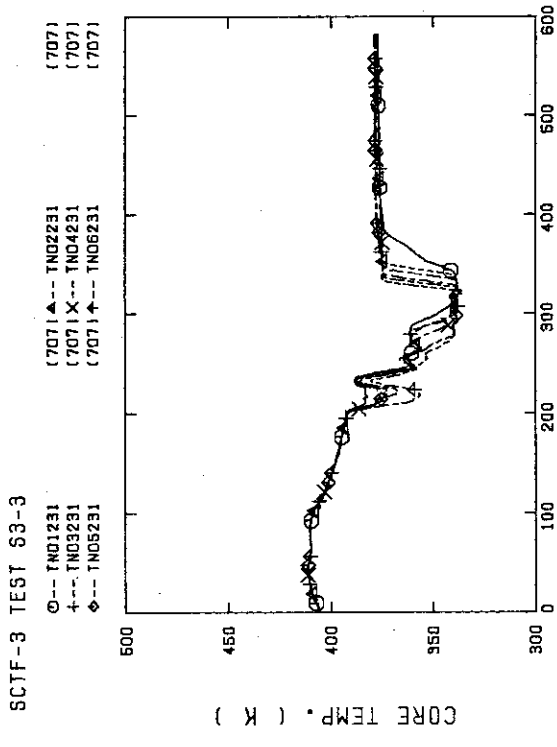

FIG. B-09 NON-HEATED ROD TEMPERATURE (BUNDLE 2-31)

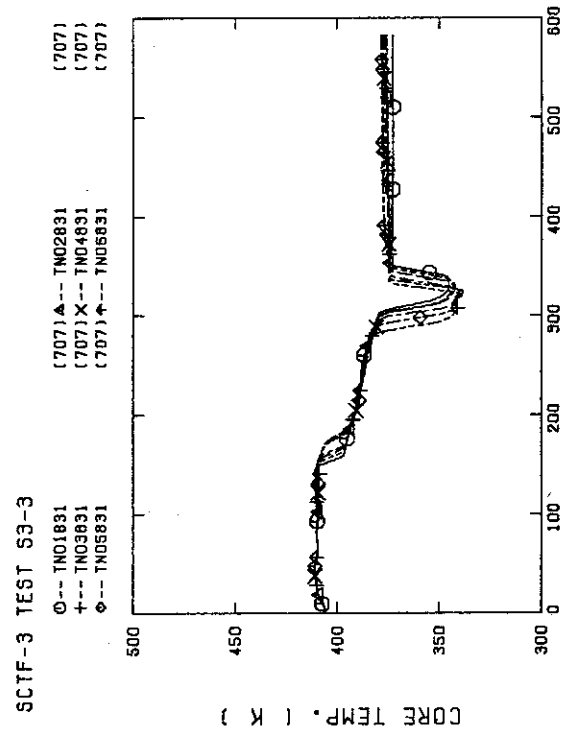

FIG. B-12 NON-HEATED ROD TEMPERATURE (BUNDLE 6-31)

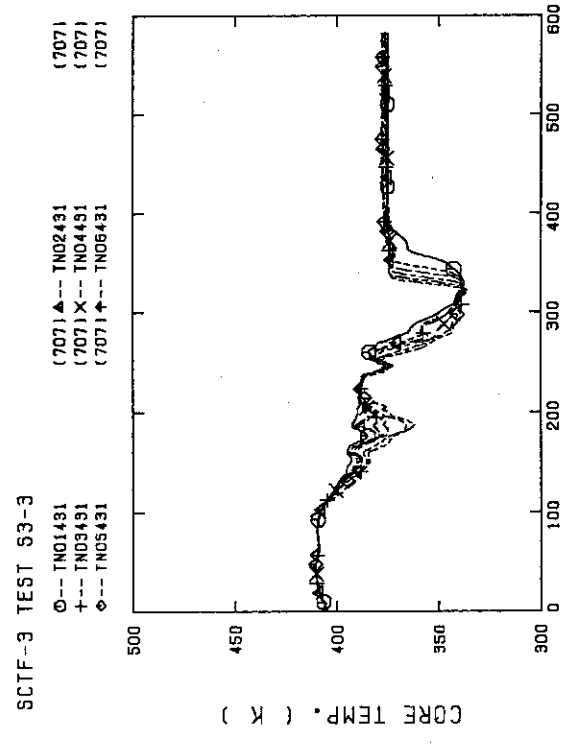

FIG. B-10 NON-HEATED ROD TEMPERATURE (BUNDLE 4-31)

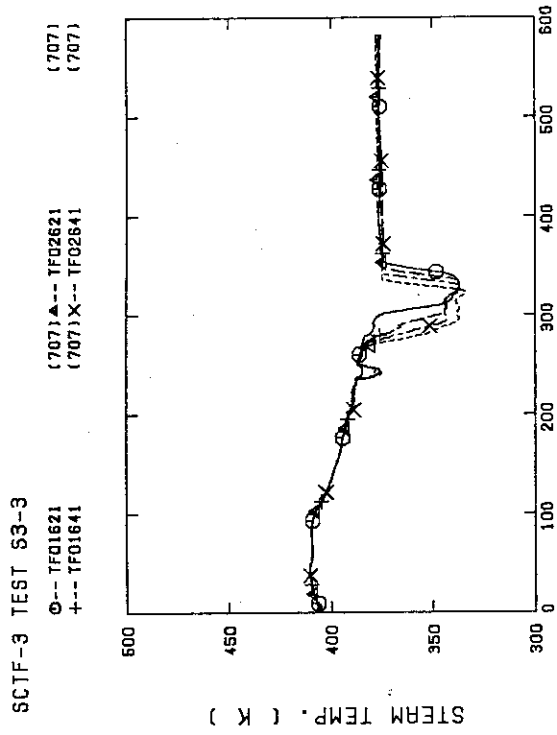

FIG. B-15 STEAM TEMPERATURE IN CORE, BUNDLE 6

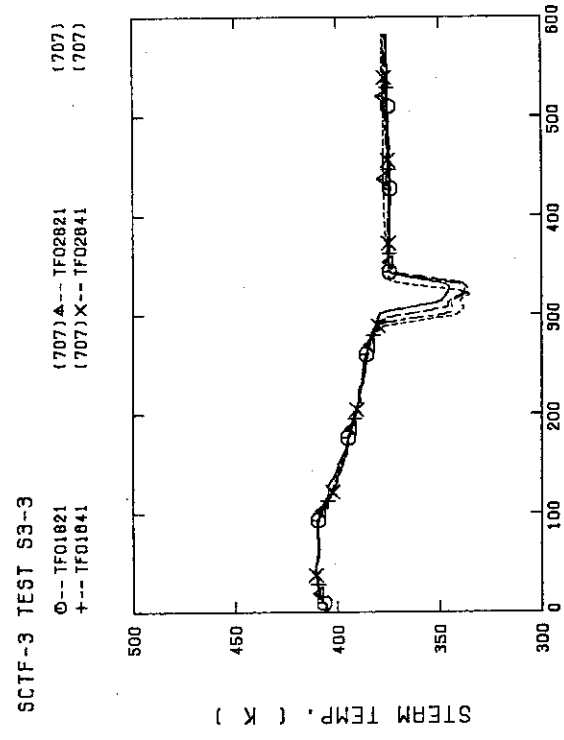

FIG. B-16 STEAM TEMPERATURE IN CORE, BUNDLE 8

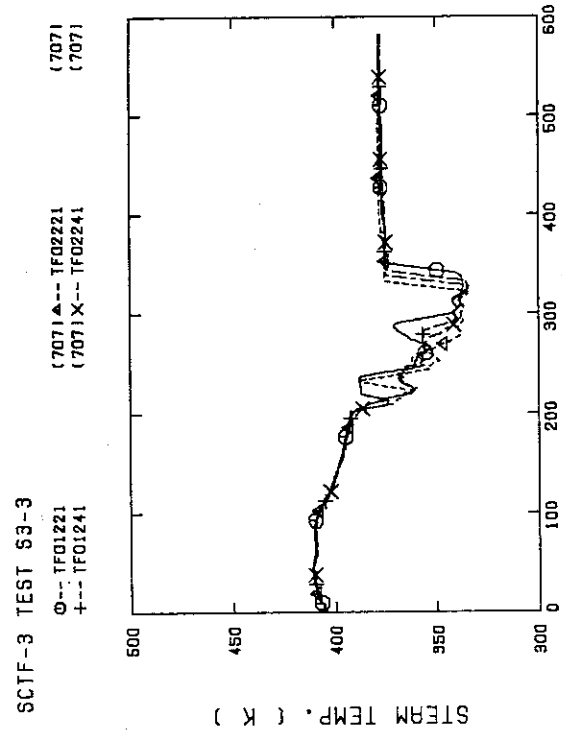

FIG. B-13 STEAM TEMPERATURE IN CORE, BUNDLE 2

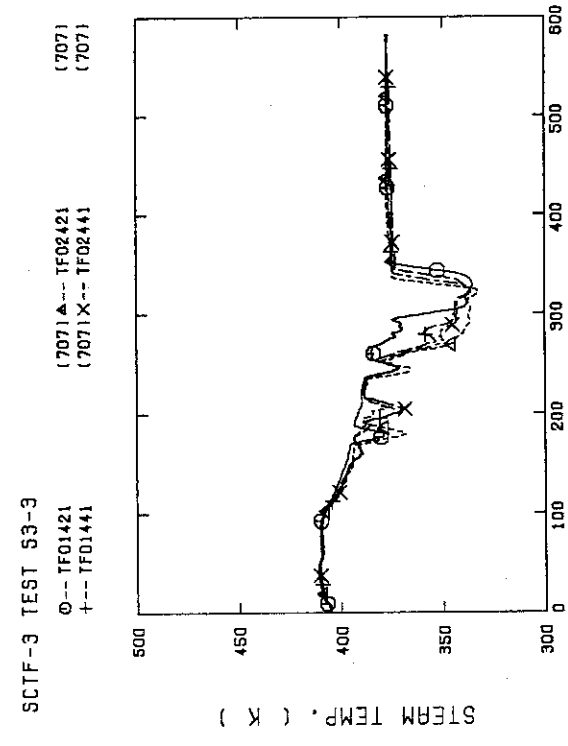

FIG. B-14 STEAM TEMPERATURE IN CORE, BUNDLE 4

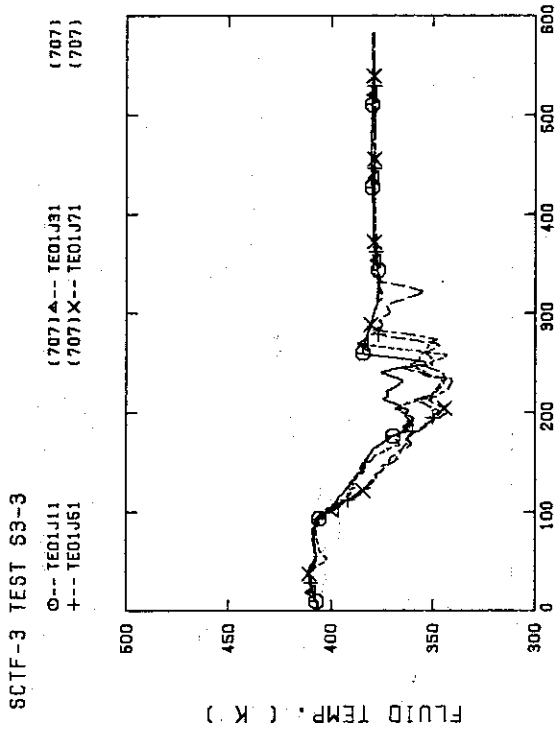

FIG. B-19 FLUID TEMPERATURE ABOVE UCSP
(BUNDLE 1,3,5,7 100MM ABOVE UCSP)

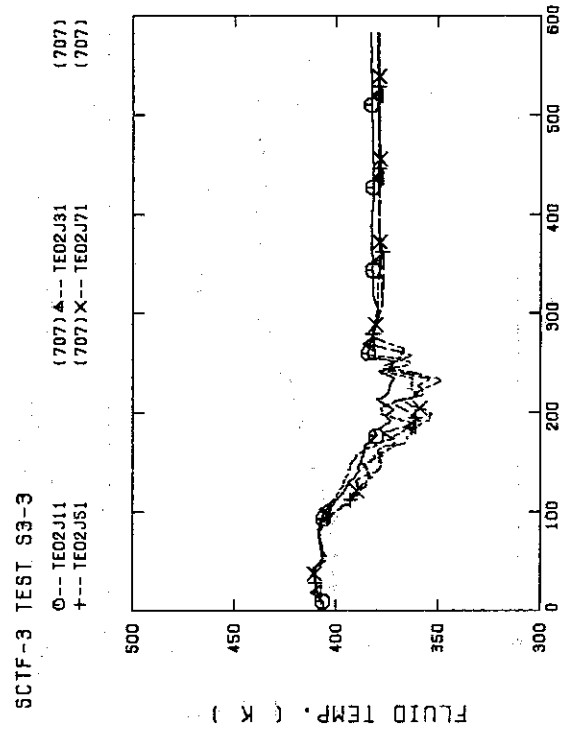

FIG. B-20 FLUID TEMPERATURE ABOVE UCSP
(BUNDLE 1,3,5,7 250MM ABOVE UCSP)

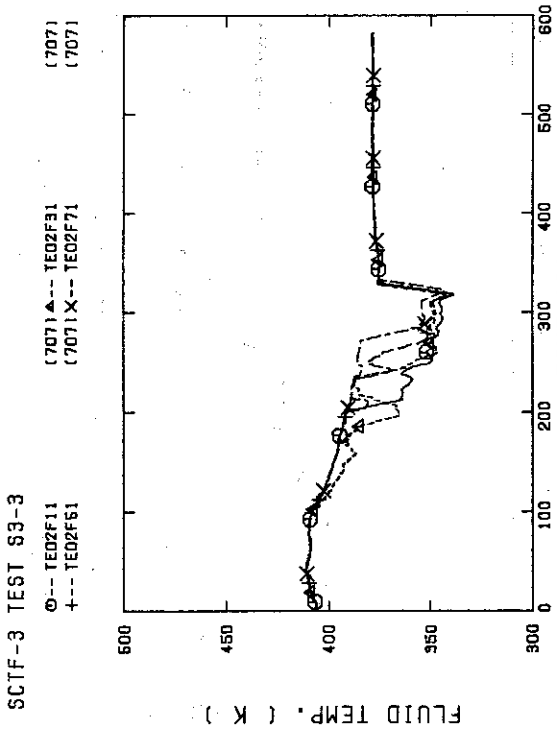

FIG. B-17 FLUID TEMPERATURE JUST ABOVE END BOX TIE PLATE
(BUNDLE 1,3,5,7 OPPOSITE SIDE OF COLD LEG, OUTER)

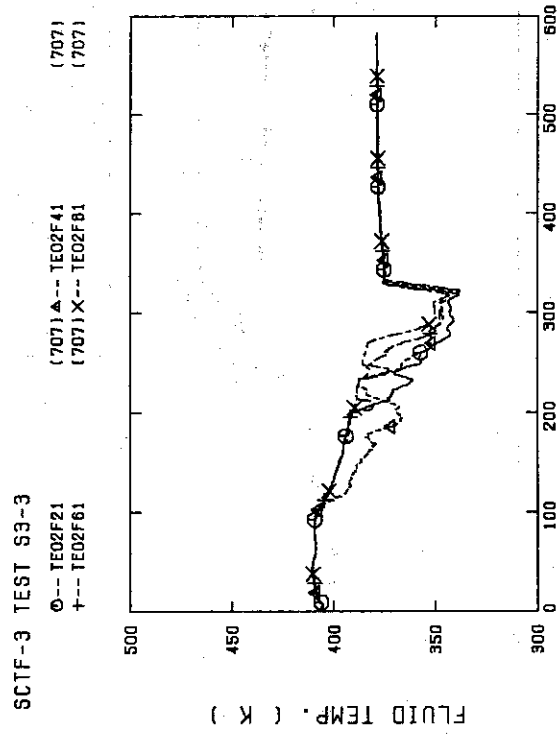

FIG. B-18 FLUID TEMPERATURE JUST ABOVE END BOX TIE PLATE
(BUNDLE 2,4,6,8 OPPOSITE SIDE OF COLD LEG, OUTER)

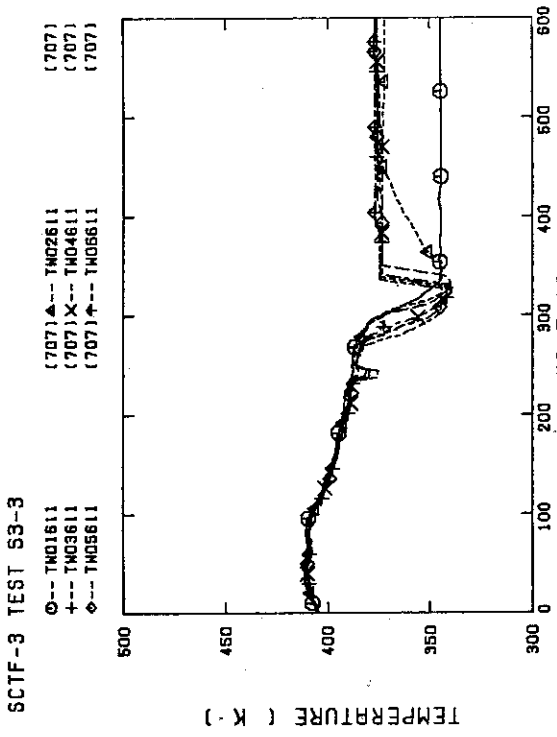

FIG. B-23 TEMPERATURE FOR SPUTTERING DETECTION BUNDLE 6 , REGION 1 , TYPE 3

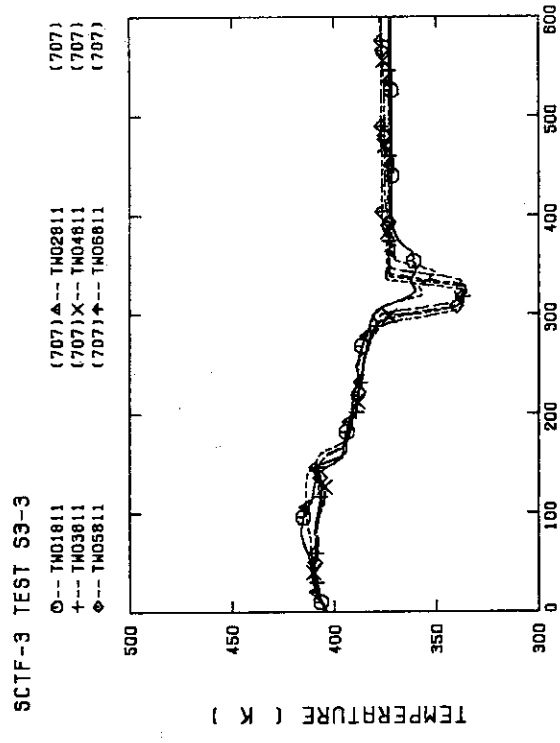

FIG. B-24 TEMPERATURE FOR SPUTTERING DETECTION BUNDLE 8 , REGION 1 , TYPE 3

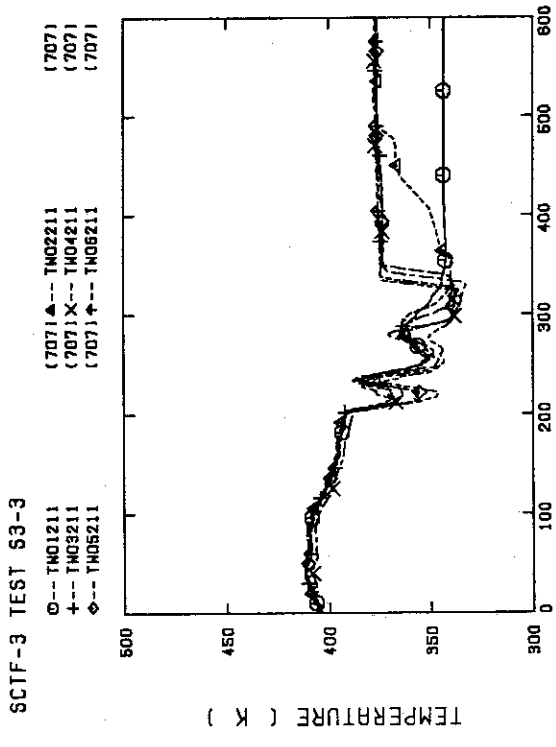

FIG. B-21 TEMPERATURE FOR SPUTTERING DETECTION BUNDLE 2 , REGION 1 , TYPE 3

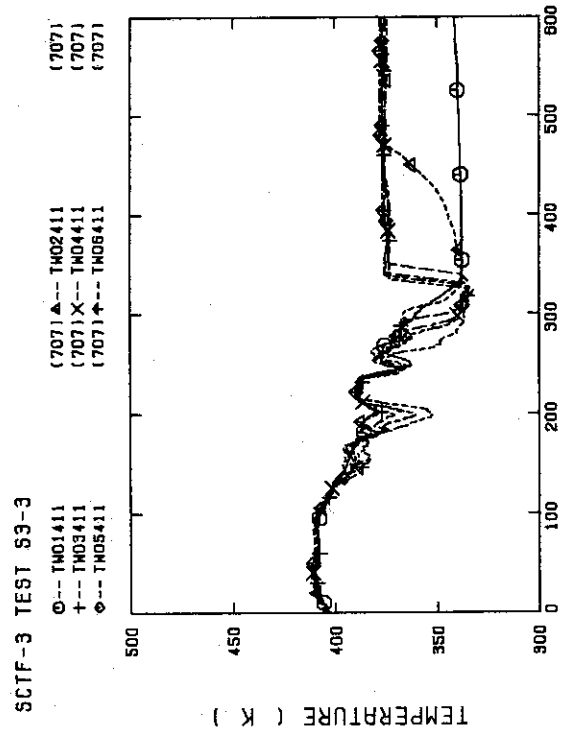

FIG. B-22 TEMPERATURE FOR SPUTTERING DETECTION BUNDLE 4 , REGION 1 , TYPE 3

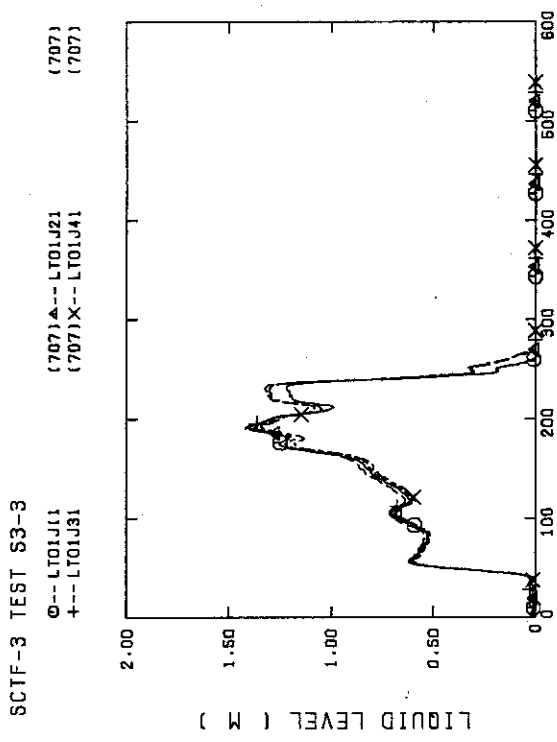

FIG. B-27 LIQUID LEVEL ABOVE UCSP (BUNDLE 1,2,3,4)

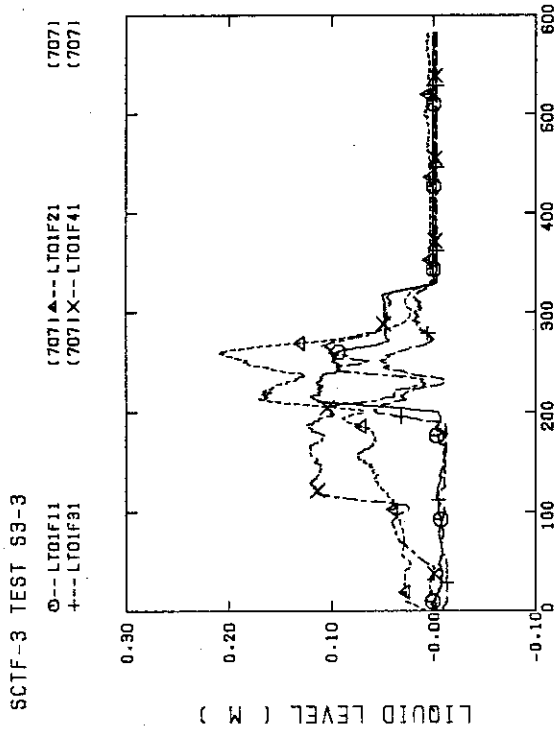

FIG. B-25 LIQUID LEVEL ABOVE END BOX TIE PLATE (BUNDLE 1,2,3,4)

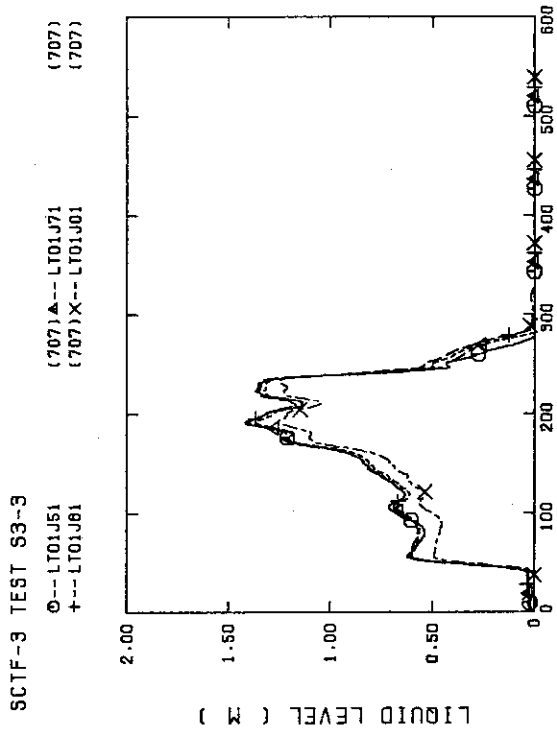

FIG. B-28 LIQUID LEVEL ABOVE UCSP (BUNDLE 5,6,7,8 AND CORE BUFFLE)

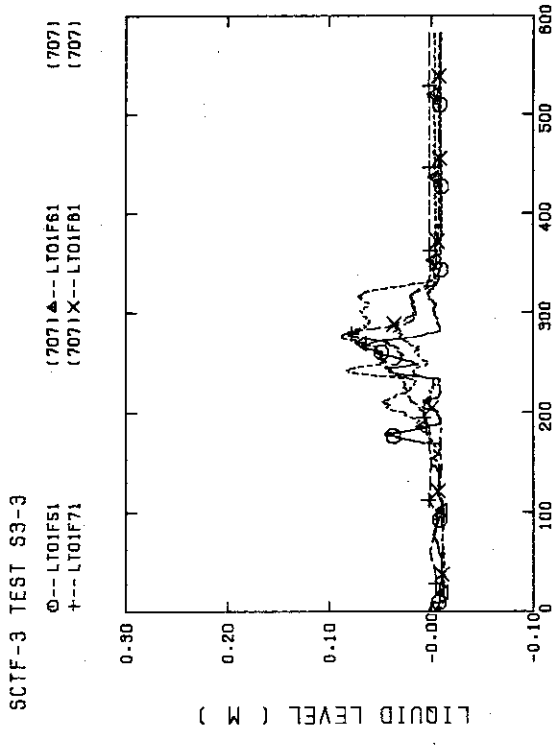

FIG. B-26 LIQUID LEVEL ABOVE END BOX TIE PLATE (BUNDLE 5,6,7,8)

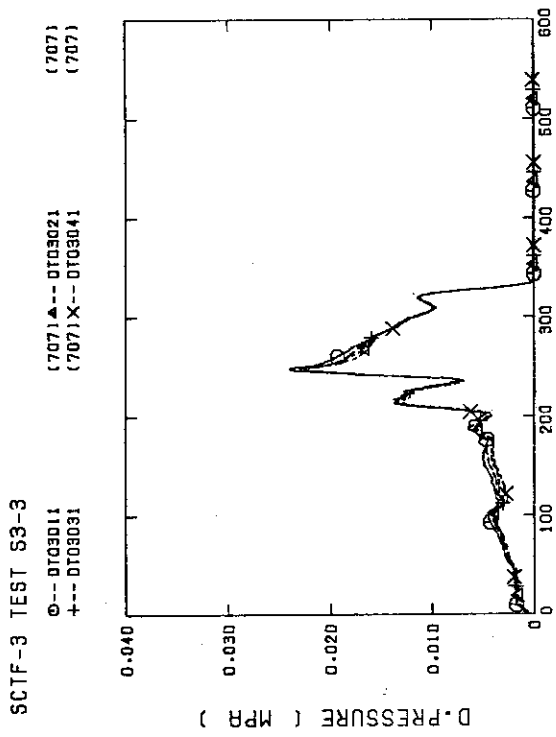

FIG. B-31 DIFFERENTIAL PRESSURE OF CORE FULL HIGHT (BUNDLE 1,2,3,4)

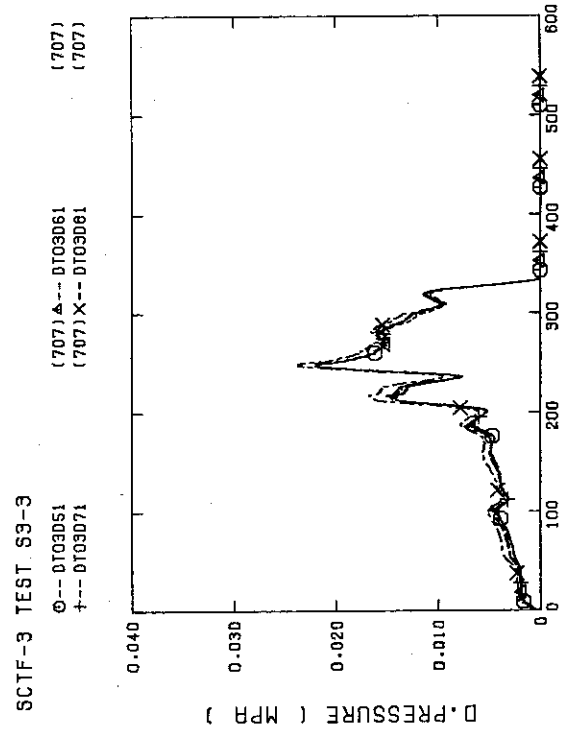

FIG. B-32 DIFFERENTIAL PRESSURE OF CORE FULL HIGHT (BUNDLE 5,6,7,8)

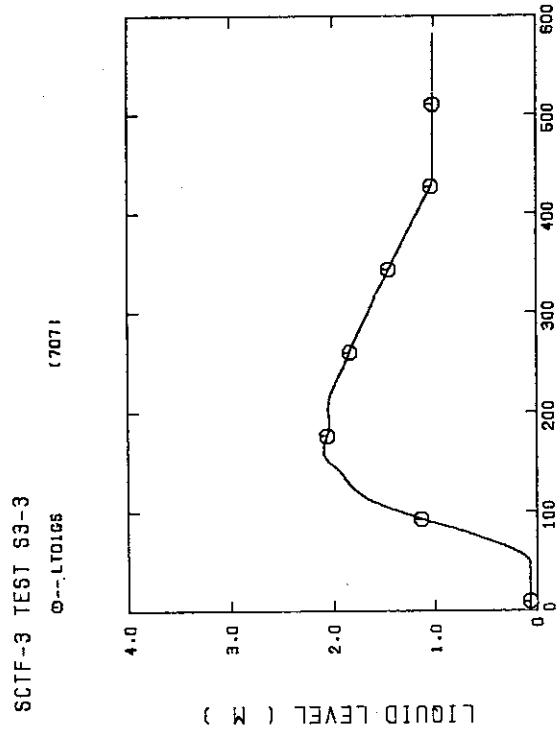

FIG. B-29 LIQUID LEVEL IN STEAM/WATER SEPARATOR

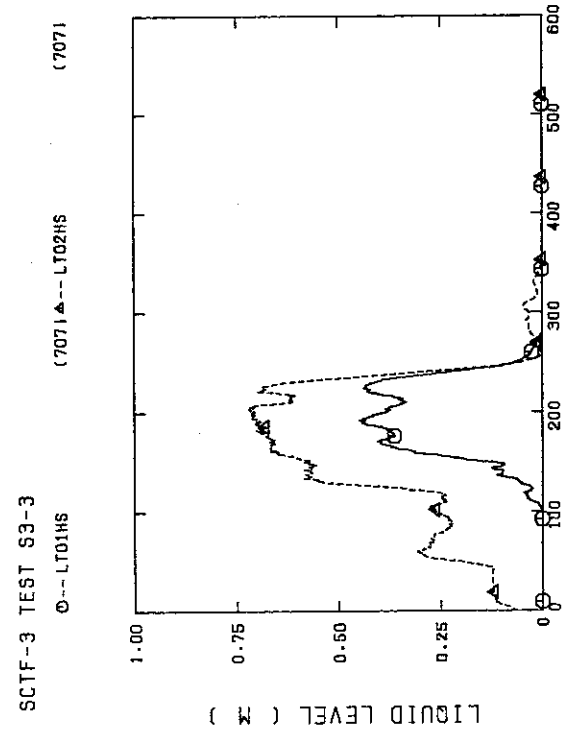

FIG. B-30 LIQUID LEVEL IN HOT LEG (01HS - PV SIDE, 02HS - STEAM/WATER SEPARATOR SIDE)

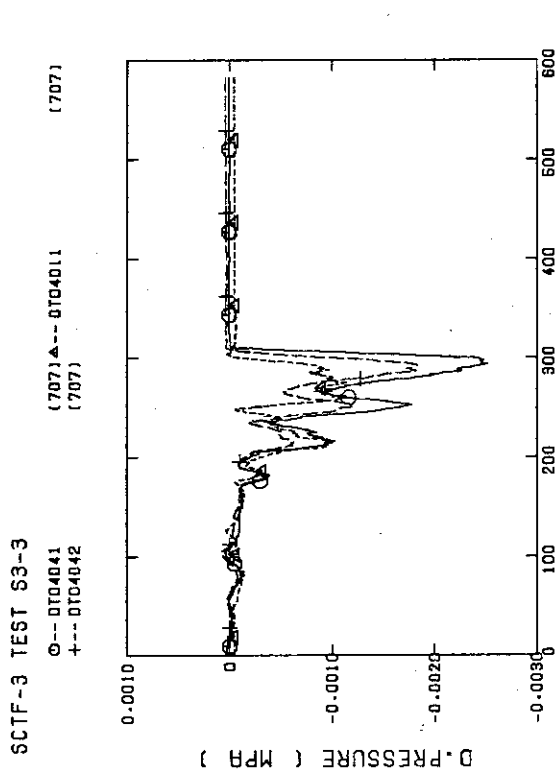

FIG. B-35 DIFFERENTIAL PRESSURE, HORIZONTAL AT 1905 MM (11-BUNDLE 1-4, 41-BUNDLE 4-8, 42-BUNDLE 4-6)

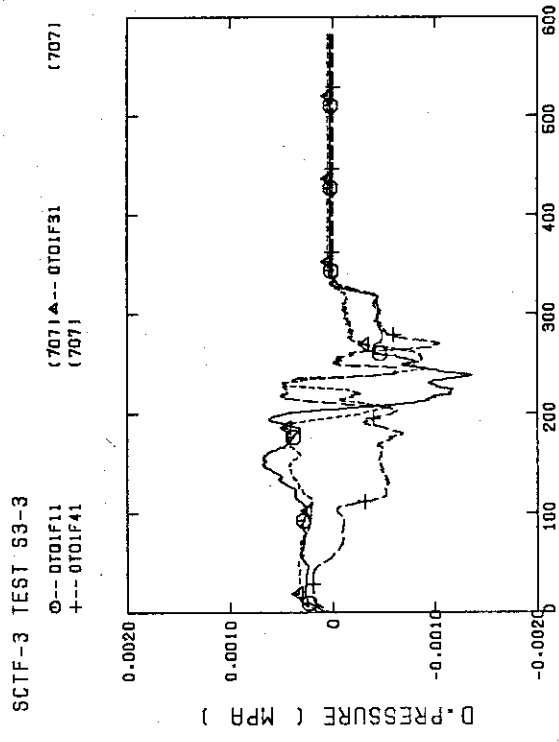

FIG. B-33 DIFFERENTIAL PRESSURE ACROSS END BOX TIE PLATE (BUNDLE 1.3.4)

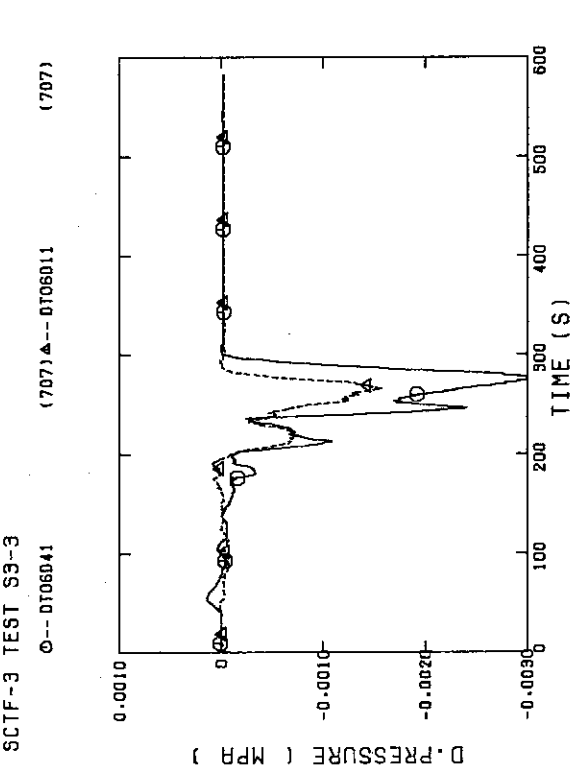

FIG. B-36 DIFFERENTIAL PRESSURE, HORIZONTAL AT 3235 MM (11-BUNDLE 1-4, 41-BUNDLE 4-8)

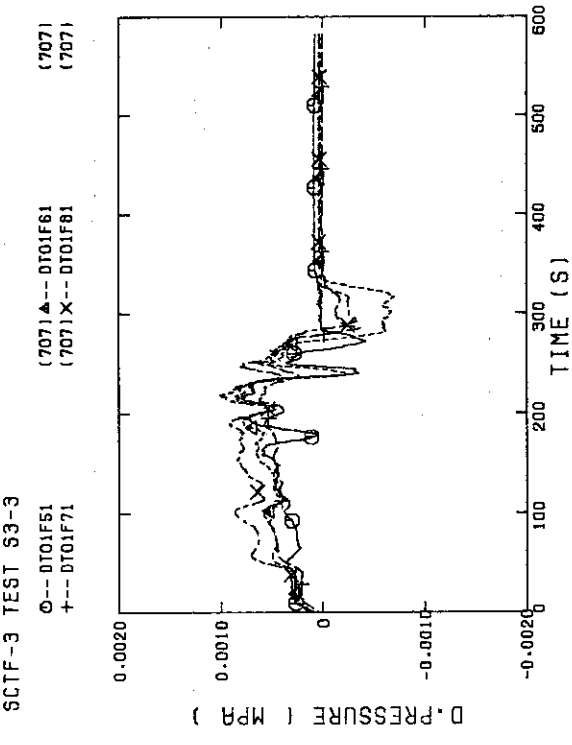

FIG. B-34 DIFFERENTIAL PRESSURE ACROSS END BOX TIE PLATE (BUNDLE 5,6,7,8)

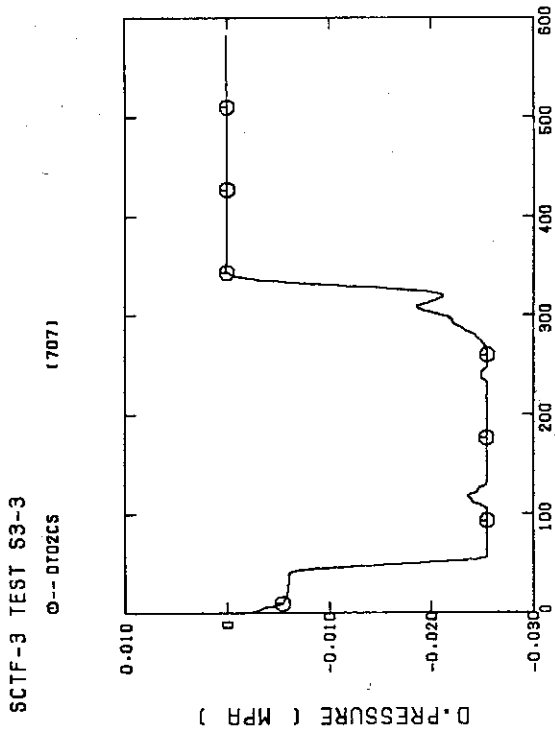

FIG. B-39 DIFFERENTIAL PRESSURE OF INTACT COLD LEG

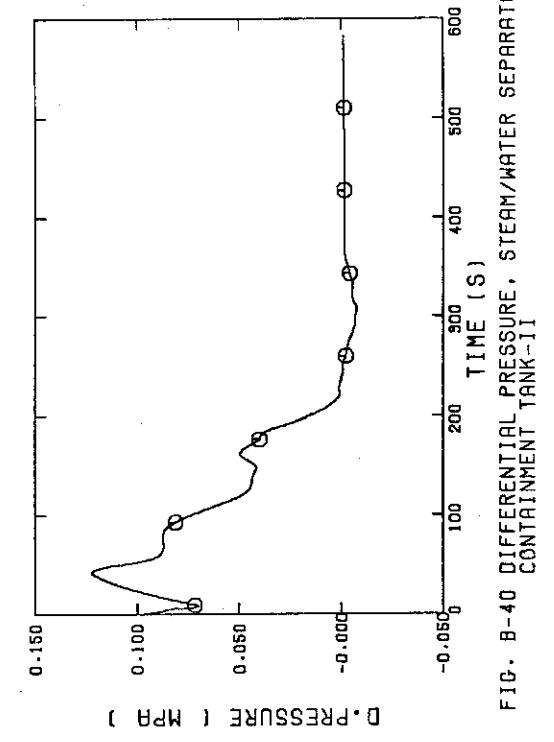

FIG. B-40 DIFFERENTIAL PRESSURE, STEAM/WATER SEPARATOR - CONTAINMENT TANK-II

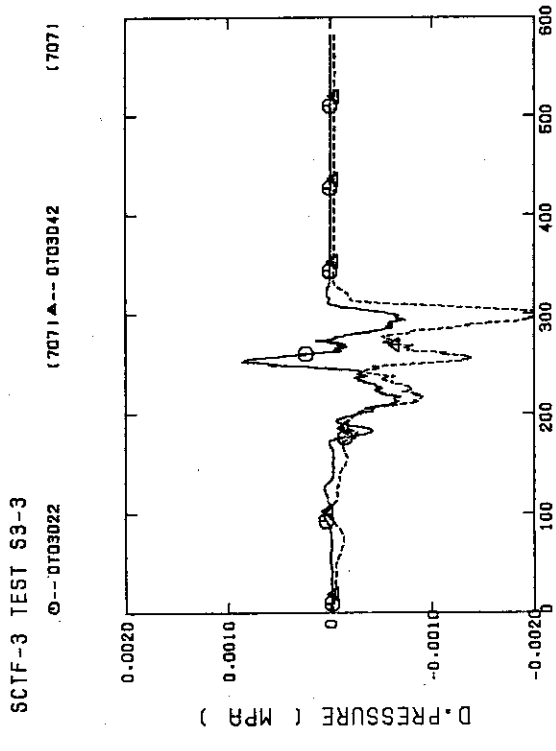

FIG. B-37 DIFFERENTIAL PRESSURE, HORIZONTAL AT 1365 MM (22-BUNDLE 2-4, 42-BUNDLE 4-8)

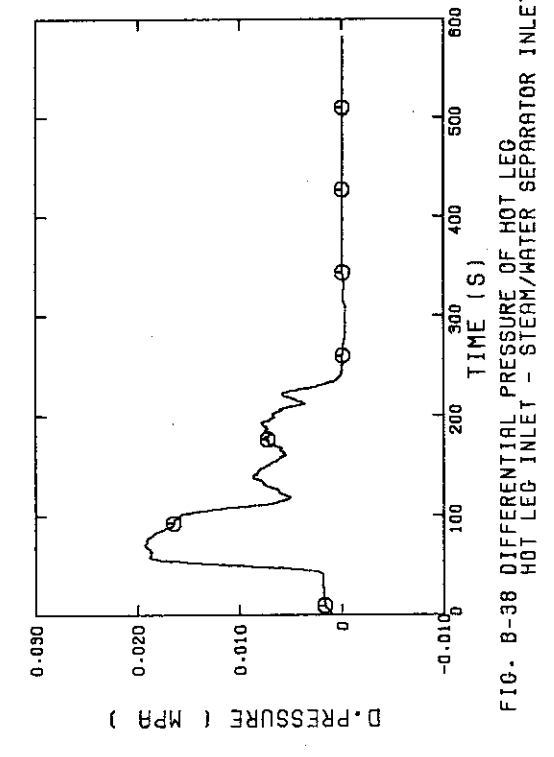

FIG. B-38 DIFFERENTIAL PRESSURE OF HOT LEG HOT LEG INLET - STEAM/WATER SEPARATOR INLET

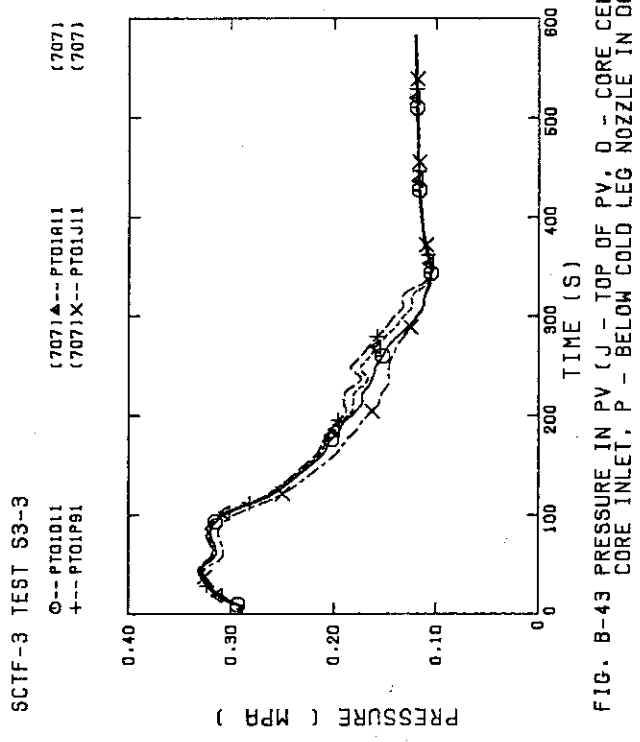

FIG. B-43 PRESSURE IN PV (J - TOP OF PV, D - CORE CENTER, A - CORE INLET, P - BELOW COLD LEG NOZZLE IN DOWNCOMER)

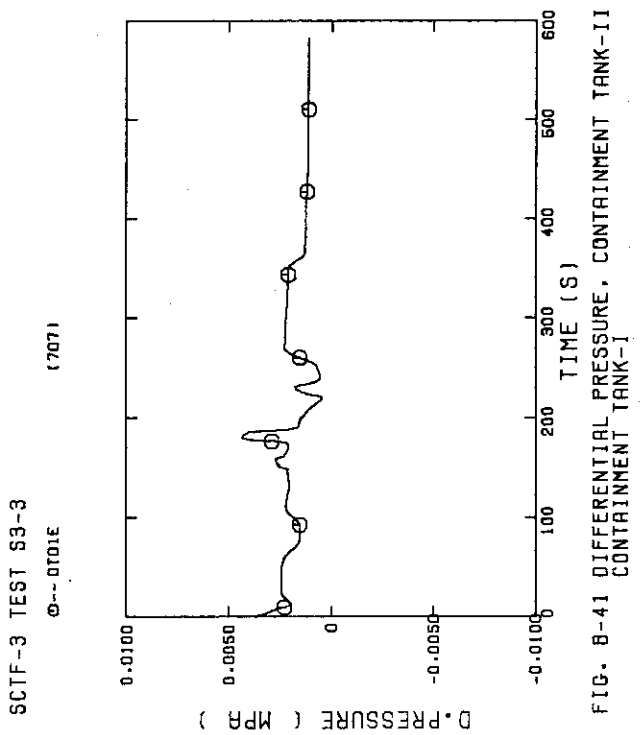

FIG. B-41 DIFFERENTIAL PRESSURE, CONTAINMENT TANK-II - CONTAINMENT TANK-I

FIG. B-44 PRESSURE AT TOP OF CONTAINMENT TANK-I AND CONTAINMENT TANK-II (F-CONTAINMENT TANK-I, B-CONTAINMENT TANK-II)

FIG. B-42 DIFFERENTIAL PRESSURE OF BROKEN COLD LEG - PV SIDE, DOWNCOMER - CONTAINMENT TANK-I

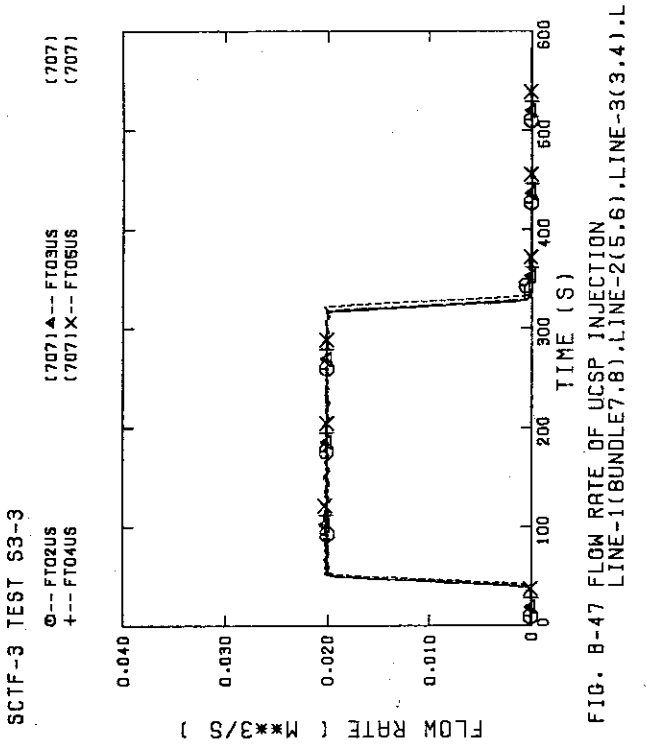

FIG. B-45 BUNDLE POWER
(BUNDLE 1,2,3,4)

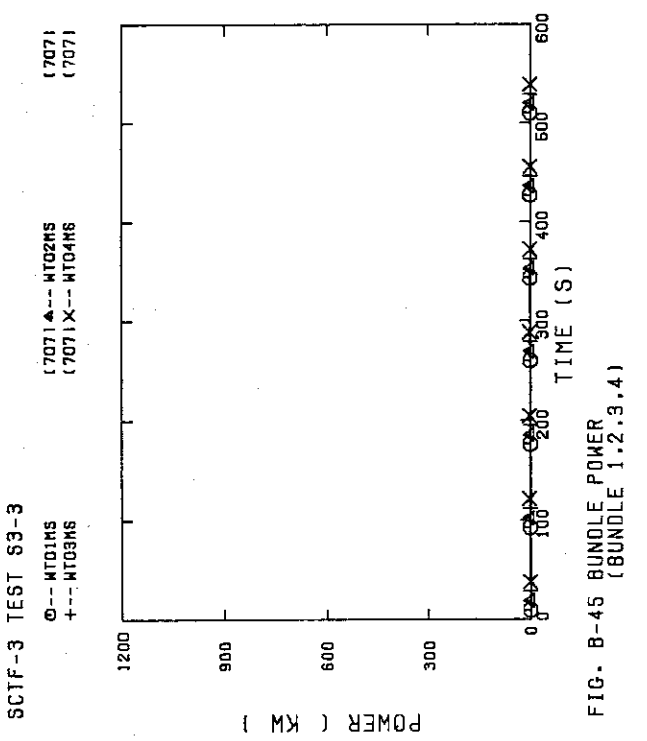

FIG. B-46 BUNDLE POWER
(BUNDLE 5,6,7,8)

FIG. B-47 FLOW RATE OF UCSP INJECTION
LINE-1(BUNDLE7,8),LINE-2(5,6),LINE-3(3,4),LINE-4
(1,2)

FIG. B-48 FLOW RATE OF UPPER HEAD INJECTION
LINE-4(BUNDLE1,2),LINE-3(3,4),LINE-2(5,6),LINE-1(7,8)

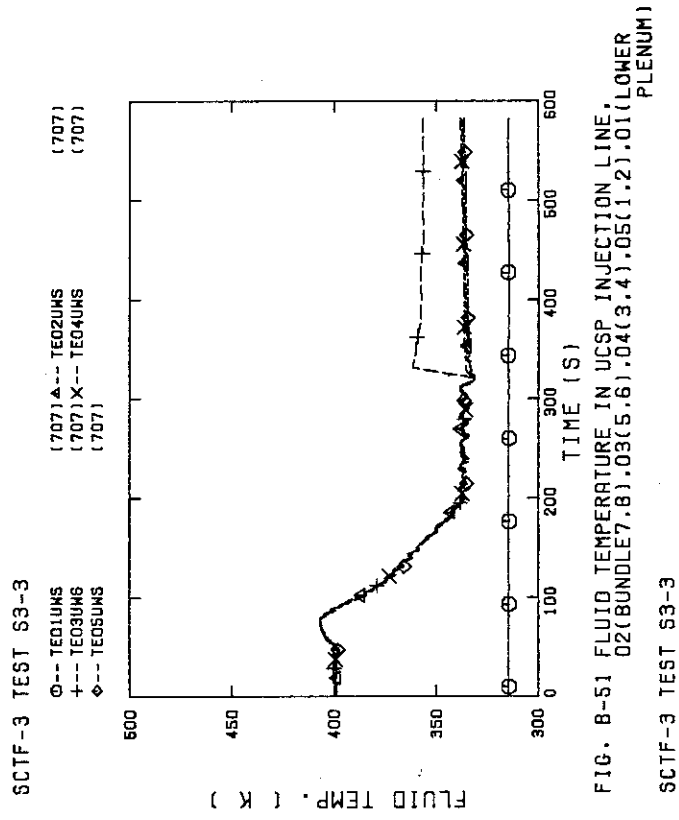

FIG. B-51 FLUID TEMPERATURE IN UCSP INJECTION LINE, 02(BUNDLE7,8),03(5,6),04(3,4),05(1,2),01(LOWER PLENUM)

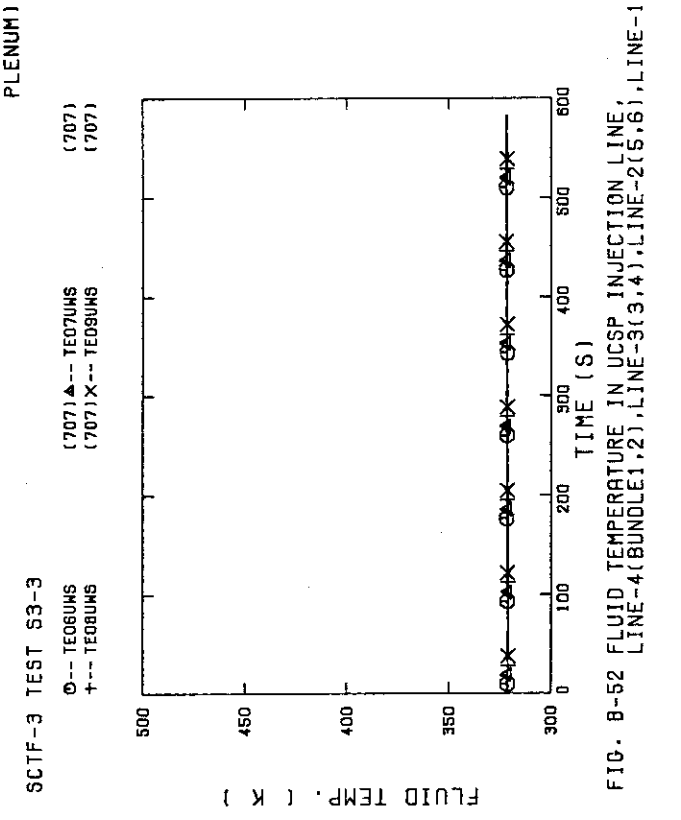

FIG. B-52 FLUID TEMPERATURE IN UCSP INJECTION LINE, LINE-4(BUNDLE1,2),LINE-3(3,4),LINE-2(5,6),LINE-1(7,8)

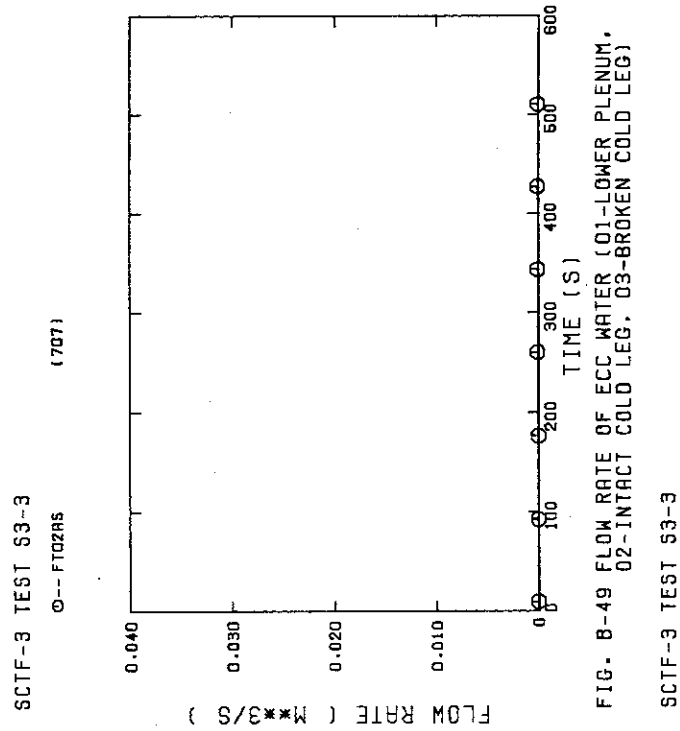

FIG. B-49 FLOW RATE OF ECC WATER (01-LOWER PLENUM, 02-INTACT COLD LEG, 03-BROKEN COLD LEG)

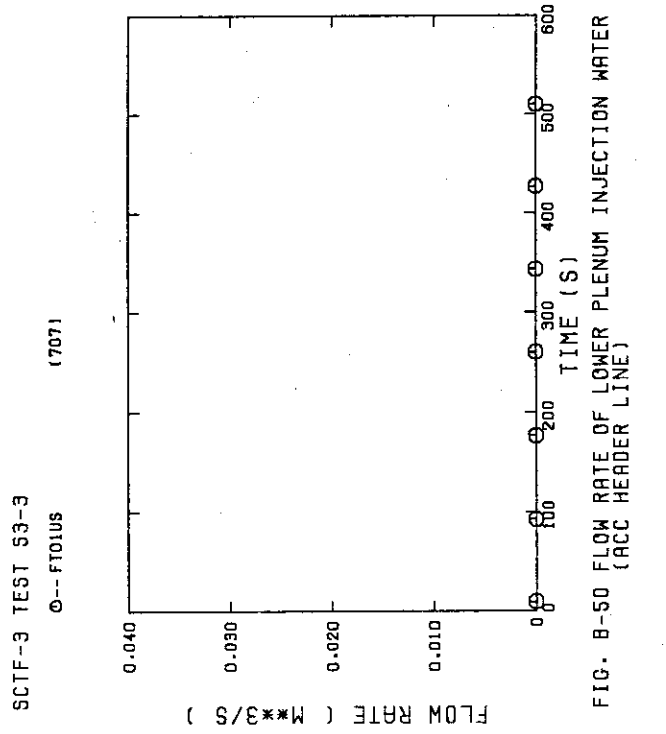

FIG. B-50 FLOW RATE OF LOWER PLENUM INJECTION WATER (ACC HEADER LINE)

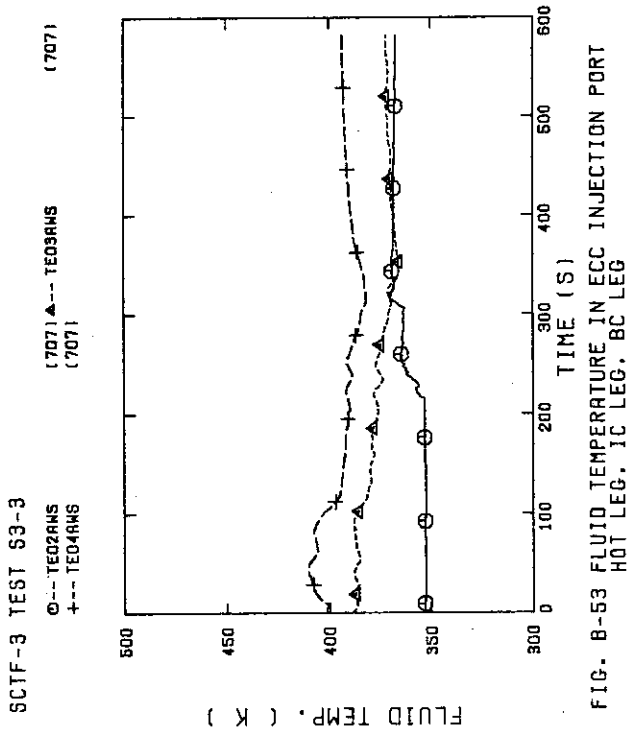

FIG. B-53 FLUID TEMPERATURE IN ECC INJECTION PORT
HOT LEG, IC LEG, BC LEG

Appendix C Selected data of Test S3-4

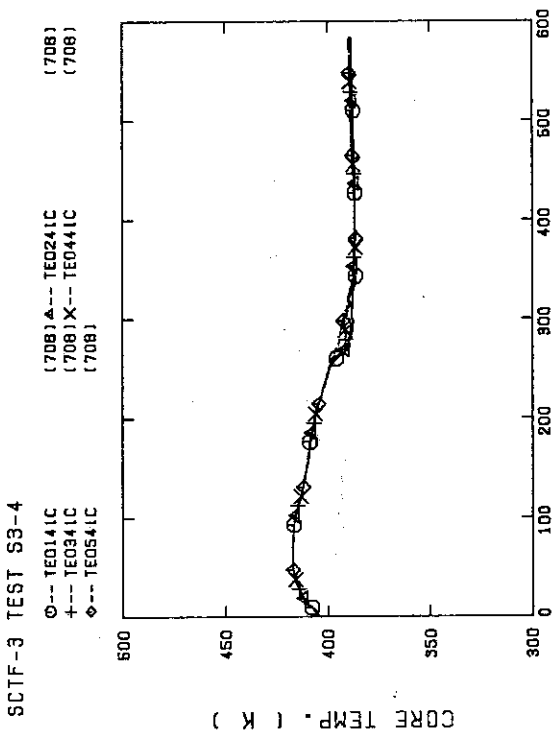

FIG. C-03 HEATER ROD TEMPERATURE (BUNDLE 4-1C, LOWER HALF)

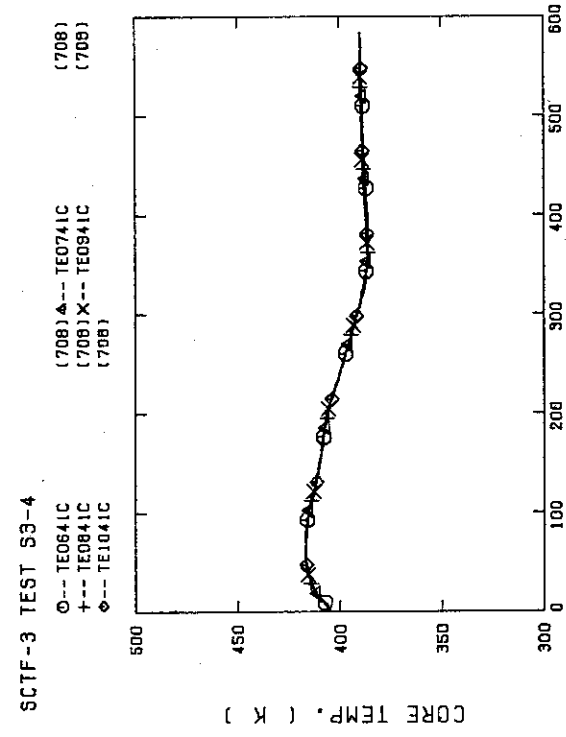

FIG. C-04 HEATER ROD TEMPERATURE (BUNDLE 4-1C, UPPER HALF)

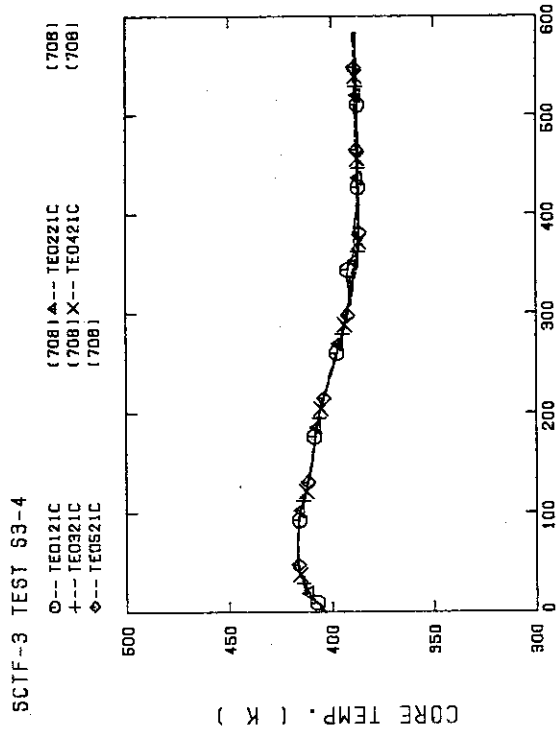

FIG. C-01 HEATER ROD TEMPERATURE (BUNDLE 2-1C, LOWER HALF)

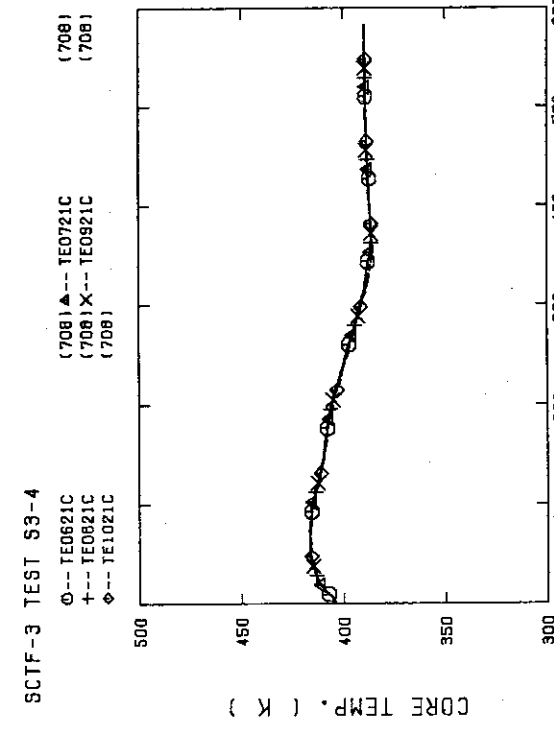

FIG. C-02 HEATER ROD TEMPERATURE (BUNDLE 2-1C, UPPER HALF)

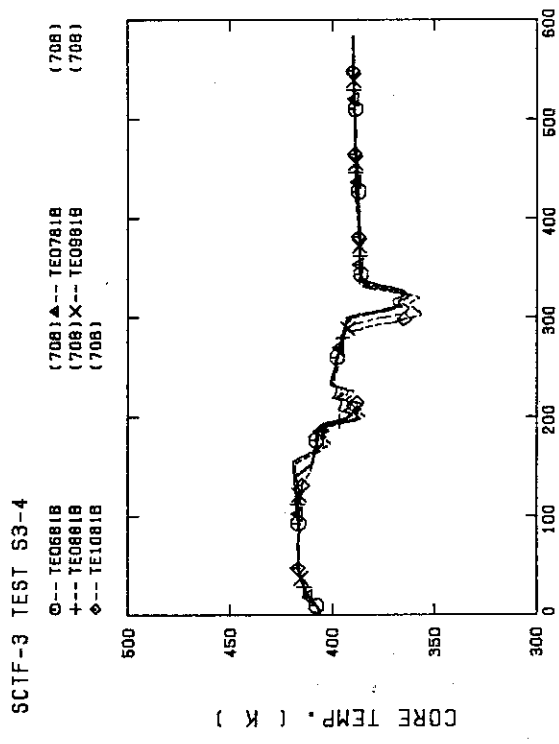

FIG. C-07 HEATER ROD TEMPERATURE
(BUNDLE 8-1B, UPPER HALF)

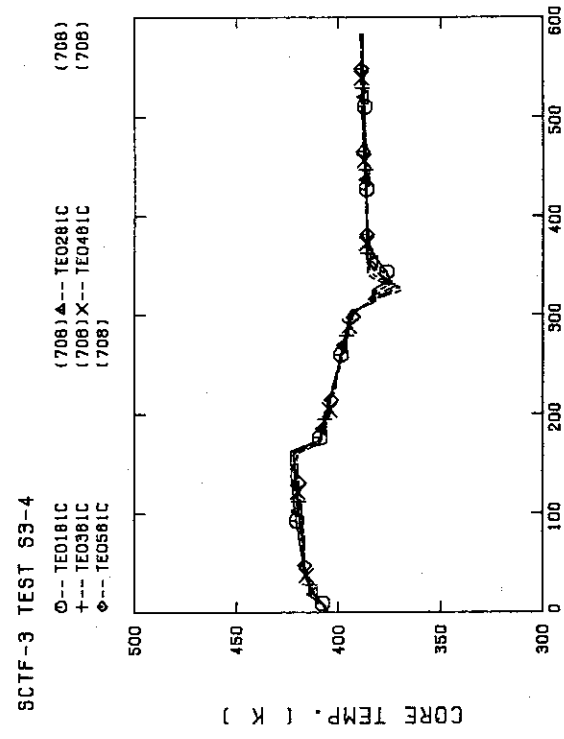

FIG. C-08 HEATER ROD TEMPERATURE
(BUNDLE 8-1C, LOWER HALF)

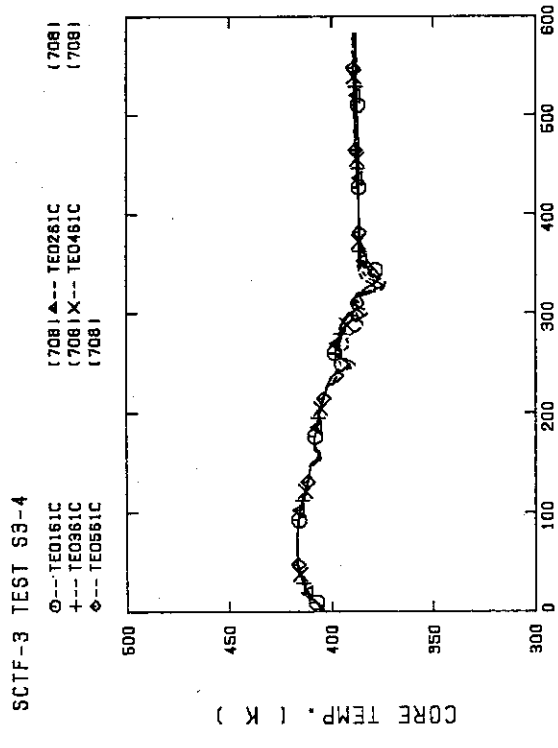

FIG. C-05 HEATER ROD TEMPERATURE
(BUNDLE 6-1C, LOWER HALF)

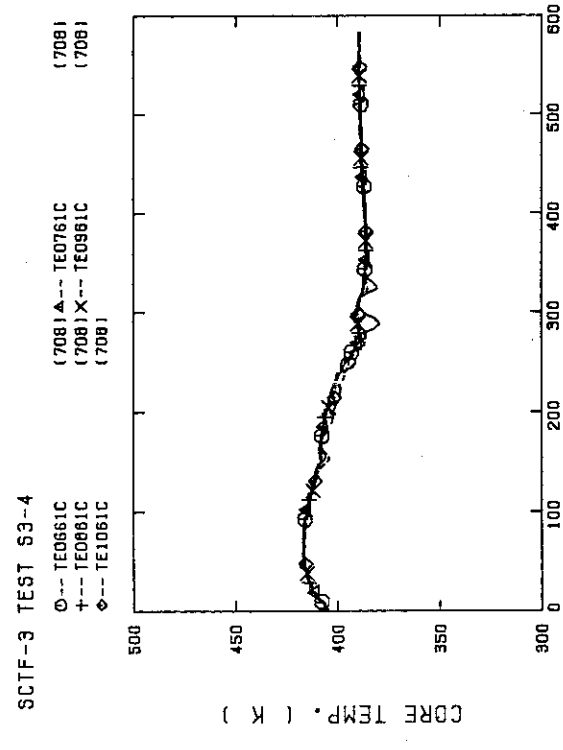

FIG. C-06 HEATER ROD TEMPERATURE
(BUNDLE 6-1C, UPPER HALF)

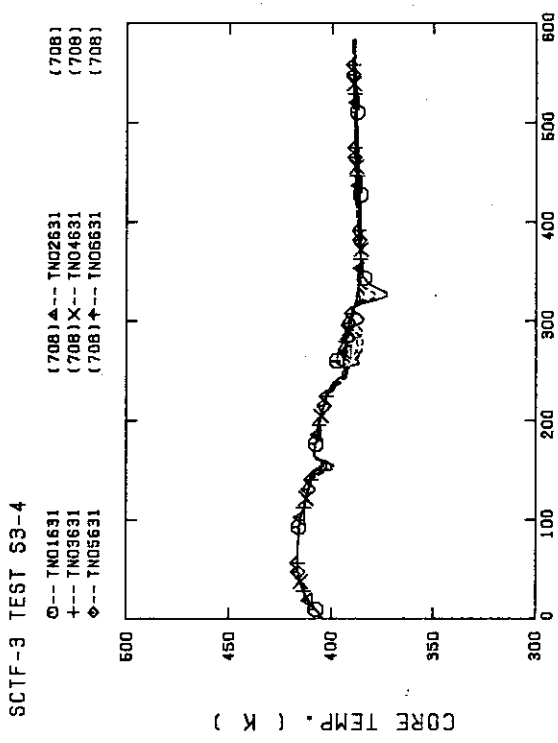

FIG. C-09 NON-HEATED ROD TEMPERATURE (BUNDLE 2-31)

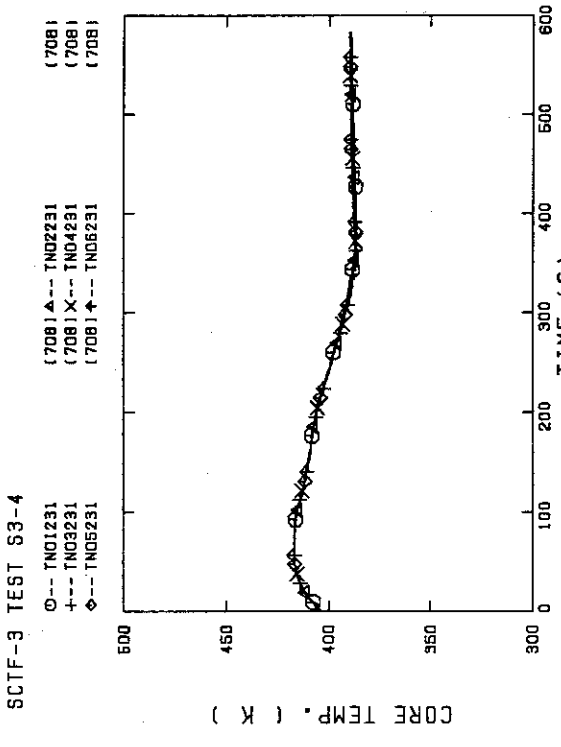

FIG. C-10 NON-HEATED ROD TEMPERATURE (BUNDLE 4-31)

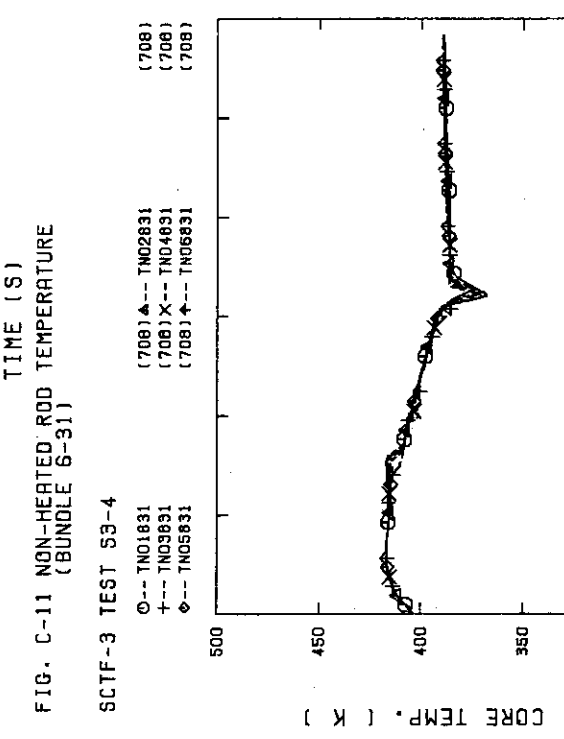

FIG. C-11 NON-HEATED ROD TEMPERATURE (BUNDLE 6-31)

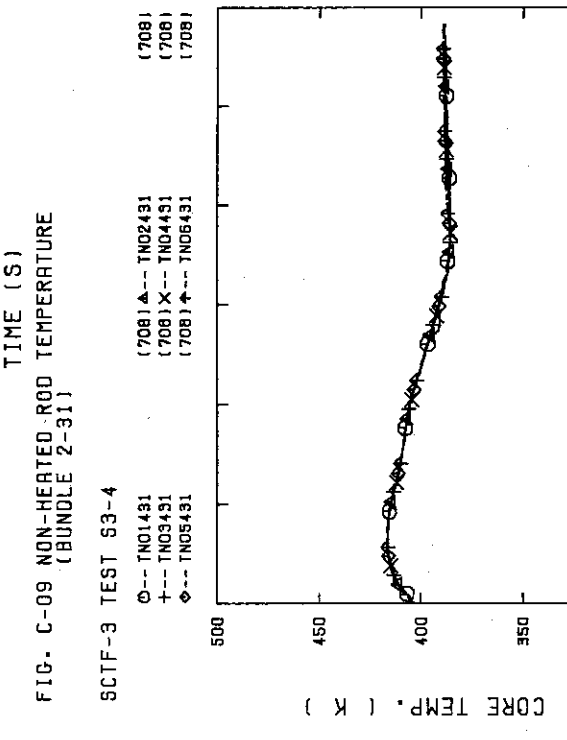

FIG. C-12 NON-HEATED ROD TEMPERATURE (BUNDLE 6-31)

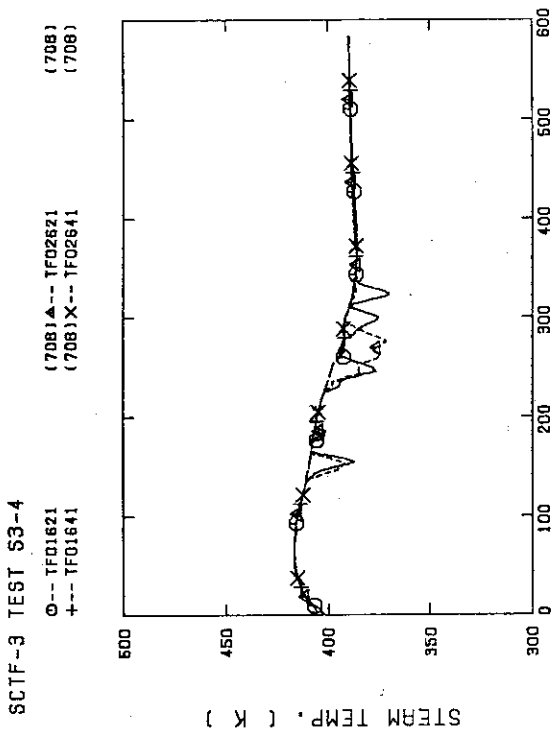

FIG. C-13 STEAM TEMPERATURE IN CORE, BUNDLE 2

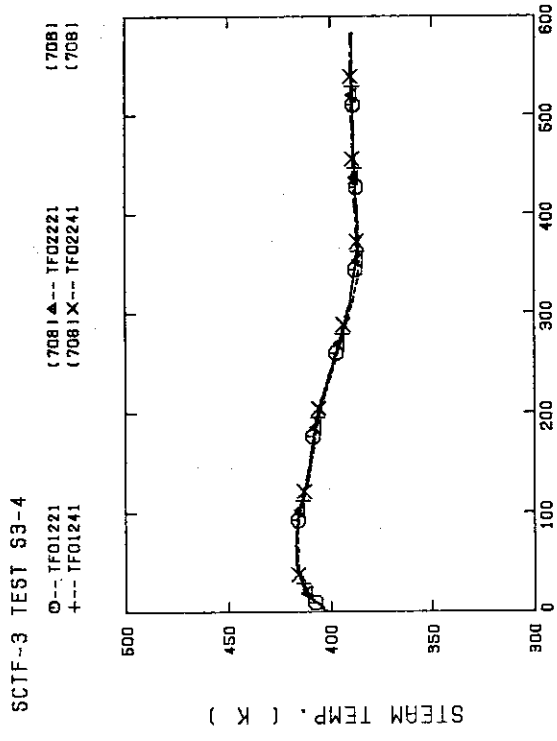

FIG. C-14 STEAM TEMPERATURE IN CORE, BUNDLE 4

FIG. C-15 STEAM TEMPERATURE IN CORE, BUNDLE 6

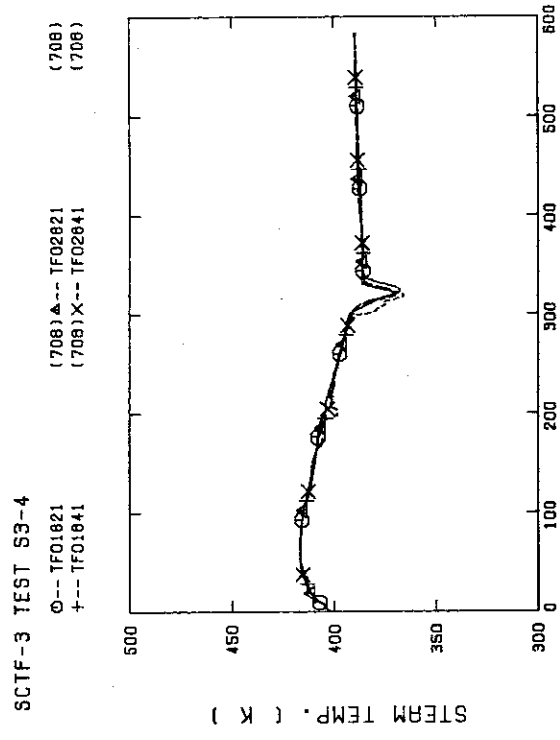

FIG. C-16 STEAM TEMPERATURE IN CORE, BUNDLE 8

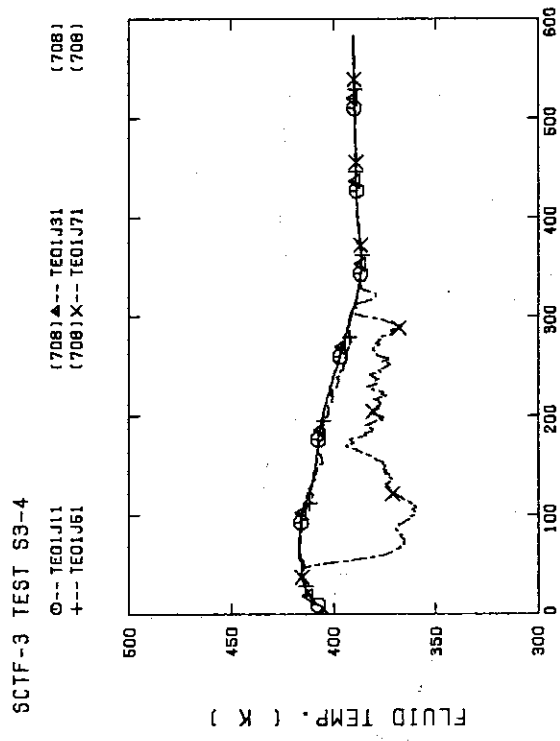

FIG. C-19 FLUID TEMPERATURE ABOVE UCSP
(BUNDLE 1.3.5.7 100MM ABOVE UCSP)

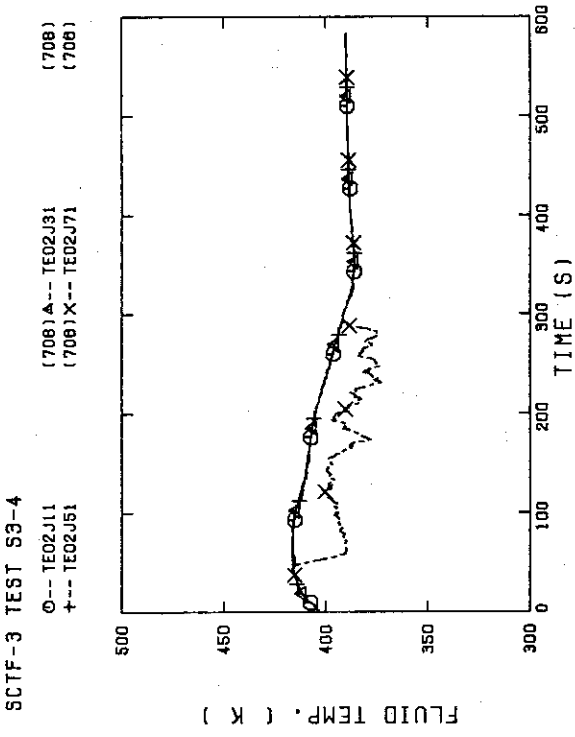

FIG. C-20 FLUID TEMPERATURE ABOVE UCSP
(BUNDLE 1.3.5.7 250MM ABOVE UCSP)

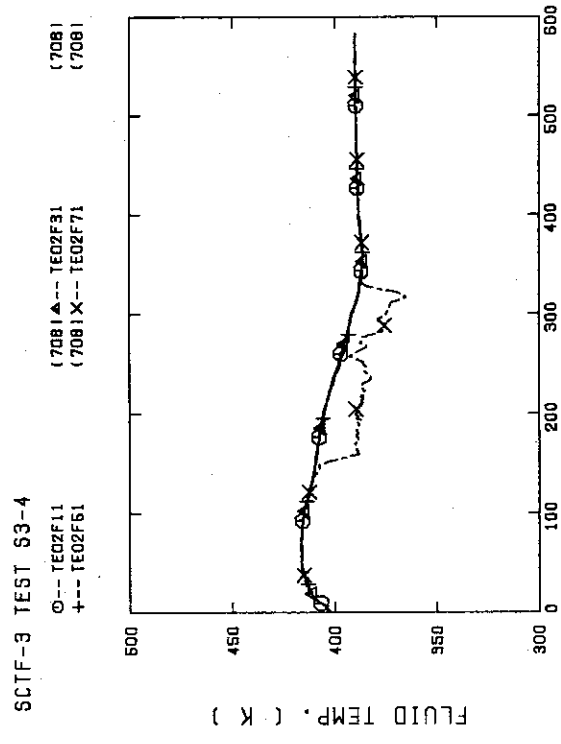

FIG. C-17 FLUID TEMPERATURE JUST ABOVE END BOX TIE PLATE
(BUNDLE 1.3.5.7 OPPOSITE SIDE OF COLD LEG. OUTER)

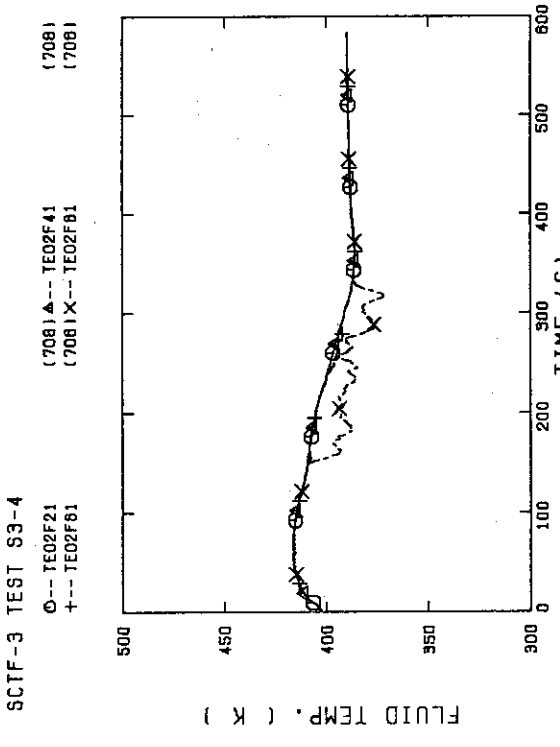

FIG. C-18 FLUID TEMPERATURE JUST ABOVE END BOX TIE PLATE
(BUNDLE 2,4,6,8 OPPOSITE SIDE OF COLD LEG. OUTER)

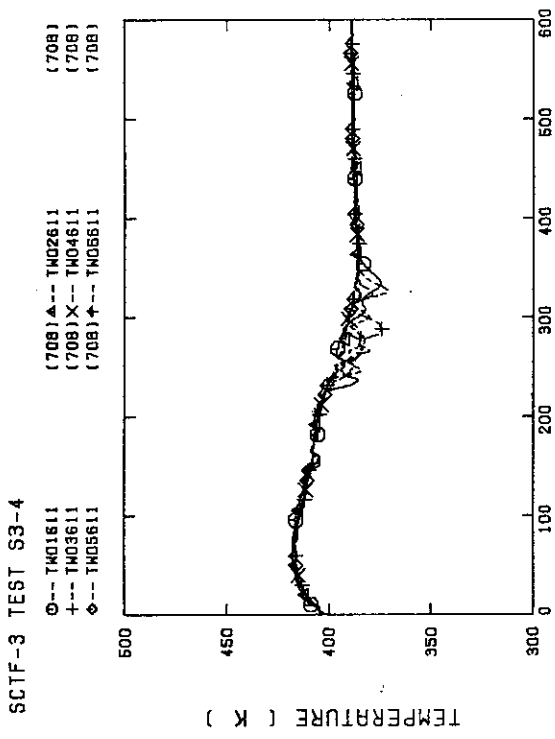

FIG. C-21 TEMPERATURE FOR SPUTTERING DETECTION
BUNDLE 2 , REGION 1 , TYPE 3

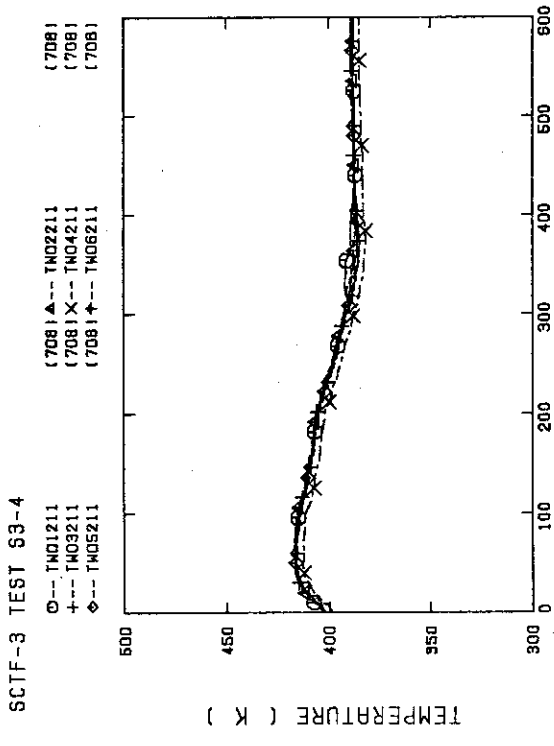

FIG. C-22 TEMPERATURE FOR SPUTTERING DETECTION
BUNDLE 4 , REGION 1 , TYPE 3

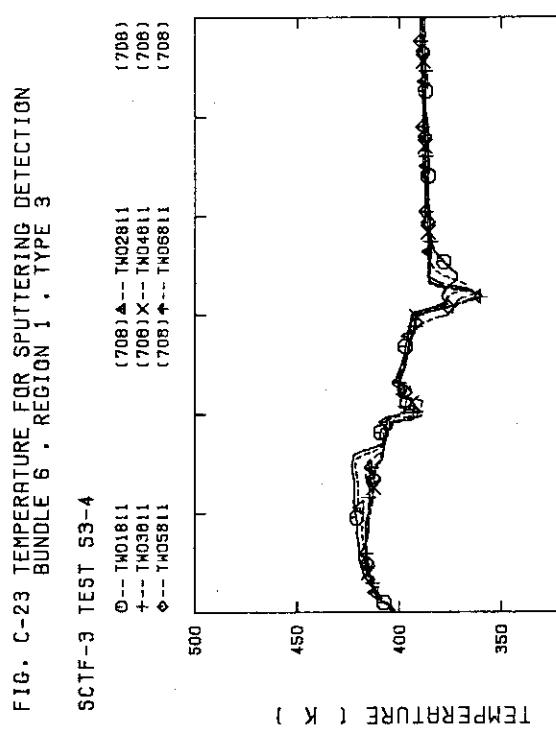

FIG. C-23 TEMPERATURE FOR SPUTTERING DETECTION
BUNDLE 6 , REGION 1 , TYPE 3

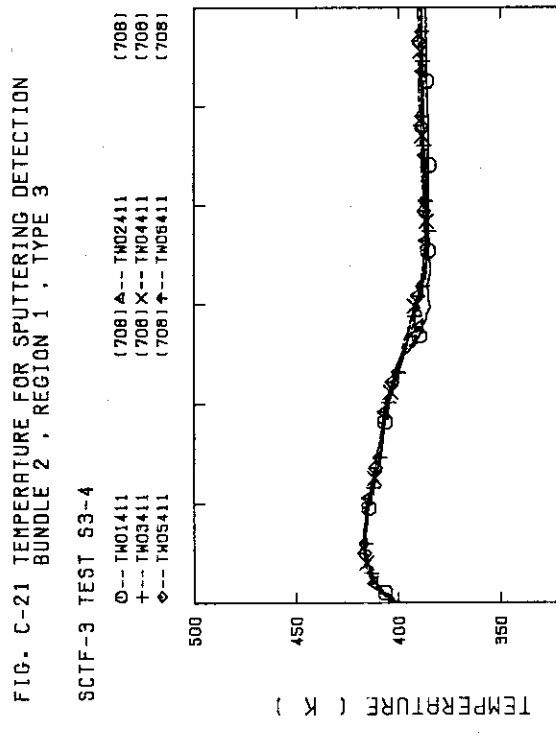

FIG. C-24 TEMPERATURE FOR SPUTTERING DETECTION
BUNDLE 8 , REGION 1 , TYPE 3

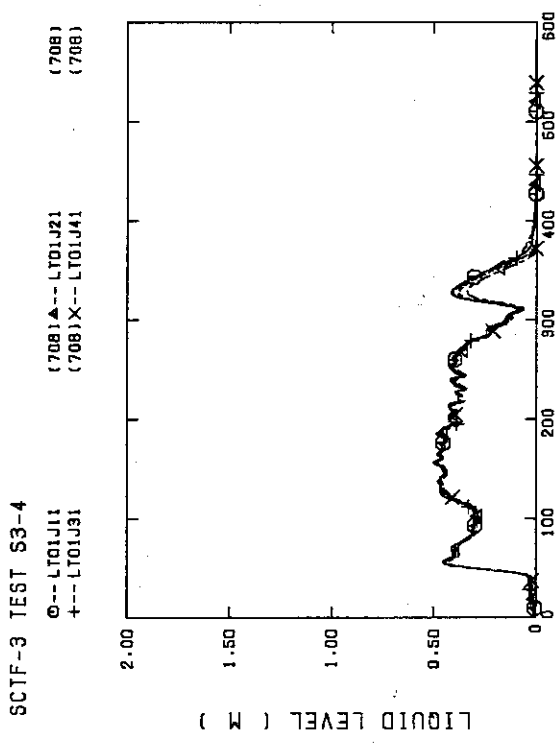

FIG. C-27 LIQUID LEVEL ABOVE UCSP (BUNDLE 1,2,3,4)

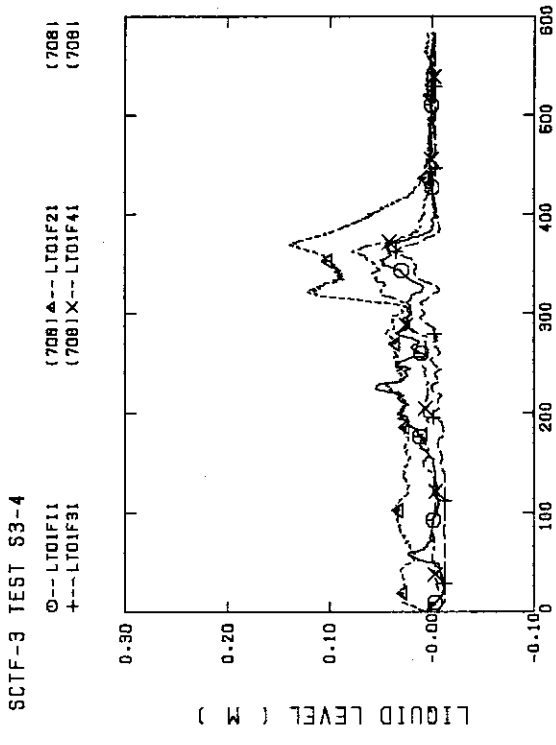

FIG. C-25 LIQUID LEVEL ABOVE END BOX TIE PLATE (BUNDLE 1,2,3,4)

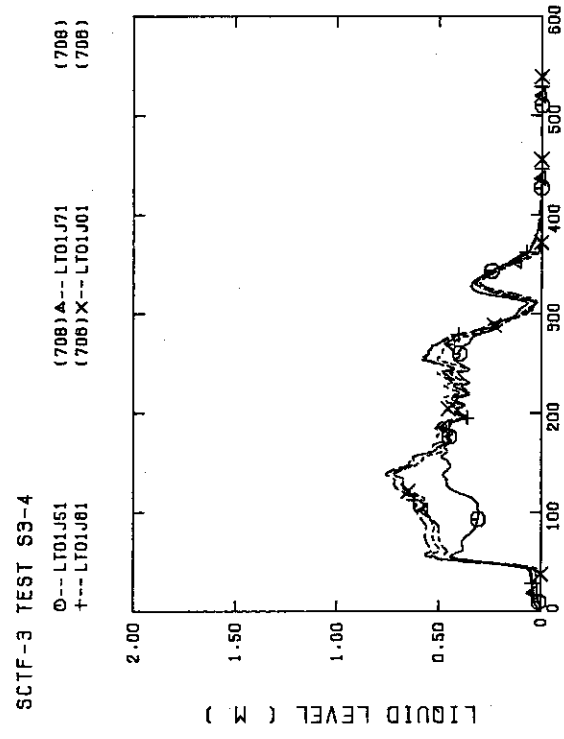

FIG. C-28 LIQUID LEVEL ABOVE UCSP (BUNDLE 5,6,7,8 AND CORE BUFFLE)

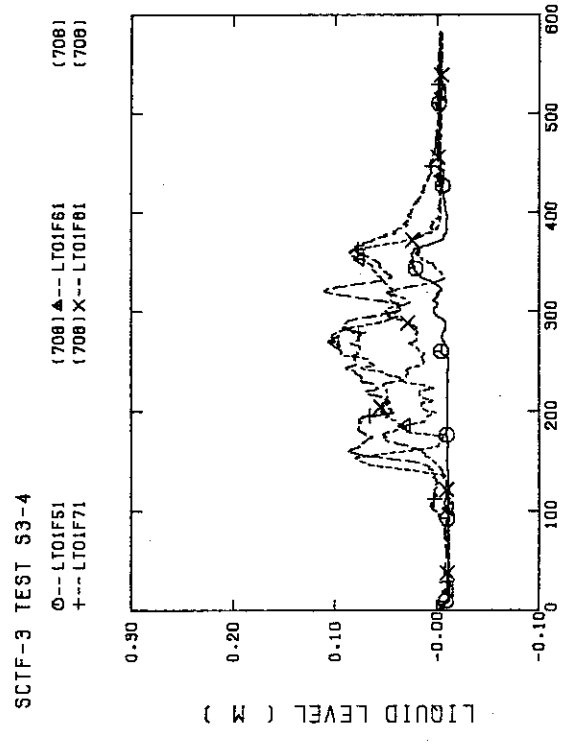

FIG. C-26 LIQUID LEVEL ABOVE END BOX TIE PLATE (BUNDLE 5,6,7,8)

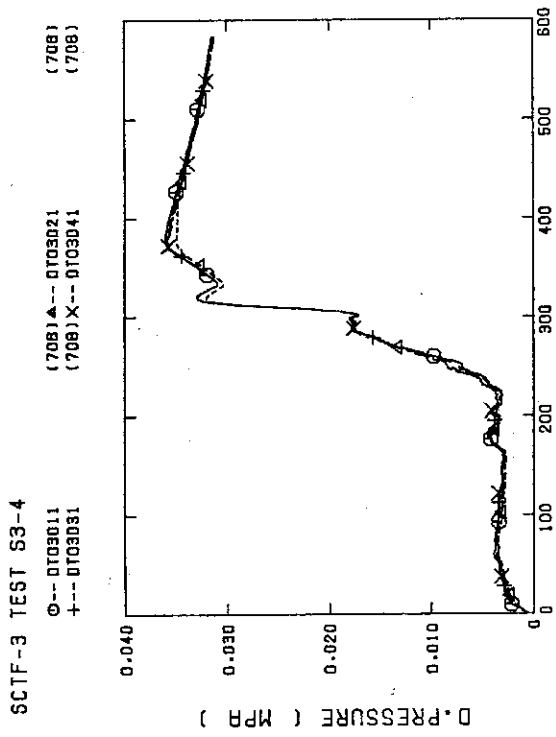

FIG. C-31 DIFFERENTIAL PRESSURE OF CORE FULL HIGHT (BUNDLE 1,2,3,4)

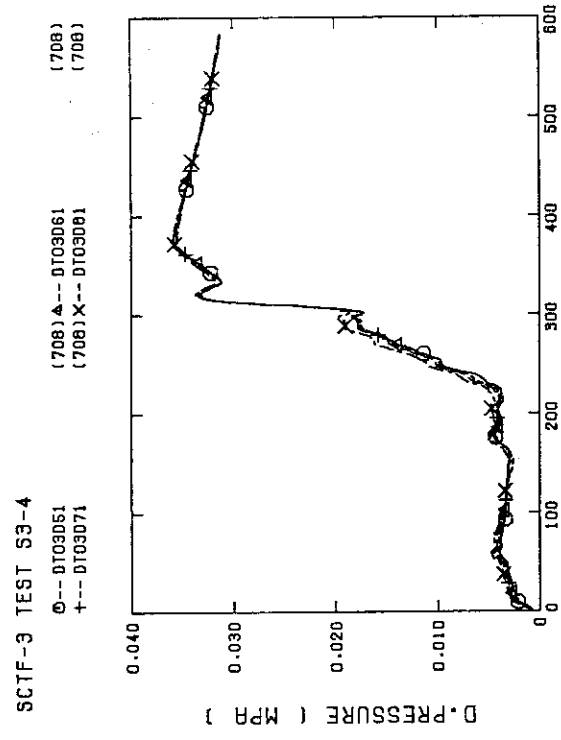

FIG. C-32 DIFFERENTIAL PRESSURE OF CORE FULL HIGHT (BUNDLE 5,6,7,8)

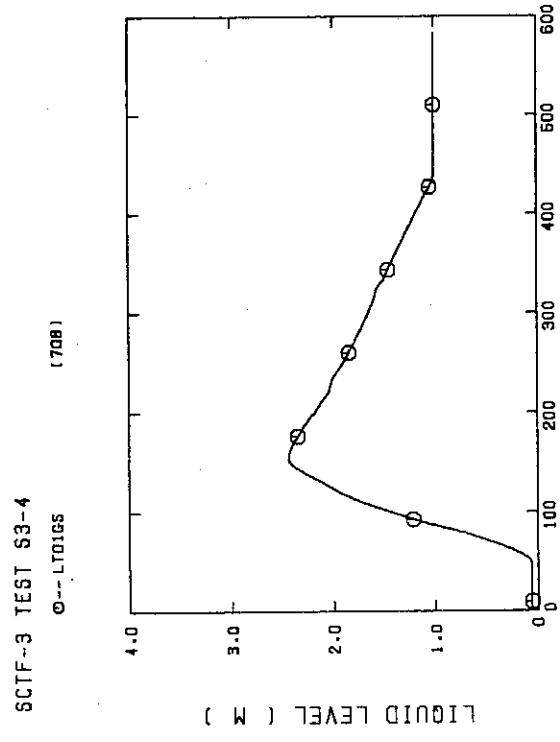

FIG. C-29 LIQUID LEVEL IN STEAM/WATER SEPARATOR

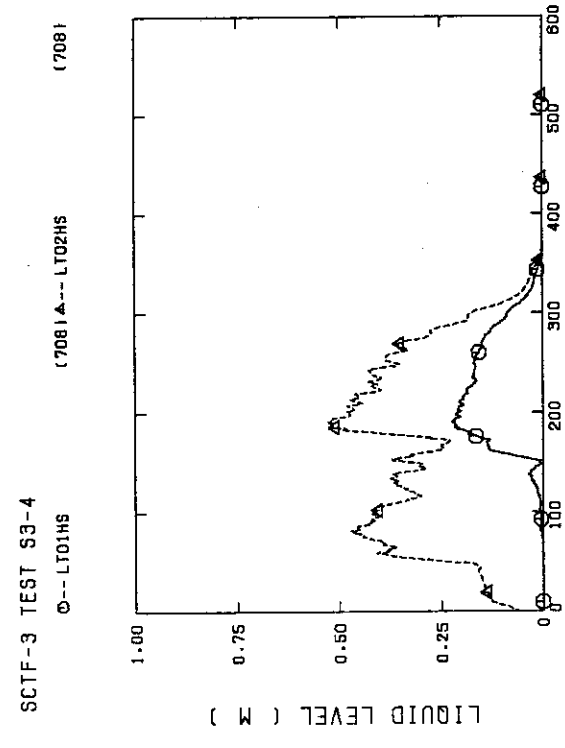

FIG. C-30 LIQUID LEVEL IN HOT LEG (01HS - PV SIDE, 02HS - STEAM/WATER SEPARATOR SIDE)

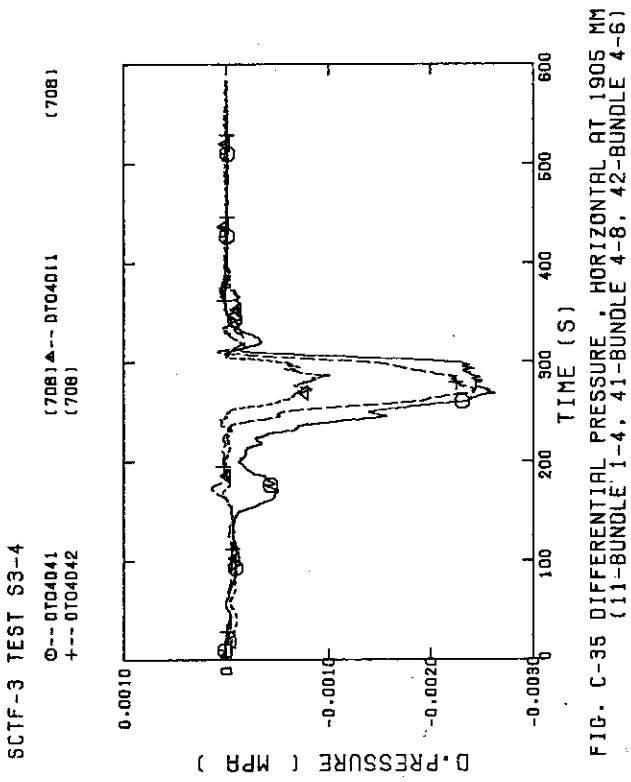

FIG. C-35 DIFFERENTIAL PRESSURE , HORIZONTAL AT 1905 MM
(11-BUNDLE 1-4, 41-BUNDLE 4-8, 42-BUNDLE 4-6)

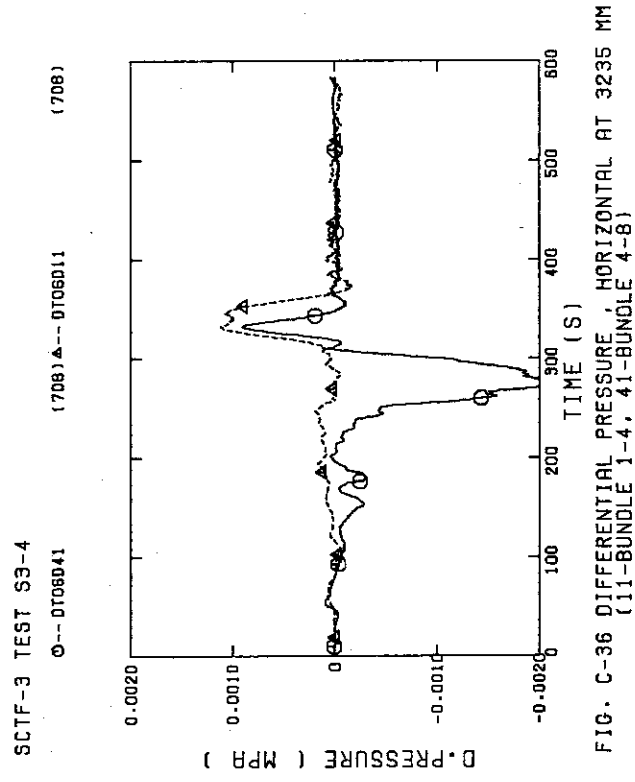

FIG. C-36 DIFFERENTIAL PRESSURE , HORIZONTAL AT 3235 MM
(11-BUNDLE 1-4, 41-BUNDLE 4-8)

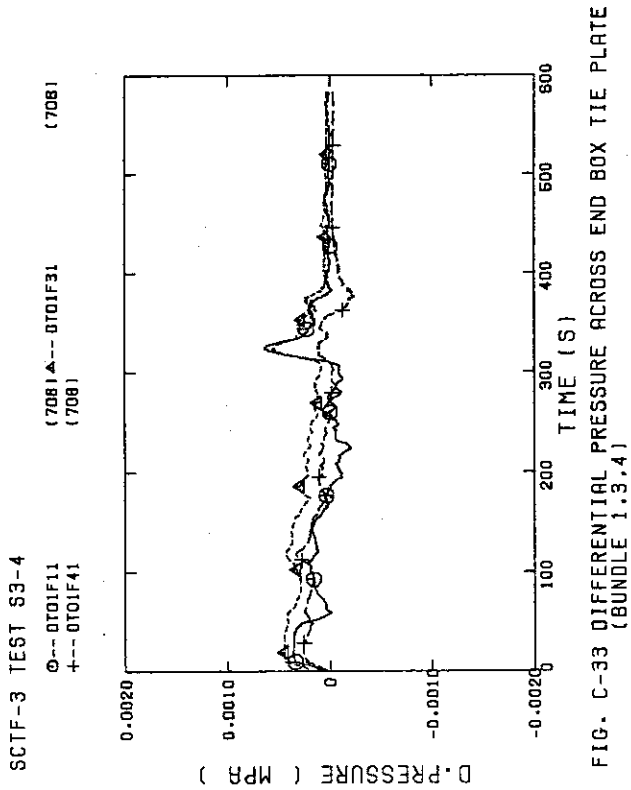

FIG. C-33 DIFFERENTIAL PRESSURE ACROSS END BOX TIE PLATE
(BUNDLE 1,3,4)

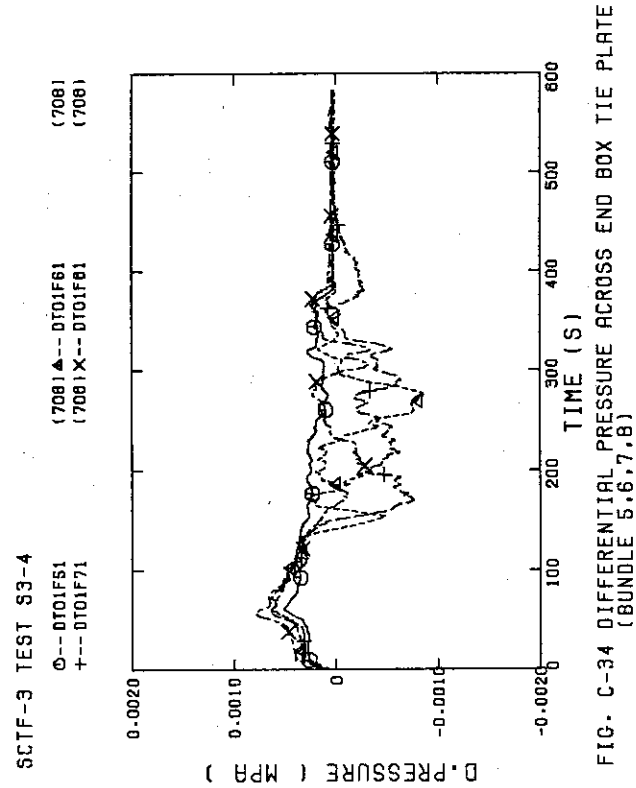

FIG. C-34 DIFFERENTIAL PRESSURE ACROSS END BOX TIE PLATE
(BUNDLE 5,6,7,8)

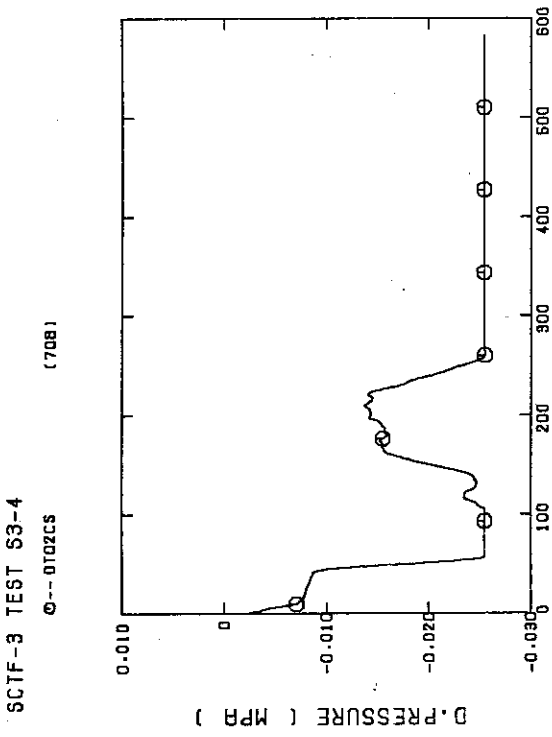

FIG. C-39 DIFFERENTIAL PRESSURE OF INTACT COLD LEG

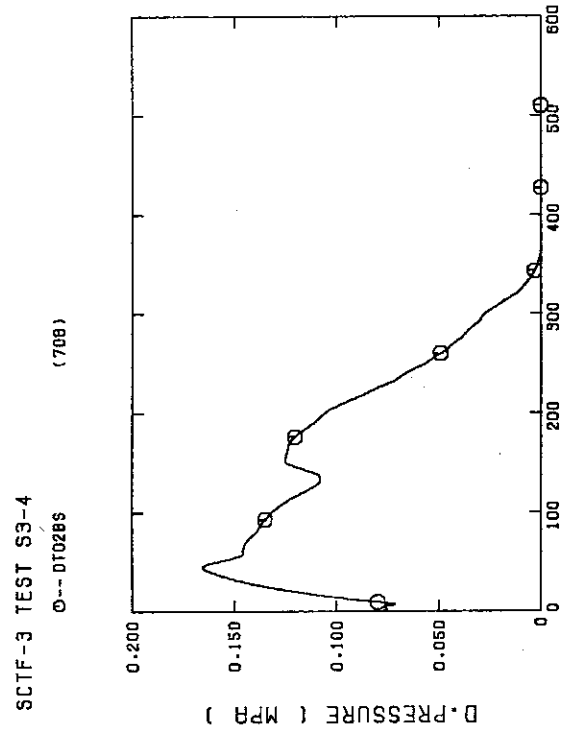

FIG. C-40 DIFFERENTIAL PRESSURE, STEAM/WATER SEPARATOR - CONTAINMENT TANK-II

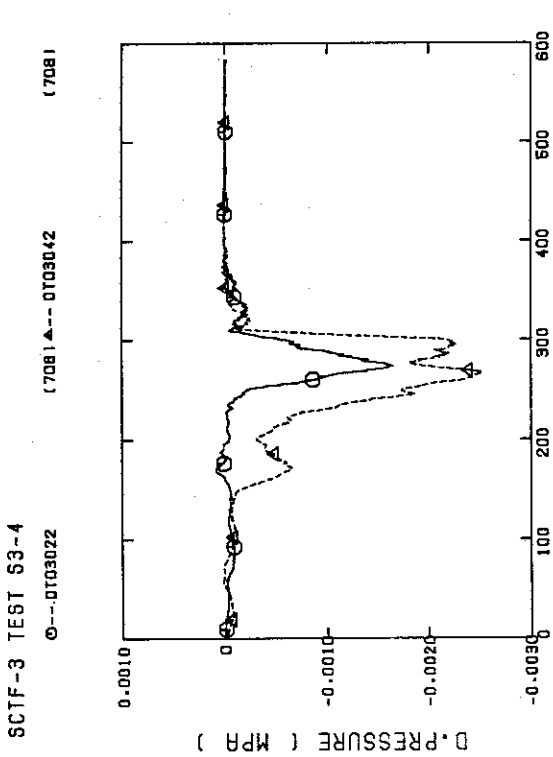

FIG. C-37 DIFFERENTIAL PRESSURE, HORIZONTAL AT 1365 MM (22-BUNDLE 2-4, 42-BUNDLE 4-8)

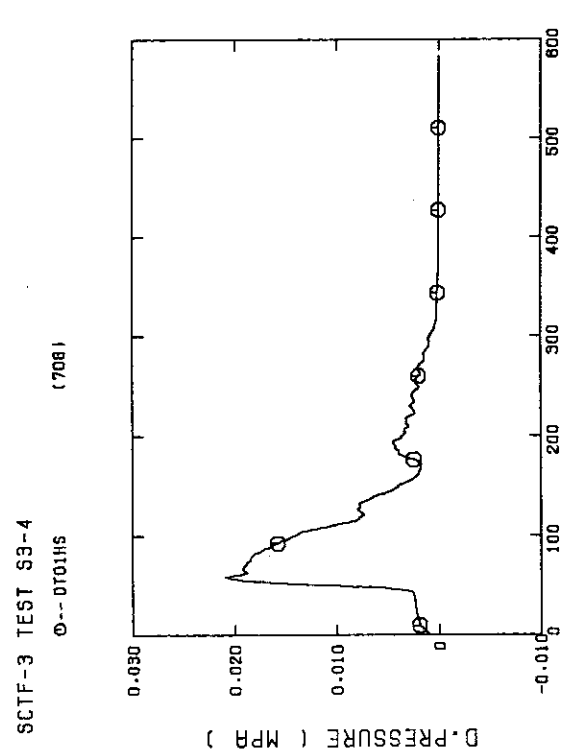

FIG. C-38 DIFFERENTIAL PRESSURE OF HOT LEG HOT LEG INLET - STEAM/WATER SEPARATOR INLET

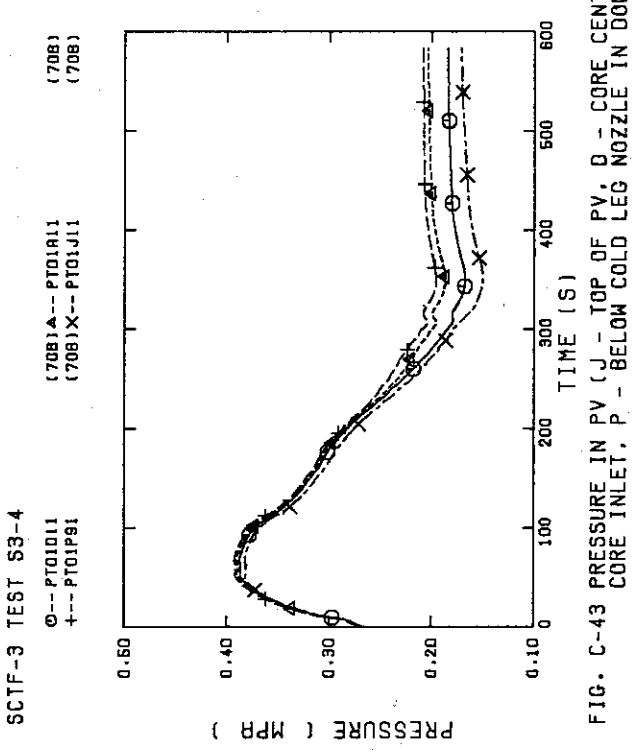

FIG. C-43 PRESSURE IN PV (J - TOP OF PV, Q - CORE CENTER, A - CORE INLET, P - BELOW COLD LEG NOZZLE IN DOWNCOMER)

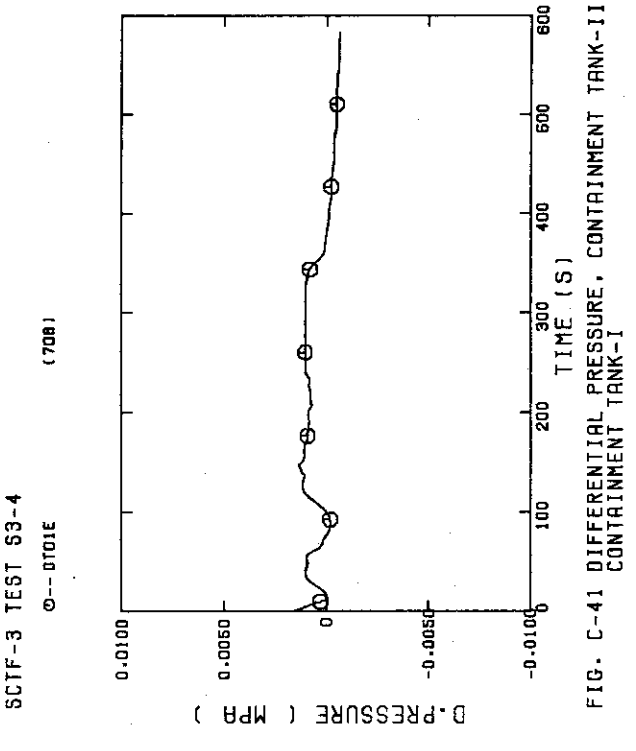

FIG. C-41 DIFFERENTIAL PRESSURE, CONTAINMENT TANK-II - CONTAINMENT TANK-I

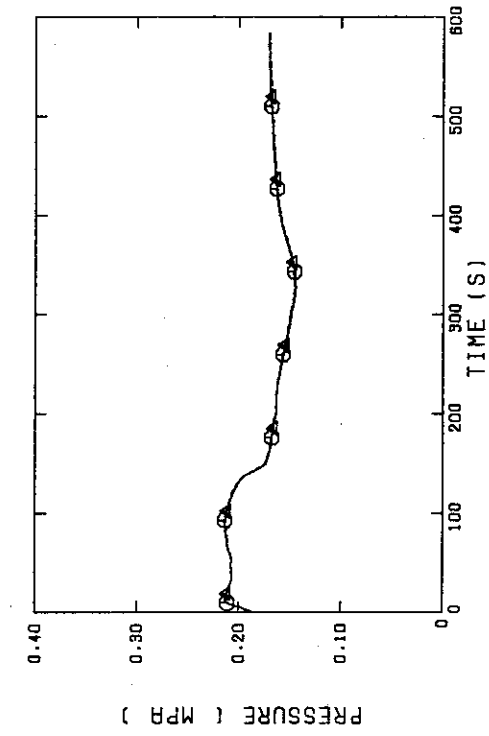

FIG. C-44 PRESSURE AT TOP OF CONTAINMENT TANK-I AND CONTAINMENT TANK-II (F-CONTAINMENT TANK-I, B-CONTAINMENT TANK-II)

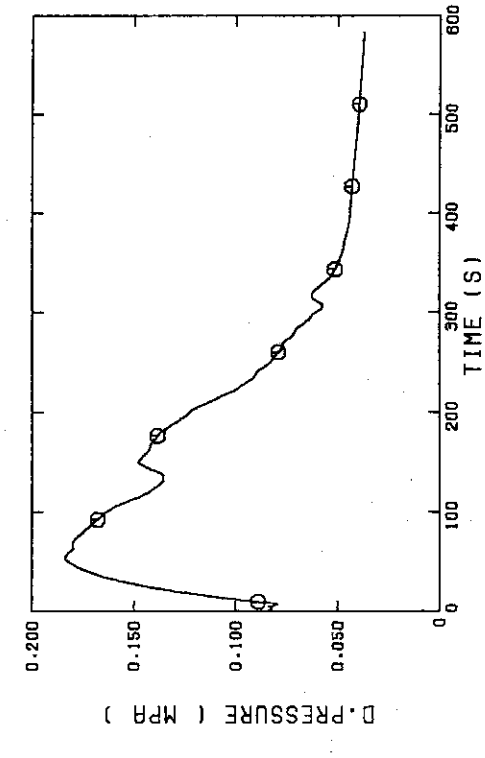

FIG. C-42 DIFFERENTIAL PRESSURE OF BROKEN COLD LEG - PV SIDE, DOWNCOMER - CONTAINMENT TANK-I

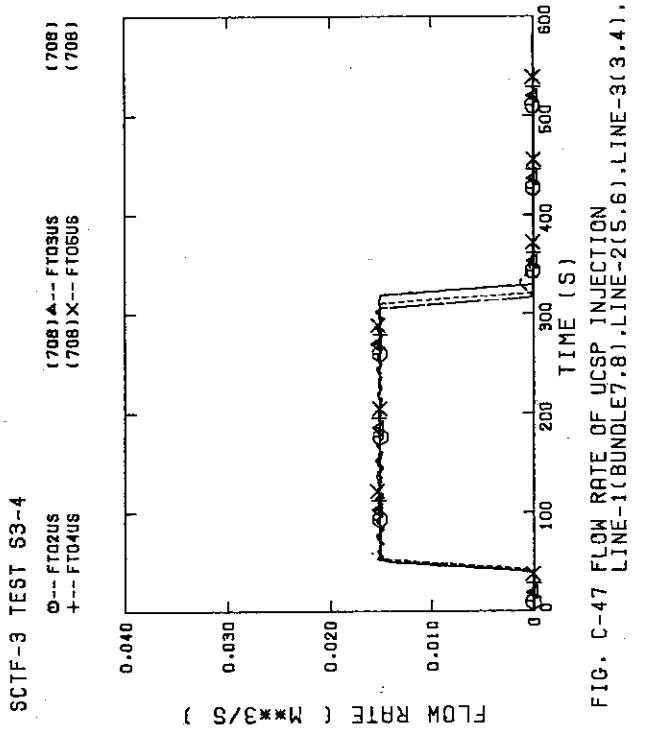

FIG. C-47 FLOW RATE OF UCSP INJECTION
LINE-1(BUNDLE7,8),LINE-2(5,6),LINE-3(3,4),LINE-4
(1,2)

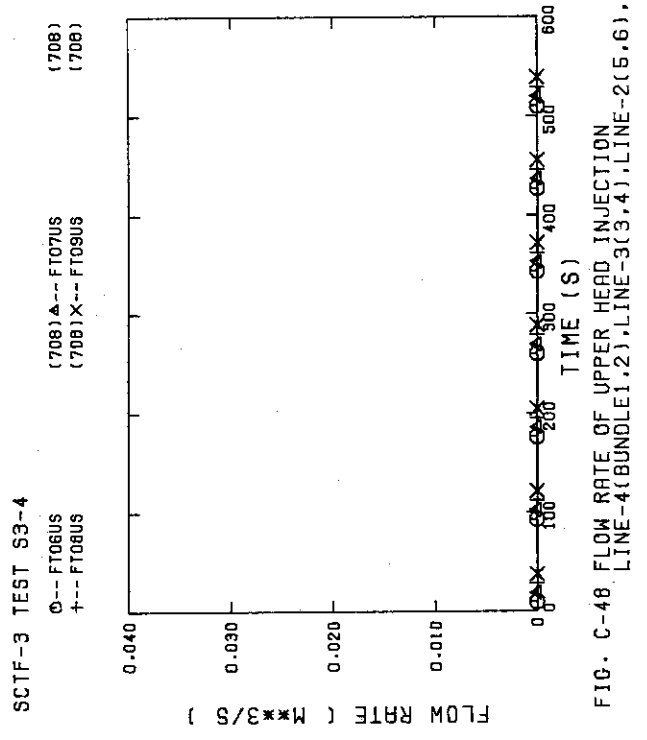

FIG. C-48 FLOW RATE OF UPPER HEAD INJECTION
LINE-4(BUNDLE1,2),LINE-3(3,4),LINE-2(5,6),LINE-1(7,8)

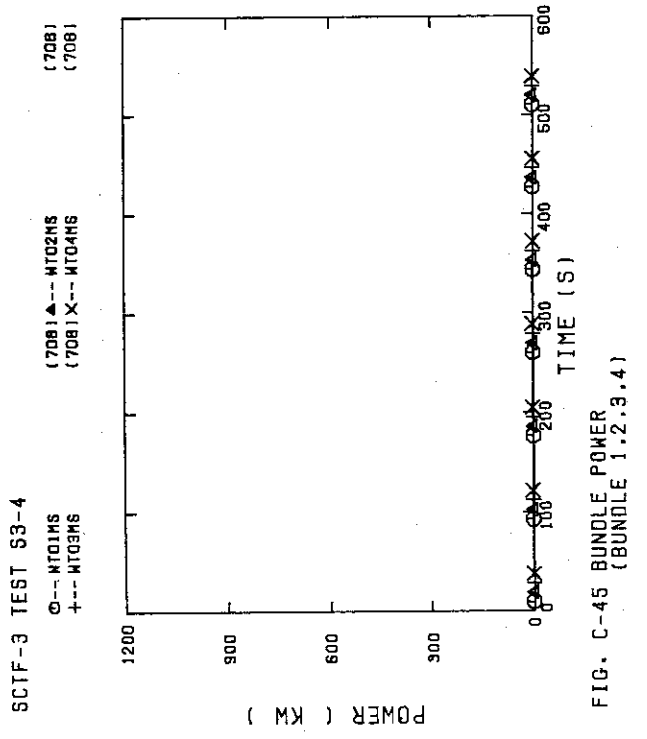

FIG. C-45 BUNDLE POWER
(BUNDLE 1,2,3,4)

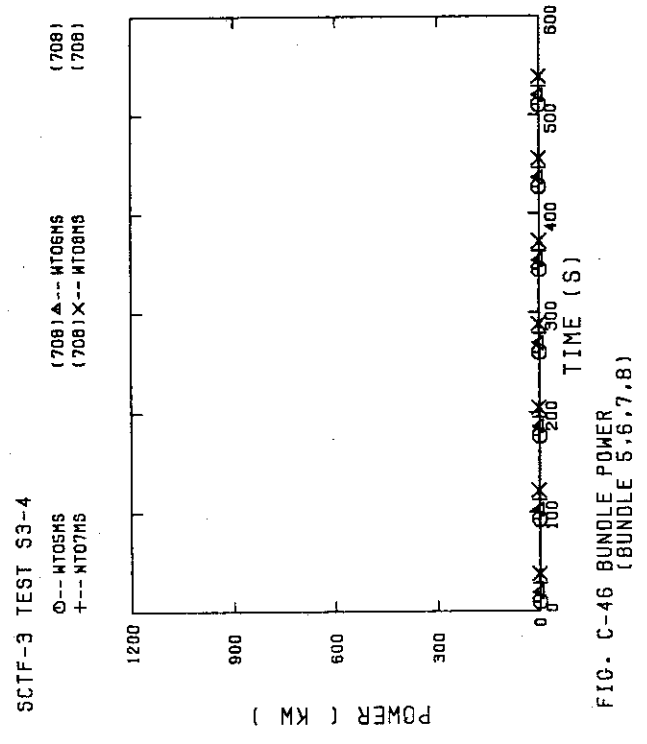

FIG. C-46 BUNDLE POWER
(BUNDLE 5,6,7,8)

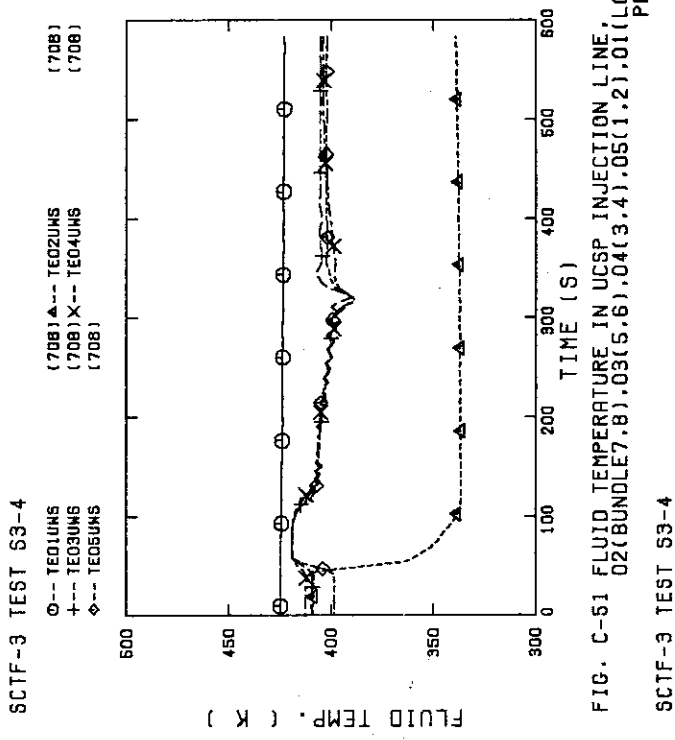

FIG. C-51 FLUID TEMPERATURE IN UCSP INJECTION LINE, 02(BUNDLE(7,8),03(5,6),04(3,4),05(1,2),01(LOWER PLENUM)

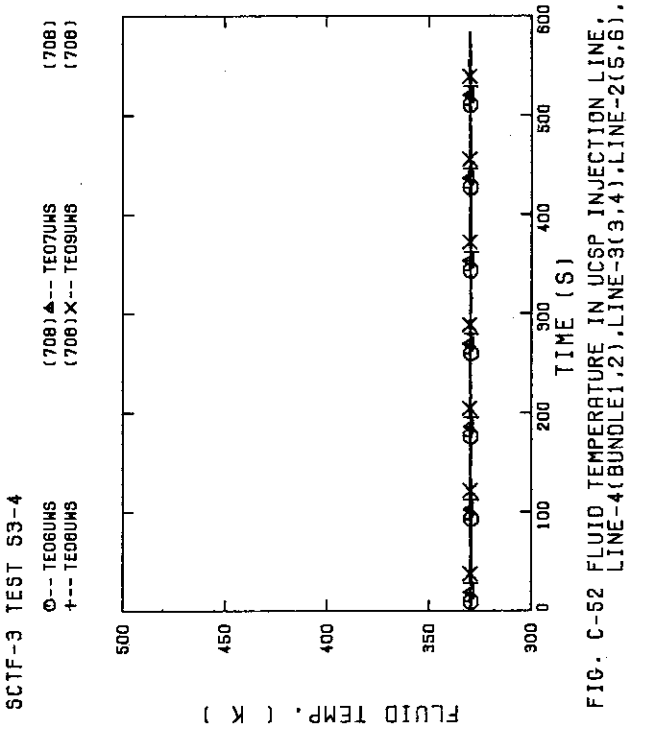

FIG. C-52 FLUID TEMPERATURE IN UCSP INJECTION LINE, LINE-4(BUNDLE(1,2),LINE-3(3,4),LINE-2(5,6),LINE-1(7,8)

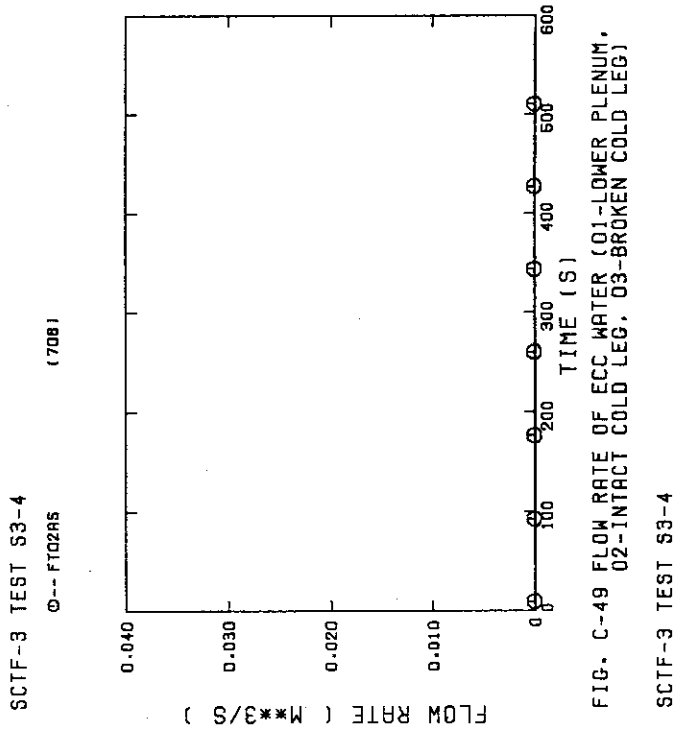

FIG. C-49 FLOW RATE OF ECC WATER (01-LOWER PLENUM, 02-INTACT COLD LEG, 03-BROKEN COLD LEG)

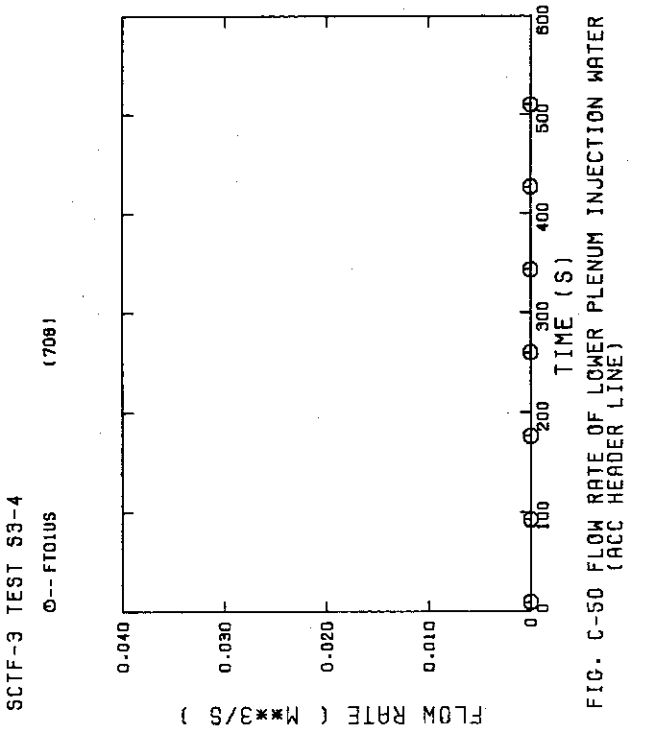

FIG. C-50 FLOW RATE OF LOWER PLENUM INJECTION WATER (ACC HEADER LINE)

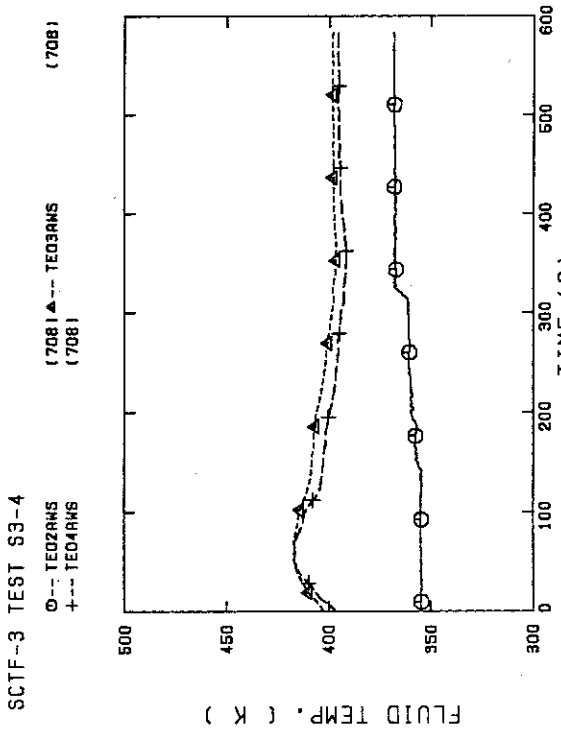

FIG. C-53 FLUID TEMPERATURE IN ECC INJECTION PORT
HOT LEG, IC LEG, BC LEG

Appendix D Selected data of Test S3-5

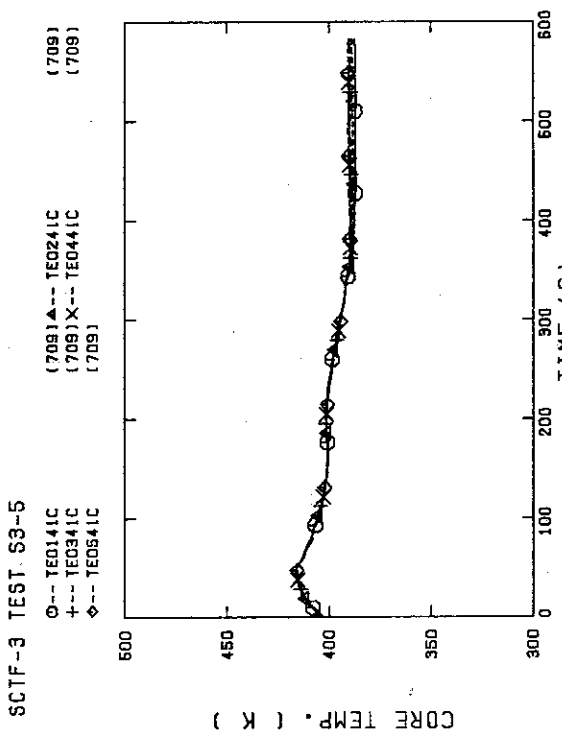

FIG. D-03 HEATER ROD TEMPERATURE (BUNDLE 4-1C, LOWER HALF)

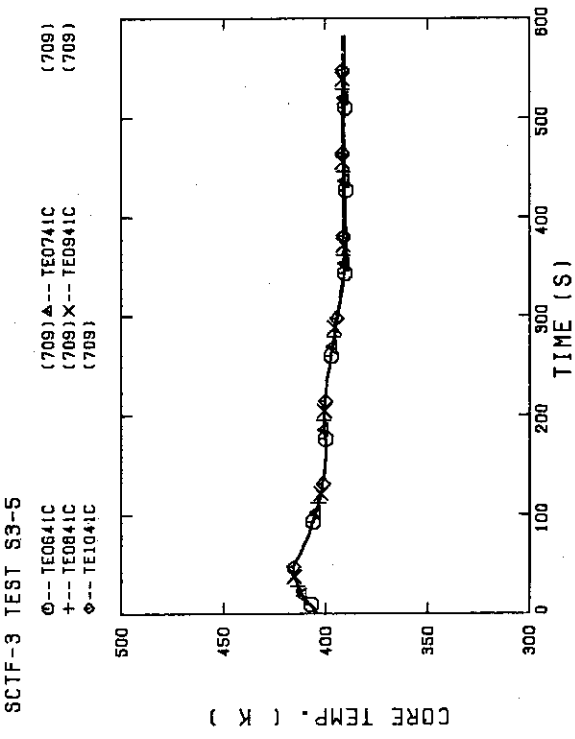

FIG. D-04 HEATER ROD TEMPERATURE (BUNDLE 4-1C, UPPER HALF)

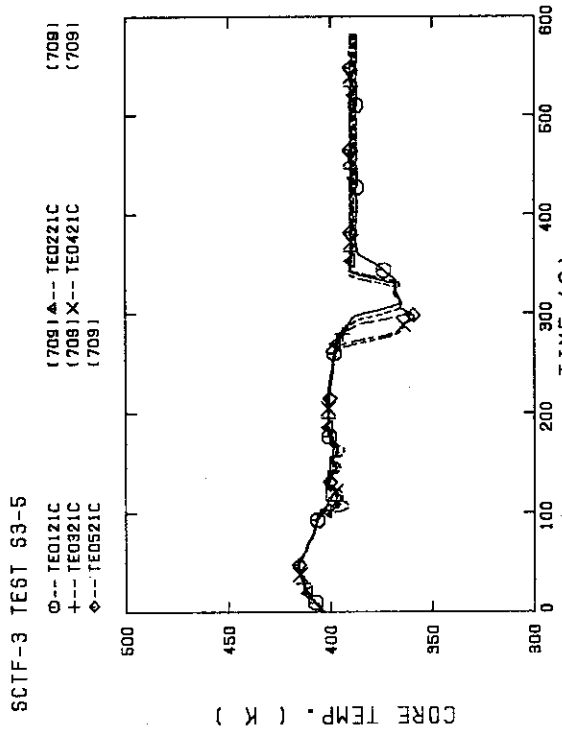

FIG. D-01 HEATER ROD TEMPERATURE (BUNDLE 2-1C, LOWER HALF)

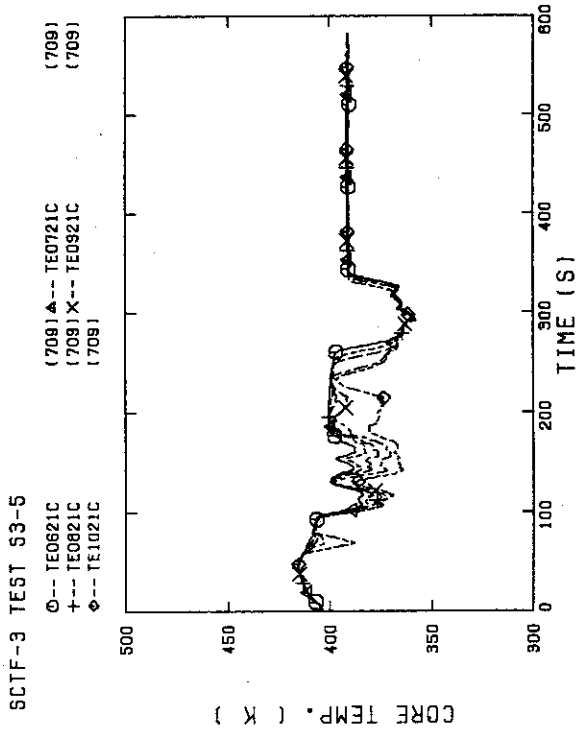

FIG. D-02 HEATER ROD TEMPERATURE (BUNDLE 2-1C, UPPER HALF)

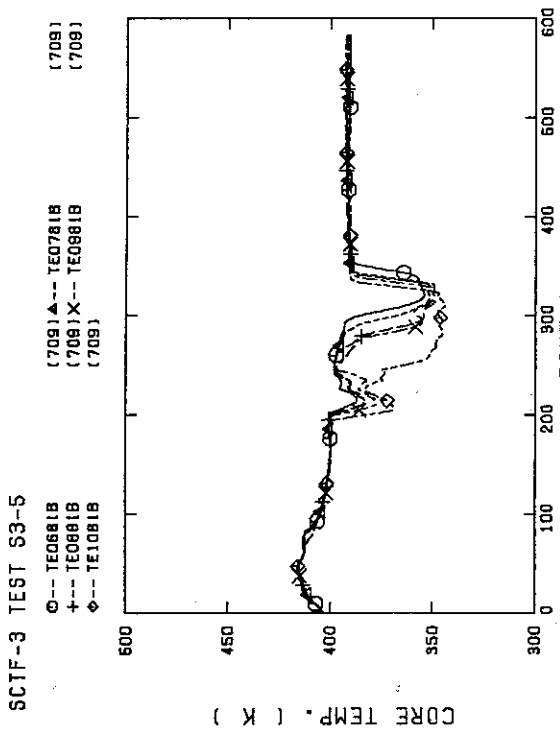

FIG. D-07 HEATER ROD TEMPERATURE (BUNDLE 8-1B, UPPER HALF)

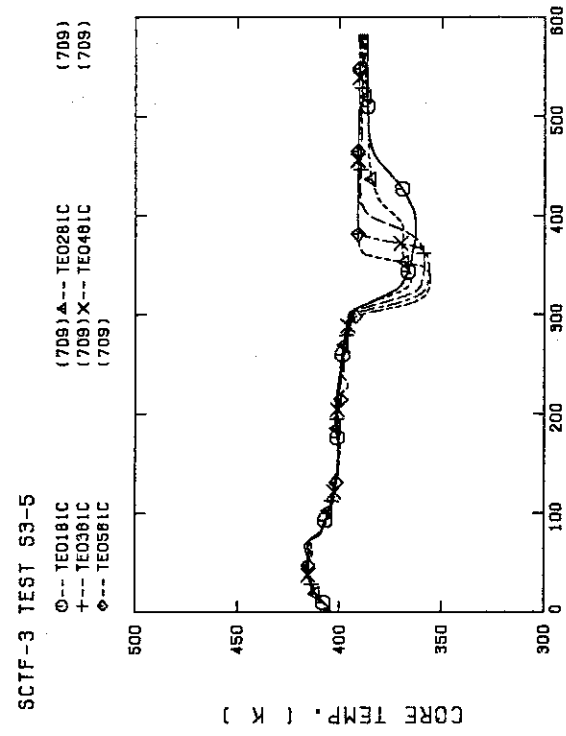

FIG. D-08 HEATER ROD TEMPERATURE (BUNDLE 8-1C, LOWER HALF)

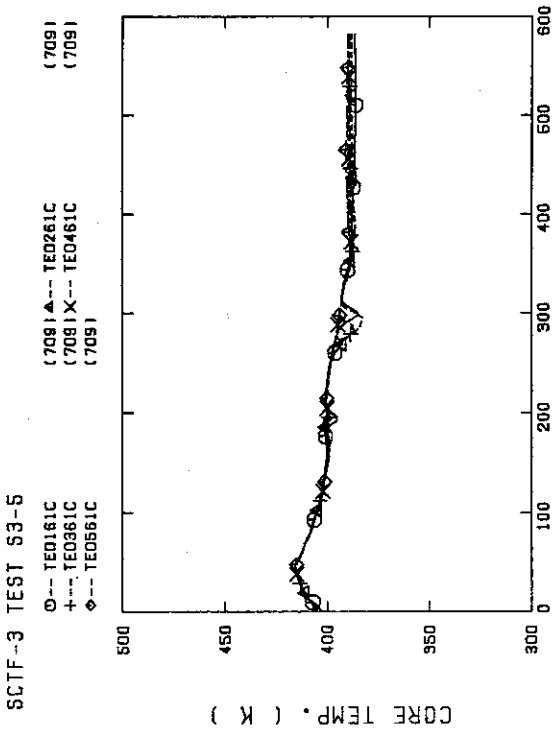

FIG. D-05 HEATER ROD TEMPERATURE (BUNDLE 6-1C, LOWER HALF)

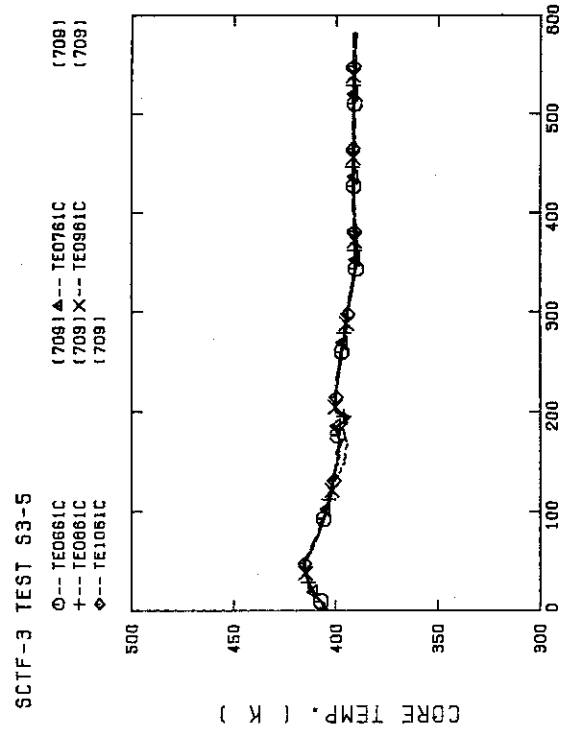

FIG. D-06 HEATER ROD TEMPERATURE (BUNDLE 6-1C, UPPER HALF)

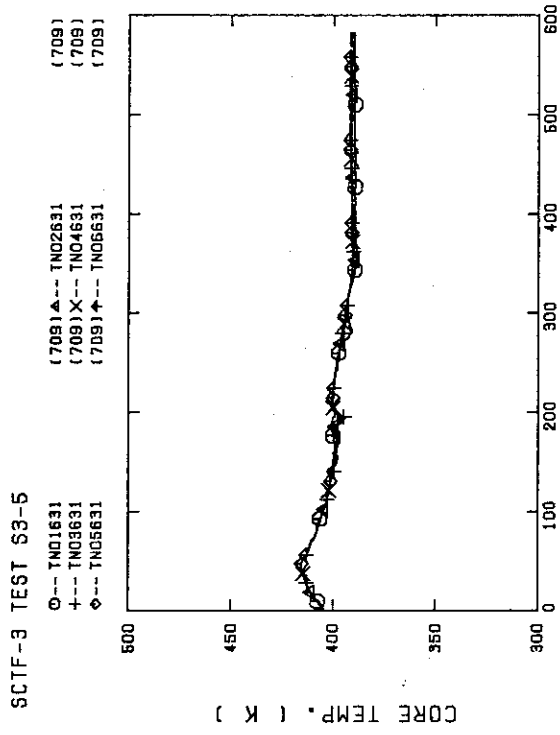

FIG. D-11 NON-HEATED ROD TEMPERATURE (BUNDLE 6-31)

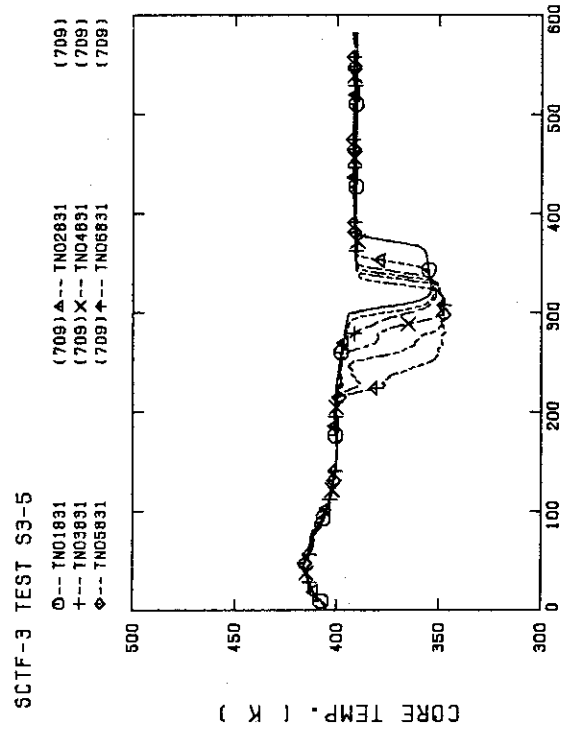

FIG. D-12 NON-HEATED ROD TEMPERATURE (BUNDLE 6-31)

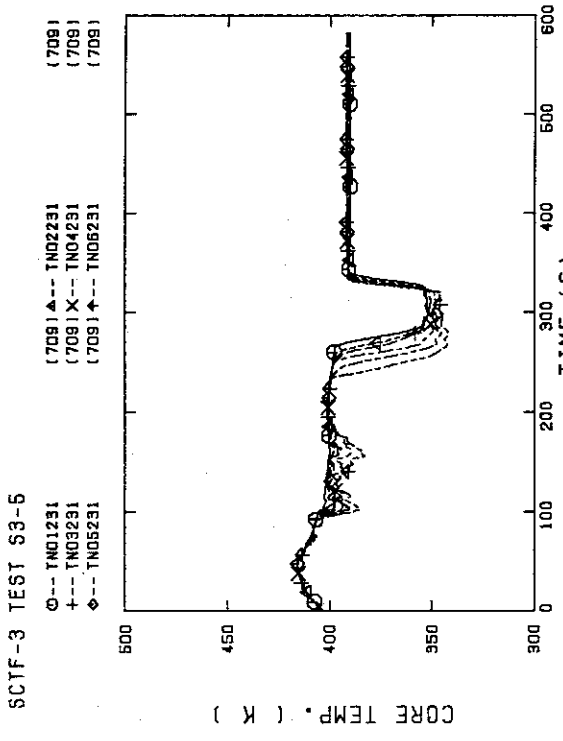

FIG. D-09 NON-HEATED ROD TEMPERATURE (BUNDLE 2-31)

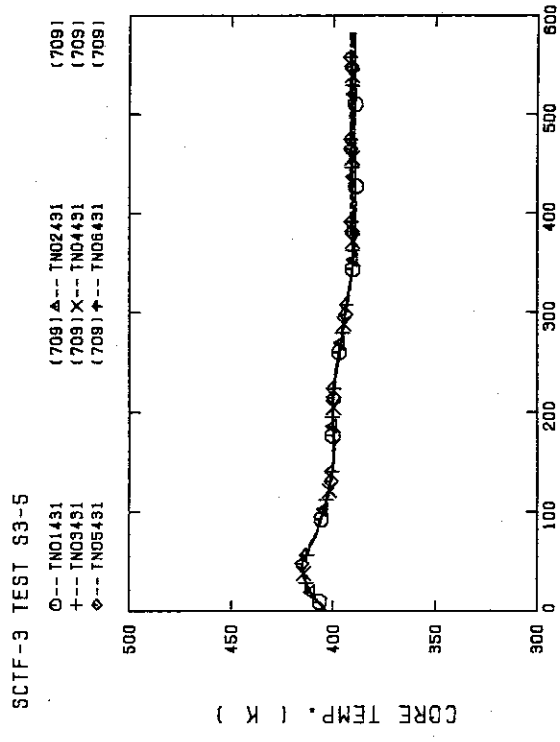

FIG. D-10 NON-HEATED ROD TEMPERATURE (BUNDLE 4-31)

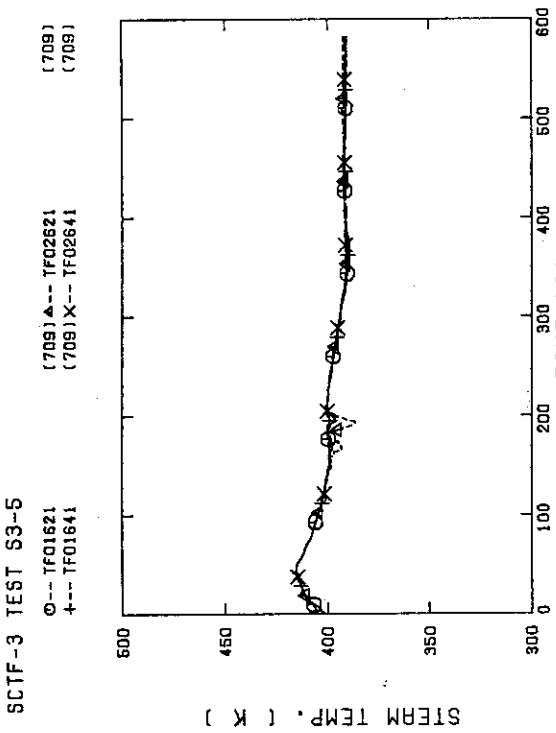

FIG. D-13 STEAM TEMPERATURE IN CORE, BUNDLE 2

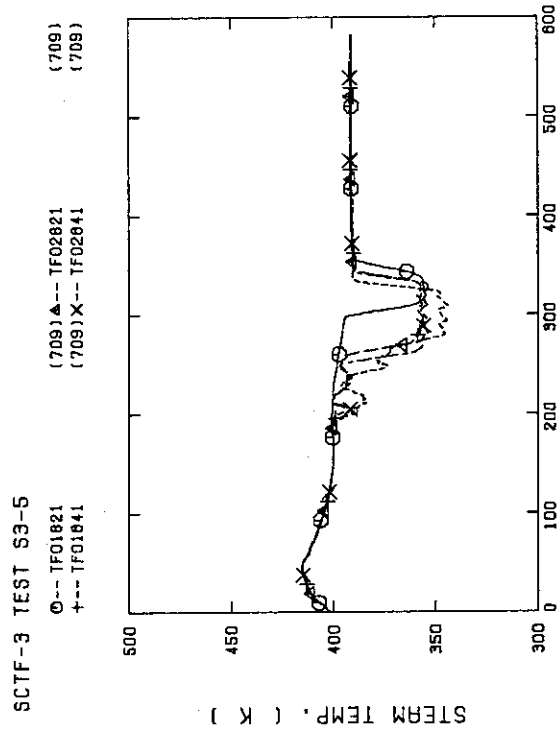

FIG. D-14 STEAM TEMPERATURE IN CORE, BUNDLE 4

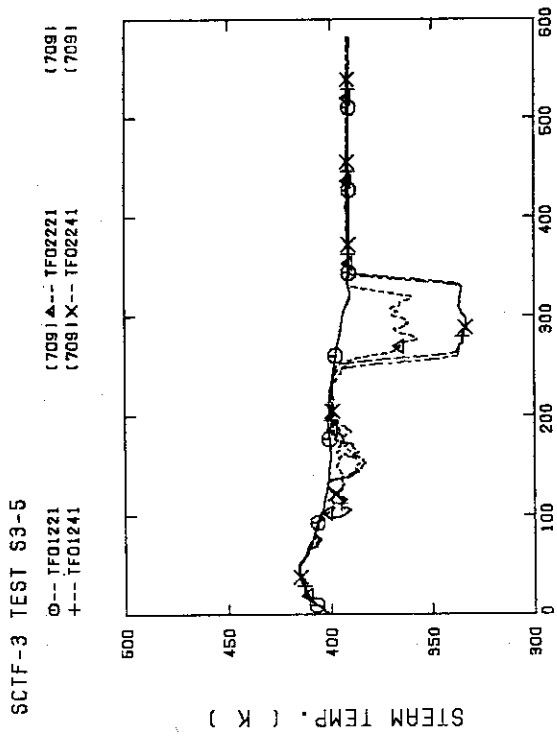

FIG. D-15 STEAM TEMPERATURE IN CORE, BUNDLE 6

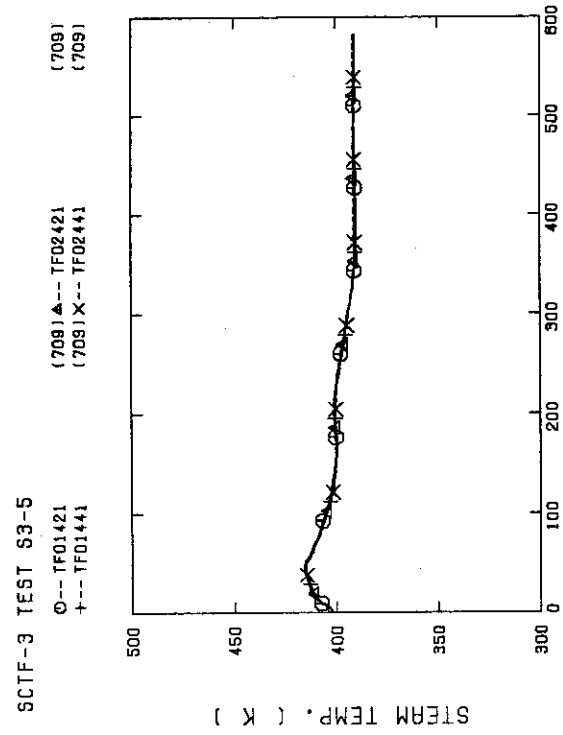

FIG. D-16 STEAM TEMPERATURE IN CORE, BUNDLE 8

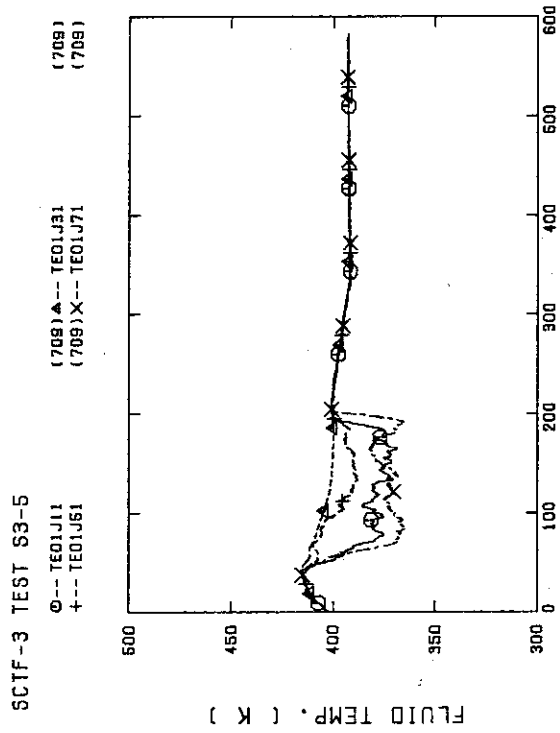

FIG. D-19 FLUID TEMPERATURE ABOVE UCSP
(BUNDLE 1,3,5,7 100MM ABOVE UCSP)

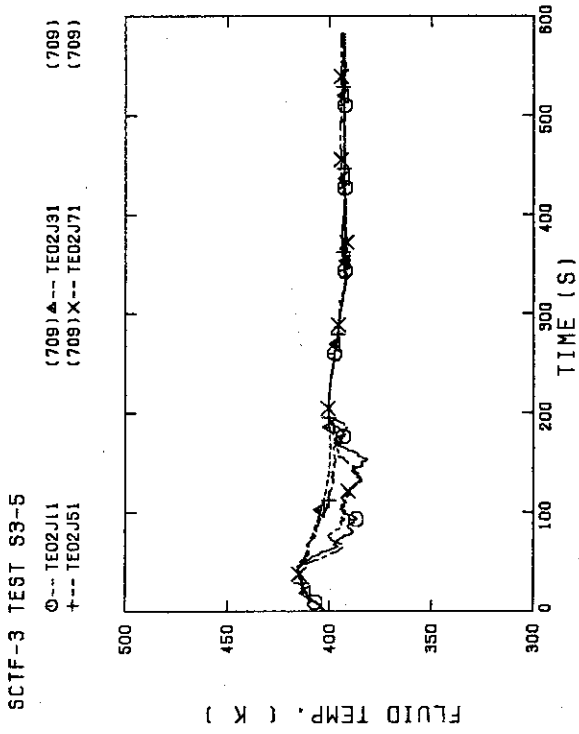

FIG. D-20 FLUID TEMPERATURE ABOVE UCSP
(BUNDLE 1,3,5,7 250MM ABOVE UCSP)

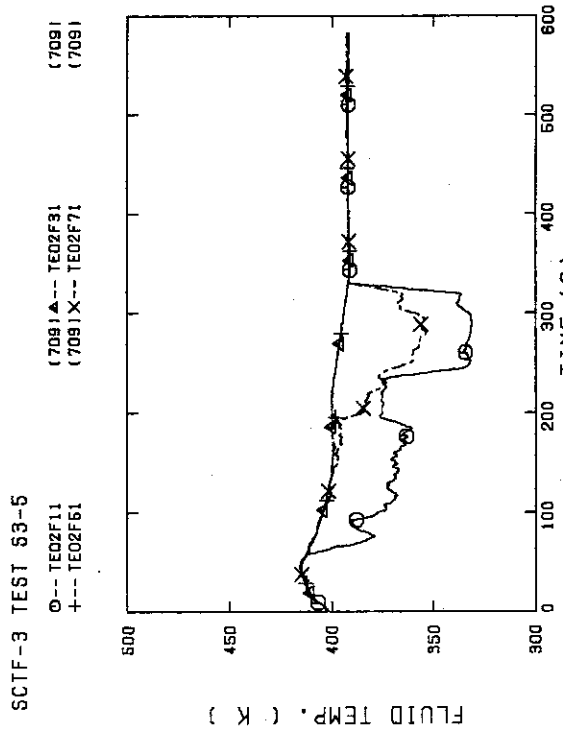

FIG. D-17 FLUID TEMPERATURE JUST ABOVE END BOX TIE PLATE
(BUNDLE 1,3,5,7 OPPOSITE SIDE OF COLD LEG, OUTER)

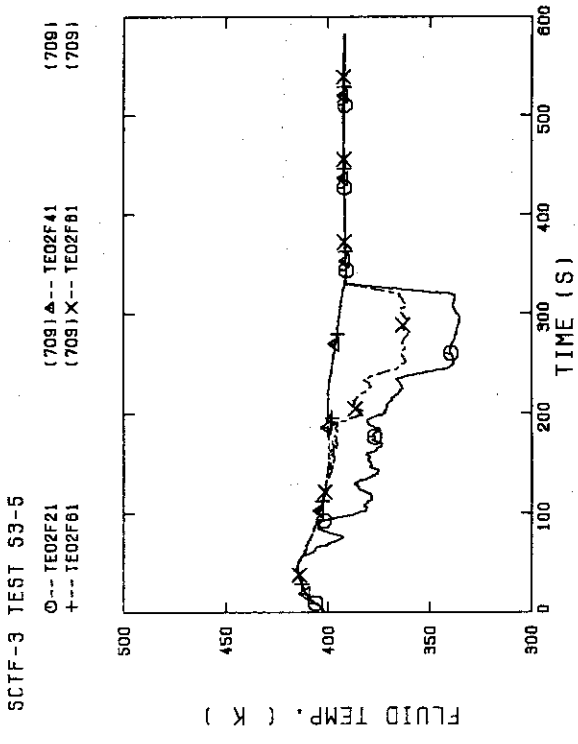

FIG. D-18 FLUID TEMPERATURE JUST ABOVE END BOX TIE PLATE
(BUNDLE 2,4,6,8 OPPOSITE SIDE OF COLD LEG, OUTER)

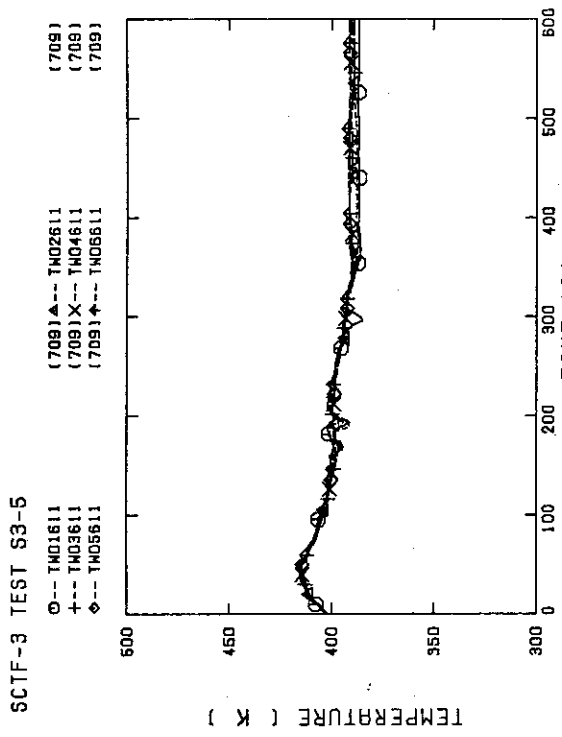

FIG. D-23 TEMPERATURE FOR SPUTTERING DETECTION
BUNDLE 6 , REGION 1 , TYPE 3

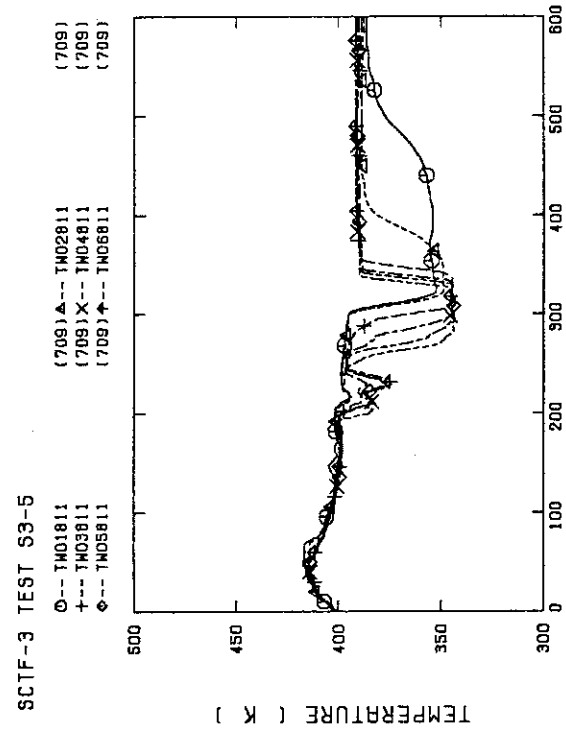

FIG. D-24 TEMPERATURE FOR SPUTTERING DETECTION
BUNDLE 8 , REGION 1 , TYPE 3

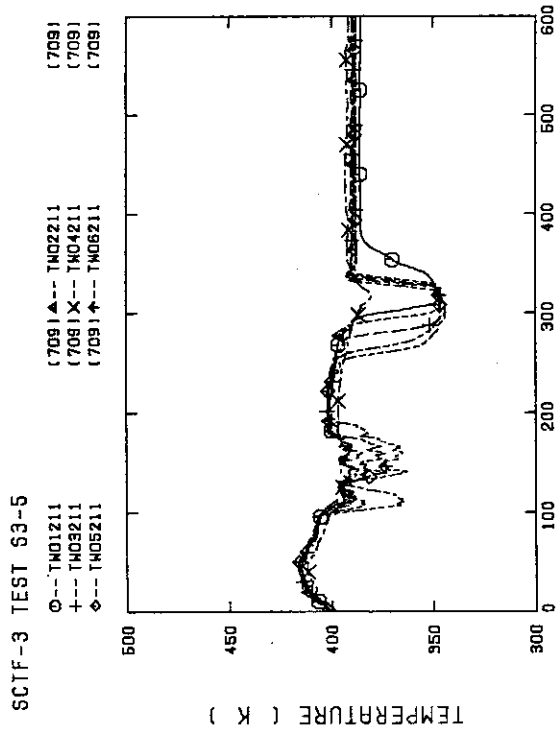

FIG. D-21 TEMPERATURE FOR SPUTTERING DETECTION
BUNDLE 2 , REGION 1 , TYPE 3

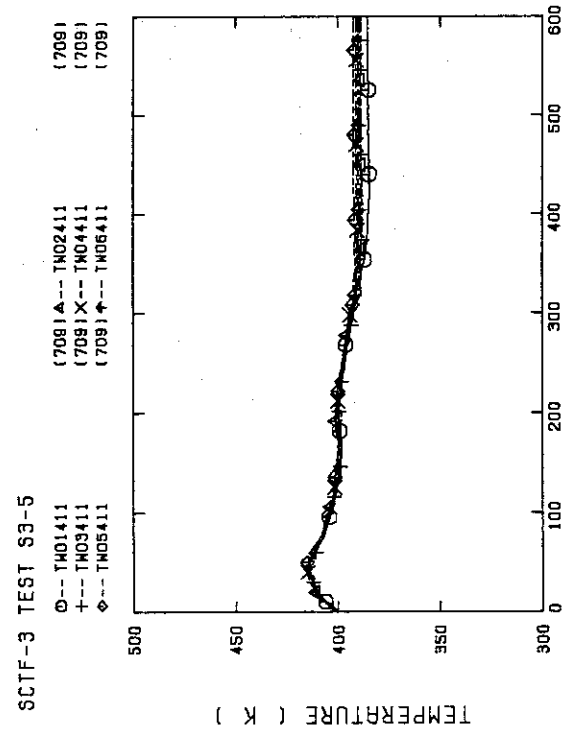

FIG. D-22 TEMPERATURE FOR SPUTTERING DETECTION
BUNDLE 4 , REGION 1 , TYPE 3

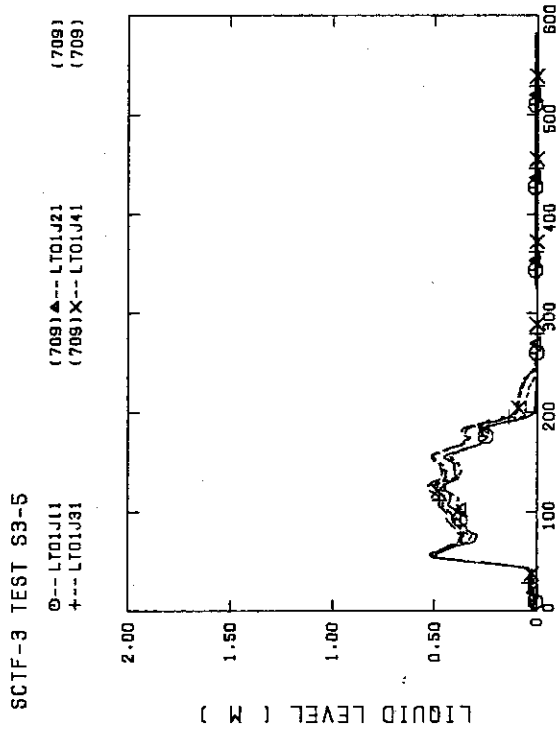

FIG. D-27 LIQUID LEVEL ABOVE UCSP (BUNDLE 1,2,3,4)

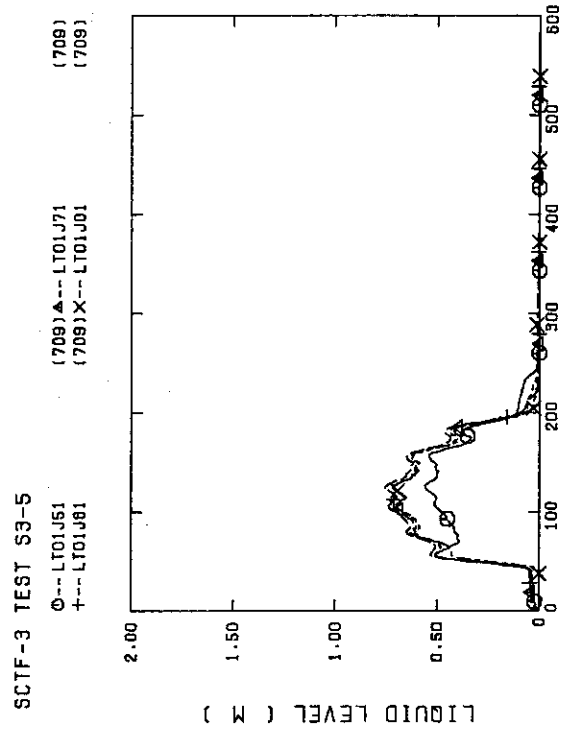

FIG. D-28 LIQUID LEVEL ABOVE UCSP (BUNDLE 5,6,7,8 AND CORE BUFFLE)

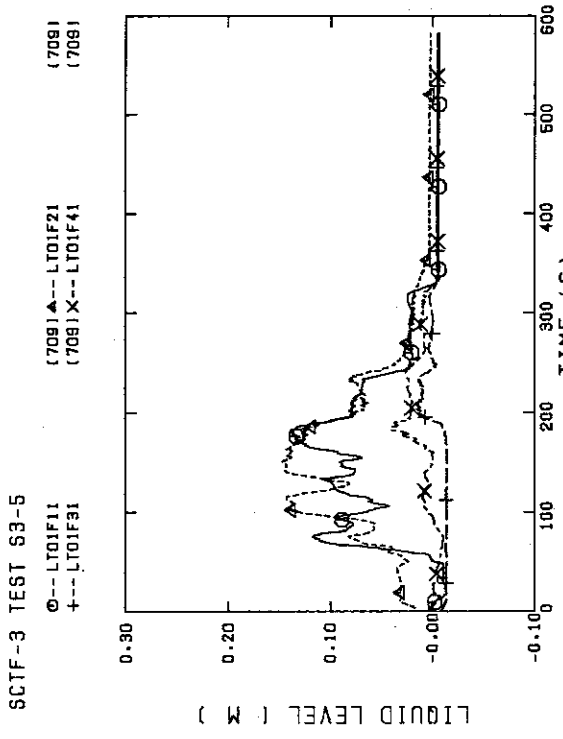

FIG. D-25 LIQUID LEVEL ABOVE END BOX TIE PLATE (BUNDLE 1,2,3,4)

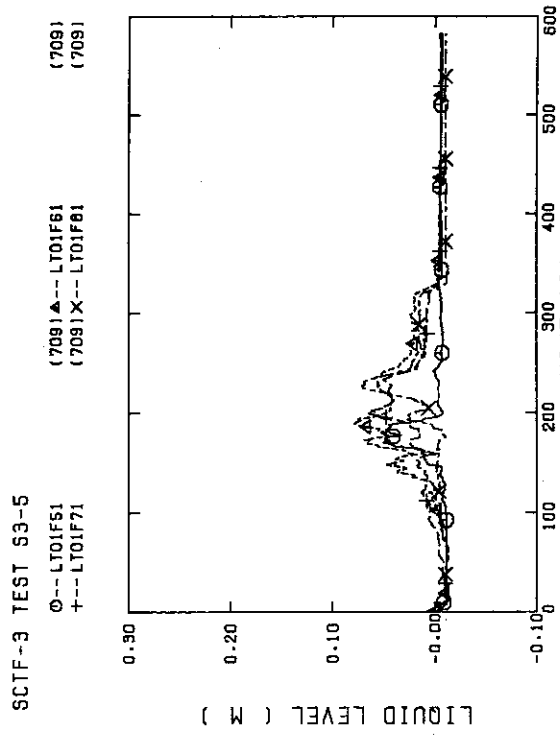

FIG. D-26 LIQUID LEVEL ABOVE END BOX TIE PLATE (BUNDLE 5,6,7,8)

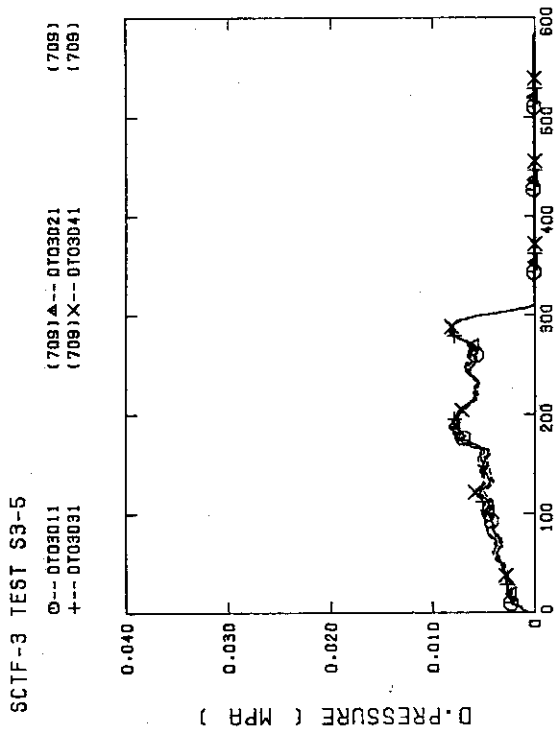

FIG. D-31 DIFFERENTIAL PRESSURE OF CORE FULL HIGHT (BUNDLE 1,2,3,4)

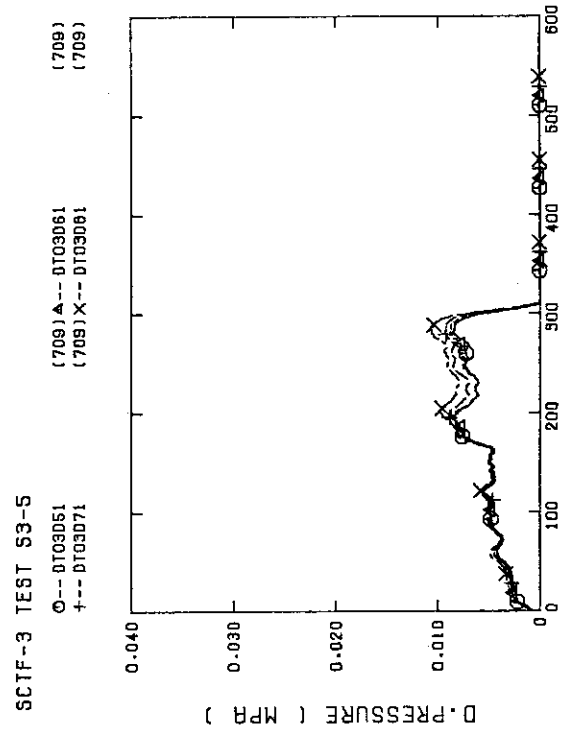

FIG. D-32 DIFFERENTIAL PRESSURE OF CORE FULL HIGHT (BUNDLE 5,6,7,8)

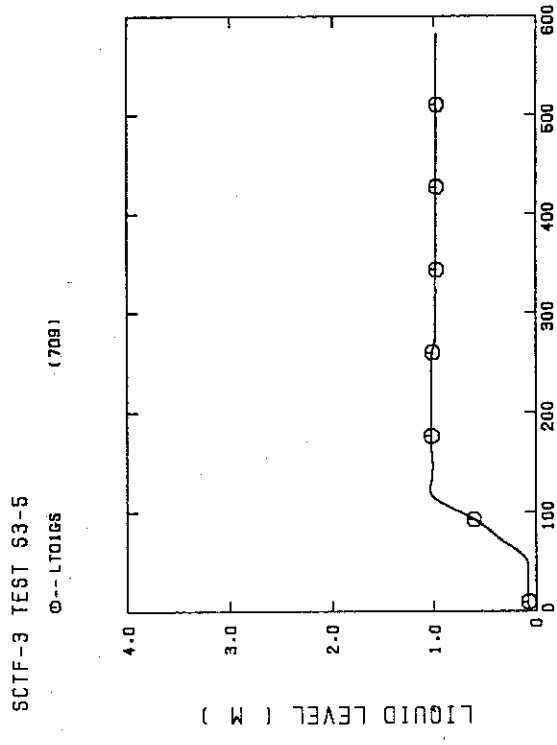

FIG. D-29 LIQUID LEVEL IN STEAM/WATER SEPARATOR

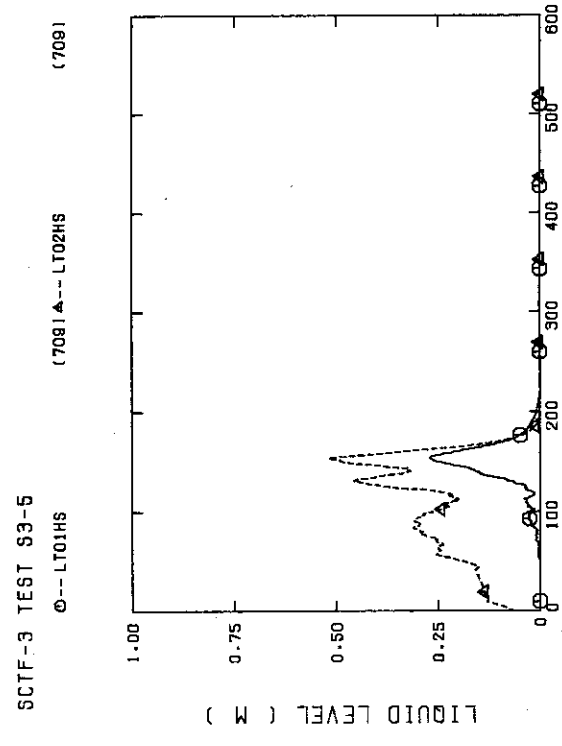

FIG. D-30 LIQUID LEVEL IN HOT LEG (O1HS - PV SIDE, O2HS - STEAM/WATER SEPARATOR SIDE)

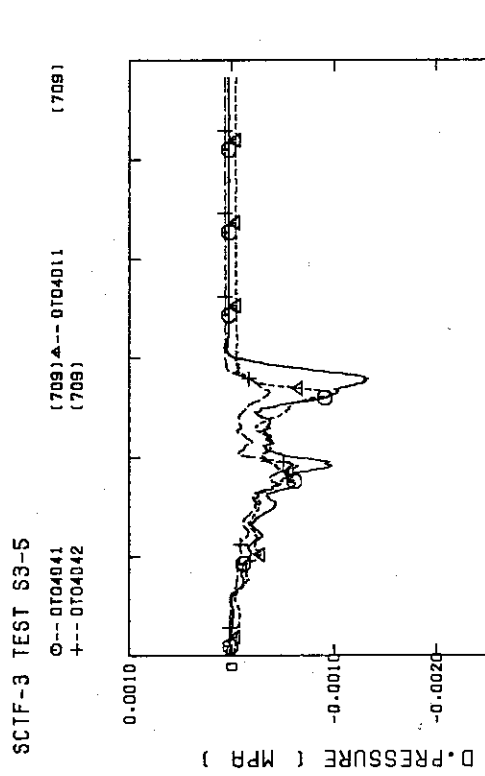

FIG. D-35 DIFFERENTIAL PRESSURE , HORIZONTAL AT 1905 MM (11-BUNDLE 1-4, 41-BUNDLE 4-8, 42-BUNDLE 4-6)

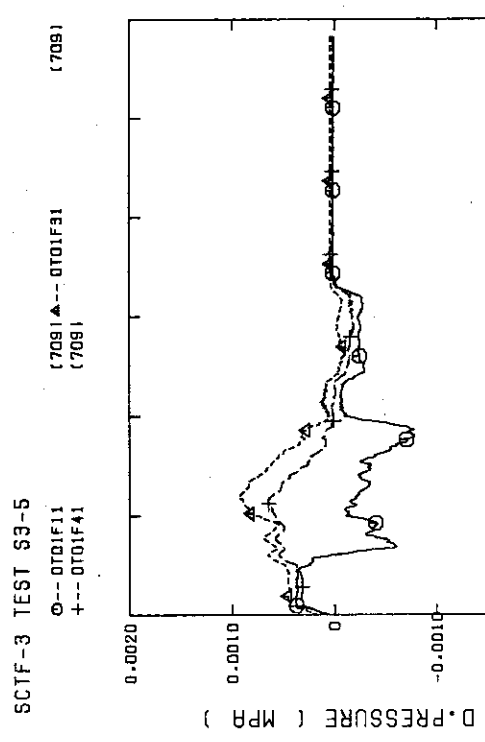

FIG. D-33 DIFFERENTIAL PRESSURE ACROSS END BOX TIE PLATE (BUNDLE 1.3.4)

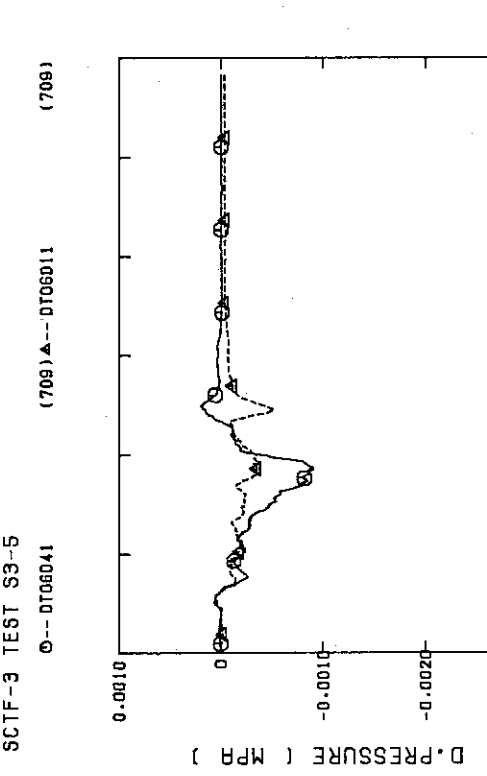

FIG. D-36 DIFFERENTIAL PRESSURE , HORIZONTAL AT 3235 MM (11-BUNDLE 1-4, 41-BUNDLE 4-8)

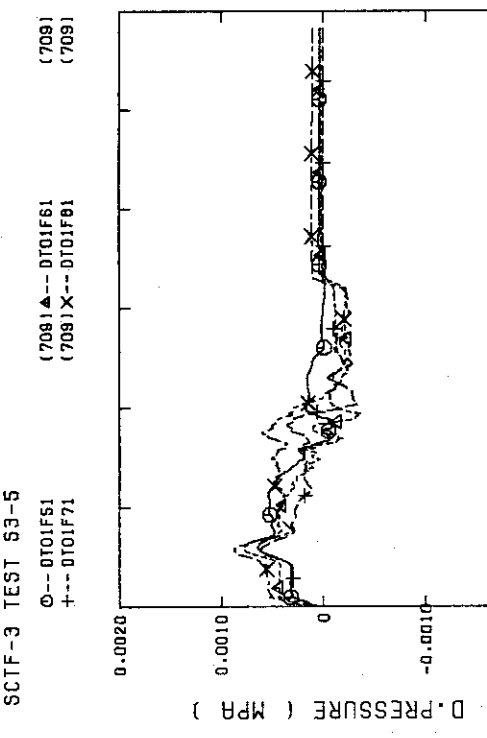

FIG. D-34 DIFFERENTIAL PRESSURE ACROSS END BOX TIE PLATE (BUNDLE 5,6,7,8)

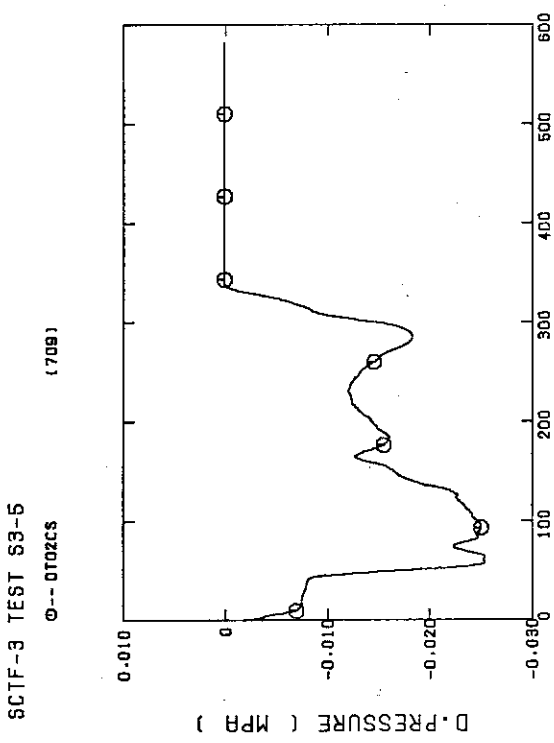

FIG. D-39 DIFFERENTIAL PRESSURE OF INTACT COLD LEG

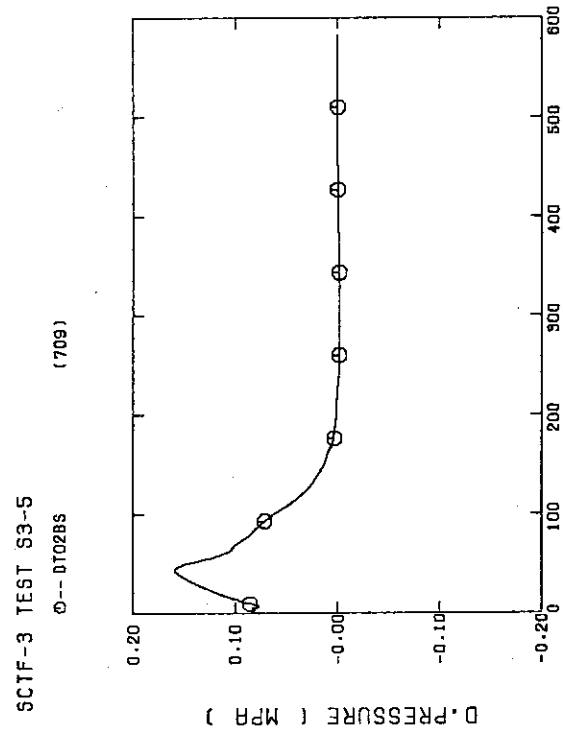

FIG. D-40 DIFFERENTIAL PRESSURE, STEAM/WATER SEPARATOR - CONTAINMENT TANK-II

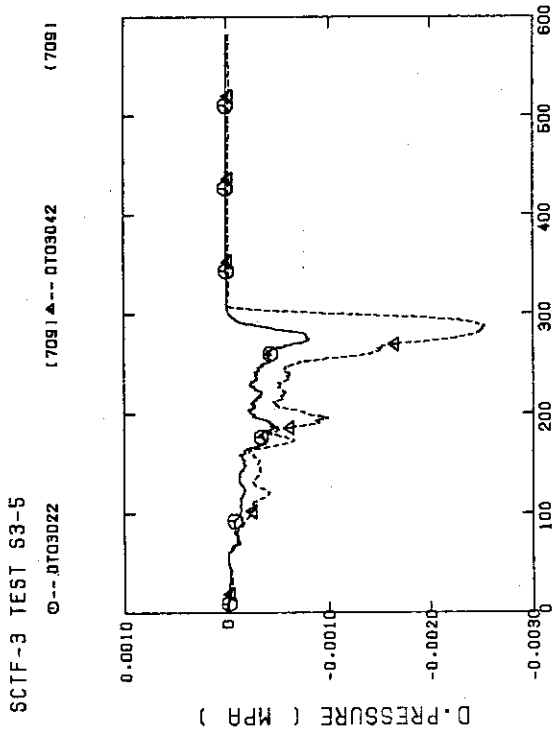

FIG. D-37 DIFFERENTIAL PRESSURE, HORIZONTAL AT 1365 MM (22-BUNDLE 2-4, 42-BUNDLE 4-8)

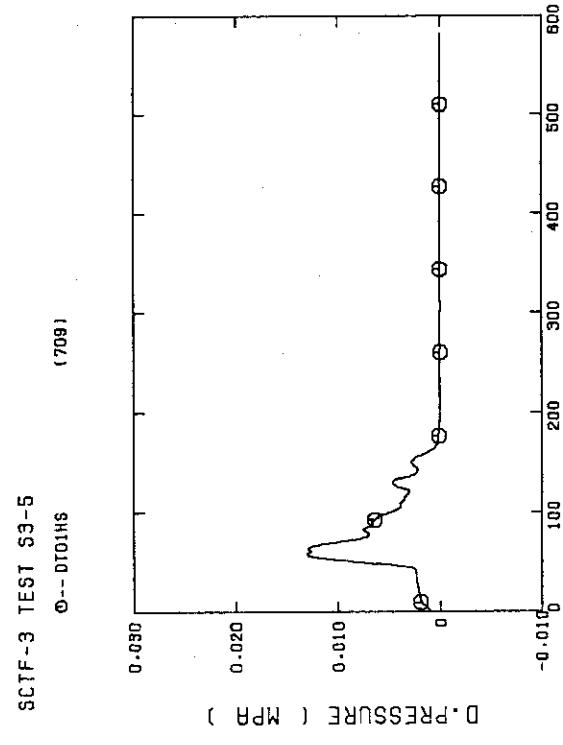

FIG. D-38 DIFFERENTIAL PRESSURE OF HOT LEG HOT LEG INLET - STEAM/WATER SEPARATOR INLET

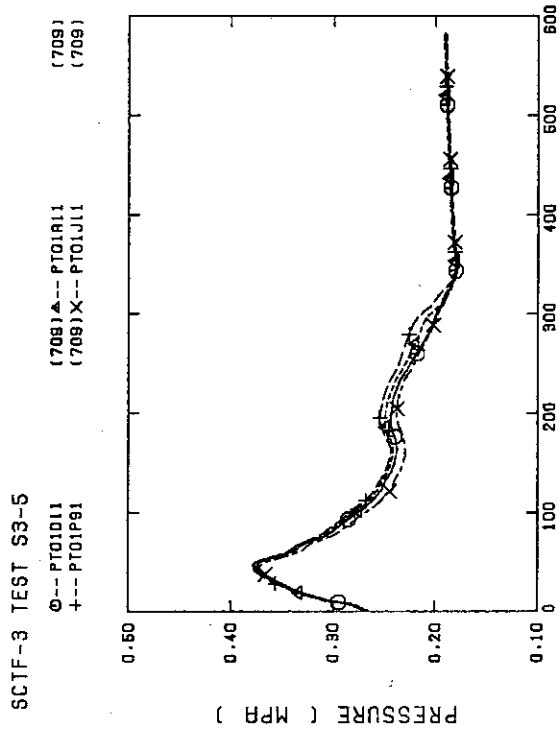

FIG. D-43 PRESSURE IN PV (J - TOP OF PV, D - CORE CENTER, A - CORE INLET, P - BELOW COLD LEG NOZZLE IN DOWNCOMER)

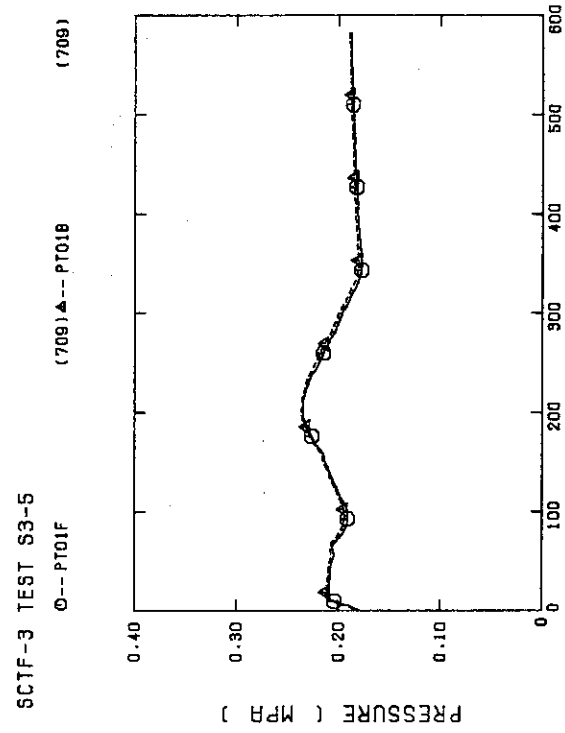

FIG. D-44 PRESSURE AT TOP OF CONTAINMENT TANK-I AND CONTAINMENT TANK-II (F-CONTAINMENT TANK-I, B-CONTAINMENT TANK-II)

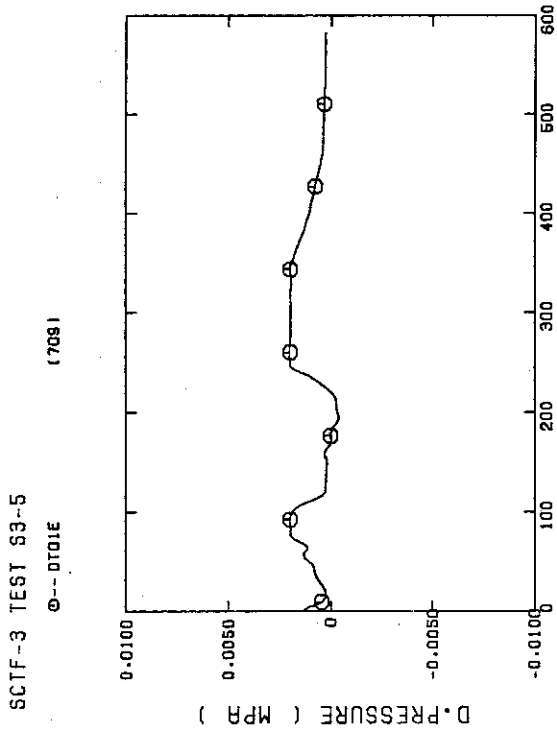

FIG. D-41 DIFFERENTIAL PRESSURE, CONTAINMENT TANK-II - CONTAINMENT TANK-I

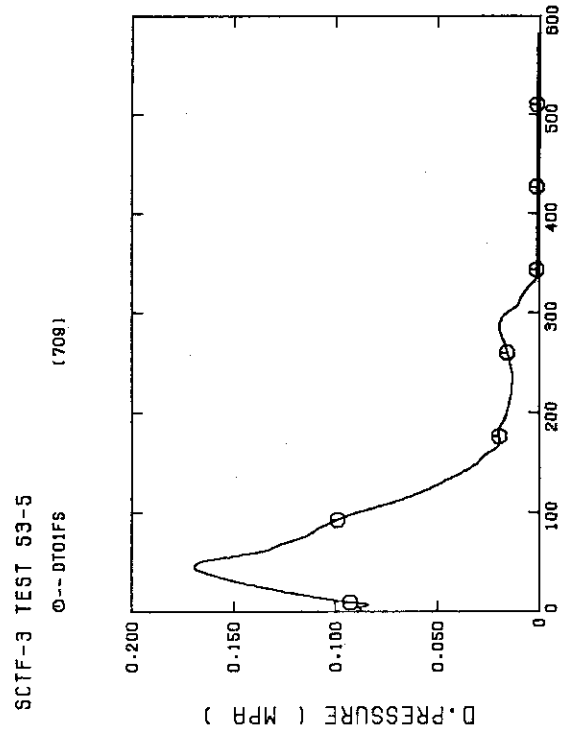

FIG. D-42 DIFFERENTIAL PRESSURE OF BROKEN COLD LEG - PV SIDE, DOWNCOMER - CONTAINMENT TANK-I

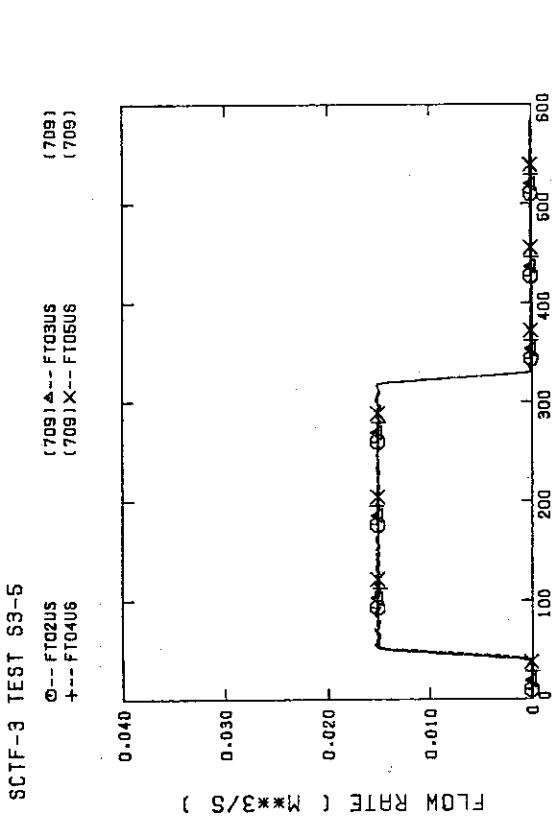

FIG. D-47 FLOW RATE OF UCSP INJECTION
LINE-1(BUNDLE7,8),LINE-2(5,6),LINE-3(3,4),LINE-4 (1,2)

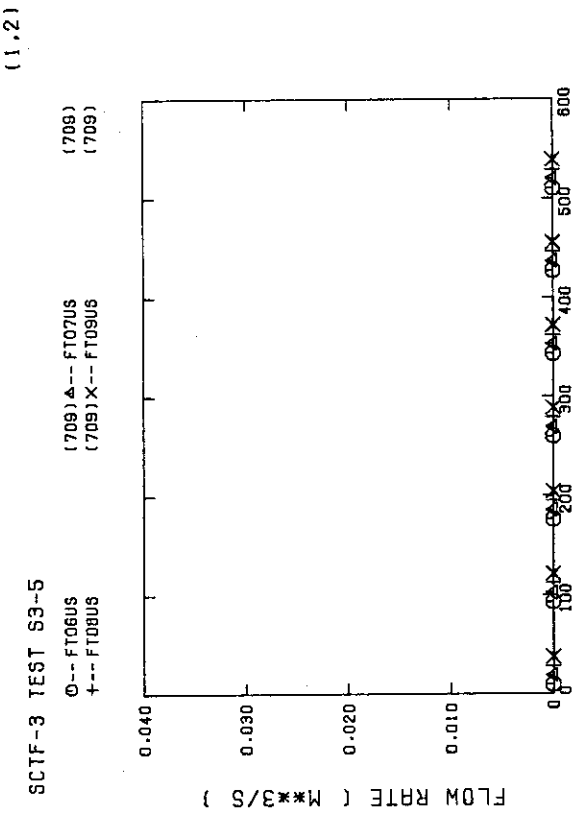

FIG. D-48 FLOW RATE OF UPPER HEAD INJECTION
LINE-4(BUNDLE1,2),LINE-3(3,4),LINE-2(5,6),LINE-1(7,8)

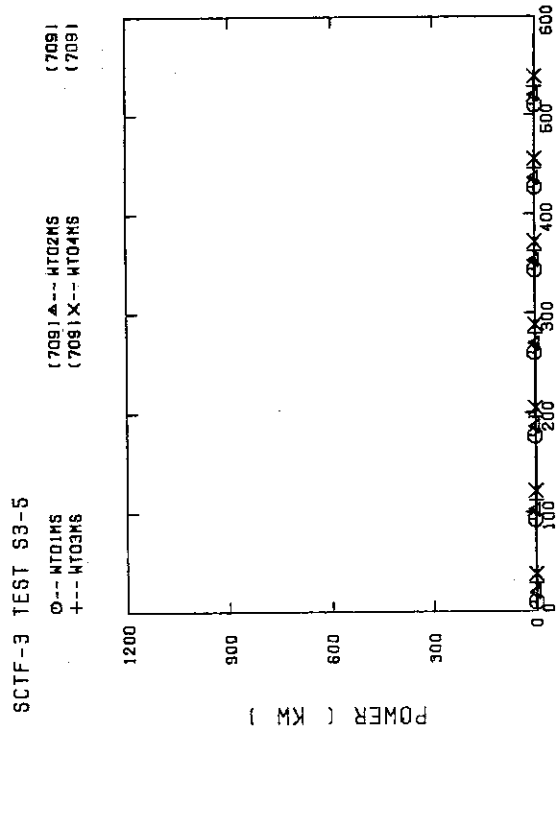

FIG. D-45 BUNDLE POWER
(BUNDLE 1.2.3.4)

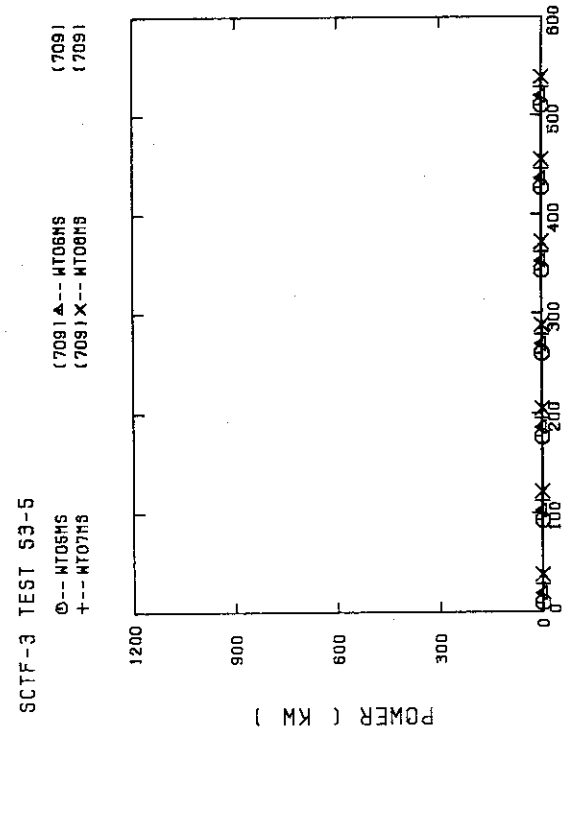

FIG. D-46 BUNDLE POWER
(BUNDLE 5,6,7,8)

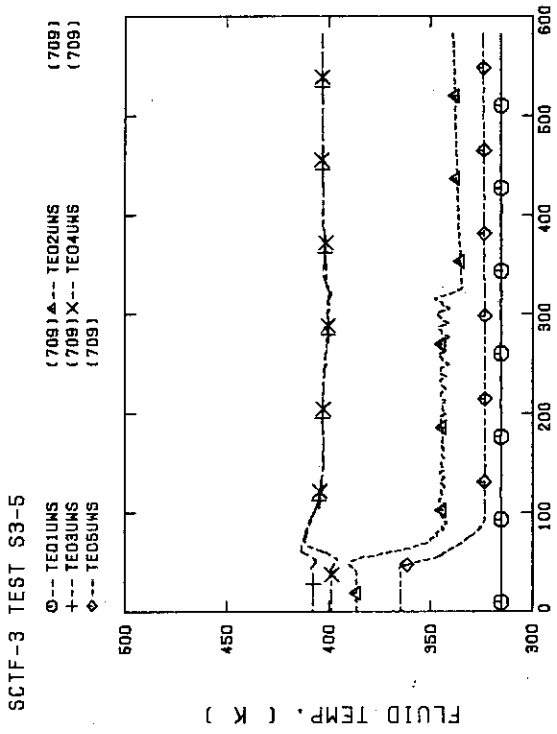

FIG. D-51 FLUID TEMPERATURE IN UCSP INJECTION LINE, O2(BUNDLE7,8),03(5,6),04(3,4),05(1,2),01(LOWER PLENUM)

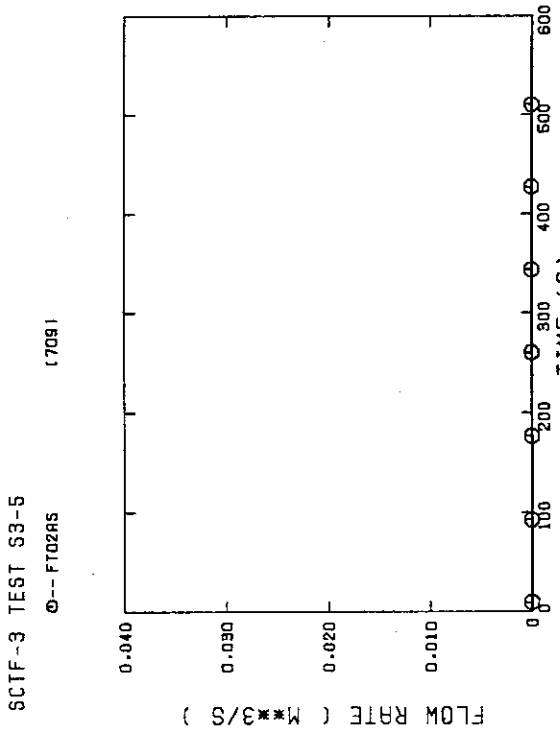

FIG. D-49 FLOW RATE OF ECC WATER (01-LOWER PLENUM, 02-INTACT COLD LEG, 03-BROKEN COLD LEG)

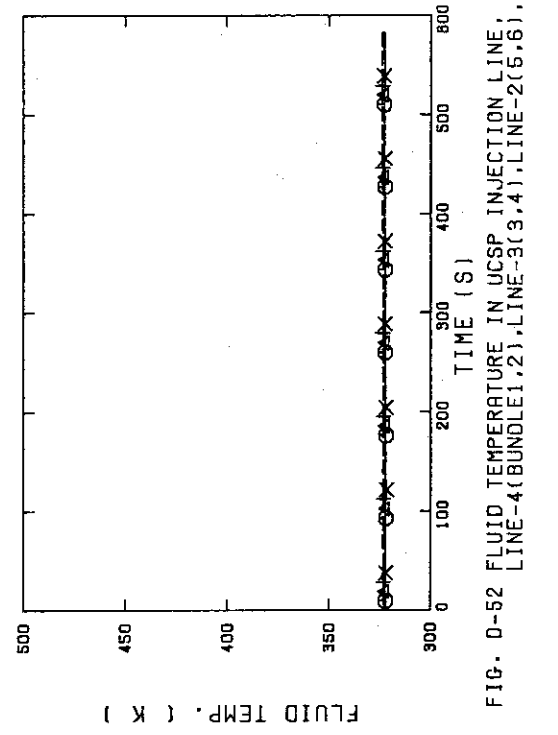

FIG. D-52 FLUID TEMPERATURE IN UCSP INJECTION LINE, LINE-4(BUNDLE1,2),LINE-3(3,4),LINE-2(5,6),LINE-1(7,8)

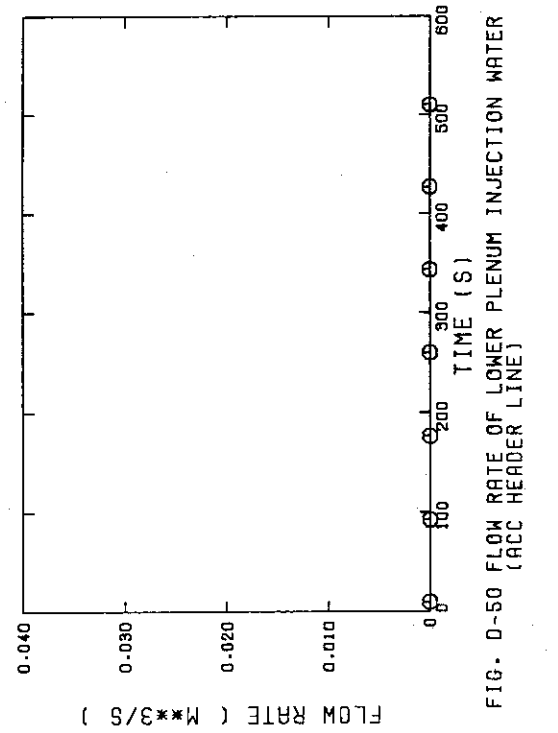

FIG. D-50 FLOW RATE OF LOWER PLENUM INJECTION WATER (ACC HEADER LINE)

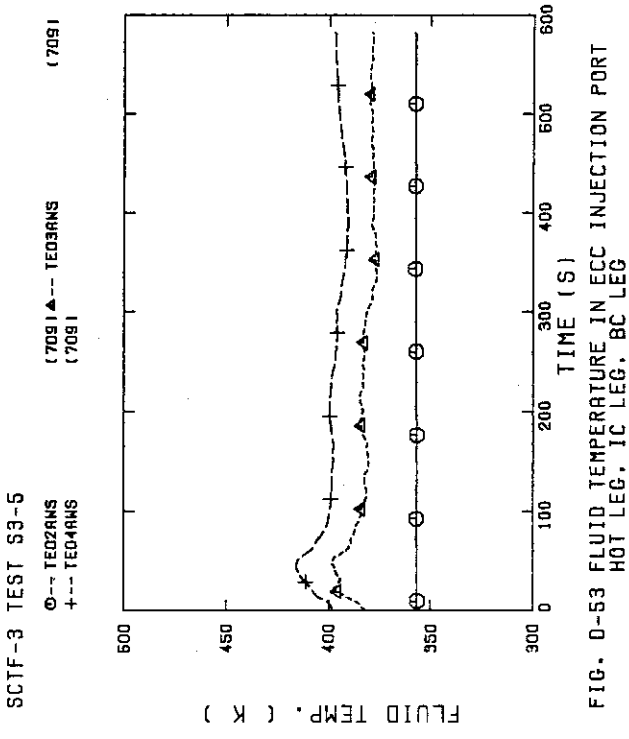

FIG. D-53 FLUID TEMPERATURE IN ECC INJECTION PORT HOT LEG, IC LEG, BC LEG